UNIVERSITY OF SOUTHAMPTON

FACULTY OF ENGINEERING, SCIENCE AND MATHEMATICS

School of Ocean and Earth Science

Implementation of a method to determine sub-nanomolar concentrations of iron in seawater and its application to the study of marine iron biogeochemistry at the ocean – shelf interface

by

Florence Nédélec

Thesis for the degree of Doctor of Philosophy

May 2006

UNIVERSITY OF SOUTHAMPTON

ABSTRACT

FACULTY OF ENGINEERING, SCIENCE, AND MATHEMATICS

SCHOOL OF OCEAN AND EARTH SCIENCE

Doctor of Philosophy

IMPLEMENTATION OF A METHOD TO DETERMINE SUB-NANOMOLAR CONCENTRATIONS OF IRON IN SEAWATER AND ITS APPLICATION TO THE STUDY OF MARINE IRON BIOGEOCHEMISTRY AT THE OCEAN-SHELF INTERFACE

By Florence Nédélec

The aim of this study was to improve our understanding of the marine iron cycle using a newly implemented technique to measure dissolved iron in seawater.

The setting up of a flow-injection analyser with chemiluminescence detection (FIA-CL) for Fe(II) proved to be non-trivial. Extensive work was undertaken to solve problems relating to our limited level of understanding of the CL reaction, and the variable behaviour of the resins prepared to preconcentrate iron. An analyser for Fe(II)+(III) was optimised, and careful assessment of data demonstrated the high quality of the information interpreted in this study, from the Celtic Sea shelf edge (Northeast Atlantic), and from the North Scotia Ridge (Southern Ocean).

The distribution of iron at the Celtic Sea shelf edge was examined, and was used to provide a conceptual framework for future studies. Dissolved Fe (< 0.4 µm) concentrations were measured in samples from nine vertical profiles taken across the continental slope (160 – 2950 m water depth). Dissolved iron concentrations varied between 0.2 and 5.4 nM, and the resulting detailed section showed evidence of a range of processes influencing the iron distributions. The presence of elevated levels of dissolved Fe near the seafloor was consistent with release of Fe from *in situ* particulate organic matter remineralisation at two upper slope stations, and possibly of pore water release upon resuspension on shelf. Lateral transport of dissolved iron was evident in an intermediate nepheloid layer and its advection along an isopycnal. Surface waters at the shelf break also showed evidence of vertical mixing of deeper iron-rich waters. The data also suggest some degree of stabilisation of relatively high concentrations of iron, presumably through ligand association or as colloids. The possibility of iron limitation of phytoplankton at the shelf edge was not ruled out despite obvious depletion of nitrate. This study supports the view that export of dissolved iron laterally to the ocean's interior from shelf and coastal zones may have important implications for the global budget of oceanic iron.

A set of surface samples collected on a survey between the Falkland Islands and South Georgia were analysed for total dissolvable iron. Results suggested a source of benthic iron near South Georgia. A shift in photo-physiology of phytoplankton towards South Georgia was probably influenced by the transition from iron-limited to iron-replete populations. These results therefore strongly support the hypothesis that South Georgia may be a "pulse-point" of iron to high-nutrient low-chlorophyll waters.

LIST OF CONTENTS

CHAPTER III. IMPLEMENTATION OF A FLOW INJECTION ANALYSER WITH CHEMILUMINESCENCE DETECTION (FIA-CL) TO SIMULTANEOUSLY DETECT FE(II) AND FE(III) IN SEAWATER

CHAPTER IV. DATA QUALITY

CHAPTER V. PROCESSES INFLUENCING DISSOLVED IRON DISTRIBUTIONS AT THE OCEAN – SHELF INTERFACE: CELTIC SEA SHELF BREAK (NORTHEAST ATLANTIC) AND SOUTH GEORGIA (SOUTHERN OCEAN)

CHAPTER VI. CONCLUSIONS AND FUTURE WORK

LIST OF FIGURES

CHAPTER I.

CHAPTER II.

CHAPTER III.

CHAPTER IV.

CHAPTER V.

LIST OF TABLES

CHAPTER II.

CHAPTER III.

CHAPTER IV.

CHAPTER V.

LIST OF APPENDICES

DECLARATION OF AUTHORSHIP

I, Florence Nédélec, declare that the thesis entitled :

Implementation of a method to determine sub-nanomolar concentrations of iron in seawater and its application to the study of marine iron biogeochemistry at the ocean – shelf interface

and the work presented in it are my own. I confirm that:

- this work was done wholly or mainly while in candidature for a research degree at this University;
- where any part of this thesis has previously been submitted for a degree or any other qualification at this University or any other institution, this has been clearly stated;
- where I have consulted the published work of others, this is always clearly attributed;
- where I have quoted from the work of others, the source is always given. With the exception of such quotations, this thesis is entirely my own work;
- I have acknowledged all main sources of help;
- where the thesis is based on work done by myself jointly with others, I have made clear exactly what was done by others and what I have contributed myself;
- parts of this work have been published as:

Claire L. Holeton, Florence Nédélec, Richard Sanders, Louise Brown, C. Mark Moore, David P. Stevens, Karen J. Heywood, Peter J. Statham, and Cathy H. Lucas, **2005**. Physiological state of phytoplankton communities in the Southwest Atlantic sector of the Southern Ocean, as measured by fast repetition rate fluorometry. *Polar Biology*, 29: 44-52.

Florence Nédélec, Peter J. Statham, and Matt Mowlem, ***submitted***. Processes influencing dissolved iron distributions below the surface at the Atlantic Ocean – Celtic Sea shelf edge. *Marine Chemistry* (Appendix 10).

Signed: Florence Nédélec

Date: 17th May 2006

AUTHOR'S DECLARATION

At no time during the registration for the degree of Doctor of Philosophy has the author been registered for any other University award without prior agreement of the Graduate Committee.

This study was financed with the aid of a studentship from the University of Southampton and carried out in collaboration with the National Oceanography Centre, Southampton.

A programme of advanced study was undertaken, which included: Masters' lectures in Environmental Analytical Chemistry, Global Biogeochemical Cycles, Coastal and Estuarine Oceanography, and Introductory Biological Oceanography; postgraduate courses in demonstrating and communication skills.

Additional skills were acquired for working at sea with courses in personal survival techniques, risk assessments, and manual handling and lifting awareness. The author participated to two major cruises: Atlantic Meridional Transect (AMT-12, 6 weeks, May – June 2003) and Celtic Sea cruise (JR-98, 3 weeks, July – August 2003).

The author also has been demonstrating during practical in Environmental Analytical Chemistry, Chemical Oceanography, and during the Plymouth field trip organised by the Southampton Oceanography Centre.

Relevant scientific meetings, seminars, and conferences were regularly attended at which work was often presented; external institutions were visited for consultation purposes and several papers prepared for publication.

Publications:

Claire Holeton, **Nédélec F.**, Sanders R., Brown L., Moore M., Stevens D. P., Heywood K. J., Statham P., and Lucas C., **2005**. Physiological state of phytoplankton communities in the Southwest Atlantic sector of the Southern Ocean, as measured by fast repetition rate fluorometry. *Polar Biology*, **29**: 44-52

Nédélec F., P.J. Statham, and M. Mowlem, **submitted**. Processes influencing dissolved iron distributions below the surface at the Atlantic Ocean – Celtic Sea shelf edge. *Marine Chemistry*.

Presentation and Conferences Attended:

Advances in Marine Biogeochemistry (AMBIO) meeting, 5th – 6th September 2005, National Oceanography Centre, 2 talks :

C. Holeton, **F. Nédélec**, R. Sanders, L. Brown, M. Moore, D. P. Stevens, K. J. Heywood, P. Statham, C. Lucas. *Physiological state of phytoplankton communities in the Southwest Atlantic sector of the Southern Ocean, as measured by fast repetition rate fluorometry*.

F. Nédélec, P. Statham. *Dissolved iron at the Northwest European shelf break: influence of benthic and transport processes*.

AMT meeting, Southampton Oceanography Centre, 6th July 2004

F. Nédélec. *Iron distribution in the Atlantic Ocean ($50^oS – 50^oN$, AMT-12)*. Talk

F. Nédélec, 21st May 2004. Development and application of a method to study marine iron biogeochemistry. Upgrade talk, SOC seminar.

AMT meeting, 29th January 2004, Plymouth.

F. Nédélec. *Iron distribution in the Atlantic Ocean ($50^oS – 50^oN$, AMT-12)*. Talk

New Frontiers in Geochemical and Isotopic Cycles in the Oceans, London, 29th – 30th September 2003.

Surface Ocean Lower Atmosphere Study (SOLAS) International Summer School, Corsica, France, 30th June – 11th July 2003

F. Nédélec, P. Statham, R. Sanders. *Study of specific aspects of the iron cycle in different marine environments*. Poster and talk

AMT meeting, Research Student Forum, 23rd – 24th January 2003, Plymouth.

F. Nédélec. *The iron biogeochemical cycle in the Atlantic Ocean ($50^oS – 50^oN$)*. Oral presentation.

External Contacts:

Dr Simon Ussher, Biogeochemistry and Environmental Analytical Chemistry Research Group, University of Plymouth
Dr Sophie Bonnet, Laboratoire d'Océanographie de Villefranche, France
Pr Tim Jickells, School of Environmental Sciences, University of East Anglia
Dr Dorothee Bakker, School of Environmental Sciences, University of East Anglia

Word count of main body of thesis: 50,262 words

Signed: Florence Nédélec

Date: 17th May 2006

Graduate School of the
National Oceanography Centre, Southampton

This PhD dissertation by

Florence Nédélec

has been produced under the supervision of the following persons

Supervisors	Doctor Peter J. Statham
	Doctor Richard Sanders
Chair of Advisory Panel	Professor Chris German
Internal Examiner	Doctor Eric P. Achterberg
External Examiner	Doctor Malcolm Nimmo

ACKNOWLEDGEMENTS

I would like to acknowledge the help and support of my supervisors, Dr. Peter Statham and Dr. Richard Sanders. I would particularly like to thank Peter for his help and advices to solve the numerous problems that I encountered when developing the techniques.

I am also thankful to Simon Ussher and Sophie Bonnet, who kindly took the time to answer the numerous questions I had relative to the techniques they were using. I would also like to thank the officers and crew of the *R.R.S. James Clark Ross* for their support during my two cruises, and Sinhue Torres and Young Nam Kim who stayed awake all night to help me carry the sampling bottles to the container during the *JR98* cruise. This thesis was carried out with the financial support of the University of Southampton, and the George Deacon Division, Southampton, UK.

Thanks to my fellow PhD students for their support, and particularly to the “lunch-time” group including Adriana Huerta Casas, Ben Rabe, Martin Gutowski, Alan Hughes, and Nils Cornelius, who helped me going through the long frustrating hours spent in the laboratory by entertaining me during my few breaks.

Finally and not the least, I would like to thank my family, Eveline, Tanguy and Hervé Nédélec, and friends Christine Gallampois and Isabelle Qadri for their constant support during my whole PhD. It is with great love that I dedicate this thesis to them and in memory of my father.

ABBREVIATIONS

AAS	Atomic absorption spectrometry
AdCSV	Adsorptive cathodic stripping voltammetry
AMT	Atlantic meridional transect
AOU	Apparent oxygen utilisation
ASW	Acidified sea water
BNL	Benthic nepheloid layer
CL	Chemiluminescence
CR	Chart recorder
CROZEX	Crozet experiment
CTD	Conductivity temperature depth
DAl	Dissolved aluminium
DFe	Dissolved iron
DMS	Dimethylsulphide
DPD	*N*,*N*-dimethyl-*p*-phenylenediamine
EISENEX	Eisen (iron) experiment
ENACW	Eastern North Atlantic Central Water
FC	Flow cell
FIA-CL	Flow-injection analyser with chemiluminescence detection
GF-AAS	Graphite furnace atomic adsorption spectrometry
HNLC	High-nutrient low-chlorophyll
HPLC	High performance liquid chromatography
8-HQ	8-Hydroxyquinoline
ICP-MS	Inductively coupled plasma mass spectrometry
IL	Injection loop
INLs	Intermediate nepheloid layers
IronEx-1 & 2	Iron enrichment experiment 1 & 2
ITCZ	Inter-tropical convergence zone
IV	Injection valve
JR	*RRS* James Clark Ross
LDPE	Low-density polyethylene
LISW	Low-iron sea water
LISW-IS	Low-iron sea water internal standard
LoD	Limit of detection
LR	Luminol reagent
LSW	Labrador Sea Water
MOW	Mediterranean Outflow Water
NASS-5	North Atlantic surface seawater – 5

NEADW	North East Atlantic Deep Water
NOCS	National Oceanography Centre, Southampton
NOM	Natural organic matter
OED	Ocean Engineering Division
OMEX	Ocean margin exchange (programme)
OTE	Ocean technology equipment
PCC	Preconcentration column
PMT	Photo-multiplier tube
POC	Particulate organic carbon
POM	Particulate organic matter
PP	Peristaltic pump
PS	Power supply
PTFE	Polytetrafluoroethylene (Teflon)
PVC	Polyvinyl chloride (plastic)
PVP	Polyvinylpyrrolidone (wetting agent)
Q-HCl	Quartz distilled hydrochloric acid
rsd	Relative standard deviation
RW	Rinsing water
SAF	Sub-Antarctic front
SBDW	Sub-boiled distilled water
sd	Standard deviation
SeaWiFS	Sea-viewing Wide Field-of-view Sensor
SEEDS	Subarctic Pacific iron experiment for ecosystem dynamics study
SERIES	Sub-arctic ecosystem response to iron enrichment study
SNL	Surface nepheloid layer
SOFeX	Southern Ocean iron fertilisation experiment
SOIREE	Southern Ocean iron-release experiment
SPM	Suspended particulate material
TDFe	Total dissolvable iron
TETA	Triethylenetetramine
TSK	A registered trade mark of Toyosoda
UKORS	United Kingdom ocean research services
UoP	University of Plymouth
UoS	University of Southampton
UV	Ultra-violet

CHAPTER I.

INTRODUCTION AND OBJECTIVES

I.1. Overview

Iron is the fourth most abundant element in the Earth's crust and is essential for all known living organisms. However, because of its high reactivity and very low solubility in the oxidised form, dissolved Fe (defined here as the fraction < 0.4 μm) remains at nanomolar or sub-nanomolar concentrations in surface waters for most of the open ocean (Johnson *et al.*, 1997). Some very iron-poor waters do not exhibit the high marine primary productivity expected for waters with elevated conventional nutrients. These areas of the open ocean are generally called "High-Nutrient, Low-Chlorophyll" (HNLC) regions, and represent about 40% of the world's ocean. They include the sub-arctic Pacific, the equatorial Pacific, and the Southern Ocean (Watson, 2001). More than 15 years ago, John Martin (1988) postulated that iron is one limiting factor for new production in these HNLC waters. The "iron hypothesis" has been validated as a result of several major iron fertilisation experiments: in the equatorial Pacific (IronEx-I (October 1993) (Martin *et al.*, 1994), IronEx-II (May-June 1995) (Coale *et al.*, 1996b)), in the Southern Ocean (SOIREE (February 1999) (Boyd *et al.*, 2000), and more recently in the sub-arctic Pacific (SEEDS (July-August 2001) (Takeda and Tsuda, 2005), and SERIES (July 2002) (Boyd *et al.*, 2004)) and again in the Southern Ocean (EISENEX (November 2000) (Gervais *et al.*, 2002) ; and SOFeX (January - February 2002) (Coale *et al.*, 2004)). All these experiments showed a significant increase in biological activity after the addition of dissolved Fe. Iron is therefore indirectly linked to the carbon cycle through this limitation of primary production, and potentially plays an important role in the uptake and production of gases associated with climate change such as carbon dioxide and dimethylsulphide (Martin *et al.*, 1990; Zhuang *et al.*, 1992). Martin and co-workers suggested that it might be possible to perform an artificial iron-fertilisation of the Southern Ocean and stimulate its absorption of carbon dioxide, thus reducing the "green-house" effect (Martin, 1990). However fertilisation experiments showed that the carbon export to the deep ocean due to enhanced photosynthesis and subsequent sinking of dead organisms was less important than initially thought (Dalton, 2002; Buesseler *et al.*, 2004). The possibility of fertilising the oceans with iron for ocean farming (Schueller, 1999), and to reduce carbon dioxide in the atmosphere is still under debate, and involves both economic considerations, and issues of environmental preservation (Chisholm *et al.*, 2001; Johnson and Karl, 2002; Buesseler and Boyd, 2003; Schiermeier, 2003; Zeebe and Archer, 2005). To fully understand the implications for carbon drawdown, it is therefore crucial to understand the iron cycle in the oceans in

order to determine the environmental effect and efficiency of artificial iron fertilisation of the ocean.

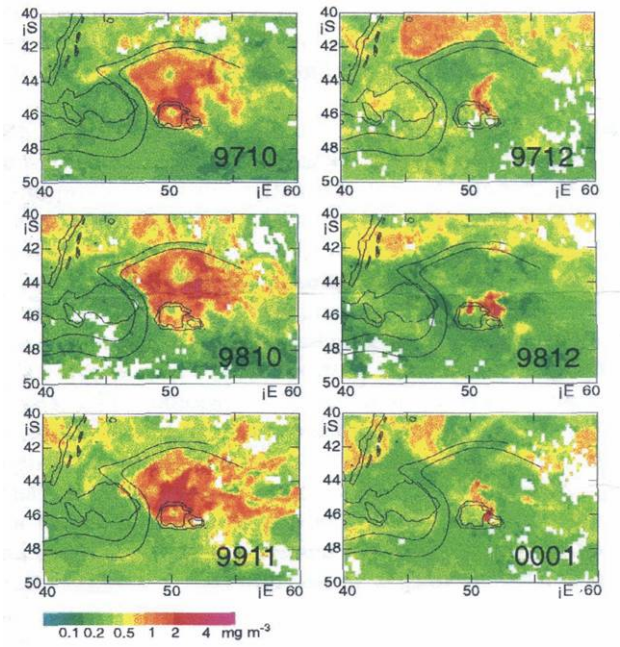

Figure I.1: SeaWiFS derived surface chlorophyll *a* concentrations around the Crozet Plateau in October / November and December / January of 1997 – 1999. Also shown are the stream-function lines defining the Circumpolar Current, as derived by Pollard and Read (2001).

Knowledge of the iron biogeochemical cycle is important when, for example, trying to understand algae blooms such as those that develop each year in the Crozet basin (Figure I.1), around Kerguelen (Blain *et al.*, 2001), and South Georgia (Korb *et al.*, 2004) in the Southern Ocean. These islands are located in HNLC areas south of the Sub-Antarctic Front (SAF) in the Indian (Read *et al.*, 2000) and Atlantic (Arhan *et al.*, 2002) sector of the Southern Ocean, respectively. A natural bloom develops during the austral Spring and lasts for up to two months in the Crozet Basin, and up to 4-5 months around South Georgia (Atkinson *et al.*, 2001). Understanding why these blooms occur is important in terms of our global comprehension of the oceans but also environmentally as these events have a significant influence on local ecosystems (Atkinson *et al.*, 2001). Atmospheric deposition is thought to be very low in the Southern Ocean (Duce *et al.*, 1991). It is hypothesised that the iron released from particulate Fe resuspended from sediments from the Crozet Plateau during winter mixing induces the plankton bloom observed in satellite images in the Crozet Basin during the austral Spring when light is not limiting (P. Statham, 2001, personal communication). This bloom is thus thought to result from the release of Fe from benthic sources in a similar way to the bloom observed 1,000 km away around the Kerguelen islands (Blain *et al.*, 2001; Bucciarelli *et al.*, 2001), and also likely around South Georgia (Holeton *et al.*, 2005). The study of these blooms involves many aspects of the iron cycle that are not fully understood such as the inputs of Fe to the upper ocean, and the processes leading to its bioavailability.

I.2. Overview of the current knowledge of the iron cycle in the ocean

The ocean distributions and biogeochemical behaviour of dissolved (< 0.4 μm) and particulate Fe (> 0.4 μm) are controlled by complex interactions including input, internal cycling, and removal processes coupled with physical transport (de Baar and de Jong, 2001) (Figure I.2). Interactions between iron and these processes in remote open ocean areas where inputs are low result in a nutrient-like distribution of dissolved iron closely correlated with that of nitrate and phosphate (Johnson *et al.*, 1997). As with major nutrients, much of the dissolved iron is taken up by phytoplankton in surface waters and is then recycled below. The cycle is completed when iron is returned to the euphotic zone through transport processes (*i.e.* advection, and vertical mixing, Figure I.2). The resulting dissolved iron profile is characterised by very low concentrations (< 0.3 nM) in surface waters, increasing to 0.4 to 1.5 nM in deeper waters (Johnson *et al.*, 1997; Ussher *et al.*, 2004). However, the distribution of dissolved iron can be considerably modified in regions affected by internal and/or external sources of iron but fluxes are still not well quantified (de Baar and de Jong, 2001; Ussher *et al.*, 2004) (Figure I.2). Residence times of dissolved iron are known only to an order of magnitude, at best, ranging from days in surface waters to a few years in deeper waters, well below the inter-oceanic mixing time of ~1000 years (de Baar and de Jong, 2001; Sarthou *et al.*, 2003; Croot *et al.*, 2004b; Statham and Hart, 2005). A single ocean residence time for the global ocean is thus not a viable concept for iron, as opposed to the major nutrients (Johnson *et al.*, 1997). It is therefore essential to determine the importance of the sources, removal, transport, and recycling of iron, and, if possible, its speciation in the environment in order to properly understand the dissolved iron distribution.

I.2.1. Sources of dissolved iron to the ocean

Iron may be supplied by external sources: laterally by rivers (coastal and shelf waters), from above via atmospheric deposition (coastal, shelf and open ocean), and/or melting sea-ice (polar waters); and by internal sources: from below through reductive benthic fluxes (coastal and shelf), and potentially at deep ocean ridges by hydrothermal venting (ridges and hot spots) (de Baar and de Jong, 2001; Ussher *et al.*, 2004) (Figure I.2). Source terms are briefly presented below in order of increasing importance, as some of the sources listed above are very small and may affect only restricted areas of the ocean.

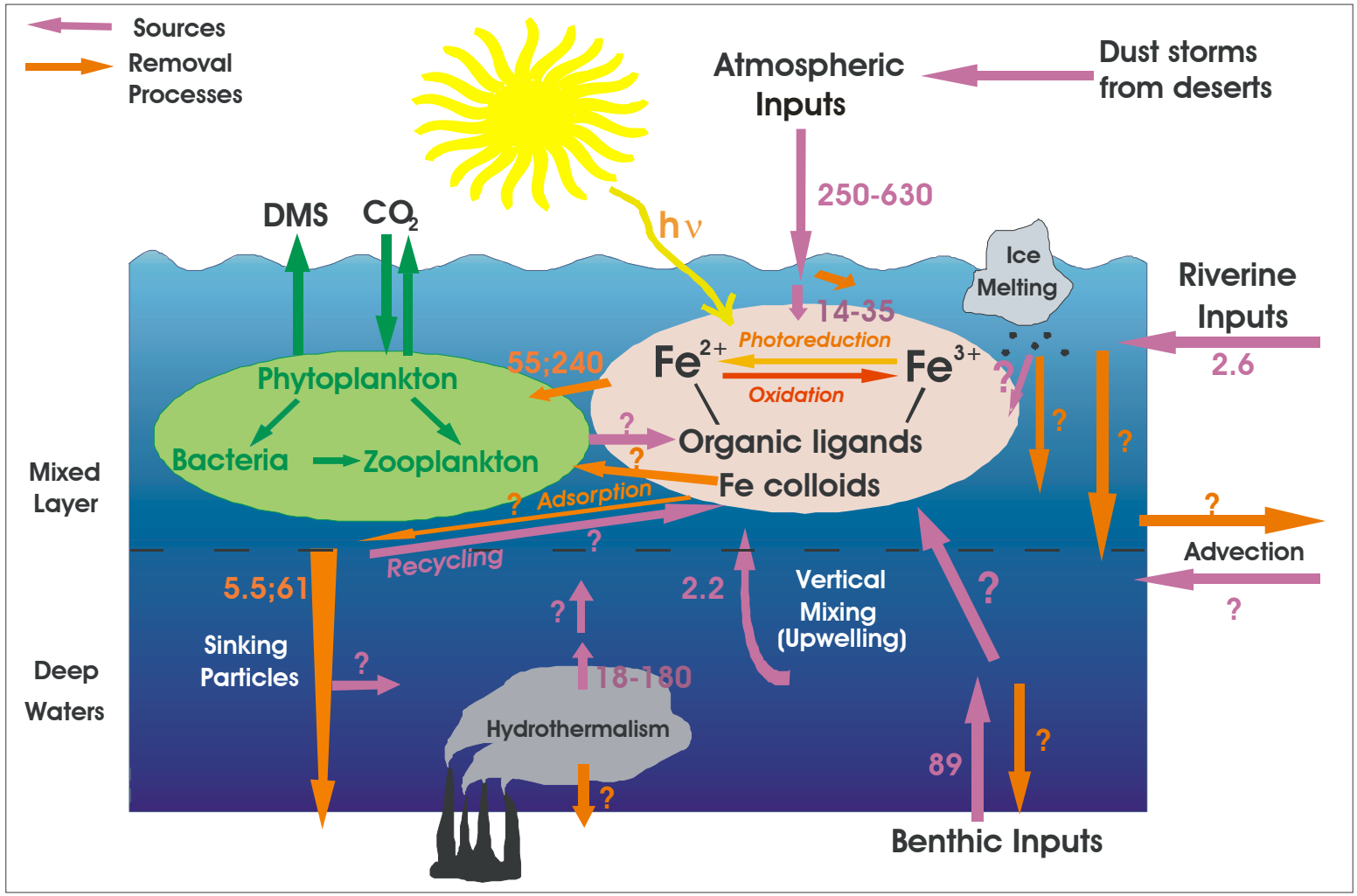

Figure I.2: Diagram representing the global iron biogeochemical cycle. Purple arrows indicate sources and orange arrows show removal of dissolved iron. Estimates of main fluxes (in Gmol.y^{-1}) are indicated. Atmospheric fluxes include both wet and dry deposition. The first number of fluxes for removal by biological uptake (55; 240) and through sinking particles (5.5; 61) is given for open ocean, and the second number for coastal waters. See text for references.

Inputs of dissolved iron released from particles in melting sea-ice, including icebergs, are likely to be very small, and localised (no estimation of flux available). Sea-ice is mostly formed and lost every year so that the release of dissolved iron, and thus phytoplankton blooms, will depend on the dynamics of the pack ice melting. Only a few studies have been carried out on the importance of melting sea ice in the fertilisation of polar waters (Loscher *et al.*, 1997; Sedwick and DiTullio, 1997; Measures, 1999; Grotti *et al.*, 2001; Croot *et al.*, 2004a), and little is known about the mechanisms releasing dissolved iron from particles trapped in the ice.

Hydrothermal activity can be found between hundreds of meters below the surface (*e.g.* Manus Island, western Pacific (Mackey *et al.*, 2002)) and as deep as 3000 m on the Mid-Atlantic Ridge (German *et al.*, 1991; Fouquet *et al.*, 1994). The global flux of dissolved iron from hydrothermal activity is estimated between 18 – 180 $Gmol.y^{-1}$ in plumes (Ussher *et al.*, 2004). However upon cooling of the metal-rich (milli-molar concentrations of iron) hydrothermal fluid either within the seafloor or by admixture of colder ambient seawater, most dissolved iron rapidly precipitates out (≥ 95%) in various mineral forms, mostly as oxy-hydroxides (German *et al.*, 1991; Field and Sherrell, 2000). Export of dissolved iron in deep waters is therefore thought to be very small and negligible compared with other sources (de Baar and de Jong, 2001; Statham and Hart, 2005). Additionally the deep hydrothermal plume will be sufficiently buoyant to rise through the weakly stratified deep waters, but may not be able to penetrate the thermocline so that only deep waters may be enriched in dissolved iron if any remains in solution (Mackey *et al.*, 2002). However, a small component of the total hydrothermal flux may be preserved (Field and Sherrell, 2000), and would still represent a significant source of dissolved iron to the deep ocean that may be at a later stage transported to surface waters, but this implies that dissolved iron is stabilised in seawater (Statham *et al.*, 2005).

Riverine inputs of iron to coastal waters are relatively important (estimated flux = 2.6 $Gmol.y^{-1}$ (de Baar and de Jong, 2001; Ussher *et al.*, 2004)) despite intense removal during estuarine mixing between river and sea waters. Most of the iron colloids present in river waters flocculate and settle as soon as the salinity increase (between salinities of 0 and 10) so that about 70 – 95% of riverine iron is removed from solution (Boyle *et al.*, 1977; Sholkovitz, 1978; Sholkovitz *et al.*, 1978). Fine particulate iron may be transported through the salinity gradient to shelf waters where desorption may release some dissolved iron in coastal waters (Turner and Millward, 2000; Sokolowski *et al.*,

2001). However, little is known about the possible flux of riverine iron into open ocean waters (Ussher *et al.*, 2004).

Atmospheric deposition of continental aerosols is thought to be the largest source of iron to the oceans even though it is highly episodic and spatially unevenly distributed (Swap *et al.*, 1996; Jickells and Spokes, 2001; Prospero and Lamb, 2003; Statham and Hart, 2005; Baker *et al.*, 2006). The largest sources for atmospheric mineral particles are in arid or semi-arid regions on the continents (*e.g.* central Asia, North Africa, India, and the Arabian peninsula) (Duce and Tindale, 1991). Atmospheric deposition is the only source of dissolved iron in several areas of the open ocean. However, dissolution rates of iron from dry aerosols are very low (< 2%) in seawater, and depend on many factors including the aerosol source (*i.e.* natural or anthropogenic) and particle concentration (Bonnet and Guieu, 2004; Mackie *et al.*, 2005; Baker *et al.*, 2006), pH-dependent adsorption-desorption processes (Mackie *et al.*, 2005; Baker *et al.*, 2006), photoreductive dissolution (Sulzberger and Laubscher, 1995), and the presence of organic species (Borer *et al.*, 2005). Iron may be more soluble in rainwater by reaction with sulphur and light, and lower pH, which may lead to significant dissolved Fe(II) levels (Kieber *et al.*, 2001; Kieber *et al.*, 2003). Atmospheric deposition in iron-depleted regions of the ocean may be important enough to fulfil the requirements of the biota and relieve temporarily iron limitation of primary production (Blain *et al.*, 2004). The total flux of iron in dust was estimated at 250-630 $Gmol.y^{-1}$ of which 70% is dry deposition (assuming 2% Fe solubility, flux = 3.5-9 $Gmol.y^{-1}$), and 30% is wet (assuming 14% Fe solubility, flux = 10.5-26 $Gmol.y^{-1}$) (Jickells and Spokes, 2001). Wet deposition of iron is of particularly important in the Inter-Tropical Convergence Zone where precipitation can be as high as 2 $m.y^{-1}$ (Bowie *et al.*, 2002b; Sarthou *et al.*, 2003).

In coastal and shelf waters, the major source of dissolved iron is likely to be mobilisation of iron from marine sediments. This source is clearly observed from the large increasing concentration gradients of both dissolved and particulate Fe (and Al) in surface waters towards the continental margin (Wu and Luther III, 1996; Croot and Hunter, 1998; Bowie *et al.*, 2002b; Boye *et al.*, 2003). The main processes potentially releasing dissolved iron are remineralisation from particulate organic matter exported from the euphotic zone (Berelson *et al.*, 2003; Elrod *et al.*, 2004), and diffusion or resuspension of Fe(II)-rich pore water (Hong and Kester, 1986; Canfield, 1989). It was recently suggested that benthic sources might have been under-estimated in the global iron budget (Elrod *et al.*, 2004). An estimate of the flux of dissolved iron from

continental shelves based on remineralisation of organic matter gave 89 Gmol.y^{-1} (Elrod *et al.*, 2004), which is far greater than the estimated dissolved iron input from atmospheric deposition (see above). However, little is known about the quantity of this flux reaching the euphotic zone in coastal/shelf waters.

In summary, sources of dissolved iron to the ocean are multiple and are highly variable, both spatially and temporally. Levels of dissolved iron however remain low in seawater due to its chemical reactivity and speciation, and as a result of removal processes.

I.2.2. The dissolved iron pool

The chemistry of iron in seawater is complex. Iron exists in two redox states, Fe(II) and Fe(III), within a variety of soluble coordination complexes with organic or inorganic ligands, or in a variety of colloidal and/or particulate forms (Ussher *et al.*, 2004) (see also Chapter II.2.1). In oxygenated seawater, iron is found primarily as the thermodynamically stable form, Fe(III), which is highly reactive with respect to hydrolysis, adsorption, and complex formation (Ussher *et al.*, 2004).

There are several reductive processes responsible for maintaining measurable Fe(II) concentrations in oxic surface waters, which is the most bio-available form of iron. These mechanisms are the retardation of Fe(II) oxidation rates by formation of Fe(II) organic complexes, direct or indirect photo-reduction (Kieber *et al.*, 2001; Moffett, 2001), bio-reduction at cell surfaces (Maldonado and Price, 2000), and chemical or microbial reduction in reducing macro-environments (anoxic basins and sediments) and micro-environments (*e.g.* faecal pellets) (Sunda, 2001; Ussher *et al.*, 2004).

It has been shown that dissolved Fe is highly complexed (> 99%) with dissolved organic ligands in open ocean waters (Rue and Bruland, 1995; van den Berg, 1995; Wu and Luther III, 1995). The total concentration of Fe-binding ligands is generally in excess of ambient dissolved iron concentrations (Rue and Bruland, 1997; Boye *et al.*, 2001; Boye *et al.*, 2003). Little is known about the sources, sinks and role of these organic ligands, but their stability constants are comparable to those of natural organic compounds released by micro-organisms (*e.g.* siderophores (Macrellis *et al.*, 2001), porphyrins (Hutchins *et al.*, 1999) and domoic acid (Rue and Bruland, 2001)) (Ussher *et al.*, 2004).

Measurements of iron in seawater are typically made in size-fractionated samples (see Chapter II.2.1). The previously defined "dissolved iron" (< 0.4 μm) may thus include a higher fraction of iron colloids which are operationally defined by filtration (~ 0.01 – ~ 1 μm), than was previously thought (Moran *et al.*, 1996; Nishioka *et al.*, 2001; Wu *et al.*, 2001). Given that dissolved iron is highly complexed by organic ligands, colloidal iron is likely to be mostly organically complexed (Kuma *et al.*, 1998) but may also include inorganic colloidal iron complexes.

The determination of dissolved iron speciation in seawater is therefore essential to understanding the dynamics of iron in the water column. However, the origin, nature, role of organic complexes and colloids, and their interaction with other processes remain poorly understood. Additionally these iron species are likely to be important in stabilising iron in solution and in the mechanisms of iron uptake by primary production.

I.2.3. Removal of dissolved iron from seawater

Removal of dissolved iron occurs through biological (*i.e.* uptake) and physical (*i.e.* precipitation and adsorption) processes, which are expected to operate simultaneously with inputs and result in the observed dissolved iron concentrations.

Iron is known to play a major role in key metabolic processes in most living organisms, and in the detoxification of reactive oxygen species (Price *et al.*, 1991; Sunda and Huntsman, 1995). The minimum growth requirements of marine phytoplankton significantly differs between species (Sunda and Huntsman, 1995; Berman-Franck *et al.*, 2001; Ho *et al.*, 2003; Price, 2005). Because of the low levels of iron in seawater, the biological pool develop different strategies to acquire iron according to their growth requirements (Whitfield, 2001), in competition with other species (Hutchins *et al.*, 1999). The currently known iron uptake mechanisms are: membrane bound porter sites (Hudson and Morel, 1990); release of Fe-binding ligands (Granger and Price, 1999; Hutchins *et al.*, 1999; Barbeau *et al.*, 2001; Rue and Bruland, 2001); ingestion (Nodwell and Price, 2001), digestion (Barbeau *et al.*, 1996); ligand exchange at cell surfaces (Chen *et al.*, 2003) of iron colloids; and extra-cellular reduction of organically bound Fe (Maldonado and Price, 2000) (Sunda, 2001; Ussher *et al.*, 2004). Uptake by primary production is a major removal mechanism for iron in coastal and open ocean waters (estimated fluxes = 240 $Gmol.y^{-1}$ and 55 $Gmol.y^{-1}$, respectively (de Baar and de Jong, 2001)). The bioavailability of iron is therefore an important factor to consider in the

study of its role in the biological loop, and reciprocally the influence of primary production on the speciation of iron by the release of organic ligands. However, several aspects of the interaction between iron and the biology remain unclear including the form of iron taken up.

Physical removal of iron and its export from the euphotic zone through sinking particles is also a major sink for iron in coastal and open ocean waters (estimated flux = 61 $Gmol.y^{-1}$ and 5.5 $Gmol.y^{-1}$, respectively (de Baar and de Jong, 2001)). This flux of detritus includes undissolved mineral particles and precipitated iron, iron adsorbed onto particles, and intra-cellular iron within biogenic particles (*e.g.* settling plankton, skeletal material, faecal pellets). Precipitation of free iron(III) occurs within seconds after addition to oxygenated seawater, and its solubility is very low (< pM) when Fe(III) hydroxides age (Rose and Waite, 2003a). Additionally dissolved iron adsorbs onto particles by electrostatic attraction to sinking particle surfaces due to their small net negative charge at the pH of seawater. However, despite these important removal mechanisms, a small fraction of dissolved iron remains in seawater, is recycled and may be supplied to the euphotic zone through transport processes.

I.2.4. Recycling and transport of dissolved iron

Iron is recycled at all depths in the water column. In the euphotic zone, iron is recycled by biological processes such as grazing, excretion, viral lysis, and bacterial remineralisation (Hutchins *et al.*, 1993). Below the euphotic zone, a significant portion (> 90%) of sinking biogenic particles is consumed by respiration of heterotrophic bacteria. The oxidation of particulate organic matter thus results in the remineralisation of macronutrients as well as biogenic iron. This process also occurs at the seafloor so that elevated dissolved iron concentrations may be observed (Elrod *et al.*, 2004) (see Chapter V). These iron-enriched bottom waters may then be advected vertically in waters affected by wind-driven upwelling (Johnson *et al.*, 1999), and in shelf waters by mixing caused by local currents.

Wind-driven upwelling processes are found in HNLC regions (Watson, 2001), and in specific coastal areas such as those off the Californian and off Peruvian coast lines. These systems provide an effective transport route for high levels of iron released from sediments to surface waters in association with macronutrients (Hong and Kester, 1986; Johnson *et al.*, 1999) (estimated flux of benthic iron upwelled to surface = 2.2 $Gmol.y^{-1}$

(Elrod *et al.*, 2004)), and lead to enhanced primary production (Martin and Gordon, 1988). However the supply of iron is limited by the discontinuity of these upwelling events (Coale *et al.*, 1996a; Fitzwater *et al.*, 2003) and by the width of the continental margin (Bruland *et al.*, 2001; Bruland *et al.*, 2005; Chase *et al.*, 2005), which leads to different degrees of iron limitation or stress (Hutchins and Bruland, 1998; Hutchins *et al.*, 1998; Hutchins *et al.*, 2002; Firme *et al.*, 2003). This limitation is particularly valid in HNLC regions of the Southern Ocean where upwelled waters are poor in iron due to the lack of an adjacent shelf (de Baar *et al.*, 1999), except in the vicinity of islands (*e.g.* Kerguelen (Bucciarelli *et al.*, 2001), Crozet (Pollard, 2004) and South Georgia (Korb and Whitehouse, 2004) islands).

Additionally a few studies have reported increased iron concentrations in open ocean waters of the Equatorial Pacific, North Atlantic, and Southern Ocean, which possibly originated from continental margins (Coale *et al.*, 1996a; Wu and Luther III, 1996; Gordon *et al.*, 1997; Laes *et al.*, 2003; Croot *et al.*, 2004a). Recently, another mechanism for the horizontal transport of these iron-enriched bottom waters was found in eddy formation (Johnson *et al.*, 2005). The possibility for dissolved iron transport to the ocean's interior from shelves may therefore be non-negligible and may be important, particularly at shelf edges.

In summary, the biogeochemical cycle of iron in the ocean is complex as it includes many processes involving its chemistry and physico-chemistry in seawater, its interaction with living organisms, and hydrography. Many aspects of these processes remain unclear, as the study of the iron biogeochemistry has been hindered by analytical limitations until recently. One of the major problems encountered when measuring sub-nanomolar concentrations of iron is contamination, since Fe is ubiquitous, especially on ships. New sampling and analytical techniques have since been developed with a better appreciation of the sources of contamination, and of its high reactivity in seawater.

I.3. Objectives

The initial aim of this study was to improve our understanding of the marine iron cycle by investigating the processes influencing the dissolved iron distribution in two different environments where samples were collected as part of this project: the Celtic Sea shelf edge, and the open Atlantic Ocean. However some of the open ocean samples from an Atlantic Meridional Transect (*AMT-12*) cruise were found to be contaminated

for iron (see Chapter IV). The focus of this project was therefore limited to the study of processes (*i.e.* sources, removal and transport) influencing dissolved iron distribution at the Celtic Sea shelf edge with the aim of giving a conceptual framework for future studies in highly dynamic environments of this sort.

An appropriate analytical tool was needed that would overcome problems due to the ultra-low Fe concentrations expected, risks of contamination, and high reactivity of iron. The first objective was to develop a working and compact analyser which would have an appropriate limit of detection (pico-molar), requiring very little sample handling to minimise risks of contamination, and allowing close to real-time measurements. The chosen technique was a flow-injection analyser with chemiluminescence detection (FIA-CL) which currently exists in two versions to determine: **i)** Fe(II), and Fe(II+III) by reducing Fe(III) to Fe(II) (Fe(II) technique); and **ii)** both Fe(II) and Fe(III) directly (Fe(II)+(III) technique), in seawater.

In Chapter II, a literature review is presented to give the principles of both versions of the FIA-CL. The chosen version, the Fe(II) technique, was based on an existing method (Bowie *et al.*, 1998) to allow the determination of dissolved iron(II) in seawater or dissolved Fe(II+III) after a reduction step. This technique was relatively easy to mechanically set up with the collaboration of Dr. Matt Mowlem from the Ocean Engineering Division (OED, NOCS), but its operation was found more difficult than at first thought. Full descriptions of the analyser are given in Appendices 1 and 3 to 5. The developmental stages are explained and an overview of the analytical problems and experiments carried out to solve them is presented. However, given the difficulty of obtaining a reliable calibration curve, it was decided to move on to the alternative method.

The FIA-CL analyser was modified to the Fe(II)+(III) technique since only a few modifications in instrumentation were required and descriptions are presented in Appendices 6 and 7. Despite some difficulties, this version of the Fe(II)+(III) based on the design of Obata *et al.* (1993) and de Jong *et al.* (1998), was successfully developed. The development of the technique and the solutions found for the problems experienced as well as a full description of the working analyser in its final stage are described in Chapter III.

The analyser was then used to determine dissolved iron in the samples collected. A rigorous data quality check was carried out on both the analysis and the integrity of the samples, to ensure the quality of these data. The quality of the analysis was checked based on its accuracy, precision, blank level, and limit of detection. At this stage, some samples were discarded from the data set due to suspicion of contamination. Investigations were carried out in order to determine its source(s). Criteria are given for the evaluation of the quality of the analysis and samples. A full description of this procedure is presented in Chapter IV.

The second objective was to examine the dissolved iron data in order to investigate processes influencing its distribution, using associated data obtained simultaneously. This study was carried out on samples collected at the Celtic Sea shelf edge during the summer of 2003 and is described in Chapter V. Oceanographic data at each station are presented in Appendix 9. Several processes were examined: **i)** sources of dissolved iron in near-seafloor waters; **ii)** removal and stabilisation of dissolved iron near the seafloor; **iii)** transport of dissolved iron both horizontally and vertically; and **iv)** the influence of primary production on the dissolved iron distribution in the euphotic zone, and the possibility for iron limitation at the Celtic Sea shelf edge was considered. Part of this work (*i.e.* sources and transport of dissolved iron) has been submitted to Marine Chemistry, and a copy of the first draft of the manuscript is included as Appendix 10.

An additional sample set collected during a transect along the North Scotia Ridge between the Falkland Islands and South Georgia not carried out within this project, was analysed for total dissolvable iron (leachable at pH ~ 2). These iron data were used to investigate primary production limitation in these polar waters (see Chapter V). A paper has already been published using the results presented here. Claire Holeton *et al.* (2005) examined variations in physiological state of phytoplankton communities in the Southwest Atlantic sector of the Southern Ocean using fast repetition rate fluorometry. The article had already been submitted once when the samples collected for iron were analysed, using the newly developed technique presented here. These iron data were used to support the data already presented in the paper. As Claire Holeton carried out the majority of the work towards this paper, a copy was not included in the main body of the thesis.

CHAPTER II.

IMPLEMENTING A METHOD TO DETERMINE VERY LOW CONCENTRATIONS OF DISSOLVED Fe(II) IN SEAWATER

II.1. Analytical challenges

It was as early as the 1930s that the potential role of iron as a limitation to marine primary production was first suggested (Gran, 1931). This idea was however not investigated further until the 1980s owing to the low data quality when attempting to measure nanomolar seawater concentrations of iron, as a result of sample contamination and not sufficiently low analytical limits of detection. Since then, new analytical techniques have been developed with a better appreciation of the sources of contamination. Ultra-clean sampling procedures (*e.g.* (Bruland *et al.*, 1979)) are now used, including careful washing of the sampling bottles; working in clean rooms; using high purity reagents (Moody and Lindstrom, 1977). Such procedures now permits the measurement of picomolar concentrations of iron in open ocean waters (Moody, 1982; Achterberg *et al.*, 2001). The methods used to determine iron concentrations in natural waters can be divided into two groups (Table II.1).

Iron measured	Technique used	Detection limit (pM)	Reference
LAND-BASED TECHNIQUES			
Fe(II+III)	Chelex-100 + GF-AAS	50 (2*s*)	(Landing and Bruland, 1987)
	8-HQ + ICP-MS	640	(Sohrin *et al.*, 1998)
	Isotope dilution ICP-MS	50	(Wu and Boyle, 1998)
SHIPBOARD TECHNIQUES			
Fe(II)	FIA + Ferrozine + spectrophotometry	100	(Blain and Treguer, 1995)
Fe(II), or Fe(II+III)	FIA + phenanthroline + spectrophotometry	42	(Adams and Powell, 2001)
Fe(II+III)	FIA + DPD + spectrophotometry	16	(Weeks and Bruland, 2002)
Total Fe, Fe(III), or organically complexed Fe	AdCSV	80	(Gledhill and van den Berg, 1995)
		~ 10	(Rue and Bruland, 1995)
		100	(Croot and Johansson, 2000)
		13	(Obata and van den Berg, 2001)
Fe(III), or Fe(II+III)	FIA-CL luminol + H_2O_2	50 10	(Obata *et al.*, 1993) (Obata *et al.*, 1997)
Fe(II) or Fe(II+III)	FIA-CL luminol	8-12	(Bowie *et al.*, 2002a)

Table II.1: Figures of merit of some of the most recent techniques used to determine iron in seawater. Analytical limit of detection = 3 times the standard deviation of the blank (3*s*), unless specified otherwise.

1) Land-based techniques, *i.e.* graphite furnace atomic absorption spectrometry (GF-AAS), or inductively coupled plasma mass spectrometry (ICP-MS). These methods are not used at sea because of the size, weight, and fragility of the instruments, in addition to the costs involved. Low detection limits are obtained using solvent extraction as a

preconcentration step, but resins (*e.g.* Chelex-100 or 8-hydroxyquinoline (8-HQ)) are nowadays generally preferred as sample handling and pre-treatment are minimised (Table II.1). However, these techniques do not allow measurement of redox or organically complexed iron (Achterberg *et al.*, 2001).

2) Shipboard techniques commonly require compact, portable, robust, and relatively low-cost instrumentation. The adsorptive cathodic stripping voltammetry (AdCSV) method has a relatively good sensitivity, and allows inorganic and organic iron speciation determination (Table II.1). However, its limit of detection is not always sufficient for measurements in iron limited regions, and analysis requires a long deposition time (up to 10 minutes) to achieve a sufficiently high sensitivity. Such long deposition could be disrupted by the ship's vibrations (Achterberg *et al.*, 2001). A recent development of the AdCSV method has significantly lowered its limit of detection and shortened the analysis time using 2,3-dihydroxynaphthalene (DHN) as ligand and the calatytic effect of the Fe(II)/Fe(III) redox couple on the reduction of bromate (Obata and van den Berg, 2001), resulting in a method adapted to work in iron-poor waters.

Most of the current shipboard techniques involve the use of flow-injection analysis (FIA) with in-line preconcentration. These methods consume small amounts of reagents and simplify sample handling (thus reducing contamination risks) and increase throughput. Different types of detectors can be used including spectrophotometric methods using ferrozine to determine Fe(II) (King *et al.*, 1991; Blain and Treguer, 1995); or 1,10-phenanthroline (Adams and Powell, 2001); or *N*,*N*-dimethyl-*p*-phenylenediamine (DPD) to determine Fe(II+III) (Measures *et al.*, 1995; Weeks and Bruland, 2002)) (Table II.1). However, ferrozine may shift the iron redox speciation reducing Fe(III) to Fe(II) (Hong and Kester, 1986), and may not be sensitive enough for open ocean surface waters in iron-depleted regions, whereas the DPD method is sensitive enough but does not allow measurements of the iron redox speciation (Achterberg *et al.*, 2001).

The most commonly used technique to determine iron in HNLC regions is flow-injection analysis with chemiluminescence detection (FIA-CL) using luminol (5-amino-2,3-dihydro-1,4-phthalazinedione) (Bowie *et al.*, 1998). This method has a flow-injection system coupled to a photo-multiplier tube (PMT) to detect the light produced

by the chemiluminescence reaction of luminol induced by iron (see Chapter II.2.3). This technique has been chosen for the current work because it potentially allows close to real-time measurements (3-10 minutes), it requires relatively low-cost, compact and portable instrumentation, it has very good sensitivity (pico-molar), and potentially allows direct Fe(II) determination.

II.2. Principle

Two versions of the FIA-CL with luminol currently exist: the Fe(II) FIA-CL designed to measure dissolved Fe(II) concentrations or total iron after reduction of Fe(II) in seawater based on the method of Bowie *et al.* (1998) (Fe(II) technique) and the FIA-CL to measure dissolved Fe(II) and Fe(III) developed by Obata *et al.* (1993) and de Jong *et al.* (1998) (Fe(II)+(III) technique). Both techniques involve three major analytical steps: **i)** sample pre-treatment to determine which size fraction and oxidation state of iron is analysed; **ii)** a pre-concentration step to collect Fe(III) or Fe(II)+Fe(III), to remove interfering trace-metals as well as sea-salts and to lower the limit of detection; and **iii)** the detection step using the chemiluminescence reaction with luminol.

II.2.1. Pre-treatment of samples

The first pre-treatment step is **sample filtration**. This procedure depends mainly on which form of iron is to be studied. The speciation of iron is complex as its two oxidation states (Fe(II) and Fe(III)) are involved in the formation of soluble inorganic and organic complexes, colloidal phases and particulate forms (Figure II.1).

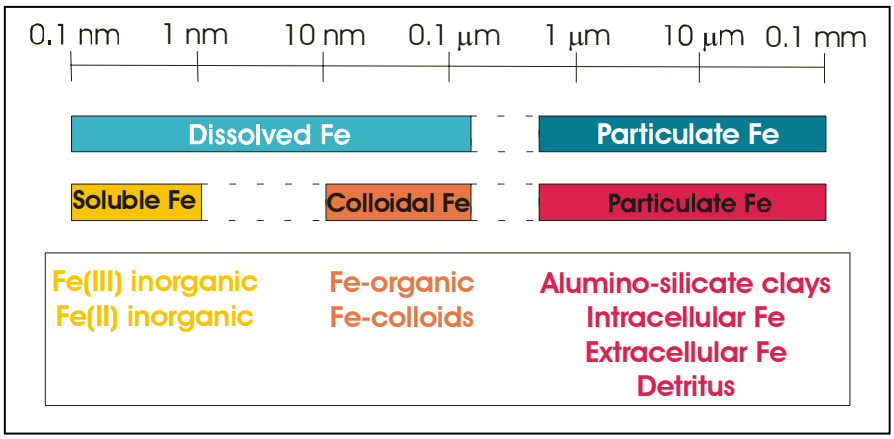

Figure II.1: The size distribution of iron species in seawater. Diagram modified from (Bruland and Rue, 2001)

The particulate phase of iron was initially operationally defined as that fraction retained on a 0.4 μm filter, and thus defining the fraction less than 0.4 μm as dissolved iron. However, it has been shown that this dissolved phase may contain an important fraction of iron colloids (80 – 90% in near-surface waters and 30 – 70% in deep waters (Wells and Goldberg, 1991; Nishioka *et al.*, 2001; Wu *et al.*, 2001)), which may be available to some organisms (Barbeau *et al.*, 1996; Nodwell and Price, 2001; Chen *et al.*, 2003). As shown in Figure II.1, boundaries between the different phases are not clearly defined, but generally the particulate phase is considered as the fraction over 0.4 μm, the colloidal fraction is between 0.1 or 0.2 μm to 0.4 μm, and the soluble fraction is below 0.1 or 0.2 μm. Recently the soluble fraction has also been divided into two phases: the soluble iron (below 200 kDa or 0.03 μm) and the small colloidal fraction (between 200 kDa or 0.03 μm to 0.1 or 0.2 μm) (Nishioka *et al.*, 2001; Wu *et al.*, 2001). This distinction between the different fractions in the dissolved phase is important in understanding the dynamics of iron in seawater; therefore the choice of filter pore size is critical in defining the form of iron studied. More recently, 0.2-μm pore size filters were used as the norm to define the dissolved fraction, in order to eliminate bacteria.

The second pre-treatment step is the **sample acidification**. Iron is a highly reactive element in seawater as Fe(III) is the thermodynamically stable form at seawater pH but is highly insoluble through the formation of oxy-hydroxides, and Fe(II) is rapidly oxidised to Fe(III) in oxygenated waters (Waite, 2001). However, Fe(II) has been found at measurable concentrations (up to 37% of total dissolved iron (Bowie *et al.*, 2002a)) thanks to photo-reduction processes and recycling from organic matter in surface waters (O'Sullivan *et al.*, 1991; Gledhill and van den Berg, 1995), and anaerobic sediment inputs (Hong and Kester, 1986). The kinetics of Fe(II) oxidation depends on several factors such as the pH (the rate decreases as it is lowered), temperature and dissolved oxygen concentration (the rate increases as these parameters are highered) (Millero, 1989; Croot and Laan, 2002). The use of an underway-sampling system is an important way to determine Fe(II) concentration as it rapidly brings surface water to the analyser, thus minimising any temperature and dissolved O_2 change in the sample (de Jong *et al.*, 1998; Vink *et al.*, 2000; Croot and Laan, 2002). When this underway system is not used, acidification keeps Fe(II) stabilised for analysis on the time scale of hours to days but this will change other aspects of speciation (*e.g.* organic complexation) (Weeks and Bruland, 2002). When the sample is stored for a long period of time (weeks to years), this procedure limits iron loss from solution by adsorption onto the walls of the

container (Moody, 1982), and Fe(II) oxidises to Fe(III) so that only total dissolved iron can be determined.

A third optional pre-treatment step is the **reduction of Fe(III)** to measurable Fe(II). This procedure is necessary for the measurement of total (Fe(II+III)) dissolved iron with the Fe(II) FIA-CL technique only. Excluding biological processes, the two major routes to reduce iron that have been found to occur in seawater are chemical reduction (Behra and Sigg, 1990; Millero *et al.*, 1995a), and photo-reduction (Voelker and Sedlak, 1995; Barbeau *et al.*, 2001). The reduction of nanomolar concentrations of Fe(III) with sulphite has been studied in seawater by Millero *et al.* (1995a). It was found that the rate constant for this first order reaction with respect to Fe(III) and S(IV) is a strong function of pH and solution composition (Millero *et al.*, 1995a). At pH 2 with [Fe(III)] = 100 nM and [S(IV)] = 100μM, the rate constant was 4.08 ± 0.03 M^{-1} min^{-1} in seawater (Millero *et al.*, 1995a). In the case of an analysis by chemiluminescence (CL) detection, sodium sulphite was identified as a reducing agent which does not interfere with the CL reaction (O'Sullivan *et al.*, 1995). This reagent was added to acidified samples and allowed to react for several hours (> 4h) for the reaction to be complete with the Fe(II) FIA-CL to determine total Fe(II+III) (O'Sullivan *et al.*, 1995; Powell *et al.*, 1995; Bowie *et al.*, 1998).

Many experiments have also shown the importance of light in reducing Fe(III) to Fe(II) (photo-reduction reaction) (O'Sullivan *et al.*, 1991; Zhu *et al.*, 1993), and that the reaction is more efficient at low pH (Behra and Sigg, 1990; King *et al.*, 1993). Both chemical and photo-reduction reactions were found to occur in cloud droplets leading to measurable concentrations of dissolved Fe(II) (Behra and Sigg, 1990; Sedlak and Hoigne, 1994). It may thus be possible to combine these two processes (*i.e.* chemical reduction with sodium sulphite and UV irradiation) together to allow effective in-line determination of total dissolved iron. This process is suggested here and may be effected by positioning an UV-light source in the centre of a quartz coil where samples with sodium sulphite added flow past, following the UV digestion design of Achterberg *et al.* (2001a) for cobalt determination.

II.2.2. Preconcentration

The second critical step during the analysis of iron in seawater with both Fe(II) and Fe(II)+(III) techniques, is the preconcentration procedure. This stage of the analysis is

important in that: **i)** it allows separation of iron from some of the interfering metal cations for the CL reaction, with quantitative recovery of the element; **ii)** it permits a large enrichment factor, thus lowering the limit of detection with a high sample throughput; and **iii)** it removes the sea-salt matrix which, at higher pH, may lead to precipitates in the manifold.

Conventional Chelex-100 resin, which has often been used to separate metals from solutions, is not appropriate in FIA-CL systems because of the swelling and contraction of the resin itself when the pH changes (Obata *et al.*, 1993). Chelating resins containing 8-hydroxyquinoline (8-HQ) have been made, which is a well-characterised reagent that reacts with over 60 metal ions to form stable complexes, and can be immobilised on a support matrix. In early studies 8-HQ was immobilised onto silica gel, which has a good mechanical strength, resistance to swelling and rapid overall exchange kinetics in column application (Sturgeon *et al.*, 1981). It was however found unstable at high pH (> 9), the chelating group potentially "bleeding" by hydrolysis and subsequently potentially showed contamination for iron from the newly exposed silica surface (Sturgeon *et al.*, 1981). Therefore in later systems the silica substrate was replaced by a polymer such as Fractogel TSK which is a highly porous, mechanically and chemically stable hydrophilic organic gel more stable at high pH (Landing *et al.*, 1986). However, this synthesis was time-consuming (> 20 h) and sometimes failed for unknown reasons. A new single- or double-step protocol (depending on the starting chemical) was found to link 8-HQ to the TSK polymer *via* an amino link instead of an ester linkage, which reduced the "bleeding" of 8-HQ from the resin (Dierssen *et al.*, 2001). Later studies suggested that TSK resins may leach colour (8-HQ bleeding) when eluted with a concentration of hydrochloric acid higher than 0.1 M as used with the Fe(II)+(III) technique, making the determination of Fe(III) at low concentrations impossible due to the masking effect of the leached functional group (Obata *et al.*, 1993; Weeks and Bruland, 2002). The choice of the resin therefore depends on the technique used and the compromise made between loading capacity, elution profiles and stability to acids (Obata *et al.*, 1993; Weeks and Bruland, 2002).

The seawater matrix is complex and may potentially create interferences during the detection step. Sea-salt ions such as Mg^{2+}, Ca^{2+} and Cl^- tend to significantly suppress (for cations) or increase (for halides) the chemiluminescence signal (Chang and Patterson, 1980; Bowie *et al.*, 1998). These ions may also precipitate (*e.g.* to $Mg(OH)_2$)

after mixing with basic luminol solution at a pH > 10 and clog the detector (de Jong *et al.*, 1998). A rinsing step with ultra pure water after passing the sample through the column is therefore necessary to remove sea-salts still present in the dead volume of the column. According to the results of Obata *et al.* (1993) and de Jong *et al.* (1998), Fe(III) was quantitatively collected at a pH between pH 2.6 and 4, and Fe(II) was completely recovered at pH 5 and above. Using a basic pH (> 8) may lead to the formation of iron colloids so that iron was not fully recovered from the sample stream and may even precipitate (Weeks and Bruland, 2002). Chromium(III), Co(II), Cu(II), and Mn(II) are the few elements susceptible of interfering with the chemiluminescence reaction (see below), however only Co(II) and Cu(II) are collected onto the resin at a pH of 5 – 5.5 (Obata *et al.*, 1993; de Jong *et al.*, 1998; Weeks and Bruland, 2002). Both Fe(II) and Fe(III) can thus be selected from some of the interfering trace metals by carefully buffering the pH to 5.5 (Bowie *et al.*, 2002a; Weeks and Bruland, 2002). At this pH, Fe(II) is susceptible of oxidising to Fe(III) on the order of few minutes, but this reaction can be minimised by adding the buffer just prior loading the sample onto the 8-HQ resin, when using the Fe(II) technique (see below).

The preconcentration column is therefore important for separating iron from many trace-metals, lowering the limit of detection, and removing sea-salts. A limitation may be that, while the reagent blank could be made negligible, there still might be a column blank that may be non-negligible when measuring sub-nanomolar iron levels (Weeks and Bruland, 2002). Additionally several factors can impact on the chelating efficiency onto the 8-HQ resin, such as the pH of the buffered sample, the loading flow rate, the eluent concentration, the column preconditioning, the column size, and the organic speciation of iron in the sample (Bowie *et al.*, 2003; Bowie *et al.*, 2004). Factors such as the particle size, porosity, and texture of the resin will also have an impact on the extraction efficiency from the 8-HQ resin (Bowie *et al.*, 2003). It was also recently shown that the presence of organic ligands in seawater samples modify the quantity of iron collected onto preconcentration resins (Ndung'u *et al.*, 2003; Ussher *et al.*, 2005). In order to ensure that all Fe complexes are destroyed and dissolved iron is loaded onto the resin, micro-wave treatment (Weeks and Bruland, 2002) or UV-digestion (Guéguen *et al.*, 1999; Ndung'u *et al.*, 2003) of the acidified sample prior analysis have been recommended. Alternatively, it has been suggested that stored samples should not be analysed before a minimum of 6-months after collection to allow complete release of iron from organic complexes and colloids (Bowie *et al.*, 2004).

II.2.3. Chemiluminescence reaction of luminol

The chemiluminescence (CL) reaction of luminol is widely used in analytical procedures because of its greater analytical performance detecting trace concentration levels of metal ions compared to other spectroscopic methods. Since it was used with both Fe(II) and Fe(II)+(III) techniques within this project, current knowledge of both mechanisms, Fe(II)/O_2/luminol and Fe(II)+(III)/H_2O_2/luminol, is presented here.

In the system Fe(II)/O_2, Fe(II) is quickly oxidised by O_2 producing the hydroxyl radical $^{\bullet}OH$, H_2O_2 and superoxide $^{\bullet}O_2^-$ (Reactions 1 – 4) (King *et al.*, 1995). Due to the rapid Fe(II) oxidation rate at pH > 9, its reaction is kinetically favoured relative to other metal ions (Xiao *et al.*, 2002). At pH ~10.5 the Fe(II) oxidation by O_2 is insensitive to low concentrations of H_2O_2 as Fe(II) is oxidised too quickly to allow free H_2O_2 to slowly form the complex Fe(II)-H_2O_2 or to decompose (Rose and Waite, 2001) (see below)**.** However, if the concentration of H_2O_2 is increased, the complex will form sufficiently rapidly to produce some hydroxyl-like radicals and therefore increase the CL signal (Reaction 3) (Rose and Waite, 2001).

(1) $Fe(II) + O_2 \rightarrow Fe(III) + {}^{\bullet}O_2^-$

(2) $Fe(II) + {}^{\bullet}O_2^- + 2H^+ \rightarrow Fe(III) + H_2O_2$

(3) $Fe(II) + H_2O_2 \rightarrow Fe(III) + {}^{\bullet}OH + OH^-$

(4) $Fe(II) + {}^{\bullet}OH \rightarrow Fe(III) + OH^-$

When H_2O_2 is present in excess, its decomposition is catalysed by free transition metal ions or their complexes through two possible mechanisms: **i)** a radical chain reaction catalysed by any cation having at least two oxidation states available such as Cu, Fe, Co, Ni, Cr and Mn (Reactions 5 – 7); or **ii)** a two-electron oxidation where H_2O_2 first reacts with free metal species to form an intermediate complex M^{n+}-H_2O_2, which can either react with organic compounds such as luminol, or decompose into O_2 and the original metal species (Reaction 7) (Xiao *et al.*, 2000). In the system Fe(II)+(III)/ H_2O_2, Reactions 5 and 6 lead to the production of the hydroxyl radical $^{\bullet}OH$ which initiates the chemiluminescence reaction.

(5) $M^{n+} + H_2O_2 \rightarrow M^{(n-1)+} + {}^{\bullet}OOH + H^+$

(6) $M^{(n-1)+} + H_2O_2 \rightarrow M^{n+} + {}^{\bullet}OH + OH^-$

(7) $2\ {}^{\bullet}OOH \rightarrow O_2 + H_2O_2$

Experiments with or without triethylenetetramine (TETA) proved that the CL reaction can significantly be enhanced when TETA is present (Obata *et al.*, 1993). This was due to the decomposition of hydrogen peroxide being more efficient when adding TETA (Wang, 1955). The splitting mechanism of the O=O bound in H_2O_2 by the reaction with the complex (TETA)$Fe(OH_2)^+$ is energically more favourable (6.6 kcal) than the free radical mechanism (see above, 35 kcal) involving isolated H_2O_2 molecules (Wang, 1955). Among trace metals, only Fe(III) and Mn(II) showed the highest catalytic activity with TETA (Wang, 1955), thus ensuring the specificity of the reaction. Therefore TETA was added to the luminol reagent in the Fe(II)+Fe(III) FIA-CL in order to enhance the decomposition of H_2O_2 , and thus of the CL reaction.

Despite being extensively studied, the detailed mechanism of the chemiluminescence reaction remains unclear. For both systems (Fe(II)/O_2 and Fe(II)+(III)/H_2O_2), the CL-generating mechanism for luminol oxidation is thought to occur in three steps: **1)** oxidation of luminol to the luminol radical (Reaction 8); **2)** oxidation of the luminol radical to luminol α-hydroperoxide, the key intermediate (Reaction 9); and **3)** decomposition of luminol α-hydroperoxide resulting in emission of blue light at 425 nm wavelength under alkaline conditions (Reaction 10) (Figure II.2) (Lind *et al.*, 1983). The luminol radical is produced by reaction of luminol with the hydroxyl radical (${}^{\bullet}OH$) formed by radiolysis of water and Reactions 3 and 6, or the carbonate radical (${}^{\bullet}CO_3^-$) when carbonate is present in the system (Xiao *et al.*, 2000; Rose and Waite, 2001). It was also suggested that the superoxide radical (${}^{\bullet}O_2^-$) produced from oxygen may initiate the CL reaction (Lan and Mottola, 1996).

(8) Luminol + ${}^{\bullet}OH$ (or ${}^{\bullet}CO_3^-$) → luminol radical + other products

(9) Luminol radical + HOO^- → luminol α-hydroperoxide

(10) Luminol α-hydroperoxide → aminophthalate + N_2 + $h\nu$

(11) 2 luminol radicals → luminol + diazaquinone

(12) Diazaquinone + ${}^{\bullet}O_2^-$ → luminol α-hydroperoxide

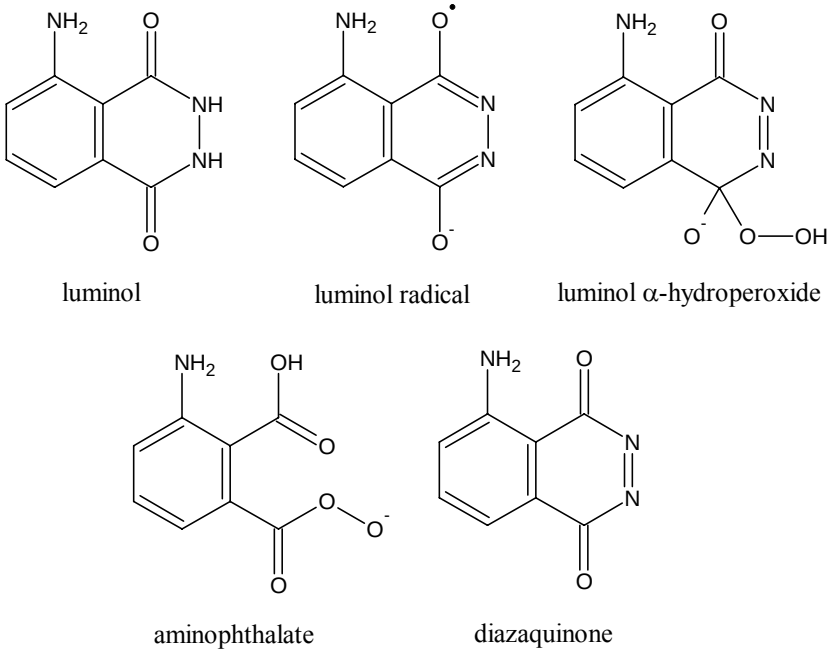

Figure II.2: Chemical structure of luminol and derivatives involved in the chemiluminescence reaction.

The decomposition of luminol α-hydroperoxide depends only upon the pH of the solution once it has been formed, resulting in an increase of the CL efficiency around pH 10.5 and a decrease over pH 11 corresponding to a decrease in the fluorescence quantum yield of aminophthalate (Lind *et al.*, 1983; O'Sullivan *et al.*, 1995; Rose and Waite, 2001). The luminol radical may also undergo self-recombination producing luminol and diazaquinone (Reaction 11) which can react with the superoxide radical $^{\bullet}O_2^-$ if it is present in the system to form luminol α-hydroperoxide (Reaction 12) (Xiao *et al.*, 2000). The Fe(II) CL yield depends upon the solution pH once the luminol α-hydroperoxide is formed (Rose and Waite, 2001) so that the optimum CL pH is 10.5 as this corresponds to its increased formation (O'Sullivan *et al.*, 1995).

Considering the kinetics of the CL reaction, the rate-limiting step is the production of hydroxyl-like radicals by oxidation of Fe(II) by O_2 or by decomposition of H_2O_2 catalysed by cations such as Fe(II) and Fe(III) depending on the system used (Xiao *et al.*, 2000). In the Fe(II)/O_2/luminol system, the oxidation of Fe(II), and therefore the production of hydroxyl radicals, occurs within a few hundreds of milliseconds, which makes the reaction easy to use in-line and allows rapid determinations (Seitz and Hercules, 1972). In the Fe(II)+(III)/H_2O_2/luminol system, decomposition of H_2O_2 is the rate-limiting step and therefore requires an initiation time which can be obtained using a reaction loop of optimised length (Xiao *et al.*, 2000). It is also generally observed that

increasing the temperature favours the decomposition of H_2O_2 with or without metal catalysts (Xiao *et al.*, 2000).

Recent studies showed that the presence of carbonate greatly enhances the CL signal (Xiao *et al.*, 2000; Xiao *et al.*, 2002). This effect is likely due to the reaction of sodium carbonate, used to buffer the luminol reagent, and hydrochloric acid, used to elute iron from the preconcentration column, which produces gaseous carbon dioxide ($CO_{2(g)}$) (Lan and Mottola, 1996). Enhancement of the CL reaction by $CO_{2(g)}$ bubbling has been previously studied (Lan and Mottola, 1996; Xiao *et al.*, 2002), and showed great increases in the CL signal. One mechanism may be that hydroxyl radicals produced by the oxidation of Fe(II) or decomposition of H_2O_2 catalysed by transition metal ions, may react with dissolved carbonate to form a carbonate radical $^{\bullet}CO_3^-$ (Reaction 13). Another mechanism may be that $CO_{2(aq)}$ produced by dissolution of $CO_{2(g)}$ may react with the superoxide radical $^{\bullet}O_2^-$ to form the peroxycarbonate radical $^{\bullet}CO_4^-$ (Reaction 14). The oxidation of luminol by $^{\bullet}OH$ (Reaction 8) leads to the production of various species other than the luminol radical since $^{\bullet}OH$ is very reactive and attacks several carbon sites on the aromatic ring of luminol (Xiao *et al.*, 2000). In contrast, $^{\bullet}CO_3^-$ and $^{\bullet}CO_4^-$ almost selectively react with luminol yielding the luminol radical, which therefore enhances the CL intensity by increasing the steady-state concentration of luminol radical (Xiao *et al.*, 2000). The effect that ageing of the luminol reagent increases sensitivity mentioned by several authors (Lan and Mottola, 1996; Bowie *et al.*, 1998; Xiao *et al.*, 2000), may thus be explained by the luminol reagent equilibrating with the carbon dioxide in the solution freshly prepared, producing more carbonate radicals capable of enhancing the CL reaction when initiated.

(13) $^{\bullet}OH + CO_3^{2-} \rightarrow OH^- + {}^{\bullet}CO_3^-$

(14) $CO_{2(aq)} + {}^{\bullet}O_2^- \rightarrow {}^{\bullet}CO_4^-$

For the Fe(II)+(III) technique, where both hydrogen peroxide (H_2O_2) and luminol are in excess, the CL emission intensity is proportional to the cation concentration over a wide working range and down to very low concentrations for many trace metals such as Cr(III), Mn(II), Fe(II), Fe(III), Co(II), Ni(II) and Cu(II). Obata *et al.* (1993) showed that only Cr(III), Mn(II), Co(II) and Fe(II) interfered with the Fe(III) signal at natural seawater concentrations. However, Cr(III) and Mn(II) are not collected onto the 8-HQ resin at pH 5.5 (see above), and Co(II) which is as sensitive as Fe(III) in this CL reaction, may be masked by the aqueous ammonia forming a stable amine complex

(Obata *et al.*, 1993). Therefore, both Fe(II) and Fe(III) can be detected with the H_2O_2 – luminol CL reaction as Fe(II) gives almost equal sensitivity to Fe(III) (Obata *et al.*, 1993).

In the absence of H_2O_2 as used in the Fe(II) technique of Bowie *et al.* (1998), the CL reaction is selective towards Fe(II) over Fe(III), and is relatively insensitive to interference from other trace metals (Seitz and Hercules, 1972; Klopf and Nieman, 1983; O'Sullivan *et al.*, 1995; Lan and Mottola, 1996; Rose and Waite, 2001). Cobalt(II), Mn(II) and Cu(II) are the only elements likely to cause an interference to the CL reaction at natural seawater concentration levels (Seitz and Hercules, 1972; O'Sullivan *et al.*, 1995; Bowie *et al.*, 1998). At pH 10, Mn(II) and Cu(II) may oxidise Fe(II) to Fe(III) and then be re-oxidised back, so that they provide an alternative path for Fe(II) oxidation which does not induce the CL reaction (Seitz and Hercules, 1972). However, Mn(II) can only be collected onto the 8-HQ column at pH values greater than 8 (Obata *et al.*, 1993) and Cu(II) and other trace-metals did not show any interference when the sample is loaded onto the 8-HQ resin column at pH 5.0 (Bowie *et al.*, 1998). Cobalt(II) has been shown not to exhibit any interference below concentrations of 500 pM, which allows open-ocean water analyses where Co(II) concentrations range from 100-300 pM (Bowie *et al.*, 1998). However Co(II) may become a problem when analysing coastal samples where its concentration may be as high as 10 nM (Cannizzaro *et al.*, 2000). Cobalt interference can then be minimised adding dimethylglyoxime (20 μM) to the luminol reagent to complex it (Bowie *et al.*, 2002a). Whilst interfering metals may reduce the sensitivity, nevertheless the signal observed is due to Fe(II) and not to other species (Seitz and Hercules, 1972; Bowie *et al.*, 1998). Moreover, no interference was observed by Powell *et al.* (1995) when analysing natural samples.

Several parameters should be optimised to maximise the CL reaction, and obtain a better sensitivity. Since the CL reaction is induced by Fe(II) within 100 ms in the Fe(II) technique, optimising the flow cell design can improve the light collection efficiency. As the CL reagents residence time in the flow cell is a critical step in the detection, reagent flow rates and concentrations and length of the PMT loop are critical to obtaining the best reproducibility (Seitz and Hercules, 1972). The concentration of luminol should be optimised to give the best compromise between signal enhancement and the baseline level (O'Sullivan *et al.*, 1995; de Jong *et al.*, 1998). The acid concentration of the eluent is also critical in that it must be high enough to fully elute

iron from the resin but low enough to minimise production of $CO_{2(g)}$ bubbles in the stream after mixing with luminol buffered with carbonate. For the Fe(II)+(III) technique, careful optimisation of the reaction coil length and temperature is crucial to ensure sufficient time and efficiency for H_2O_2 to decompose before entering the flow cell without generating too many bubbles in the liquid stream (Xiao *et al.*, 2000). Finally, as the CL reaction is highly pH dependant, this parameter should also be carefully optimised. For the Fe(II) technique, the maximum CL intensity (pH 10.5) is achieved by adjusting the luminol reagent pH with sodium hydroxide (Seitz and Hercules, 1972; Klopf and Nieman, 1983; O'Sullivan *et al.*, 1995; Bowie *et al.*, 1998). For the Fe(II)+(III) technique, the optimum CL reaction (pH 9.5) is obtained by adjusting the ammonia concentration (Obata *et al.*, 1993).

Despite the apparent desire of researchers to fit a straight line to calibration data (Seitz and Hercules, 1972; Klopf and Nieman, 1983), calibration curves are frequently non-linear (Rose and Waite, 2001). This is due to variations between experimental conditions and to the presence of radicals in the reagents. Hydrogen peroxide produces hydroxyl radicals $^{\bullet}OH$ depending on light conditions and concentration of impurities, which can both potentially enhance the CL reaction (Xiao *et al.*, 2002). Exposure of the H_2O_2 reagent to light should be therefore minimised in order to limit increases in radical concentrations. Luminol is also very photosensitive and its exposure to light is likely to produce luminol radicals by photo-oxidation, producing a low level of CL background that varies in response to light conditions in the laboratory (Rose and Waite, 2001). The luminol stock and reagent solutions and the luminol reagent tubing should thus be kept in the dark as much as possible to minimise this effect. It is necessary to perform a calibration for each batch of reagents and attempting to linearise the curve may introduce additional errors into the technique (Rose and Waite, 2001).

II.3. Development of a flow injection analyser with chemiluminescence detection (FIA-CL) to detect Fe(II) in seawater

The Fe(II) technique of Bowie *et al.* (1998) was chosen here as it allows near real-time determination of dissolved Fe(II) as well as total dissolved Fe(II+III) after a reduction step, which potentially can be done in-line. It also requires less reagents for the CL reaction and is slightly faster than the Fe(II)+(III) technique, due to the kinetics of the elution of Fe(II) from the resin and of the CL reaction.

The development of the Fe(II) technique was achieved through three major stages: a simple manifold to detect Fe(II) in de-ionised water, then a manually controlled analyser to detect Fe(II) in seawater, which was subsequently modified to be automated. Xiao *et al.* (2000) suggested that optimum conditions found by one laboratory (reagent pH and concentration, sample and reagent mixing ratio, detector design) may not be ideal for others with very similar setups. Each stage of the technique was firstly set up as suggested in the literature before being modified through optimisation. An overview of the extensive work carried out to develop the Fe(II) technique is given below.

II.3.1. Manual FIA-CL system to detect Fe(II) in de-ionised water

Initially, a simple analyser to measure Fe(II) in de-ionised water based on the method of King *et al.* (1995) was built in order to test the response from the photomultiplier tube and learn about the chemistry of the CL reaction. This first work on the analyser was undertaken in an open laboratory space without any particular precautions to avoid contamination, and used relatively high concentrations of iron.

This system was divided into two parts: **i)** the flow injection system including a peristaltic pump (PP), an injection valve (IV) and an injection loop (IL); and **ii)** the detection system including a flow cell (FC), a photomultiplier tube (PMT), two power supplies (PS), and a chart recorder (CR) (Figure II.3). Details about instrumentation, reagent preparation, and the analytical sequence are given in Appendix 1.

Analyses were done using a new low-voltage photomultiplier tube (PMT) (Hamamatsu Photonics). This PMT was powered and the signal acquired through an electronic board designed by Dr. Matt Mowlem (OED, NOCS). The PMT showed very good sensitivity to the CL reaction but also to ambient light. The high baseline due to stray light entering the flow cell *via* the tubes and detected by the PMT was reduced using black tubing to shield the PTFE tubing going to and from the flow cell.

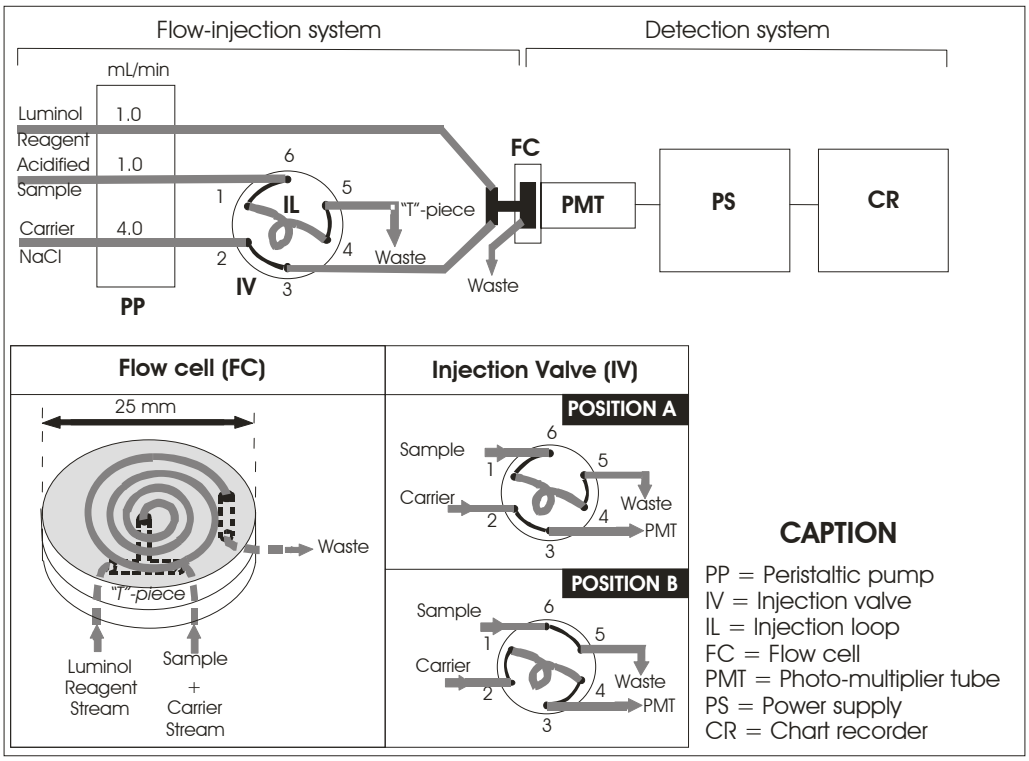

Figure II.3: Diagram of the Fe(II) FIA-CL analyser according to King *et al.* (1995). Thick grey lines represent PTFE or PVC tubing.

Enhancement of the CL signal was observed when a carbonate buffer was used instead of the borate buffer (7-fold increase in sensitivity with Fe(II) standards of 12 and 25nM in 0.7 M NaCl and 10 μM luminol reagent), a trend previously shown by Klopf and Nieman (1983). A broad optimum pH of the CL reaction in de-ionised water was also found at around 10.2 (Figure II.4), as suggested in the literature (Seitz and Hercules, 1972; O'Sullivan *et al.*, 1995).

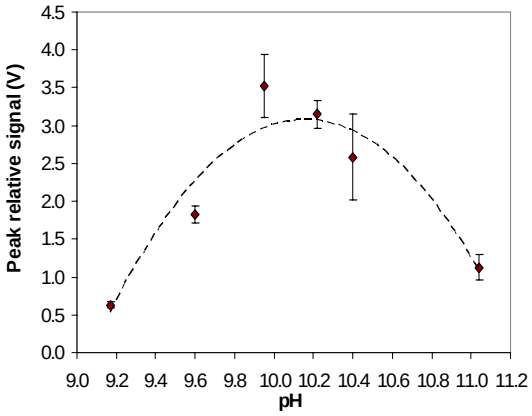

Figure II.4: Effect of CL pH on Fe(II) peak height. [Fe(II)] = 100 nM in 0.7 M NaCl acidified with 0.2 M Q-HCl.

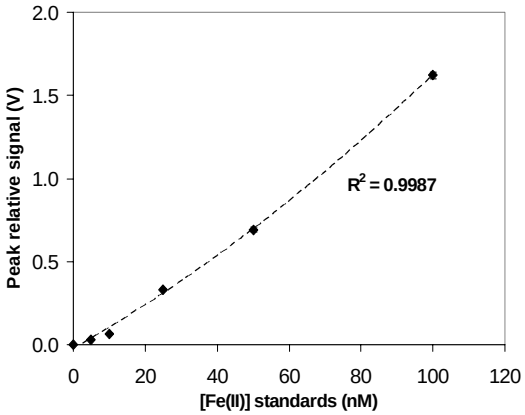

Figure II.5: Calibration curve performed with the Fe(II) FIA-CL according to King *et al.* (1995) with a polynomial trend line (2nd degree). Standards prepared in 0.7M NaCl acidified with 0.2M Q-HCl.

A calibration curve was produced for the range 5-100 nM by standard additions to acidified sodium chloride (0.7 M) solutions. The signal peaks were acquired with a chart recorder, and calculations were made using peak heights. The curve was slightly non-linear, as suggested by King *et al.* (1995) and Rose *et al.* (2001), due to the photosensitivity of luminol, as it was not kept away from light during storage at this time (Figure II.5). Precision ranged between 1.0% and 2.1% (n = 6) for a 5nM and 10 nM Fe(II) standard respectively. The limit of detection (= 3sd of the blank) was estimated at 500 pM with a blank value of 1 nM, which was satisfactory at this stage of the development.

II.3.2. Manual FIA-CL system to detect Fe(II) in seawater

The next critical stage was to develop an iron analyser allowing dissolved Fe(II) (and Fe(II+III) after a reduction step) measurements at sub-nanomolar concentrations in seawater. The main objective in the system development was thus to include a preconcentration column and adapt the chemistry in order to reach a limit of detection of about 40 pM using the analyser design of Bowie *et al.* (1998). The use of a preconcentration column in the manifold led to the addition of ammonium acetate (NH_4OAc) buffer to the sample prior to loading onto the column to collect iron, and to the introduction of an eluent stream to release it from the resin and carry it to the detection flow cell. The addition of these two components to the system required careful pH adjustment of the standard/buffer mixture (loading pH) and eluent/luminol reagent (CL pH) to optimise the loading of iron onto the column at *circa* 5.5 and the CL reaction at 10.5 respectively, as suggested by the literature (see Chapter II.2).

II.3.2.1. Preconcentration resin and column

A resin for the preconcentration of iron in a seawater matrix was prepared. As the protocol of Landing *et al.* (1986) was time-consuming (> 20 h) and sometimes failed for unknown reasons (Dierssen *et al.*, 2001), the preparation of the 8-hydroxyquinoline (8-HQ) resin following the procedure described by Dierssen *et al.* (2001) was chosen. This new protocol included only two reaction steps (2 h and 6 h) (Dierssen *et al.*, 2001). The 8-HQ resin was prepared using Toyopearl HW-65F (fine, 30-60-µm, Anachem) as the polymeric support. The 8-HQ resin obtained was homogeneously dark brown when freshly prepared, indicating that 8-HQ was efficiently bound to the resin since the

darker colour is due to the amount of 8-HQ (Weeks and Bruland, 2002). Details concerning reagent preparations, protocols, and the resin complexing capacity experiments performed to test the resin are described in Appendix 2.

The complexing capacity of the 8-HQ resin prepared (100.1 ± 9.7 μmol Cu/g of resin (*n* = 4), Appendix 2) was in agreement with the value reported by Dierssen *et al.* (2001). Bowie *et al.* (1998) reported that there was 54.7 mg of dried fine 8-HQ resin in the volume (45 μL) of their column. In this study, the volume of 8-HQ resin (of similar pore size as that of Bowie *et al.* (1998)) in the column was varying between approximately 38 and 50 μL depending whether the column was completely filled or not. As copper shows a similar behaviour as iron as regards the 8-hydroxyquinoline, the complexing capacity of the resin would be 4.5 to 6.1 μmol of Fe for the quantity of resin packed in the preconcentration column. Given the results obtained with copper, the 8-HQ resin prepared should allow determination of iron in most marine environments where it is found at nano- to pico-molar concentrations.

The development of the column to hold the 8-HQ resin was time consuming as the design of Bowie *et al.* (1998) was judged unsatisfactory due to backpressure problems and leaks (A. Bowie, 2001, personal communication) (Figure II.6). The column used in the present system was thus made of clear Perspex (polymethylmethacrylate), and the resin was kept inside the column by two polyethylene frits at either end (Figure II.6). Packing the 8-HQ resin in the columns was carried out very carefully in order to minimise the presence of the finest particles, blockage, and backpressure problems. To this end, the 8-HQ resin was suspended in water and allowed to settle for a few minutes and the supernatant removed. This procedure maximised the selection of the biggest particles, as fine ones may clog the frits.

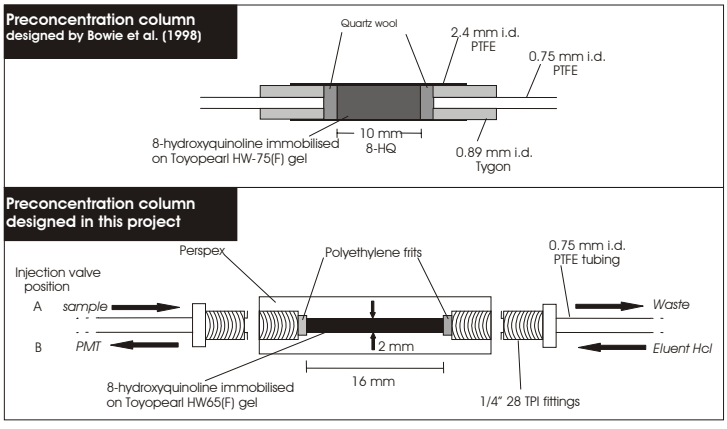

Figure II.6: Preconcentration columns designed by Bowie *et al.* (1998) and as used in this project (PMT = photo-multiplier tube).

II.3.2.2. Description and optimisation of the manual system

Prior to a computer control system being available, the analyser was controlled manually (Figure II.7). A manual valve was placed before the pump to switch between the buffered sample and the Milli-Q water to rinse the column. The injection valve was manually controlled by a two-position switching valve. The injection loop was changed for a 8-HQ preconcentration column as described above. Details on the instrumentation, reagent preparation, and analytical sequence (4 minutes) are described in Appendix 3.

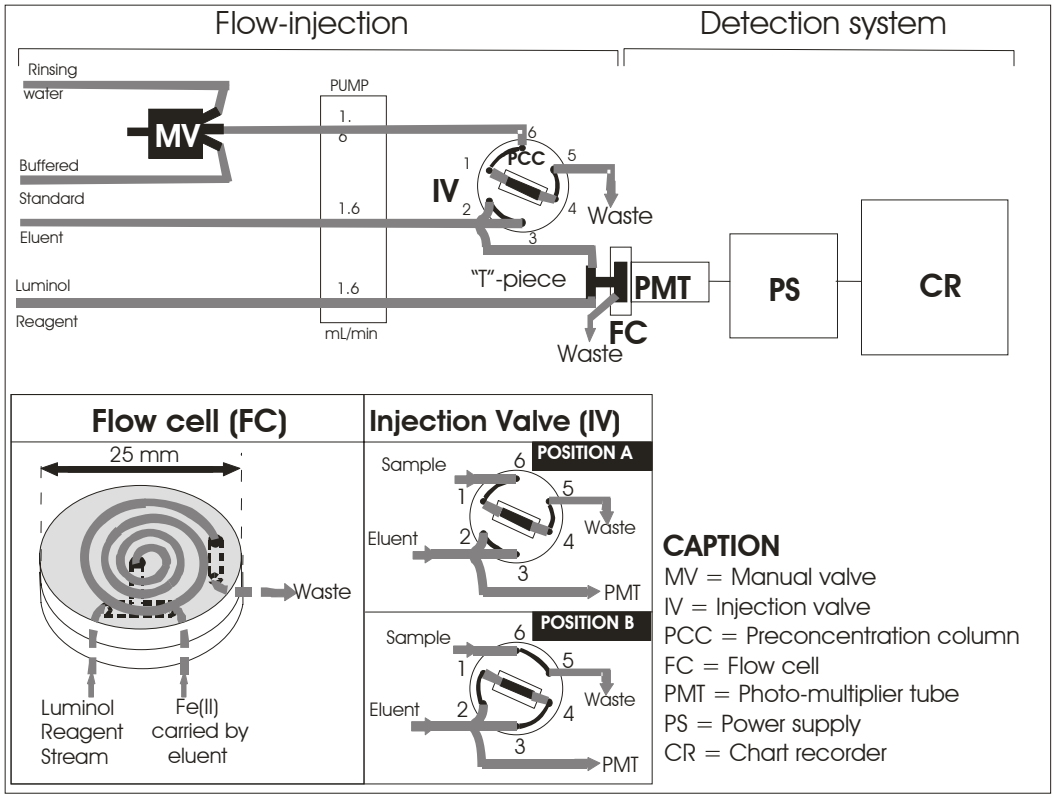

Figure II.7: Diagram of the Fe(II) manual FIA-CL with preconcentration step based on the design of Bowie *et al.* (1998). Thick grey lines represent PTFE or PVC tubing.

During the first tests with a preconcentration step, high double peaks were observed when the rinsing step was not included in the sequence. This high signal was likely due to sea-salts, as halides tend to increase the CL signal (Bowie *et al.*, 1998). A rinsing step with Milli-Q water was therefore added. In addition, a small negative peak was seen before the positive CL peak (Obata *et al.*, 1993; Bowie *et al.*, 1998). This was produced by the pH change of the elution solution sent into the flow cell as a small amount of rinsing Milli-Q water remained in the void volume of the extraction column and was sent prior to the acidic eluent.

Several experiments were carried out to optimise the loading pH by changing the pH of the 0.4 M ammonium acetate (NH_4OAc) buffer added to 100 nM Fe(II) standards. According to the literature, Fe(III) is collected by 8-HQ from pH 2.6 and Fe(II) at pH > 5 (Obata *et al.*, 1993; de Jong *et al.*, 1998). However results gave maximum signal for a pH of about 3.5 for this batch of resin (Figure II.8). One possible explanation for these unexpected results would be that Fe(II) was not collected, as the highest pH obtained was 4.9 at which Fe(II) may not yet be collected. The decrease in signal between pH 3.5 and about 5 might be due to precipitation of iron since the buffer was added off-line to the system, but it was highly improbable to have almost complete precipitation of 100 nM iron so rapidly.

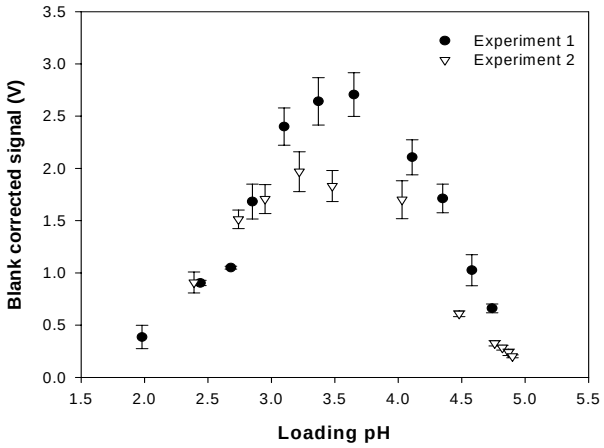

Figure II.8: PMT response for two loading pH optimisation experiments to collect Fe(II).

The hypotheses given above do not however explain why a CL signal was monitored when the loading pH would only allow collection of Fe(III) according to the literature. If most of Fe(II) was oxidised to Fe(III) and Fe(III) collected onto the resin at pH 3.5, hardly any signal should have been recorded due to the specificity of the CL reaction to Fe(II) without hydrogen peroxide (see Section II.2.3). This would only be possible if Fe(II) was oxidised to Fe(III) before collection onto the resin, and Fe(III) was subsequently photo-reduced to Fe(II) after elution and before entering the detection flow cell. However, photo-reduction was highly improbable as the distance was kept to a minimum between the column and the detection cell, and the tube covering that distance was protected from sunlight with black tubing. There was thus no obvious reason why the resin behaved as observed, but it was clear that the response was not that expected. The possibility of a problem with the behaviour of this batch of 8-HQ resin was also considered given that experiences in other laboratories showed that the first

batch of resin prepared can sometimes fail for unknown reasons (S. Ussher, 2003, personal communication, and (Dierssen *et al.*, 2001)).

Despite the unexpected results for the optimisation of the loading pH, this system was useful in developing and adapting the chemistry. This was not a viable system for long-term use, as either the injection valve or the manual valve had to be manually switched at precisely 60 second intervals to give reproducible data, which is difficult to achieve over long periods of time. Additionally the problems encountered trying to determine the optimum loading pH may have been caused by the addition, off-line of the buffer to the standard, which may have promoted the precipitation of a significant fraction of iron before analysis. These results would imply that solutions should be buffered in-line to minimise this effect, which can only be done with an automated method. It was therefore subsequently modified to be computer controlled and further optimisation was carried out with a new batch of resin prepared as described in Appendix 2, in order to determine whether the resin may have been partly responsible for the unexpected results obtained for the loading pH.

II.3.3. Development of an automated FIA-CL system to detect Fe(II) in seawater

II.3.3.1. Description of the system

The system was subsequently modified to be computer controlled (Figure II.9). Low voltage pumps (B and C), switching valves (V1, V2 and C3), and other components were chosen to simplify control circuits, to allow safe operation of the system, and were set up as described by Bowie *et al.* (1998).

Instrument control was performed using a National Instruments 12-bit multifunction input/output (I/O) DAQPad-6020E card, and the signal acquisition using a National Instruments 96-bit Digital I/O DAQPad-6507. The power supply and amplifier to control peristaltic pumps, valves and photomultiplier tube were designed and made in the laboratory by Drs. Matt Mowlem and Ralf Prien (OED, NOCS). The sensitivity (or gain) of the PMT could be changed on a scale from 1 to 10 using the instrument control software. Data acquisition and processing were performed using software written in LabVIEW 6.1 (National Instruments) on a Toshiba Satellite Pro laptop. Details about instrumentation, reagent preparation, and analytical sequence are described in Appendix 4. Information about the programme LabView used for the data

acquisition and processing, together with diagrams of the electronic control, are given in Appendix 5.

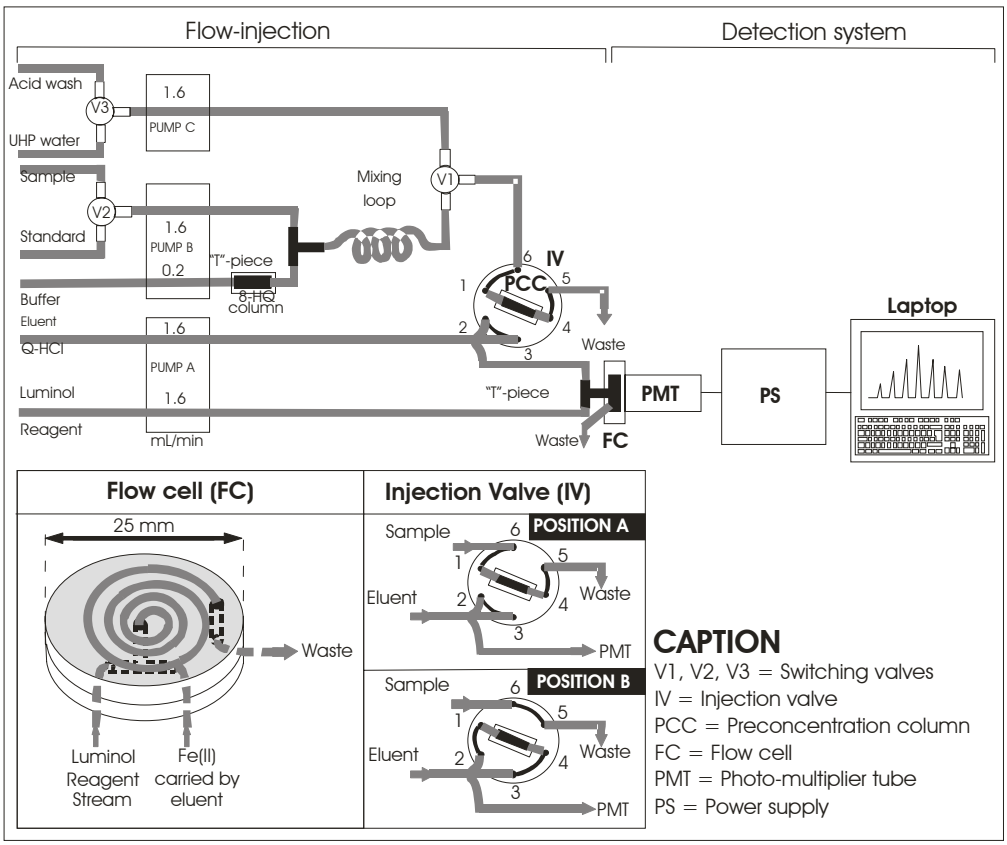

Figure II.9: Diagram of the Fe(II) automated FIA-CL with preconcentration step based on the design of Bowie *et al.* (1998). Thick grey lines represent PTFE or PVC tubing.

During initial tests the baseline was high and unstable to allow detection of low-iron concentrations, presumably because of low levels of iron contamination of the reagents. It became clear that all reagents needed further purification. The luminol reagent was purified through about 10 g of Chelex-100 resin. It was observed later that the baseline level could be lowered further by passage through 8-HQ resin to remove iron and other trace metals. Furthermore, the noise and stability of the baseline could be further improved by preparing the luminol reagent 24 h in advance as suggested by Bowie *et al.* (1998), and protecting the solution from light. The working buffer was purified through an off-line 8-HQ resin column and further purified in-line with an additional 8-HQ resin column in the FIA-CL system.

A reducing reagent (sodium sulphite, approximately 40 mM) was prepared to convert Fe(III) to Fe(II) in samples for Fe(II+III) determination. This reagent was also purified through a 8-HQ resin column to minimise its contribution to the blank. In order to achieve a concentration of 100 μM of sulphite in the sample, 2.5 μL of reducing

reagent were added per mL of acidified seawater as suggested by Bowie *et al.* (1998). The reducing reagent was left to react for a minimum of 8 h before analysis. Iron stock solutions were kept in a fridge to slow down the oxidation of Fe(II).

Calibrations were carried out by standard additions to seawater collected in the open Atlantic Ocean during the *AMT-12* cruise. A 10 μM Fe(II) stock solution was prepared by dilution of a 10 mM Fe(II) stock solution where 0.3921 g ammonium ferrous sulphate (Fisher) was dissolved in 0.1 M quartz distilled hydrochloric acid (Q-HCl). A 500 nM Fe(II) working standard was prepared in 0.01 M Q-HCl (similar to the acid strength in acidified samples) by diluting the 10 μM Fe(II) stock solution. Calibration standards were prepared daily by adding the required quantity of 500 nM Fe(II) working standard to acidified seawater (ASW) and adjusting volumes with diluted acid (0.01 M Q-HCl) in order to achieve the same total volume for all standards (*e.g.* Table II.2).

	Volume ASW (mL)	Volume 500nM Fe(II) standard (μL)	Volume 0.01M Q-HCl (μL)	Total volume (mL)
Blank (0.01 M Q-HCl)	0	0	20 mL	20
ASW	20	0	200	20.2
ASW + 0.5 nM	20	20	180	20.2
ASW + 1 nM	20	40	160	20.2
ASW + 2 nM	20	80	120	20.2
ASW + 5 nM	20	200	0	20.2

Table II.2: Example of standards preparation for a calibration in the range 0 to 5nM Fe(II). ASW = Acidified seawater.

It was observed by experience that slight variations occurred in the peak shape between replicate peaks (data not shown). Peak areas were thus used for measurements in order to better define peaks.

The mechanical development of the automated Fe(II) analyser was relatively simple with Dr. Matt Mowlem's help, and therefore the main work was to optimise and calibrate it. Given the time and equipment constraints, the unoptimised technique was taken onboard ship during the *AMT-12* (6 weeks) and *JR98* (3 weeks) cruises, in a clean trace-metal container to minimise contamination, in order to progress its development. Sampling was done so measurements were possible later in the laboratory if needed.

II.3.3.2. Analytical challenges

In addition to significant complications encountered including backpressure, contamination from the Milli-Q water onboard, and problems with the available pH-meter during the first cruise, attempts to calibrate the system highlighted three major problems: **a)** poor reproducibility between replicate peaks; **b)** poor precision when switching between solutions; and **c)** poor sensitivity and negative curvature of the calibration curve.

Major progress in the understanding of the technique was achieved through the extensive work carried out to optimise the system. Experiments were undertaken to improve performance of the system focussing on precision and the calibration curvature. However, due to persistent poor calibrations and precision of the system, it was decided to seek help from the University of Plymouth where the Fe(II) FIA-CL was originally developed. Major improvements on precision were then made although the calibration remained poor. A significant number of experiments were carried out to try and solve problems as they arose. In order to limit the length of the material presented here and for clarity, these results are presented classified relative to the problems encountered rather than chronologically. An overview of the main findings is given below.

II.3.3.2.1. The resin : Loading pH and problems of backpressure

As the first batch of 8-HQ resin did not show the highest recovery of Fe(II) at the expected pH (> 5) using the manual Fe(II) technique for unknown reasons (see Section II.3.2.2), a new batch of fine 8-HQ resin was prepared following the same protocol and with the same resin bead size (see Appendix 2).

A simple loading pH experiment showed that the signal increased between pH 3.2 and 5.2 (Figure II.10), a trend suggesting that Fe(II) was collected at pHs > 5, as suggested by the literature (see Section II.2.2). However this fine 8-HQ resin was found to induce backpressure because of packing with time. This packing effect resulted in a reduced bed volume, and when flows were reversed, in the formation of channels in the column, which could provide an alternative flow path to the buffered sample solution other than through the 8-HQ resin, and affect the precision. Several time consuming attempts where made to limit this packing effect.

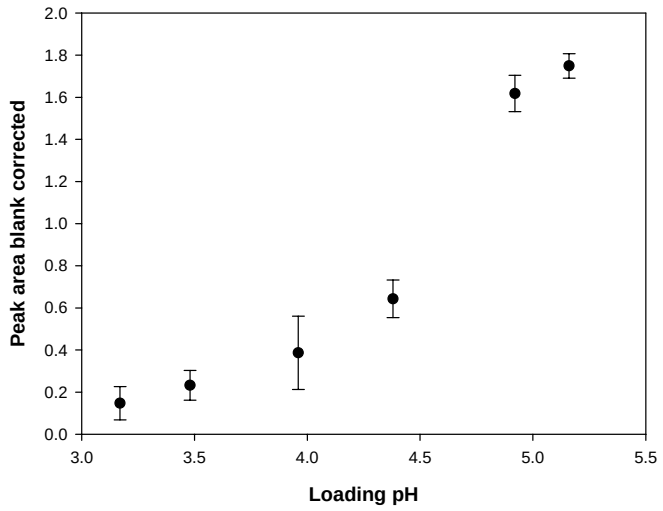

Figure II.10: Loading pH experiment with the new 8-HQ resin. [Fe(II)] = 20 nM prepared in Milli-Q water.

In order to avoid backpressure problems, a new 8-HQ resin with a coarser particle size (HW-40C, 75 μm) was subsequently prepared following the protocol of Dierssen *et al.* (2001) (see Appendix 2). The 8-HQ (HW-40C) resin obtained was homogeneously black, and no backpressure problems were encountered with its use with a half-full column. This new resin showed optimum uptake of iron at pHs > 5 for filtered seawater containing sulphite and spiked to 20 nM Fe(II). The new coarser resin was therefore more adapted to the configuration of this version of the FIA-CL relative to a finer resin.

II.3.3.2.2. Problem a: Poor reproducibility

All the following experiments were carried out using surface seawater collected along the track of the *AMT-12* cruise, filtered through 0.4 μm pore size filters, acidified with 1 μL Q-HCl per mL seawater stored in polycarbonate bottles, and allowed to react with the reducing reagent (sodium sulphite, 2.5 μL per mL seawater) for more than 10h in polycarbonate bottles. The iron concentration of this seawater was estimated at about 1 nM.

The problem of reproducibility was identified when several experiments showed that after a gradual increase in peak height, the CL signal for acidified filtered seawater with sulphite seemed to stabilise, but with relatively reproducibility (*e.g.* Figure II.11, precision = 12.3% *rsd* (n = 16) in this example). Several components and parameters of the system may influence reproducibility and were thus tested (Table II.3), and their influence on precision was reported when possible.

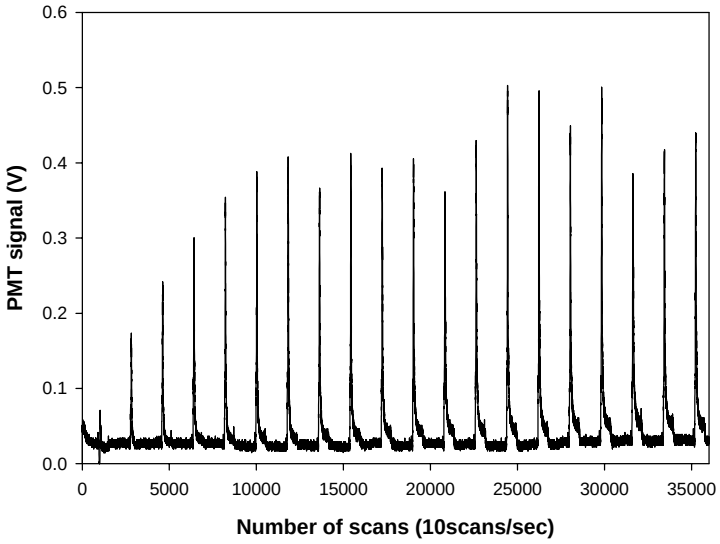

Figure II.11: Reproducibility experiment of 20 analytical cycles with acidified filtered seawater with sulphite (PMT gain = 6). Atlantic surface water with [Fe(II)] ~ 1 nM, [S(IV)] = 100 μM.

Experiments	**Precision (% *rsd*)**
i) Performance of the equipment	
Change valves	14.4% (*n* = *11*)
Change PMT and flow cell	13.1% (*n* = 14)
Change low-voltage pumps	9.6% (*n* = *9*)
ii) Effect of flow rates and eluent strength	
Flow rates	9 – 18% (*n* = *5-7*)
Increased eluent concentration	poor
iii) Effect of the flow cell design	
Change design flow cell	poor
iv) Other factors: Changes in pH	
No change in CL pH monitored	

Table II.3: Summary of the experiments performed to improve reproducibility.

i) Performance of the equipment

Almost all mechanical components of the system were tested to check for variations in their repetitive functioning. Air bubbles were observed in the standard/sample line on using the switching valve (V2), and this and one other valve (V3) were removed from the system (Figure II.9), but did not result in any obvious amelioration in precision (14.4% (*n* = 11)). In order to test other components of the system, the photomultiplier tube, flow cell, and switching valve (V1) were all exchanged with spares, but these modifications did not appear to improve the precision (13.1% (*n* = 15) before and 13.0% (*n* = 14) after changing components).

Variability in the standard/sample flow rate would change the quantity of iron loaded onto the resin. Relatively high pulsing was observed with the lab-made low-voltage pumps initially used, due to their slow rotating speed. These pumps were therefore

exchanged with Ismatec pumps which showed much less pulsing as their rotation speed was much faster. Variations in the volume delivered by the pump with time were monitored and the volume of solution delivered was found to only decrease by about 1.7% over 40 analytical cycles (data not shown). Peristaltic pump tubing was changed regularly to minimise this effect. Precision was thus slightly improved (9.6% (n = 9)).

ii) Effect of flow rates

Variability in the elution efficiency was tested by changing reagent flow rates. Decreasing flow rates of the luminol reagent and eluent changed the peaks shape and intensity as the residence time in the flow cell varied, but did not seem to improve reproducibility significantly (Figure II.12). Moreover, if the elution was not complete during the elution step, a carry over effect would be expected between peaks. However, increasing the eluent strength and elution time did not change peak area (data not shown), suggesting that the strength of the eluent and elution time used previously were close to optimum.

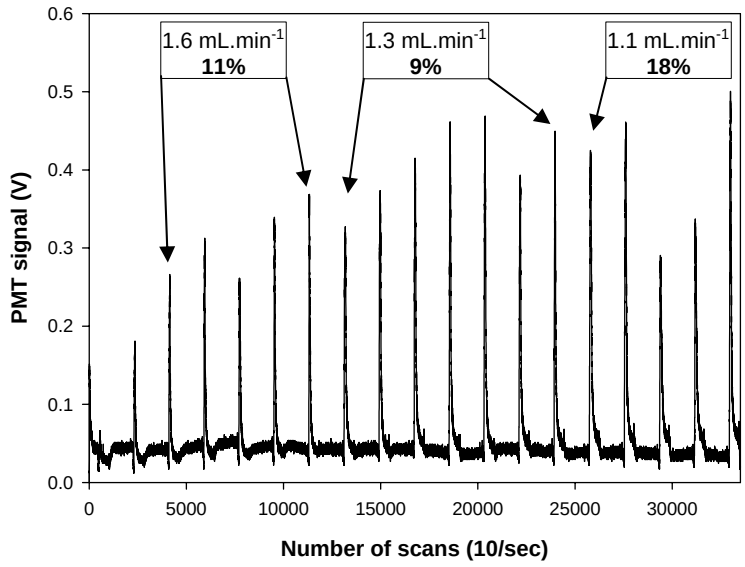

Figure II.12: Experiments where luminol reagent and eluent flow rates were changed by ± 25%. Flow rates (mL.min^{-1}) and the precision (% *rsd*) for each of the tests are indicated. Atlantic surface water with [Fe(II)] ~ 1 nM, [S(IV)] = 100 μM.

iii) Effect of flow cell design

As the CL light emitting reaction is very rapid (~ 100 ms), signal loss is possible if the mixing of reagents occurs away from the PMT. Thus another design for the flow cell was tested (Figure II.13). Instead of having the luminol reagent and eluent mixing just before entering the flow cell, the reagents mixed in front of the PMT window as the critical factor is the time for mixing of reagents in front of the PMT window. Peak

shape was similar with both designs but the response was weaker with the new design which may be due to a modification in the mixing efficiency. The first design was therefore retained in subsequent experiments.

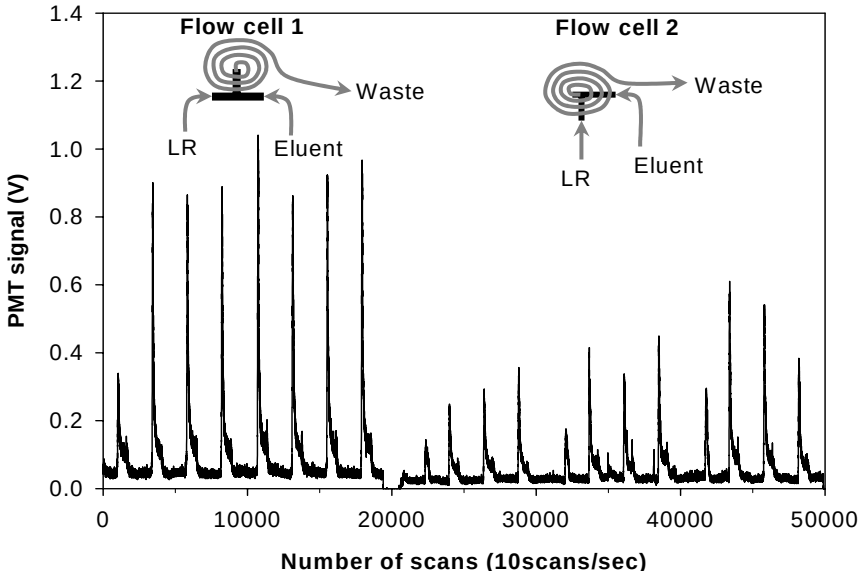

Figure II.13: Experiment comparing two flow cell designs with acidified filtered seawater. Atlantic surface water with [Fe(II)] ~ 1 nM, [S(IV)] = 100 μM.

Variability in the CL pH in the flow cell would change the efficiency of the CL reaction. However, measurements of the pH in waste showed that there was no variation in the CL pH between replicate peaks during the detection step.

Given that most of the above experiments showed little improvement on precision, it was hypothesised that poor reproducibility was due to the 8-HQ resin, which seemed to require several cycles before stabilising when starting a new experiment. This problem was investigated further with the help of S. Ussher from the University of Plymouth (see Section II.3.3.4).

II.3.3.2.3. Problem b: Poor precision on changing solutions

In addition to the poor reproducibility, a problem with the precision during calibrations was identified as a carry-over effect was observed on the first replicate peak of a new solution contributing to the poor precision of the system during calibrations. This feature can be minimised when adjusting the loading time for the first replicate peak (S. Ussher, 2003, personal communication). A sequence of four analytical cycles was set up to be able to change the loading time of the first peak of four replicates (Table II.4).

Sequence	Loading	Rinsing	Eluting	Rinsing
Valve 1	ON	OFF	OFF	OFF
Pump B	ON	OFF	OFF	OFF
Pump C	OFF	ON	ON	ON
IV	Position A	Position A	Position B	Position A
Cycle 1	**60s**	30s	60s	30s
Cycle 2	60s	30s	60s	30s
Cycle 3	60s	30s	60s	30s
Cycle 4	60s	30s	60s	30s

Table II.4: Description of the timing sequence for the automated analyser. The time in bold was modified between each experiment. (See Figure II.9 for definition of Valve 1, Pump B, Pump C and IV)

Loading times of 120, 105 and 90 seconds were used to find the optimum precision during calibrations in the range 0.5 to 5 nM. The best precision was obtained for 105 seconds loading time (Table II.5). Within a calibration, however, precision was poorer for the highest standards suggesting that adjusting the timing was not sufficient to minimise the carry-over effect on the first replicate peak. The problem was then approached in a different way.

Experiment	Loading time cycle 1	Precision *(average, n = 4)*	Analytical sequence
A Increasing first loading time	120 s	11 – 49% *(26%)*	Table II.4
	105 s	4 – 27% *(18%)*	
	90 s	15 – 25% *(20%)*	
B Addition of switching valve	60 s	6 – 12% *(9%)*	Table II.6
		3 – 19% *(11%)*	
		4 – 15% *(9%)*	
		6 – 12% *(9%)*	

Table II.5: Precision of calibrations carried out by standard additions to acidified filtered seawater (Atlantic surface water with [Fe(II)] ~ 1 nM, [S(IV)] = 100 μM) in the range 0.5 to 5 nM.

A carry-over effect between standards was evident where a lower (or higher) first peak was caused by previous solution remaining in the tubing between the container and the adjacent valve (V1), which had a lower (or higher) concentration than the new standard (Figure II.9). To minimise this carry-over effect, an extra switching valve (V2) was added before V1 to reduce the dead volume in the flow system (Figure II.14).

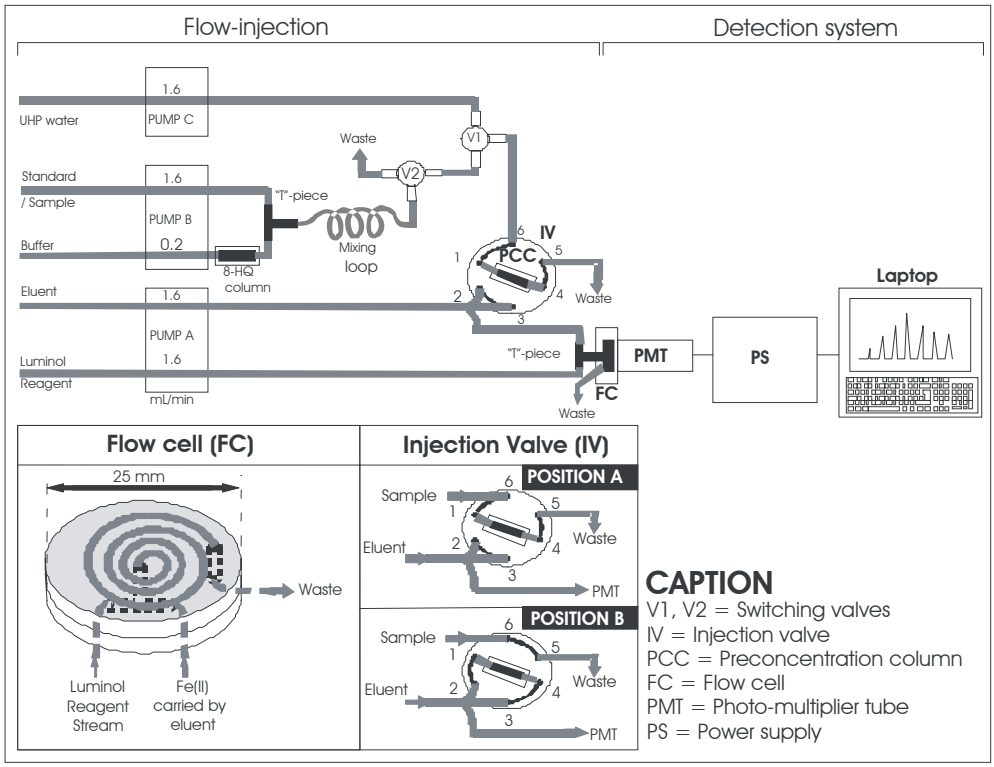

Figure II.14: Diagram of the automated Fe(II) FIA-CL after addition of V2 to improve the precision. Thick grey lines are PTFE or PVC tubing.

Additional experiments were carried out to determine the time needed for the new solution to reach the added valve (V2). Results (data not shown) showed that the rinsing time of the last cycle should be increased from 30s to 55s. The new analytical sequence is shown in Table II.6.

Sequence	Loading	Rinsing	Eluting	Rinsing
Valve 1	ON	OFF	OFF	OFF
Valve 2	OFF	OFF	OFF	ON
Pump B	ON	OFF	OFF	ON
Pump C	OFF	ON	ON	ON
IV	Position A	Position A	Position B	Position A
Cycle 1	**60s**	30s	60s	30s
Cycle 2	60s	30s	60s	30s
Cycle 3	60s	30s	60s	30s
Cycle 4	60s	30s	60s	**55s**

Table II.6: Description of an analytical sequence after addition of valve (V2). Parameters changed are in bold. See Figure II.14 for definition of Valve 1 & 2, Pump B & C and IV.

Several calibrations with standard additions in the range 0.5 to 5 nM were then carried out and showed that precision was improved (average 10%) but occasionally remained high (up to 19%) (Table II.5B).

The addition of an extra valve therefore improved precision during calibrations although it was still occasionally high, suggesting that another factor, such as the behaviour of the 8-HQ resin may be responsible for the poor performance.

II.3.3.2.4. Problem c: Poor calibration

An additional problem was identified when attempting to calibrate the analyser, which did not seem related to the issues of reproducibility and precision. Several calibrations using standard additions to different batches of acidified filtered seawater containing sulphite (as described in Section II.3.3.2.1) were carried out in the range 0.5 or 1 to 5 or 10 nM. The problem was that calibration curves did not show positive curvature as expected (see Section II.2.3), but had negative curvature (*e.g.* Figure II.15). In almost all cases and even after adding the extra valve, which improved precision (see Section II.3.3.2.3), calibrations showed that the most concentrated standards typically gave a lower signal than expected, resulting in a negative curvature.

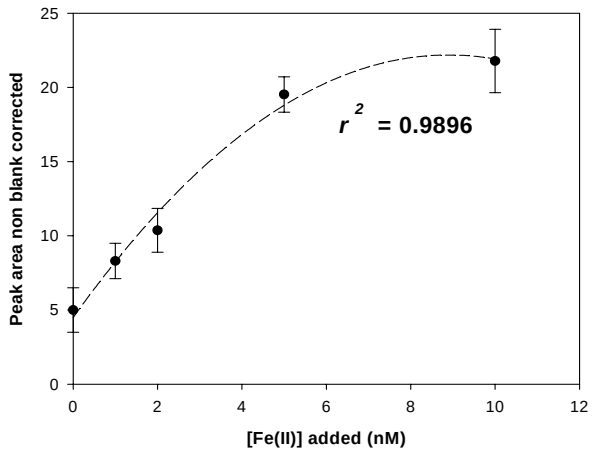

Figure II.15: Calibration curve using standard additions of Fe(II) to acidified filtered surface seawater from the Atlantic Ocean ([Fe] = 1.6 nM) and containing 100 µM sulphite. CL pH = 10.4 and Loading pH = 4.9. Values not blank corrected. Curve fitted with a second degree polynomial trendline. Fe(II) stock solutions prepared with reducing reagent, bubbled with nitrogen, and kept in a fridge. Precision ranged between 6 - 30% rsd (n = 5-7, average 15% rsd). The reagent blank value lower than the limit of detection (estimated at 430pM).

Subsequent work was thus focussed on identifying the factor(s) leading to poor calibration of the system. Working reagents (luminol, eluent, and ammonium acetate buffer) were not thought to be responsible for this behaviour as a new batch was used for each experiment with a different seawater matrix. The response of the anlyser in different Fe(II) concentration ranges was checked, and several parameters susceptible of influencing the response of the analyser during calibrations tested (see Table II.7).

Calibrations with ...	**Sensitivity with linear fit (average)**	*n*
Fe(II) standards range 0.5 – 10 nM	0.1 – 43.2 (5.4)	27
i) Concentrated standards range 1 – 200 nM	1.5 – 3.1 (2.4)	5
iii) Reduced Fe(III) standards	1.1 – 6.3 (3.7)	7
iv) Random calibration	1.2 – 4.6 (3.0)	3

Table II.7: Summary of the experiments carried out to investigate on the poor response of the Fe(II) FIA-CL during calibrations.

i) Calibrations with high concentration standards

In order to test the response of the analyser at relatively high concentrations, several calibrations in the range 5 – 200 nM were carried out with acidified filtered seawater containing sulphite (as described in Section II.3.3.2.2). The CL pH and loading pH were checked and if needed adjusted to the optimum pHs of 10.4 and > 5.5, respectively. These curves were linear, with a precision for each point ranging from 3% rsd for a 10 nM standard up to 27% rsd for seawater alone (Table II.8).

I.D.	Correlation for linear trendline	Precision *rsd* (*n=4*) *(average)*	Limit of detection (nM)	Blank level (nM) (*n=4*)
1	0.999	5 – 27% *(13%)*	3.87	8.00
2	0.9973	3 – 10% *(7%)*	0.53	0.60
3	0.9971	3 – 8% *(6%)*	0.96	< LoD
4	0.9698	10 – 19% *(13%)*	0.81	2.68

Table II.8: Figures of merit of four calibrations by standard additions in the range 5 to 200 nM to acidified filtered seawater collected during the *AMT-12* cruise ([DFe] ~ 1 nM).

The response of the analyser at high iron concentrations was satisfactory over a wide range of Fe(II) concentrations (0 - 200 nM) and did not show the negative curvature observed at lower concentrations. These results suggest that at high concentrations the system is responding satisfactorily, and that the problem only affects low levels of iron.

ii) Stability of Fe(II) standards

The stability of Fe(II) standards was suspected to be an issue in the calibrations. The Fe(II) stock solutions were initially prepared by dissolving ammonium ferrous sulphate in 0.1 M quartz-distilled hydrochloric acid (Q-HCl). These acidified stock solutions were simply stored in the fridge, as low temperature is reported to slow down the oxidation rate of Fe(II) (Croot and Laan, 2002).

A stability experiment was carried out to check on variations of Fe(II) with time (t = 0 to 3h15min) in a freshly prepared working standard of 40 nM Fe(II) in 0.1 M Q-HCl. Iron(II) concentration decreased linearly to up to 2 h (R^2 = 0.97), and continued decreasing more slowly thereafter (Figure II.16). Results showed that in weak acid media, the Fe(II) was 30% oxidised less than one hour after preparation of the 40 nM standard. Assuming that the initial signal measured corresponded to 40 nM Fe(II) as initially prepared, the rate of oxidation would be 0.23 $nM.min^{-1}$ during the first two hours of the experiment. Iron(II) would have a half-life of 87 min at about pH 1 in 0.1 M Q-HCl, which is far greater than its half-life in seawater (~ 1.5 min (Ussher *et al.*, 2004)) at pH 8, as expected in an acidic medium.

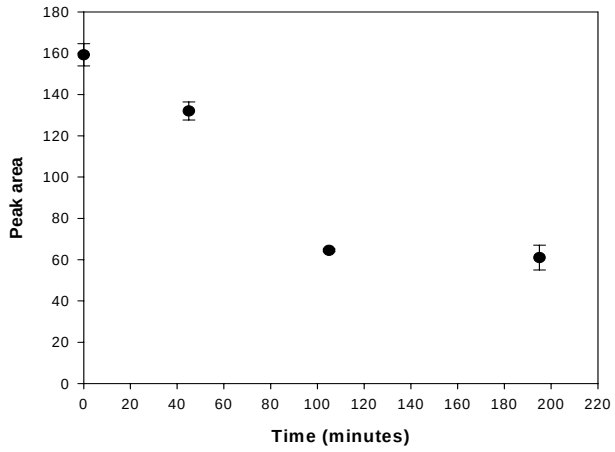

Figure II.16: Standard stability experiment with a 40 nM Fe(II) standard prepared in 0.1 M Q-HCl (eluent) carried directly to the flow cell, without any preconcentration step.

This experiment clearly showed that stability of Fe(II) standards is a major issue. Sodium sulphite was therefore added to the 10 mM and 10 µM Fe(II) stock solutions prepared in 0.1 M Q-HCl to keep iron in the reduced form as suggested by Bowie *et al.* (1998), and were stored in a fridge to lower the oxidation rate (Croot and Laan, 2002). These stock solutions and diluted 1 µM working solutions were prepared weekly and daily, respectively. The Fe(II) standard additions to seawater with sulphite were carried out immediately prior to analysis to minimise Fe(II) oxidation.

iii) Reduced Fe(III) standards

A test was performed to check whether the calibration was still showing the same feature when using reduced Fe(III) standards for the same low range of concentrations. A series of calibration experiments was carried out using Fe(III) standards reduced with sulphite for > 7 hours to ensure complete reduction of Fe(III). All seven calibrations performed showed negative curvature (*e.g.* Figure II.17). This result suggests that the

reduction of Fe(III) may not have been complete or the concentration of sulphite may have been too small to reduce all Fe(III) in the most concentrated standards, however sulphite was added in excess (100 μM) relative to iron, therefore all Fe(III) would be expected to be reduced. It may nevertheless be possible that sulphite was not as efficient as expected in reducing Fe(III), but this eventuality was not considered at the time.

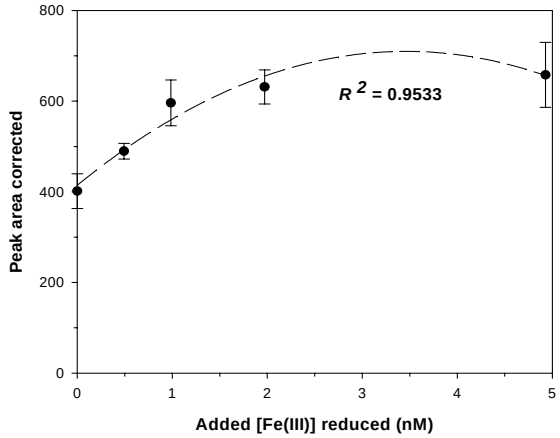

Figure II.17: Calibration curve by standard addition of reduced Fe(III) to acidified filtered surface seawater from the Atlantic Ocean ([Fe] = 1.5 nM) reduced for 17h with sulphite (100 μM). Blank = 0.4 nM and limit of detection = 0.2 nM

When using Fe(II) standards, sodium sulphite is used to keep Fe(II) in the reduced form, and additions of Fe(II) from the 500 nM stock solution to seawater were made less than a minute before analysis. Therefore oxidation of Fe(II) in the standards was expected to be minimum, and sulphite was expected to reduce any oxidised Fe(II), suggesting that the negative curvature was presumably not due to oxidation in the Fe(II) standards.

iv) Random calibrations

More calibration experiments were carried out where Fe(II) or reduced Fe(III) standards (prepared by standard additions to acidified filtered seawater with sulphite (100 μM) as used before in the range 0.5 to 5 nM) were analysed in random order rather than in order of increasing iron concentration as performed before. The aim was to test whether the negative curvature of the calibration was due to a technical feature of the system, however all calibrations showed negative curvature. These results infer that the negative curvature was therefore not a feature of the system, and that this problem originated from a parameter likely not related to the standards.

II.3.3.3. Comparison with the analyser from the University of Plymouth

Given the difficulty in isolating the factor(s) leading to the negative curvature of the calibration, poor precision and time constraints in the present project, it was decided to compare the University of Southampton (UoS) system to the one developed at the University of Plymouth (UoP) by Bowie and co-workers, and used at that time by S. Ussher and co-workers; see Table II.9 for a comparison of the systems.

Differing components	**Fe(II) FIA-CL Southampton**	**Fe(II) FIA-CL Plymouth**
Luminol reagent	Purification through 8-HQ resin	Through Chelex-100 with acid wash each 500 mL
	Protected from light	No protection
FIA-CL system	Gilson, Ismatec pumps, control unit	Gilson pumps, control unit
	Additional valve (V2) to avoid carry-over effect	Longer first loading time or do not consider first peak
Preconcentration column	Protocol Dierssen *et al.* (2001)	Protocol Landing *et al.* (1986)
	Coarse bead size (HW-40C)	Fine bead size (HW-75F)
	Column design as in Figure II.6	Column design as Bowie *et al.* (2002)

Table II.9: Comparison of the main differing components between Fe(II) FIA-CL systems developed at the University of Southampton and at the University of Plymouth.

Experiments were carried out to compare the preconcentration column (PCC) and the luminol reagent (LR). Conditions for the experiments (Experiments 1, 2 and 3) are summarized in Table II.10.

	Southampton	**Plymouth**	**Number of cycles**	**Average peak area**	**Precision (% rsd)**
Experiment 1	PCC & LR	------	8	132.4	18.3%
Experiment 2	LR	PCC	9	362.8	7.1%
Experiment 3	------	PCC & LR	12	203.7	7.2%
Luminol preparation	10 μM luminol in 0.1 M Na_2CO_3	10 μM luminol in 0.1 M Na_2CO_3			
Luminol pH	12.3	10.4			
CL pH	10.4	9.5			

Table II.10: Description and results (average peak area and precision % rsd) of the experiments carried out to compare the Fe(II) FIA-CL of this project response changing the preconcentration column (PCC) and/or the luminol reagent (LR).

Results showed that the PCC and therefore the UoP resin, was about threefold more sensitive than the UoS one (Figure II.18 and Table II.10). The signal during Experiment 3 was lower using the UoP LR with the Southampton system (Figure II.18 and Table

II.10) as the CL pH was not optimal. The UoP LR solution was prepared and purified at a slightly different pH than that of UoS, and any subsequent adjustment of the pH of LR was expected to result in an increased baseline and lower precision due to the presence of impurities from the added sodium hydroxide. These results also indicated that the resin prepared following the protocol of Dierssen *et al.* (2001) was not as sensitive as the resin prepared according to the protocol of Landing *et al.* (1986).

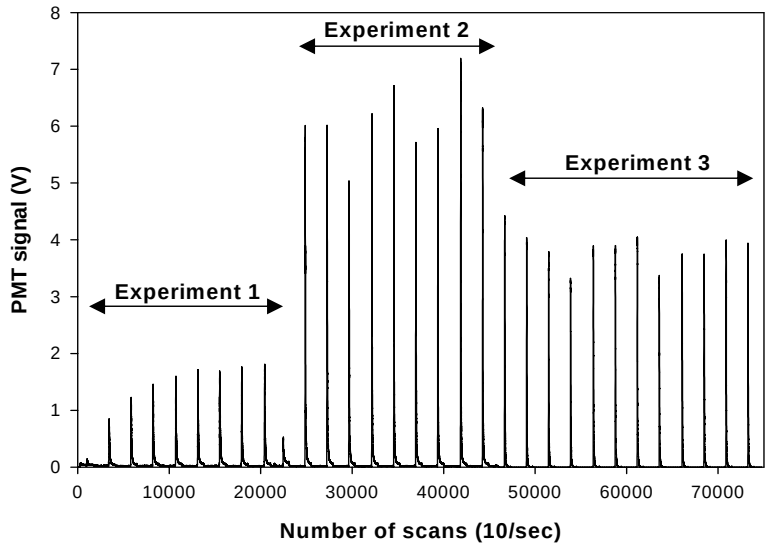

Figure II.18: Signal obtained from the comparison of the preconcentration column and luminol reagent used at the University of Southampton and at the University of Plymouth. Experiment carried out with acidified filtered surface seawater from the Atlantic Ocean ([DFe] = 1.5 nM) with sulphite (100 μM).

As it was clear the UoP resin was behaving better that UoS resin, it was decided to use the 8-HQ resin from the University of Plymouth in the subsequent experiments at Southampton (courtesy of S. Ussher, University of Plymouth).

II.3.3.4. Comparison of the 8-hydroxyquinoline resins

In Southampton, a qualitative experiment to test the cation breakthrough of the resins (*i.e.* uptake and elution) was performed with HW-65F and HW-40C 8-HQ resins prepared at UoS with the protocol of Dierssen *et al.* (2001) ("Dierssen 8-HQ resins"), and HW-75F 8-HQ resin from UoP prepared following the protocol of Landing *et al.* (1986) ("Landing 8-HQ resins"). The configuration of the manifold was simplified and included a peristaltic pump for the luminol reagent and the Fe(II) standard/eluent, a preconcentration column on the standard/eluent line, a PMT flow cell where the luminol reagent and the standard/eluent mixed, and the signal was detected using a PMT. The luminol reagent was continuously flowing directly to the PMT flow cell. The procedure consisted of two steps: **1)** a 1 μM Fe(II) standard (in 0.08 M Q-HCl containing sulphite)

was pre-concentrated onto the resin until the signal stabilised to its maximum value, indicating that the resin iron binding sites were saturated with iron; and **2)** the loaded Fe(II) was eluted with the acid eluent (0.08 M HCl).

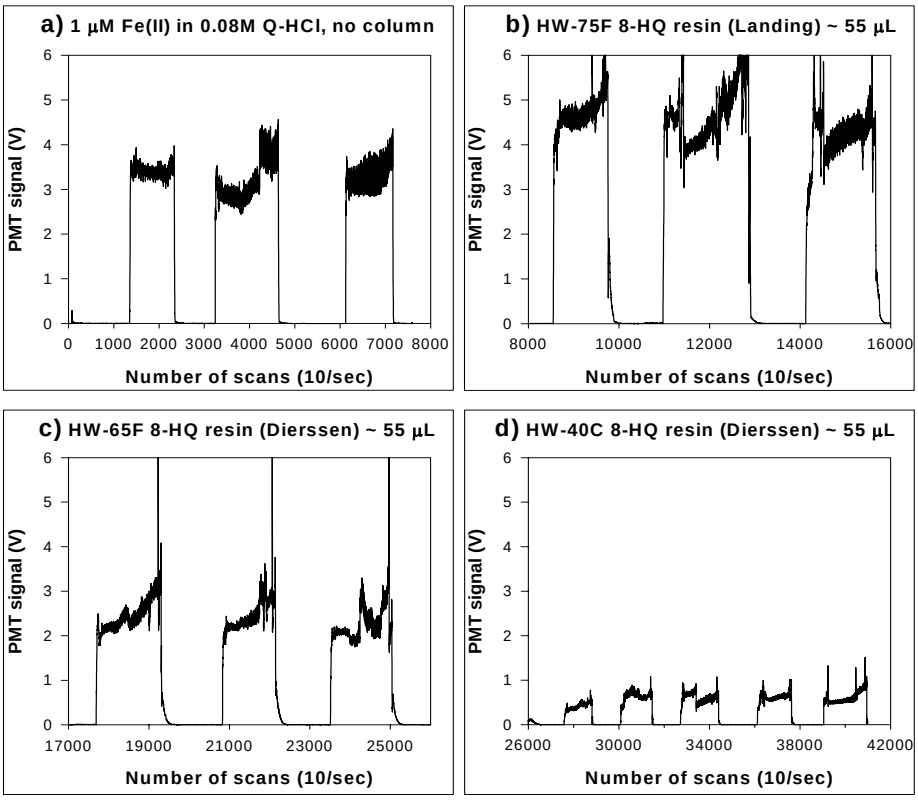

Figure II.19: Breakthrough experiments performed with three 8-HQ resins prepared with different protocols. Figures show 3 (a - c) or 5 (d) loading/elution cycles of a 1 µM Fe(II) standard. Quantity of resin packed in columns is indicated. Resins HW = Hydrophilic Water-compatible polymeric base resins; F = Fine; C = Coarse. HW-75F = 30-60 µm particle size, > 1000 Å pore size; HW-65F = 30-60 µm particle size, 1000 Å pore size; HW-40C = 50-100 µm particle size, 50 Å pore size.

The PMT signal given by the 1 µM Fe(II) standard without a preconcentration column was *circa* 3.5 V (n = 3, Figure II.19a**)**. The PMT signal showed that, at first, the resin bounded Fe(II) until reaching its maximum capacity leading to the PMT signal to increase and stabilise (Figure II.19b, c and d**)**. The eluent was then pumped and Fe(II) eluted so that the PMT signal decreased and stabilised at its background level. Results showed that while the "Landing 8-HQ resin" retained all the iron passing through and fully released it during the elution, the "Dierssen 8-HQ resins" both tended to slowly take up and only gradually release iron. Weeks *et al.* (2002) reported that the 8-HQ TSK resin prepared by attaching 8-HQ to the commercial epoxy resin (Dierssen protocol) tended not to fully release the loaded copper, as observed here for iron. It is hypothesised that the "Dierssen 8-HQ resins" may have two types of binding sites:

some easily available sites which would quickly complex and then release Fe during the elution; and some sites less easily accessed in the resin matrix which would only gradually complex Fe, but difficult to release Fe by the eluent. This feature of the "Dierssen 8-HQ resins" used in all the previous experiments carried out during the development was thought to play a major role in the problems encountered with the Fe(II) technique, especially with the reproducibility of the CL signal. In particular it may explain why a gradual increase in the signal was observed during replicate measurements in earlier experiments (see above). The "Landing 8-HQ resin" was therefore used subsequently, and there was a significant improvement in the precision; *e.g.* typically 5% rsd for standards in the 0.5 to 5 nM Fe(II) concentration range.

II.3.3.5. Subsequent calibrations with the new 8-HQ resin from Plymouth

Despite using the improved resin, a series of nine calibration experiments in the range 0.5 to 5 nM frequently showed non linear calibrations. The last calibration in the range 0.5 – 5 nM was performed without sulphite additions, to reproduce the conditions of the calibration experiments carried out during the comparison exercise at the University of Plymouth. Results showed a negative curvature as in previous experiments with precisions ranging from 2% to 5% (average 2.9%, n = 5), the blank and limit of detection were estimated at 460 pM and 220 pM, respectively, using a second-degree polynomial fitting curve (Figure II.20).

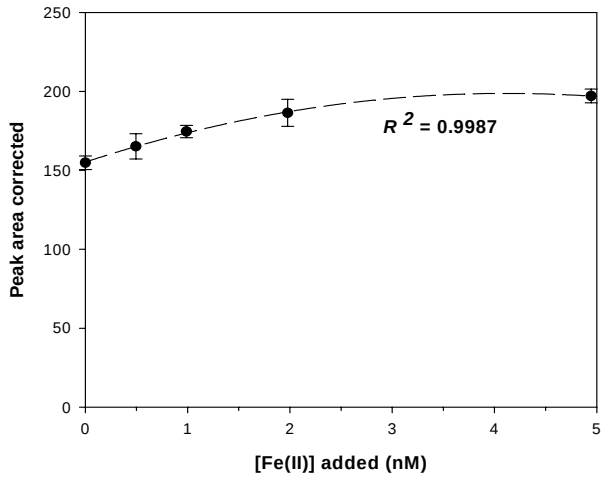

Figure II.20: Calibration curve by standard additions without sulphite to acidified filtered seawater collected in the Celtic Sea ([DFe] ~ 1.5 nM).

This last calibration showed that, at this stage, the system was still not reliable and did not allow sample analysis. The only element of the system not changed or modified in the Fe(II) technique was the luminol in the chemiluminescence reaction. Since this product was used as received, and was ordered from the same company as Bowie *et al.*

(1998), there was no reason to doubt its quality, and no comments about variability of quality of this reagent had been presented in the literature. Degradation or poor quality luminol could explain the problems encountered with calibrations, however this possibility had not yet been considered at this stage. Because of time constraints in the project, it was decided at this point to move on to the alternative version of the FIA-CL system for total dissolved Fe.

Subsequently, a comparison of calibrations obtained with the luminol used above and a new luminol were compared to investigate on the role of luminol in the negative curvature often observed in calibrations.

II.3.3.6. Comparison of calibrations with old and new luminol

Before the end of this project, two experiments were carried out to investigate the effect that the quality of the luminol reagent may have had on calibrations, to determine whether it may have been responsible for the negative curvature of calibrations with the Fe(II) technique. Reagents and standards were prepared for the Fe(II) technique as it was set up in its last stage of development (see Chapter II.3.3 and Appendix 4). Two luminol reagents were prepared: one with the luminol ("old luminol") used in earlier experiments, and one with a newly bought luminol ("new luminol"). All conditions (*i.e.* reagents concentration, ageing, pHs, flow rates) were kept as similar as possible between experiments, which were both performed in a single day.

Calibration curves were slightly different as the curve with "old luminol" was linear whereas the "new luminol" calibration had a clear positive curvature (Figure II.21). The signal for non-spiked and + 0.5 nM seawater were similar for both experiments and then differed for additions ≥ 1 nM. Additionally the peak area for the NASS-5 certified seawater measured after each calibration increased by 17% between the two experiments. These results are unlikely to be due to the 8-HQ resin since both experiments were carried out with the same resin column and standards.

The difference between calibrations may be related to the response of the system to additions of Fe(II). From 0 to + 2 nM the sensitivity was 0.5 V/nM using peak heights with the "old luminol", and the peak height of + 3.5 nM and + 5.0 nM standards were lower than expected from this trend (-11% and -14% of the peak area,

respectively). These results are similar but less pronounced than those obtained earlier with the Fe(II) technique with the "old luminol" (see Section II.3.3.2.).

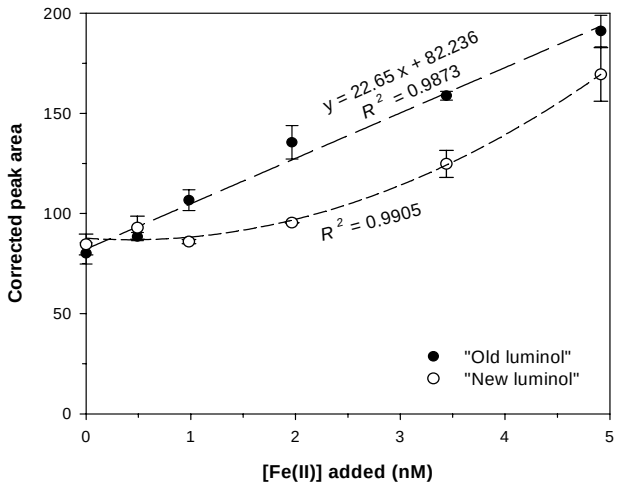

Figure II.21: Comparison of calibrations carried out with the "old" or "new" commercial luminol. "New luminol" calibration fitted with a second-degree polynomial regression.

The "new luminol" calibration was carried out after the "old luminol" therefore Fe(II) could have been significantly oxidised between the two experiments. However sulphite was added to the standards to keep Fe(II) in solution and therefore oxidation of Fe(II) should have been very limited. The calibration with the "new luminol" did not have a linear regression however the curvature was positive. Values obtained for the certified seawater NASS-5 were within the 95% confidence level for the "old luminol" calibration, and significantly higher for "new luminol" (Table II.11). This latter result may be due to the poor precision on the NASS-5 measurement or to the lower signal obtained with the standards with the "new luminol" experiment.

Calibration with	CL pH	Precision (*average*) (*n* = 3-4)	Blank (nM)	NASS-5 ± 1*sd* *(3.71 ± 0.63nM)*
"Old luminol"	10.43	2.3-6.6% *(4.8%)*	< LoD	4.33 ± 0.12 nM
"New luminol"	10.46	0.01-7.9% *(4.3%)*	< LoD	5.81 ±1.84 nM

Table II.11: Figures of merit of the Fe(II) technique using the "old" or "new" commercial luminol. CL = chemiluminescence; LoD = Limit of Detection

Due to time constraints, the role of luminol quality in the problems encountered during calibration of the Fe(II) technique could not be investigated further.

II.4. Summary

The Fe(II) technique was chosen because it could give information on iron speciation, and the technique seemed simple and quick. The method had the potential to allow near

real-time measurement of transient Fe(II) in seawater, which is the most available form of iron to the biota, as well as total iron (Fe(II+III)), after a reduction step. This reduction was planned to be integrated in an in-line system combining the action of light and sulphite. However, the development of the system proved difficult. The principal problems were with the critical steps of preconcentration, and the chemiluminescence reaction.

The preconcentration step was found to be difficult to control using the laboratory prepared resin. The preparation of the first batch of resin failed for unknown reasons, and the resin created backpressure problems owing to packing. About 90 experiments were designed and carried out in order to improve the precision when using the resins prepared following the protocol of Dierssen *et al.* (2001). Best results were obtained when calculating peak area, the loading pH was adjusted to pH 5.5 instead of 5.0, and after adding an extra valve to minimise the carry-over effect between analyses. It was later found that the resin obtained from Plymouth ("Landing resin") was more efficient in loading and fully releasing iron than the "Dierssen resins" prepared in the current work. It was suggested that the "Dierssen resins" contained two types of 8-HQ binding sites, one of them being less available to Fe complexation than the other one. The resin used at the University of Plymouth was used subsequently; its finer resin bead size did not induce backpressure, and precision was significantly improved.

The second critical step, the chemiluminescence reaction, was found to be complex. Calibration curves were found to be mostly linear for concentrated standards (0 to 200 nM). However, most calibrations performed up to 10 nM showed a negative curvature. Previous studies ((King *et al.*, 1995; Rose and Waite, 2001)) have shown that calibrations were slightly curved mainly as a result of the photosensitivity of luminol and impurities (see Section II.2.3); however none suggested that the curvature could be negative. Experiments comparing the "old" and "new" luminol were not conclusive that luminol was directly responsible for this problem.

As the aim of this project was to analyse samples collected during the *AMT-12* and *JR98* cruises, given time constraints of the present project, and continuing problems with the Fe(II) method, it was decided to move on to an alternative method more widely used, the Fe(II)+(III) FIA-CL technique. It was hoped that modifying the Fe(II) technique to the Fe(II)+(III) system would help to identify the problem with the former method since these two techniques are quite similar.

CHAPTER III.

IMPLEMENTATION OF A FLOW INJECTION ANALYSER WITH CHEMILUMINESCENCE DETECTION (FIA-CL) TO SIMULTANEOUSLY DETECT Fe(II) AND Fe(III) IN SEAWATER

III.1. Introduction

Whilst the Fe(II) FIA-CL technique (with preconcentration) has been only developed and used in two laboratories (University of Plymouth (UK) (Ussher *et al.*, 2005), and Old Dominion University (USA) (Powell and Donat, 2001)), the Fe(II)+(III) technique based on the method of Obata *et al.* (1993) has much more widespread use suggesting that its optimisation may be easier. The Fe(II)+(III) technique is based on the three critical steps described in Chapter II. The main difference between the two systems is the addition of hydrogen peroxide (H_2O_2) in the CL reaction, which makes possible the simultaneous determination of Fe(II) and Fe(III). Therefore Fe(III) does not need to be reduced to Fe(II). However, the CL reaction with H_2O_2 is kinetically slower, and requires a long reaction coil and heating to enhance the reaction. An overview of the optimisation and calibration of the Fe(II)+(III) technique, and a full description of the optimised analyser are given below.

III.2. Description of the Fe(II)+(III) analyser

The Fe(II)+(III) technique developed was based on the methods of Obata *et al.* (1993) and de Jong *et al.* (1998), and modified to take advantage of the experience gained from the work on the Fe(II) technique. Main modifications to the Fe(II) technique were:

- Addition of hydrogen peroxide for the CL reaction;
- Ammonia solution added to buffer the CL reagents mixture to pH 9.5;
- Standards were prepared from a single element AAS stock solution for iron (1000ppm) and thus included Fe(III) even though Fe(II) could be formed by photo-reduction in the standard.
- 5-way junction added to mix the CL reagents (luminol reagent, ammonia, hydrogen peroxide, and eluent);
- Laboratory made thermostated heating system to increase the temperature, and thus the sensitivity of the CL reaction;
- 8-HQ resin used was that provided by the University of Plymouth;
- The ammonium acetate buffer was purified through two 8-HQ resin columns in series and further purified in-line with an additional 8-HQ resin column;
- Flow cell was a 0.8 mm internal diameter PTFE tubing coil mounted on the PMT window and backed with aluminium foil to optimise light reflection;
- A complete analytical cycle of loading, rinsing, eluting and rinsing was performed in *circa* 5 minutes for a 60 seconds preconcentration time.

The PMT and electronics in the detection system were identical to the Fe(II) technique. The modified system configuration is shown in Figure III.1, and details of instrumentation, reagent preparation, and analytical sequence are given in Appendix 6.

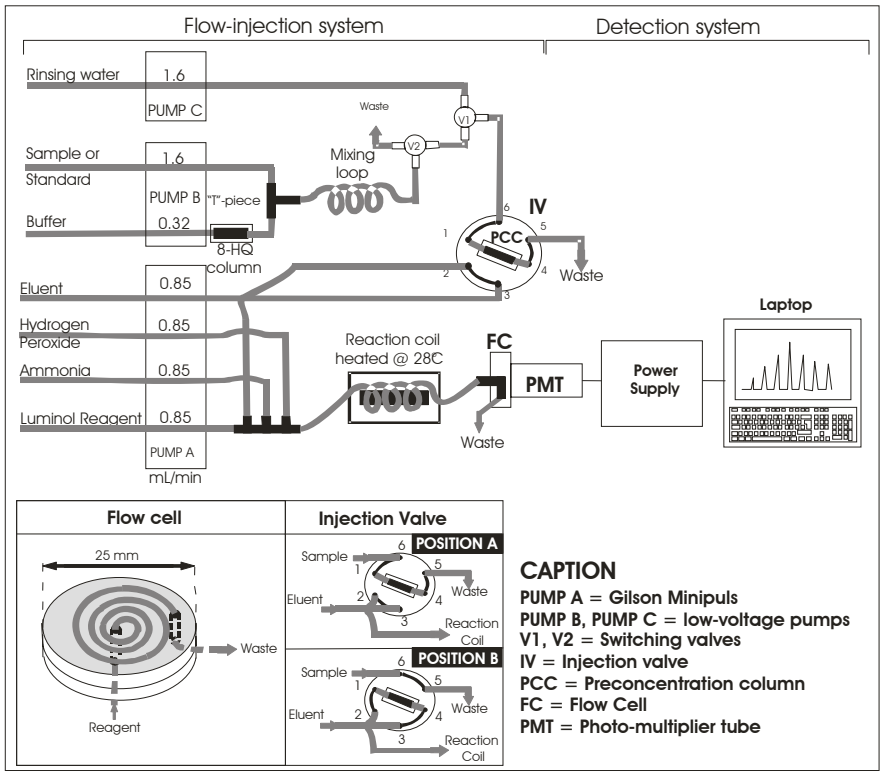

Figure III.1: Diagram of the Fe(II+III) FIA-CL analyser, based on the methods of Obata *et al.* (1993) and de Jong *et al.* (1998). Thick grey lines represent PTFE or PVC tubing.

This Fe(II)+(III) analyser was relatively easy to set up mechanically because it was very similar to the Fe(II) instrument. The main work thus focussed on the optimisation of the chemistry of the system to allow determination of Fe(II) and Fe(III), and on the calibration.

III.3. Optimisation of the analyser

III.3.1. Reaction coil length

The reaction coil length was optimised in order to ensure that the CL reaction commenced in the PMT flow cell and finished before exiting it. With the heater set to 27^{o}C (Xiao *et al.*, 2000), the signal increased with length of tubing, and reached a plateau at about 1810mm (Figure III.2). This value is close to the 1.9 m reaction coil used by Obata *et al.* (1993).

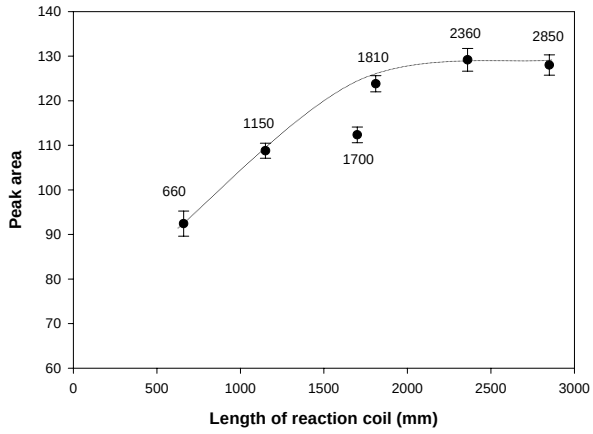

Figure III.2: Optimisation of the reaction coil length at 27°C with acidified (pH ~ 2) filtered (< 0.4 μm) surface seawater from the Atlantic Ocean ([DFe] = 1.4 nM).

III.3.2. Reaction temperature

The influence of reaction coil temperature on the CL signal was then tested between 21°C and 38°C. A linear relationship (R^2 = 0.995) was found between temperature and peak area (Figure III.3). This result is consistent with observations that higher temperature favours the decomposition of H_2O_2, which therefore enhances the CL reaction (Xiao *et al.*, 2000). The temperature was set at 28°C as a compromise between signal enhancement and minimising bubble generation as more bubbles were formed as temperature increased.

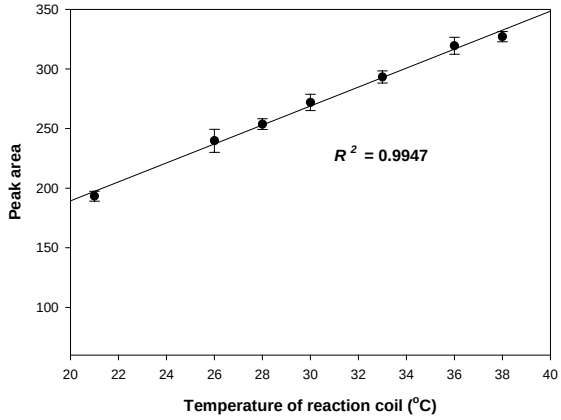

Figure III.3: Relationship between the reaction coil temperature and the CL signal with acidified (pH ~ 2) filtered (< 0.4 μm) surface seawater from the Atlantic Ocean ([DFe] = 1.4 nM).

III.3.3. Loading and CL reaction pHs

Ammonia solutions of different concentrations were added to the CL reagents to find the optimum CL pH. A pH of *circa* pH 9.5 gave the highest signal as reported in the literature (Obata *et al.*, 1993) (Figure III.4a). The optimal CL pH was obtained using 0.6 M NH_4OH.

To find the optimal loading pH, a series of ammonium acetate buffers, giving a range of sample pHs, was used. Results (Figure III.4b) showed that the optimal pH for

collecting Fe(III) from an iron standard for atomic absorption spectrometry and any eventual Fe(II) reduced in this standard, was pH > 5 as suggested in the literature (see Chapter II).

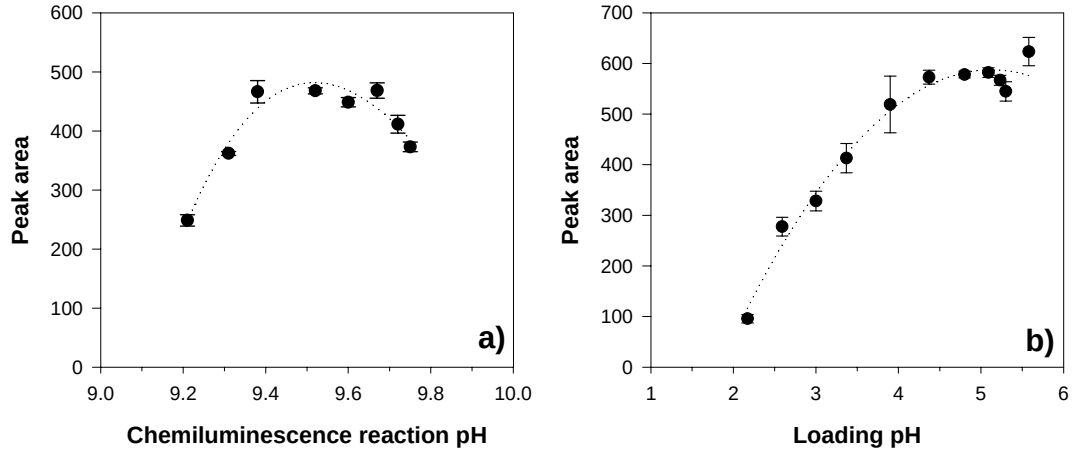

Figure III.4: pH optimisation of **a)** the CL pH and **b)** the loading pH, with acidified (pH ~ 2) filtered (< 0.4 μm) surface seawater from the Atlantic Ocean ([DFe] = 1.4 nM).

III.3.4. Luminol concentration

The luminol concentration was optimised by measuring the signal of acidified open ocean seawater the following concentrations: 750 μM (as used by Obata *et al.* (1993)), 100 μM (de Jong *et al.*, 1998), 50 μM and 10 μM (Bowie *et al.*, 1998). Results showed that there was a significant increase in the signal up to 100 μM, and the signal was little enhanced at 750 μM with a higher baseline (Figure III.5). The luminol reagent was prepared at a concentration of 100 μM as suggested by de Jong *et al.* (1998), as it showed the best compromise between signal enhancement and baseline level.

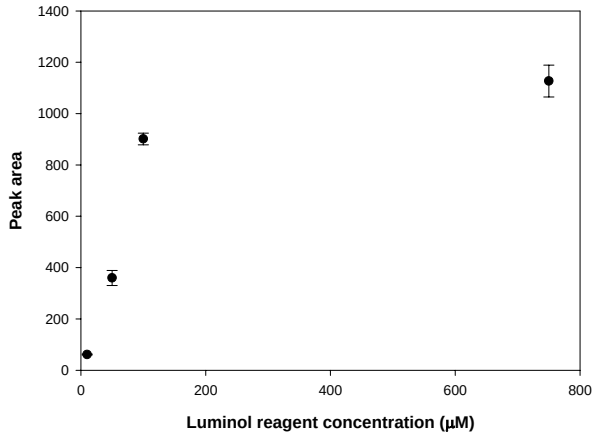

Figure III.5: Optimisation of the luminol concentration in the luminol reagent with acidified (pH ~ 2) filtered (< 0.4 μm) surface seawater from the Atlantic Ocean ([DFe] = 1.4 nM).

Luminol was found to be difficult to dissolve in 0.04 M sodium carbonate, even after sonicating for 30 min, resulting in a "cloudy" solution. Incomplete dissolution of luminol may lower sensitivity and particles may cause increased noise, and potentially blockage of tubes if particles aggregate. It was noted that whilst luminol is insoluble in water it is very soluble in alkaline solutions. The 0.04 M sodium carbonate buffer may not be alkaline enough to completely dissolve the reagent. Therefore, a 0.01 M stock solution of luminol was prepared using a stronger 0.1 M sodium carbonate solution and luminol seemed to be completely dissolved overnight as the solution looked clear.

A comparison between luminol/0.04 M Na_2CO_3/TETA (Test 1) and luminol/0.1 M Na_2CO_3/TETA (Test 2) reagents showed that the CL signal was greatly enhanced in Test 2, but the baseline and peaks were very noisy (Figure III.6). A large number of micro-bubbles were observed in the tubing shortly after the acidic eluent mixed with luminol/0.1 M Na_2CO_3/TETA presumably due to $CO_{2(g)}$ bubbles produced on mixing of acid eluent and luminol reagent, as suggested by Xiao *et al.* (2000) (see Chapter II).

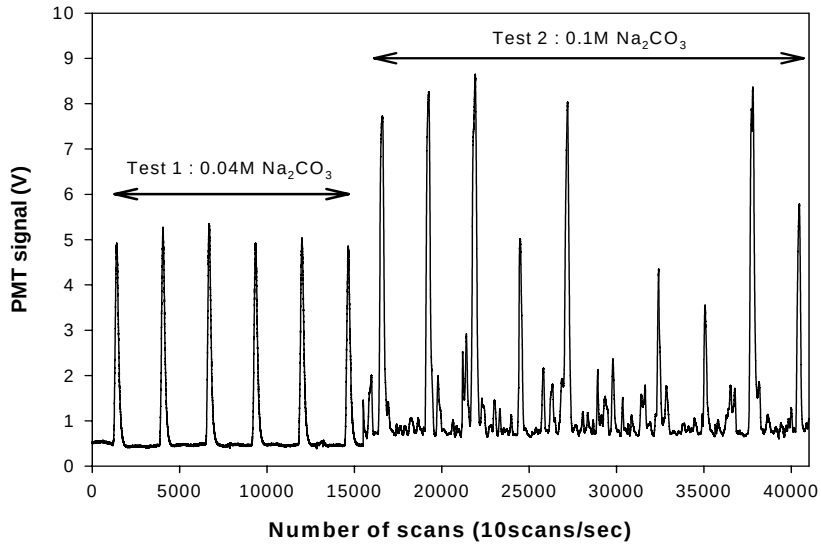

Figure III.6: Comparison of signals obtained with luminol reagents prepared in 0.04 M (Test 1) or 0.1 M sodium carbonate (Test 2) with acidified (pH ~ 2) filtered (< 0.4 μm) surface seawater from the Atlantic Ocean ([DFe] = 1.4 nM). CL pH = 9.5 in both cases.

In order to avoid excessive production of bubbles in the manifold, the luminol stock solution was prepared in 0.1 M sodium carbonate to promote its dissolution, whilst the working luminol reagent was prepared in 0.04 M sodium carbonate.

III.3.5. Hydrogen peroxide concentration

The concentration of hydrogen peroxide was changed in the range 0.05 M - 0.8 M H_2O_2, and signals measured. Results (Figure III.7) showed a plateau starting at about 0.4 M H_2O_2, which was intermediate between the concentration used by de Jong *et al.* (1998) (0.1 M), and Obata *et al.* (1993) (0.7 M). The hydrogen peroxide concentration used was therefore adjusted to 0.4 M, as a compromise between sensitivity and saving reagents.

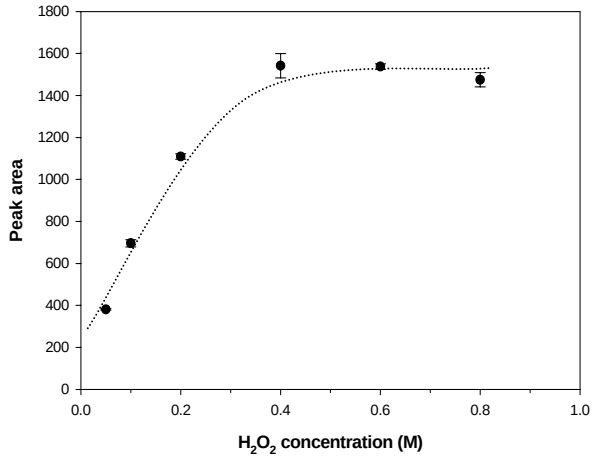

Figure III.7: Optimisation of the hydrogen peroxide concentration with acidified (pH ~ 2) filtered (< 0.4 μm) surface seawater from the Atlantic Ocean ([DFe] = 1.4 nM).

III.3.6. CL reagents flow rate

The flow rate of the CL reagents was optimised to give maximum signal in the PMT flow cell. The relationship between the CL signal and the flow rate in the flow cell after all CL reagents mixed was linear (r^2 = 0.992) in the range tested (3.3 – 5.0 mL.min^{-1}) with highest signal at lowest flow rate (Figure III.8). This result suggests that the reaction may not be finished at high flow rate when the mixture left the PMT flow cell resulting in loss of signal. Flow rates of 3.3 mL.min^{-1} were thus used subsequently for the CL reagents.

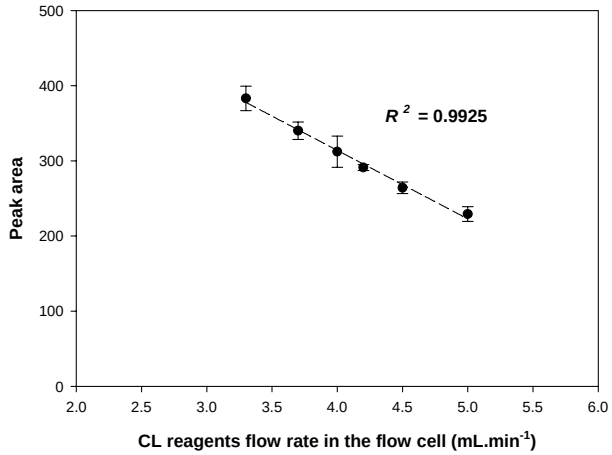

Figure III.8: Optimisation of CL reagents flow rates in the flow cell with acidified (pH ~ 2) filtered (< 0.4 μm) surface seawater from the Atlantic Ocean ([DFe] = 1.4 nM).

After optimisation of the reaction coil length and temperature, loading and CL pHs, luminol and hydrogen peroxide concentrations and CL reagents flow rate, the system was ready to be tested for its response during calibrations.

III.4. Calibration of the analyser

A calibration experiment was performed with standard additions in the range 0.5 – 5 nM to acidified filtered open ocean seawater. The CL pH was checked at 9.5 and loading pH at 5.2. The curve was linear (R^2 = 0.991) with a precision ranging from 3% to 11% rsd (n = 4) (average 6% rsd) (Figure III.9). Accuracy was checked using a NASS-5 certified seawater standard (from the National Research Council of Canada, certified value: 3.71 ± 0.63 nM), the value obtained was 3.68 ± 0.24 nM (1*sd*). The blank defined as the signal given by a 0.01 M Q-HCl solution used to prepare the standards was estimated at 1.05 nM and the limit of detection (3 *sd*) was 580 pM.

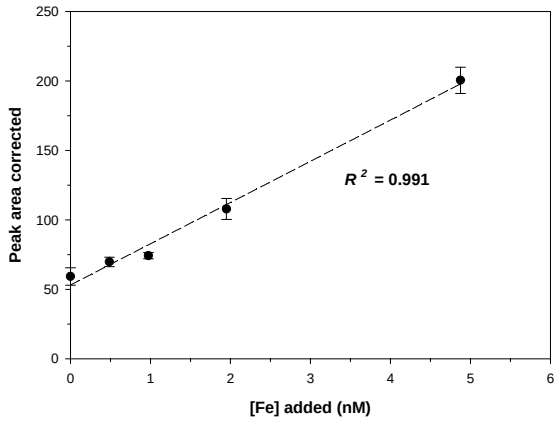

Figure III.9: Calibration curve by standard additions to acidified (pH ~ 2) filtered (< 0.4 μm) surface seawater from the Atlantic Ocean ([DFe] = 1.4 nM).

This first calibration was not negatively curved as obtained with the Fe(II) technique, precision was kept below 10% rsd, and the NASS-5 concentration was close to the certified value. However, more work was necessary to try and lower the blank value and more calibration experiments were needed to conclude that the technique was reliable.

III.4.1. Sources of contamination to the blank

A series of experiments was carried out to identify the source of the blank signal as shown in Table III.1. These experiments were carried out using the highest gain of the photomultiplier tube (G = 10, relative to G = 6 or 7 as used for calibrations) to increase its sensitivity and thus get a better qualitative appreciation of the relative importance of

each of the component of the blank. Using such a high gain prevented from performing a calibration to quantitatively determine these blank values as peaks for the usual standards used were saturating. However a calibration was carried out on the previous day using the same CL reagents with a gain of 7. By experience, it was noted that the signal decreased 3-fold when switching from a gain of 10 down to 7. The relative iron concentration of the blank for each of the experiment presented below could therefore be estimated, assuming similar reaction of the luminol reagent.

	Contribution of	Loading	Rinsing	Eluting	Rinsing
Experiment 1	CL reagents + PCC			180 s	
Experiment 2	CL reagents + PCC + RW		30 s	180 s	30 s
Experiment 3	CL reagents + PCC + RW + Buffer	60 s	30 s	180 s	30 s
Experiment 4	CL reagents + PCC + RW + Buffer + 0.01M Q-HCl	60 s	30 s	180 s	30 s

Table III.1: Description of the experiments performed to determine the sources of the blank. PCC = preconcentration column; RW = rinsing water

Experiment 1: The CL signal was recorded for several cycles with the eluent going through or not through the column, which gave information on the contribution of the CL reagents and preconcentration column (PCC) to the blank signal. Results (Figure III.10) showed that the contribution of the preconcentration column was small (estimated at 0.09 nM).

Experiment 2: The signal was recorded for several cycles including the rinsing step with Milli-Q water as rinsing water (RW). The contribution of Milli-Q water passing through the preconcentration column could be important at some occasions (here estimated at 0.13 nM (total [Fe] = 0.22 nM); Figure III.10). This was observed even when adding up to two in-line 8-HQ resin columns in the rinsing water stream.

Experiment 3: The ammonium acetate buffer used to buffer the sample to *circa* pH 5.5 was added to the sequence. Results (Figure III.10) showed that the contribution of the sample buffer to the blank signal was equivalent to the Milli-Q water at this occasion (estimated at 0.11 nM (total [Fe] = 0.33 nM)).

Experiment 4: Instead of a standard, a 0.01 M Q-HCl solution used to prepare the iron standards was loaded onto the column. Results (Figure III.10) showed that the diluted acid contributed significantly to the blank (estimated at 0.33 nM (total [Fe] = 0.66 nM)).

It was noticed that the blank was sometimes higher than the Fe signal for samples. The blank may be over-estimated when using diluted acid as a matrix; therefore the definition of the blank was reviewed.

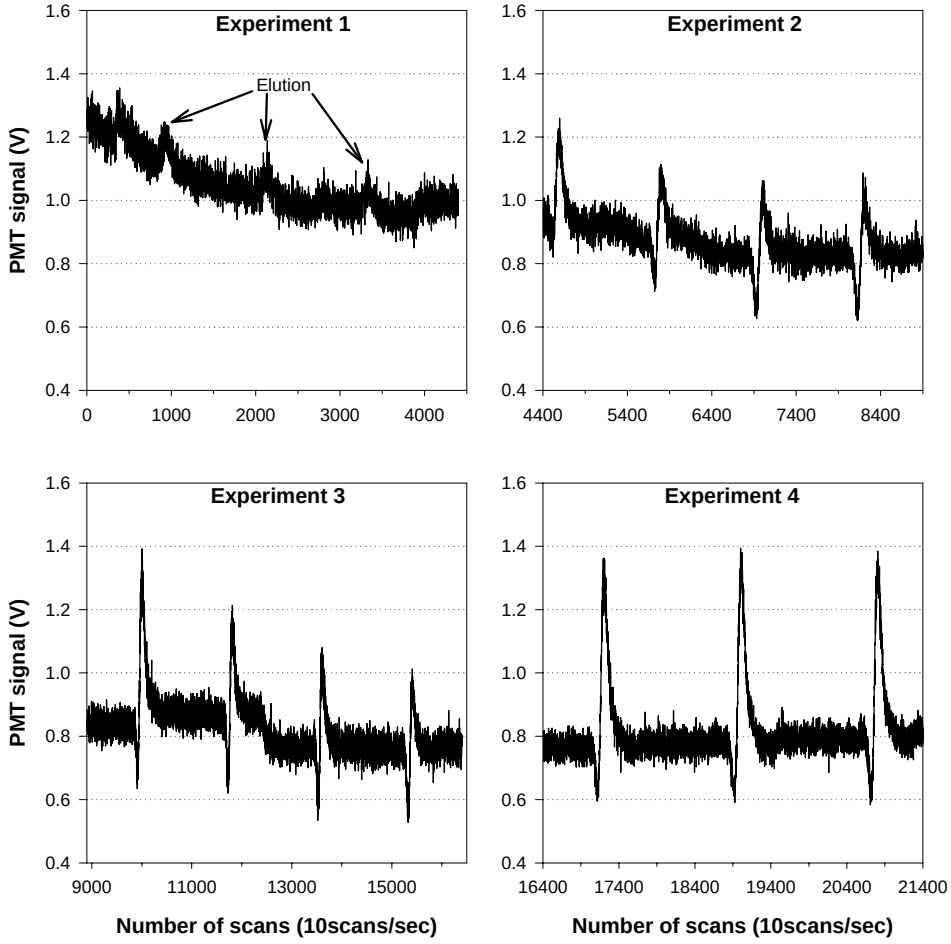

Figure III.10: Experiments to determine the sources of the blank. Experiment 1: CL reagents & preconcentration column (PCC). Experiment 2: CL reagents & PCC & rinsing water (RW). Experiment 3: CL reagents & PCC & RW & buffer. Experiment 4: CL reagents & PCC & RW & buffer & 0.01 M Q-HCl solution. PMT gain = 10 (maximum).

It was decided that the blank value would be defined as the signal obtained during a cycle with the ammonium acetate buffer only being loaded onto the column for the length of time used to analyse samples, as used by Bowie *et al.* (1998). The blank value included the contribution of the CL reagents, the preconcentration column, the rinsing water, and the sample buffer. Furthermore, the buffer was subsequently purified through two 8-HQ resin columns in series off-line in addition to the in-line 8-HQ column, and the rinsing water was taken freshly from the Milli-Q water system after leaving it to flush, and was stored in a Teflon bottle.

III.4.2. Calibration of the system

Several calibration experiments by standard additions in the range 0.5 – 5 nM were subsequently carried out in order to check on improvements in the blank, limit of detection values, and sensitivity. Figures of merit of these six calibrations are summarised as ranges in Table III.2.

Correlation *(mean)*	Slope *(mean)*	Precision *(mean)*	Blank (nM) *(mean)*	LoD (nM) *(mean)*	NASS-5 ± 1*sd* *(mean)*
0.9635 – 0.9969 *(0.9800)*	44 – 137 *(74)*	1 – 15% *(7%)*	< LoD – 1.53 *(1.18)*	0.12 – 0.46 *(0.27)*	4.11 ± 0.36 - 4.83 ± 0.69 *(4.51)*

Table III.2: Ranges of figures of merit of six calibration curves. Calibrations were fitted with a linear trendline. *rsd* = relative standard deviation (n = 4). Limit of detection (LoD) defined as three times the standard deviation of the blank. Certified value of NASS-5 for Fe : 3.71 ± 0.63nM.

Three of these calibrations had a poorer correlation due to the lower signal obtained for the two most concentrated standards, whereas the other three showed good linear or positive curvature as in the first calibration (see Figure III.9). The sensitivity and curvature fluctuated most probably because of changes in analytical conditions such as the small variations in the ageing of the luminol reagent. Values of the blank, limit of detection, and NASS-5 certified seawater material values were often high, and may have been over-estimated because of poorer calibrations, poorer quality of Milli-Q water, and/or baseline instability. These results suggest that there still was a problem with the calibration even with this version of the FIA-CL analyser.

Since the only component in the Fe(II) system not tested was luminol, a new batch was ordered from a different supplier (Fisher). The old and new batches of luminol had different colours: the new batch was pale-yellow and the old batch was greenish. An initial calibration using the new batch of luminol was linear (R^2 = 0.994, Curve 7, Table III.3), and several subsequent calibrations gave slightly non-linear curves but always with positive curvature. Figures of merit of these calibrations are summarised in Table III.3. The value for NASS-5 certified seawater standard was generally close to the certified value but was occasionally higher and often with fluctuating precision (2 – 27% rsd, average 12.5% rsd).

	Correlation *Range*	Slope	Precision *rsd* (*n=4-6*) (*average rsd*)	Blank (nM)	Limit of detection LoD (nM)	NASS-5 ± *sd* (nM) 3.71 *(± 0.63)*	Samples analysed
7	0.9937 *0.5-5nM*	138 *(linear)*	2.9 – 7.6% *(5%)*	0.43	0.24 *(n=5)*	4.08 ± 0.41	
8	0.9956 *0.5-5nM*	$7x^2 + 55x$	3.7 – 21.7% *(10.1%)*	< LoD	0.21 *(n=9)*	4.80 ± 0.43	JR98/N8
9	0.996 *0.5-7.5nM*	$11x^2 + 74x$	6.7 – 16.7% *(13.5%)*	1.23	0.32 *(n=4)*	5.58 ± 0.48	JR98/N7
10	0.9982 *1-8nM*	$4x^2 + 80x$	3.4 – 11.8% *(5.8%)*	0.47	0.27 *(n=9)*	4.20 ± 0.41	JR98/N6
11	0.9925 *0.5-5nM*	$8x^2 + 7x$	2.7 – 13.2% *(7.6%)*	1.20	0.75 *(n=4)*	4.50 ± 0.69	
12	0.9958 *2-8nM*	$3x^2 + 47x$	1.7 – 11.9% *(6.2%)*	0.86	0.64 *(n=5)*	4.52 ± 0.54	JR98/N1 &N2
13	0.998 *2-8nM*	$1x^2 + 35x$	3.5 – 8.4% *(4.9%)*	1.19	0.72 *(n=5)*	4.42 ± 0.77	JR98/N3 &N4
14	0.9993 *1-6nM*	$5x^2 + 8x$	3.8 – 13.1% *(7.9%)*	1.25	0.17 *(n=5)*	3.26 ± 0.53	JR98/N5
15	0.9999 *0.5-5nM*	$11x^2 + 49x$	2.4 – 29.7% *(8.8%)*	< LoD	0.53 *(n=5)*	3.90 ± 0.67	JR98/N9 AMT12/ CTD69
16	0.992 *0.5-5nM*	112 *(linear)*	4.7 – 8.5% *(7.6%)*	0.72	0.14 *(n=5)*	2.90 ± 0.80	AMT12/ CTD69
17	0.9973 *0.5-4nM*	$9x^2 + 36x$	4.0 – 8.5% *(5.9%)*	1.18	0.20 *(n=8)*	3.35 ± 0.21	AMT12/ CTD68
18	0.9969 *0.25-4nM*	$11x^2 + 70x$	1.6 – 5.8% *(3.8%)*	1.01	0.26 *(n=4)*	3.48 ± 0.08	AMT12/ surface

Table III.3: Figures of merit of calibration curves performed with a new batch of luminol. Limit of detection = 3*sd* of the blank. Trend lines are 2nd -degree polynomial unless stated otherwise. All the samples from the profiles listed in the table were analysed using the Obata method.

Following Curve 10 (Table III.3), there was an episode of contamination of the acid used to prepare the eluent reagent, leading to a very high and unstable baseline. The problem was solved by changing the stock Q-HCl solution. The system was also regularly washed with an acid wash mixture of 0.1 M ascorbic acid and 1 M hydrochloric acid, and rinsed with Milli-Q water subsequently. The presence of ascorbic acid should enhance the washing as it reduces Fe(III) to Fe(II), which is more soluble in water (Obata *et al.*, 1997).

The sensitivity was fluctuating and was on average similar to calibrations performed with the old batch of luminol. Variations in sensitivity and in the degree of curvature between experiments may be attributed to the changing degree of exposure of the photo-sensitive reagents to light, which may have increased the concentration of radicals in solution by decomposition of hydrogen peroxide and luminol (see Chapter II). It was also noted that there was occasionally an increase in the sensitivity of the signal over a

full day of analyses with increasing temperature in the laboratory. One standard was thus measured regularly during a day of analysis to monitor possible changes in sensitivity, and was subsequently used to eventually correct the calibration accordingly to ensure accuracy of the data (see Chapter IV). Bubbles were observed throughout the calibration and analysis procedures, and were evident as spikes in signal on the baseline. The bubbles generally did not significantly affect the peak area of measurements, however when they did, an additional replicate was measured to ensure quality of the data (see Chapter IV).

Blank and limit of detection values were improved using "fresh" Milli-Q water, but were still variable possibly due to the varying quality of that water and instability of the baseline. Uncertainty in blank estimation may increase because of shifts in the baseline between non-elution/elution stages. These shifts were due to changes of pH (data not shown) because of backpressure as the eluent was flowing through the preconcentration column. Furthermore double peaks observed when measuring the reagent blanks (data not shown) may be due to iron in the rinsing water, and made the blank determination difficult. Finally for unknown reasons, chronic instability of the baseline was observed especially at the end of the calibration (see below). It badly affected peak determination, and therefore analysis was ceased, and all data rejected.

It was very likely that the quality of luminol had been a major problem in obtaining a good calibration. However, whilst sample analyses were possible (see Table III.3), two problems remained which made the analysis and the determination of the blank value difficult: **i)** double peaks were often observed when measuring the reagent blank; and **ii)** the poor stability of the baseline with periodic shifts.

III.4.3. System improvements

III.4.3.1. Eliminating double peaks

Double peaks observed when measuring the reagent blanks may be due to: **i)** a pulse in the reagent flow when the injection valve was switched and the eluent passed through the resin in a reversed direction; or **ii)** the Milli-Q water remaining in the preconcentration column after the rinsing step, which passed to the flow cell. In the experiments to determine the sources of the blank described in Table III.1, peaks were much smaller during Experiment 1 (Figure III.10) or were often absent (data not

shown), suggesting that the first part of the double peak was not due to a pulse in the reagents flow. However the peak attributed to the Milli-Q water contribution during Experiment 2 of the experiment on the blank (Table III.1) appeared at the same timing as the first part of the double peak (Figure III.10). These results suggest that the Milli-Q rinsing water remaining in the void volume of the column was responsible for the first part of the double peak of the reagent blank due to its iron content or due to a chronic change in CL pH.

In order to minimise the aliquot of Milli-Q water remaining in the preconcentration column, a new configuration of the analyser was tested, based on the design of Johnson *et al.* (2003). These modifications involved adding a 6-port injection valve (IV2) with an elution loop in series with the existing 6-port valve (IV1) (Figure III.11) and both injection valves could be replaced by a 10-way injection valve for a more permanent change later on. Therefore after rinsing with Milli-Q water, iron was eluted from the 8-HQ resin column by the acid eluent and collected in the elution loop.

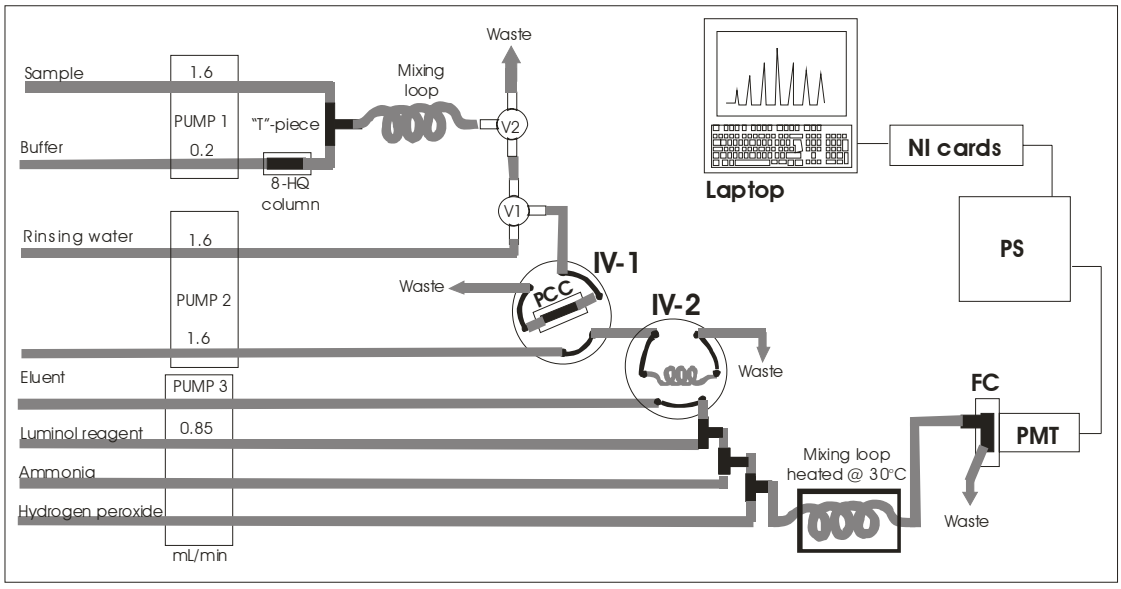

Figure III.11: Diagram of the Fe(II+III) FIA-CL analyser, based on the methods of Obata *et al.* (1993) and de Jong *et al.* (1998) after modification based on the method of Johnson *et al.* (2003). Thick grey lines represent PTFE or PVC tubing. PUMP 1 and PUMP 2 = low-voltage pumps; PUMP 3 = Gilson Minipuls peristaltic pump; V1 and V2 = Switching valves; IV-1 and IV-2 = Injection valves; PCC = Preconcentration column; FC = flow cell; PMT = photomultiplier tube; PS = Power supply; NI cards = National Instruments control cards.

Timing and elution loop length (optimum 0.5 m) were accurately determined by measuring peak area with different loop lengths and time (data not shown) so that most of the Milli-Q water was sent to waste without losing any of the eluted iron solution.

When IV2 was switched, the eluted iron solution was carried by the eluent to the PMT flow cell. This configuration lowered the blanks and also removed any steps in the baseline previously seen due to slowing of eluent through the column. The timing sequence of the new configuration (Table III.4) was complete in 262 s with a 60 sec loading step.

Sequence	Loading	Rinsing	Eluting	Detection & Rinsing	
Valve 1	ON	OFF	OFF	OFF	OFF
Valve 2	OFF	OFF	OFF	OFF	ON
Pump B	ON	OFF	OFF	OFF	ON
Pump C	OFF	ON	ON	ON	ON
IV1	Position A	Position A	Position B	Position B	Position A
IV2	Position A	Position A	Position A	Position B	Position B
Timing	60s	30s	22s	120s	30s

Table III.4: Timing sequence with the configuration based on the method of Johnson *et al.* (2003).

III.4.3.2. Stabilisation of baseline

Baseline noise and shifts were not expected to be caused by the electronics (*e.g.* light entering the PMT) since peak heights remained the same for replicate peaks despite baseline changes.

Changes in room temperature were unlikely to have caused the problem as such variations were slow relative to the often rapid baseline shifts. Additionally, the small shifts in temperature in the reaction coil heating system due to the thermostat did not correspond to observed baseline changes.

It was also unlikely that CL reagents would change their concentration with time, potentially changing the CL pH, and tubing flow rates were regularly checked. Build up of backpressure in the system and its rapid release may lead to a pH change if it occurred before CL reagents mixed and before the baseline shifts. However the problem remained despite checking the whole manifold for kinks or tubing obstructions, and changing the 5-way junction piece for three individual tee-pieces.

Further possibilities were that iron contamination from components or particles in solutions may create these periodic shifts and baseline instability. Unfortunately, nothing could be done concerning contamination from components except checking

them regularly and ensuring rigorous cleaning. To test if particles in the luminol reagent were responsible for the baseline instability, the luminol reagent was filtered in-line using an acid washed 0.4 μm polycarbonate filter unit fitted immediately after the Gilson pump. When the baseline shifted and became unstable, on filtering the luminol reagent the baseline slowly came back to its original level and stability (Figure III.12), indicating that the baseline problems were presumably due to small particles in the luminol reagent. These particles may be re-precipitated luminol, formed after dilution of the 0.1 M sodium carbonate stock solution to 0.04 M used in the final luminol reagent.

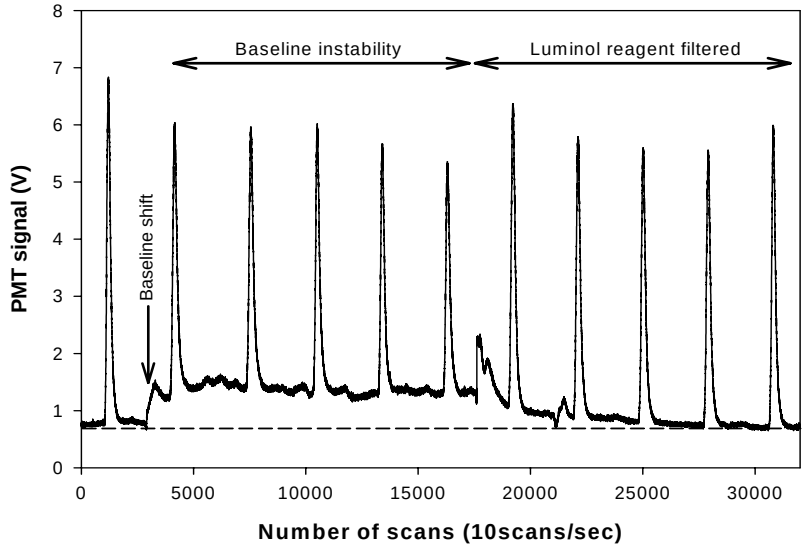

Figure III.12: Test for the effect of in-line filtration of the luminol reagent. Dashed line underlines the background baseline level (gain = 6).

III.4.3.3. Purity of water used to prepare reagents

At the beginning of the Fe(II) technique development, it appeared that using sub-boiled distilled (SBD) water to prepare reagents significantly lowered and stabilised the baseline compared to Milli-Q water stored in an aspirator. However if Milli-Q water was freshly taken, the baseline slightly increased and got noisier relative to when SBD water was used (Figure III.13), but remained reasonably low and stable compared to Milli-Q water stored in an aspirator. This may be either due to Milli-Q water slowly releasing contamination from the container walls or to the slow absorption of $CO_{2(aq)}$ with storage time which enhanced the CL reaction and thus the CL baseline. This experiment therefore showed that freshly taken Milli-Q water could be used instead of SBD water for the CL reagents, which was important for shipboard measurements, as significant quantities of water are used for each batch of reagents and SBD water is difficult to produce at sea.

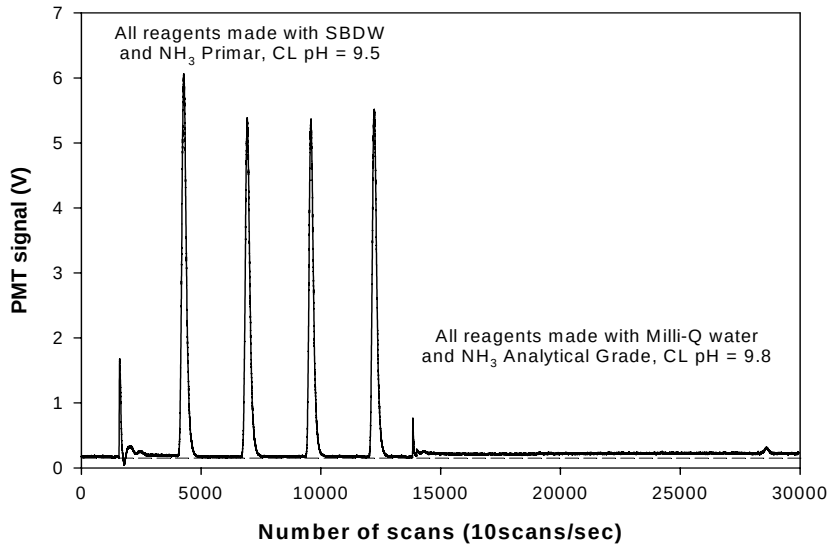

Figure III.13: Baseline level and stability using Milli-Q water instead of sub-boiled distilled water (SBDW) to prepare the reagents (Gain = 6). Dashed line indicates the underlying baseline level.

III.4.4. Comparison of data obtained using the Obata and Johnson configurations

Using the optimised system in the Johnson configuration, two linear (R^2 > 0.99) calibrations by standard additions gave NASS-5 values in the certified range (4.21 ± 0.07 nM and 3.76 ± 0.05 nM), and precision ranged from 0.4 to 7% rsd (average 3.1% rsd). Blank values were 125 and 20 pM with a limit of detection of 89 and 27 pM, respectively.

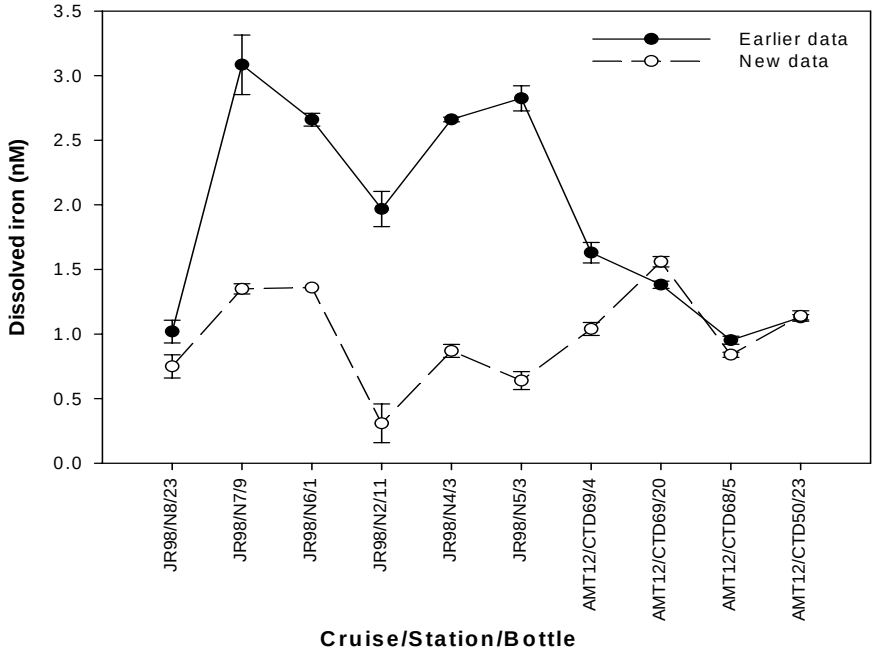

Figure III.14: Fe(II+III) concentration (nM) measured with the Obata system (closed circles) and with the new system configuration (open circles) for a sample of each profile previously analysed.

In order to test and validate earlier measurements obtained with the Fe(II)+(III) system in the Obata configuration, one sample from each profile previously quantified for iron with good precision (< 5% rsd), were re-analysed (Table III.3). The majority of the data in the two sets were different (Figure III.14). The new data were often lower than the previous data, inferring that contamination of samples during handling was not an issue. The values for NASS-5 obtained with the Obata configuration were often high with relatively poor precision (see Table III.3). These results suggest that there may have been a problem during earlier measurements with the Obata configuration, which may be due to the difficulty in estimating the blank when double peaks were observed.

As it was difficult and time-consuming at the time to determine what went wrong during earlier analyses, and since new data were obtained with a good NASS-5 value on this analysis event, it was decided to re-analyse all the samples using the optimised Fe(II)+(III) technique with the Johnson configuration, and the quality of the new data carefully checked (see Chapter IV). A full description of the optimised Fe(II)+(III) analyser is given in Appendix 7.

III.5. Figures of merit of the Fe(II)+(III) analyser

At this final stage of the development, the working Fe(II)+(III) analyser showed linear calibrations to up to 5 nM using standard additions of iron to acidified (pH ~ 2) filtered (< 0.4 μm) surface seawater collected in the Atlantic Ocean. Precision of measurements of standards ranged from 0.3% to 16.4% rsd (relative standard deviation, average 3.9% rsd) with a minimum of three replicate peaks. Blank values ranged from 20 pM up to 2.26 nM (average 490 pM), and the limit of detection from 27 pM to 474 pM (average 109 pM).

III.6. Summary

The Fe(II)+(III) FIA-CL technique set up here is based on the system of Obata *et al.* (1993) and de Jong *et al.* (1998). Given the extensive experience gained through working on the Fe(II) technique, the development and optimisation of this modified version to determine Fe(II) and Fe(III) in seawater was relatively rapid. However due to continuing problems with the baseline stability and blank level, the configuration of the

manifold was modified following the approach of Johnson *et al.* (2003) with the introduction of an elution loop. Modifications resulted in a lower blank value, which depended mainly on the quality of the Milli-Q water, and in significantly stabilising the baseline. The final Fe(II)+(III) FI-CL analyser gave linear calibrations tested to up to 6 nM, with good precision (< 5% rsd) using a 8-hydroxyquinoline resin prepared following the protocol of Landing *et al.* (1986) (courtesy of S. Ussher, University of Plymouth), and with reasonable blanks (average 540 pM) and limits of detection (average 121 pM) that allowed measurements of Fe in most oceanic and coastal environments.

The move to the Fe(II)+(III) analyser also allowed investigation of one of the problems encountered with the Fe(II) technique: the negative curvature of the calibration. The luminol was tested since it was the only component not previously changed or modified in the Fe(II) system. Although there had been no obvious reason to doubt the quality of this reagent, it appeared at this time that the luminol used was possibly degraded. It had a different colour compared to a new batch ordered from another company and this new batch had greater sensitivity with the Fe(II)+Fe(III) system, suggesting the old batch had been altered by light and/or oxygen contact. Several other workers using the flow-injection analyser with chemiluminescence detection shared this concern about the reliability of commercial luminol reagents (from P. Statham, 2005, personal communication). The question of to what extent the luminol was actually responsible for the problem with the calibration for the Fe(II) analyser has been addressed (see Chapter II); however results were not clear and due to time constraints further investigation was not possible.

The Fe(II)+(III) FIA-CL system was subsequently used to analyse samples collected in at the Celtic Sea edge. It was felt to be very important with this newly developed technique to demonstrate the precision, accuracy, and overall validity of the method. In the next Chapter, a rigorous assessment of data quality is carried out at two levels: the quality of the analyses and data of a certified seawater standard, and the quality of the data relative to high quality published data from similar marine waters.

CHAPTER IV.

DATA QUALITY

IV.1. Introduction

A major challenge in the development of a technique to determine dissolved iron at low concentrations in seawater is to demonstrate the quality of the data obtained with the method. Iron is a ubiquitous element and its analysis may be affected by contamination from many sources. Additionally the chemistry involved in the FIA-CL system is subject to small variations between batches, which may slightly change the response of the analyser so that quality of the analysis should be discussed for each new batch of reagent (Rose and Waite, 2001).

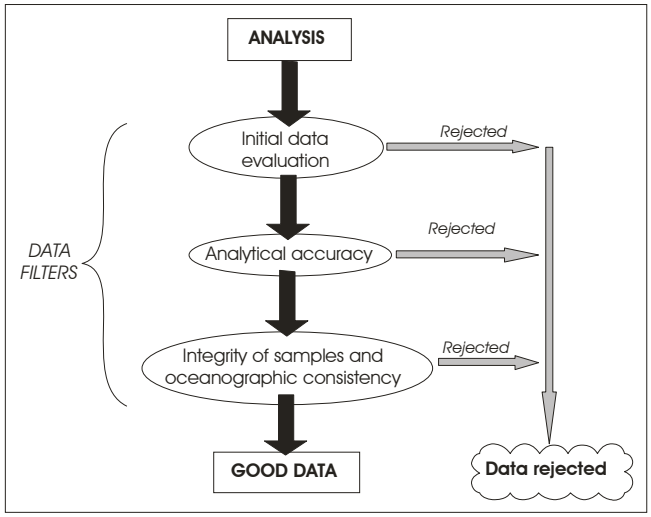

Figure IV.1: Diagram showing the procedure used to assess data quality.

A very rigorous data-quality check was carried out (Figure IV.1): **1)** an initial data evaluation was made by determining an approach to identify and assess the validity of outliers in the raw data, and by examining the figures of merit for the analyser and its variability; **2)** analytical accuracy was then considered using certified and internal seawater standards; and **3)** the quality of samples was discussed regarding problems of contamination during sampling and storage by comparing high quality data published in the literature and evaluating its oceanographic consistency. These checks were felt to be essential to ensure confidence in the data finally produced.

IV.2. Initial data evaluation

IV.2.1. Outliers

The first step in calculating the data was the determination of peak area. Occasionally, bubbles gave anomalous peaks raising the issue of identifying those peaks and deciding

whether they were valid. Gas bubbles were observed at the exit of the reaction coil where all the CL reagents met, which may be carbon dioxide formed by reaction of sodium carbonate (in the luminol reagent) with hydrochloric acid (eluent). It was shown that carbon dioxide significantly enhances the CL reaction (Xiao *et al.*, 2002) (see Chapter II). The gas may have been diffusing into adjacent segments of solution, locally enhancing the signal, which may explain why those peaks were much higher than replicates (see for example Figure IV.2). It was also observed that the larger the peak the larger the increase in the peak associated with bubbles.

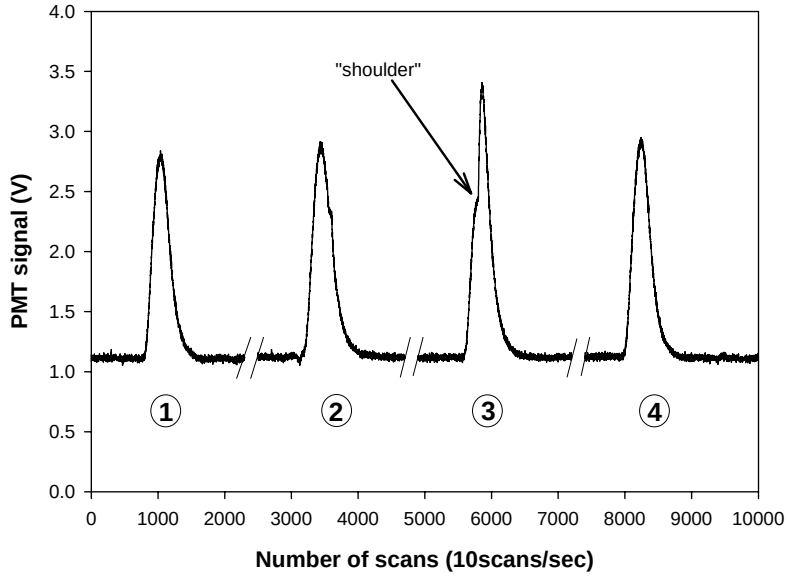

Figure IV.2: An example of the influence of gas bubbles in the liquid stream on replicate peaks. Peaks 1, 2 and 4 were reproducible whereas a shoulder was observed on Peak 3 as well as a bubble in the waste line. Baseline between peaks is shortened. [DFe] = 1.27 ± 0.05 nM excluding Peak 3.

Peaks affected by these bubbles could be recognised when processing the data, as their shape changed, with a "shoulder" in the peak (Peak 3, Figure IV.2), which increased the overall peak area. However, it was noted by experience that when bubbles appeared whilst the peak was decreasing (Peak 2, Figure IV.2) a drop in signal was observed before the shoulder so that the overall peak area was not changed. It was therefore decided that peaks showing a shoulder only whilst the signal was increasing (such as Peak 3) should be discarded provided that simultaneous bubbles were observed in the waste line. When a peak appeared to be affected by bubbles, an additional replicate was carried out to ensure the reproducibility of the signal without bubbles.

Anomalous lower peaks relative to replicates were also observed when no sample solution was pumped to the PMT because the tubing was not properly immersed into solution or all the solution had been consumed. Additional replicates were analysed after solving the problem.

Outliers may also be created during transcription of the data from the processing programme to the programme used for further calculations. However, in the LabView programme used for processing, peak area results were stored in a table that could be directly imported for calculation in another programme, therefore avoiding this type of error. Additionally all calculated data in spreadsheets were carefully checked before interpretation.

IV.2.2. Figures of merit for the analyser

The behaviour of the system during a long analytical sequence may change with time, due, for instance, to: **i)** increasing temperature in the laboratory which may enhance the sensitivity and induce more bubbles in the reagents stream; **ii)** potential contamination of the system after analysing a contaminated sample; **iii)** peristaltic tubing wear.

All calibrations were performed by standard additions of iron to low-iron seawater (LISW) to up to 6 nM following the procedure described in Chapter II.2, using a 1000 $mg.L^{-1}$ Fe AAS stock solution (Z-Tek). The figures of merit of the analyser were compiled after obvious problem data were removed (see Section IV.2.1). The Fe (II)+(III) FIA-CL system gave linear curves in this range with varying sensitivity (Table IV.1), depending on the loading time, and ageing of the luminol reagent. The loading time was modified (30s to up to 120s) in order to increase the sensitivity when low concentrations were expected for some profiles. Precision of measurements of standards ranged from 0.3% to 16.4% relative standard deviation (*rsd*), averaging 3.9% *rsd* (n = 85) with a minimum of three replicate peaks per standard (Table IV.1). Precision averaged 6.2% *rsd* for a total of 227 samples analysed (minimum n = 3, 0.2 to 49.4% rsd range). Precision of measurements was therefore satisfactory for all the analyses performed.

The main contribution to the blank was possibly from the rinsing water for the preconcentration column or from the components of the system (see Chapter III). The blank signal was relatively high on analysis events 11 to 14 and 16 (Table IV.1), which was found to be due to the poorer (17.8 – 18.0 MΩ.cm) quality of the Milli-Q water used for rinsing. Blank values ranged from 20 pM up to 2.26 nM (average 496 pM), and the limit of detection from 27 pM to 225 pM (average 90 pM). Blanks and limits of

detection could thus be improved in the future to achieve better performance of the system by using better quality rinsing water.

	R^2 *Range*	Slope	Precision *rsd* (*n=3-6*) (*average rsd*)	Blank (pM)	Limit of detection (pM)	NASS-5 ± sd (nM) (3.71 ± 0.63)	Samples analysed
1	0.997 *0.5-5nM*	221	0.4 – 5.4% *(2.5%)*	20	27 *(n=4)*	3.76 ± 0.05	
2	0.9994 *0.5-5nM*	120	2.4 – 8.4% *(4.5%)*	295	72 *(n=7)*	4.44 ± 0.14	AMT12/CTD 24/1-12
3	0.9988 *0.25-4nM*	212	1.2 – 3.8% *(2.7%)*	321	58 *(n=5)*	4.77 ± 0.03	AMT12/CTD 24/13-24
4	0.996 *0.25-4nM*	247	0.7 – 4.6% *(2.5%)*	110	28 *(n=8)*		AMT12/CTD 24/0.1µm-filtered
5	0.9979 *0.25-4nM*	314	1.4 – 5.6% *(3.1%)*	568	154 *(n=6)*		AMT12/CTD 39
6	0.9979 *0.25-4nM*	278	1.7 – 12.8% *(5.2%)*	143	76 *(n=5)*		AMT12/CTD 39/0.1µm-filtered
7	0.996 *0.25-4nM*	316	2.4 – 3.9% *(2.9%)*	179	63 *(n=8)*		AMT12/CTD 50
8	0.9996 *0.25-4nM*	475	1.3 – 6.5% *(3.5%)*	162	62 *(n=10)*	5.46 ± 0.01	AMT12/CTD 50/0.1µm-filtered
9	0.9985 *0.25-4nM*	450	1.5 – 3.4% *(2.6%)*	62	31 *(n=8)*	4.75 ± 0.04	AMT12/surf. samples
10	0.9955 *0.5-5nM*	263	1.3 – 5.3% *(3.4%)*	400	83 *(n=6)*	4.95 ± 0.02	JR80/surf. samples
11	0.9981 *0.5-5nM*	264	3.1 – 5.2% *(4.1%)*	746	128 *(n=6)*	4.70 ± 0.06	AMT12/CTD 68
12	0.9994 *0.5-5nM*	287	1.1 – 5.3% *(3.0%)*	848	73 *(n=3)*	5.17 ± 0.12	JR98/N8 & N9
13	0.9919 *0.5-6nM*	156	0.5 – 4.5% *(2.5%)*	679	225 *(n=8)*	6.66 ± 0.32	JR98/N7
14	0.997 *1-6nM*	203	1.0 – 16.4% *(8.1%)*	2260	130 *(n=3)*	5.41 ± 0.20	JR98/N1
15	0.9942 *1-6nM*	139	0.6 – 8.1% *(5.0%)*	177	32 *(n=3)*	5.03 ± 0.06	JR98/N6
16	0.9911 *1-5nM*	232	1.9 – 11.8% *(5.7%)*	1022	133 *(n=5)*	3.53 ± 0.09	JR98/N4
17	0.9994 *0.5-5nM*	286	0.3 – 8.4% *(4.8%)*	447	163 *(n=4)*	3.63 ± 0.14	JR98/N5 & N2 & N3

Table IV.1: Provisional figures of merit of calibration curves used to determine sample concentrations for each analysis event (first column). Precision is based on 3 to 4 replicate peaks of the standards and is one standard deviation. Limit of detection is defined as three times the standard deviation of the blank. No NASS-5 was available on analysis events 4 to 7.

Three data points were removed from the JR98 data set from Stations N3 (2 m-depth and 15 m) and N5 (20 m) since the iron concentrations in these samples were below detection limit. Figures of merit were adequate to use the method in many marine environments where concentrations fall within the analyser.

IV.3. Analytical accuracy

IV.3.1. NASS-5 certified reference material

The certified reference material used in this project was North Atlantic Surface Seawater (NASS-5, from the National Research Council of Canada) with an iron concentration of 3.71 ± 0.63 nM (95% of individual sub-sample concentrations fell within this range) certified after analysis by many laboratories worldwide using different techniques. When the iron value measured fell in this range, the analysis performed was considered as accurate, such as on analysis events 1, 16 and 17 where values were 3.76 ± 0.05 nM, 3.49 ± 0.08 nM and 3.63 ± 0.14 nM (± 1*sd*) respectively (Table IV.1 and Figure IV.3). However when the iron value did not fall in the range, the quality of the analysis was questionable unless a valid argument was given for the difference. The average iron concentration for all the NASS-5 analyses was 4.80 nM (*n* = 53) which corresponded to a mean enrichment of 1.1 nM relative to the certified value. The cause for these high iron values of the NASS-5 was therefore investigated.

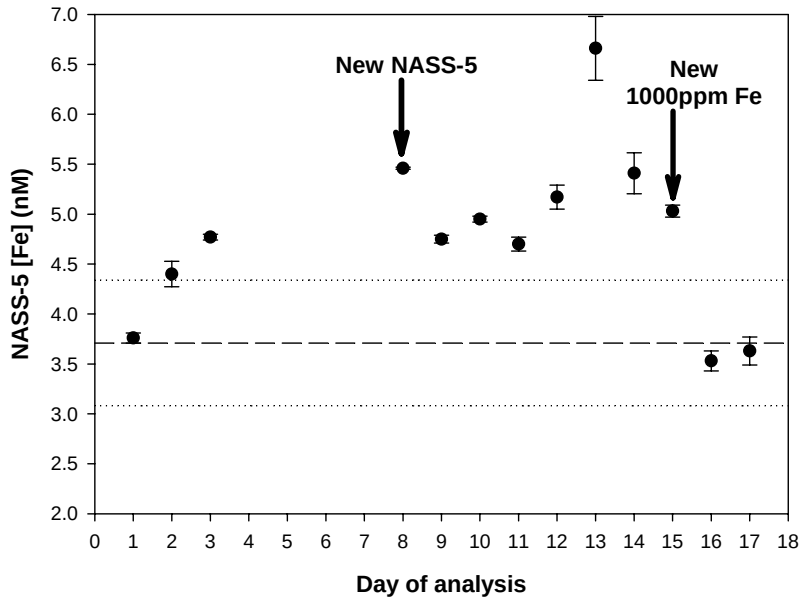

Figure IV.3: NASS-5 iron concentration (nM) determined during each analysis event (in chronological order). The dashed line represents the certified value (3.71 nM) and the dotted lines represent the lower (3.08 nM) and top (4.34 nM) limits of the 95% confidence range of the certified value.

The NASS-5 concentration is certified for 10 years, and it had been stored heavily acidified with nitric acid for at least 6 years at the time of analysis; therefore the concentration is not expected to have significantly changed from the certified value. Moreover, high values were still obtained even though a new bottle of NASS-5 seawater was used from analysis event 8, suggesting that it was not due to internal contamination (Figure IV.3). As the NASS-5 is highly acidified (pH ~ 1.6), it was found that the loading pH was often lower than for standards and samples (pH ~ 2). However,

this would only provide an explanation for low values if not all the iron was being loaded onto the resin, and does not explain the high values observed. Additionally, the preconcentration and detection steps are independent; the chemiluminescence reaction is therefore not influenced by a change in the loading pH. The 8-hydroxyquinoline resin used was provided by the team at the University of Plymouth, and was therefore considered as reliable, and did not generate an obvious blank (see Chapter III). Whilst blank values varied significantly between analysis events, the blank measurements made at the beginning and end of the analysis events showed that the blank value did not change through that particular analysis event (*e.g.* Table IV.2).

Analysis event	Blank value before calibration	Blank value after samples
5	0.58 ± 0.06 nM	0.57 ± 0.05 nM
8	0.16 ± 0.02 nM	0.21 ± 0.01 nM
17	0.45 ± 0.05 nM	0.47 ± 0.01 nM

Table IV.2: Examples of the blank value before the calibration and after all samples for three analysis events as presented in Table IV.1. Precision is 1 standard deviation.

One possible explanation for the high NASS-5 values is that the calibration slope was too low. However, it was very unlikely that the 1000 $mg.L^{-1}$ iron stock solution was diluted, and any evaporation or contamination of the Fe stock solution would give a NASS-5 iron value lower than expected, not higher as observed. Based on the assumption that the sensitivity of the analyser is increasing linearly with preconcentration time, calibration slopes were normalised at 1 min loading time. No relationship was found between the NASS-5 iron concentration and the normalised calibration slopes (data not shown), suggesting that high NASS-5 values were not due to changes in the response of the analyser. Moreover, the NASS-5 iron concentration remained high on analysis event 15 even though a brand new 1000 $mg.L^{-1}$ Fe stock solution was used (Figure IV.3).

The last hypothesis for these high values was external contamination. The NASS-5 seawater may have been subject to low levels of contamination while being poured in the sterile polystyrene tubes used for analyses or the tubes may have had residual contamination for iron. The heavily acidified NASS-5 seawater may also have released some iron from the manifold Teflon tubes internal wall or from the peristaltic pump PVC tubing. This assumption is based on the observation that 1 M HCl solutions were

used to acid wash the system overnight and were efficient to remove iron from the manifold as blanks were significantly lower after such a procedure.

Despite its high iron concentration, the NASS-5 is generally useful to demonstrate the accuracy of an analyser. However, its high acidity raises questions about occasional external contamination during handling, leaching from the manifold tubing and/or containers. It was therefore important to have an alternative way of evaluating the reliability of the response of the analyser.

IV.3.2. Low-iron seawater internal standard

An internal low-iron seawater standard (LISW-IS) was used to monitor changes in sensitivity of the analyser as well as giving another indicator of the reliability of the system. This LISW-IS was unfiltered surface seawater collected in the Northeast Pacific Ocean, and stored unacidified in a cubitener. It was acidified by adding 1 mL of Q-HCl per litre of seawater before use. This internal standard had the double advantage of: **i)** being acidified to the same degree as standards and samples, minimising changes in the loading pH; and **ii)** of having a lower concentration than NASS-5 seawater. The LISW-IS was generally analysed on four occasions during each day of analysis: after the blank, after the NASS-5 seawater, between and after samples (see procedure in Appendix 9).

Measurements showed that the signal was relatively reproducible during a single analysis event, suggesting no change in the sensitivity except on event 10, and on analysis event 13 where LISW-IS iron values were higher than previous events (Figure IV.4). There may thus have been a continuous increase in sensitivity on event 10, and a shift in the data on analysis event 13. Omitting values on analysis events 10 and 13, total dissolvable iron concentrations measured for the LISW-IS averaged 0.98 ± 0.17 nM (17% *rsd*, $n = 49$) (Figure IV.4).

Whilst the NASS-5 iron concentration was higher than the certified value except on analysis events 1, 16 and 17 (Figure IV.3), the internal standard did not show any significant difference in the signal on analysis events 16 and 17 compared to previous days (Figure IV.4). Moreover, no simple relationship was found between LISW-IS and NASS-5 measured iron concentrations (data not shown) suggesting that the factor

causing higher NASS-5 values was not impacting upton the LISW-IS values. Values outside the range of the relative standard deviation (*i.e.* 17%) were analysed on analysis events 10 and 13 (Figure IV.4). Reproducible inter-batch measurements of the LISW-IS gave confidence in the reliability of the response of the analyser despite over the range values for the NASS-5 seawater.

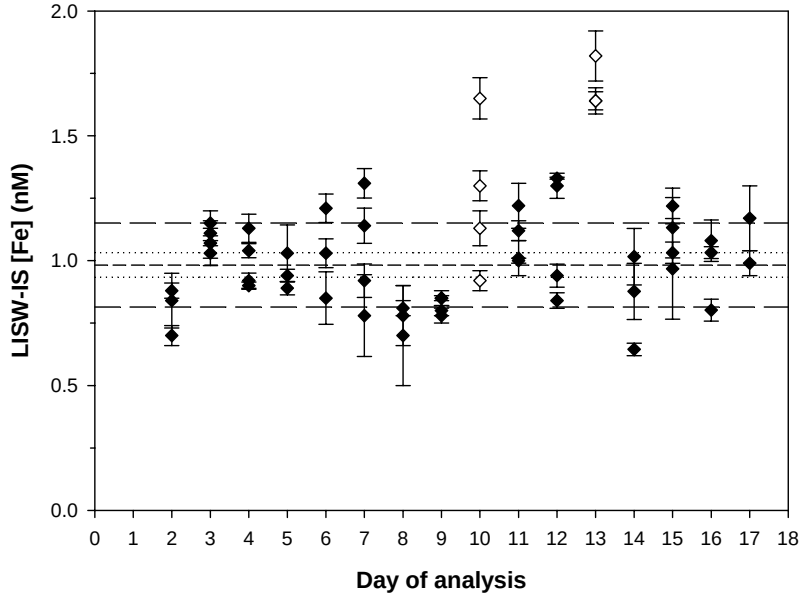

Figure IV.4: Total dissolvable iron concentrations (nM) of the low-iron seawater internal standard (3-4 replicates) with time. Lines represent: — — — mean value (0.98 nM); − − − 1 standard deviation (± 0.17 nM); ····· 2 standard deviations (± 0.34 nM). Suspect values on analysis events 10 and 13 are shown as open diamonds.

The way in which to process data from analysis events 10 and 13 was addressed.

On analysis event 10, the peak area for LISW-IS measured 4 times during the day increased linearly (R^2 = 0.986) with time (Figure IV.5), suggesting that all the data would be affected by this change in sensitivity. Data could thus be corrected using the equation given by the increasing LISW-IS signal with time. However, the NASS-5 value remained high despite correction (4.76 ± 0.02 nM) suggesting that increasing sensitivity was not responsible for the high NASS-5 value obtained on that event.

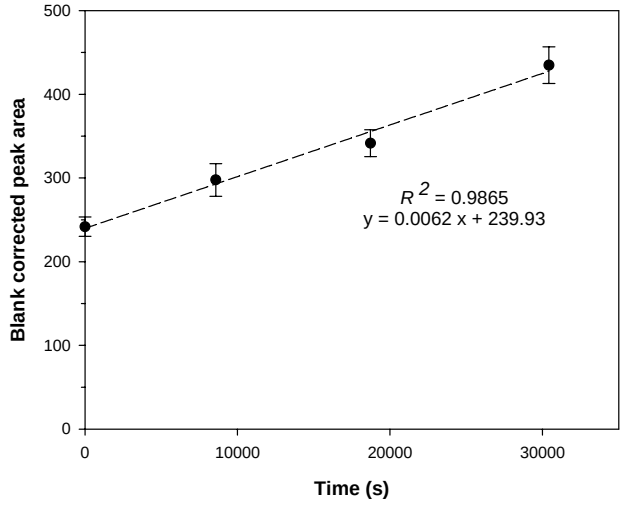

Figure IV.5: Blank corrected peak area of low iron seawater internal standard (LISW-IS, 0.99 ± 0.17 nM) with time (0 – 8h20) during analysis event 10.

On analysis event 13, all LISW-IS concentrations (average 1.7 ± 0.10 nM (1*sd*)) were on average 0.7 nM higher than the mean value (0.98 ± 0.17 nM). The NASS-5 value was unusually high on analysis event 13 (Figure IV.3). These results indicate a shift in the data, which could eventually be associated with a problem with the standards on that day. All data analysed on analysis event 13 was thus normalised (= concentration x 0.98 / 1.70) to the LISW-IS mean value (0.98 ± 0.17 nM).

At this stage, it was decided to correct data from analysis event 10 for the change in sensitivity with time. Data from analysis event 13 were normalised to the value expected for the internal standard and re-analysis another day indicated that this data was then acceptable (see below).

IV.3.3. Re-analysis of some samples from the Celtic Sea and Atlantic Ocean

An additional means of assessing the analyser reliability was to perform an inter-batch sample determination, where a selection of previously analysed samples were re-analysed on different analysis events. Data from three such sets of samples are shown here: **a)** the *JR98* cruise samples were collected during a transect across the Celtic Sea shelf edge (Northeast Atlantic) from N1 the most inner-shelf station to N9 the most off-shelf profile (see Chapter V); **b)** a set of surface samples were collected between the Falkland Islands and South Georgia (Southern Ocean) using a pole sampler during the cruise *JR80* (see Chapter V); and **c)** five profiles were also analysed from the *AMT-12* transect (Atlantic Ocean) as well as surface samples between the Equator up to 40^{o}N (see below). The procedure was carried out on several occasions, and data are shown in detail in Appendix 8.

Results are presented in Figure IV.6 as the difference between measurements of a same sample during two analytical events as a percentage of the mean of the two values (P%). Precision on individual measurements was very satisfactory when below 5% however precision may become poorer (to up to 10%) with lower concentrations or when more bubbles are created in the flow stream. The evaluation criteria were thus as follows: measurements with P% < 20% are reproducible, however the reproducibility is poor when P% > 20%. Values shown with open symbols in Figure IV.6 included a determination during analysis events 10 or 13 where data needed correcting for drift or offset. Overall, these results showed that there were small variations between analysis

events but data was reproducible. Inter-batch results thus gave further support that data were affected by a shift on analysis event 13.

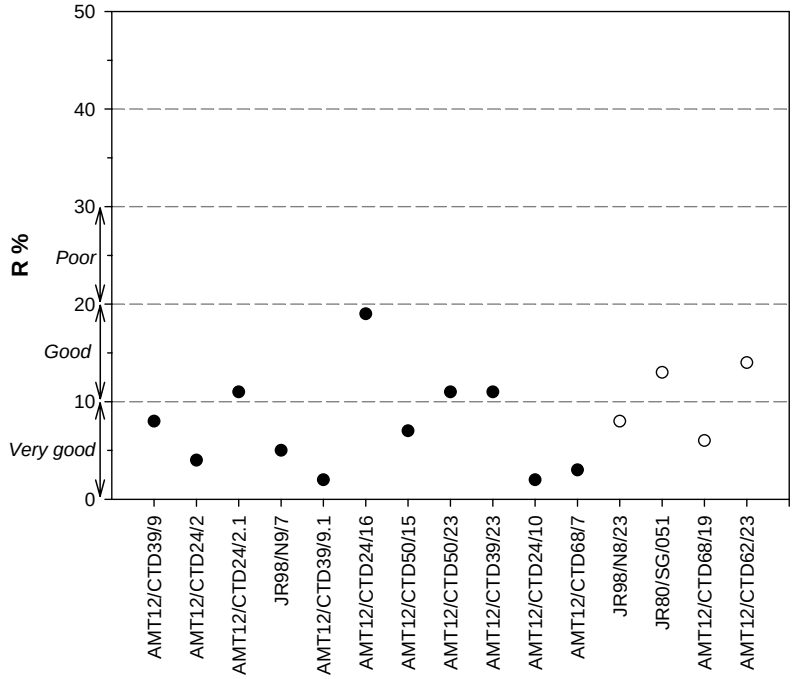

Figure IV.6: Difference between measurements of a same sample during two analytical events as a percentage of the mean of the two values (P%). Data analysed on event 10 was corrected for the change in sensitivity and on event 13 (see Table IV.1), the concentration was normalised to the low-iron seawater internal standard mean value (open symbols). Samples label = Cruise/Station/ CTD Bottle(/0.1μm filtered).

The inter-batch data check showed that after normalisation of the data on analysis event 13, most of the selected sample data showed satisfactory inter-batch agreement. A further check was the oceanographic consistency of the data from event 13 (see below). Samples from the *AMT-12* cruise were often found to have unexpectedly high concentrations. Since the analytical quality of the data appeared good, as demonstrated in this Section, the integrity of these samples was called into question.

IV.4. Integrity of *AMT-12* samples and oceanographic consistency

IV.4.1. Contamination potential during sampling

One of the challenges in measuring iron in seawater is to avoid contamination before analysis. It is therefore crucial to be aware of all potential sources and risks of contamination in order to be able to prevent as well as isolate them. All the cleaning, sampling, and handling procedures within this project were carried out following procedures that had been previously used at the National Oceanography Centre, Southampton (see below). A review of the sampling and pre-treatment techniques allowed identification of potential sources of contamination, which was useful in the attempt to explain the unexpected results obtained with the *AMT-12* samples.

IV.4.1.1. Sampling for iron

During sampling, contamination risks may vary depending on the device used to collect seawater, and the main source of contamination is without doubt the ship itself. A CTD rosette was built to minimise trace-metal contamination and was made from Titanium and plastic, with the sensors all being housed in titanium cases without any zinc sacrificial electrodes. Even though the CTD cable was made of steel, it was assumed that any contribution of the cable would be highly diluted by the surrounding currents. Additionally even stainless steel CTD systems have been used to collect good samples for iron (Statham *et al.*, 2005). The 10L Teflon coated Ocean Technology Equipment (OTE) Niskin style bottles were adapted to minimise metallic components and potential contamination. They were acid-washed before use at sea and thoroughly rinsed with ambient seawater before collecting samples for analysis. Between casts, the Titanium CTD rosette was protected from particles generated from the ship with a plastic cover. The OTE bottles were carried to the clean container laboratory wearing latex powder-free gloves and without touching the Teflon taps.

An alternative sampling device allowed collection of surface seawater samples. A “pole sampler” (Sherrell and Boyle, 1988) was used during the *JR80* cruise where a bottle was employed to collect unfiltered samples which were then poured directly into storage bottles. However as the “pole sampler” was not available during the *AMT-12* cruise, a “dipper” was built onboard by Richard Phipps (UKORS), using a plastic tube that held a 500mL bottle, with weights at the bottom isolated in plastic bags (Figure IV.7).

Figure IV.7: **a)** The "dipper" with a 0.5 L LDPE bottle (18 cm-height); and **b)** The "dipper" seen from above.

The "dipper" was thrown over board as the ship was slowing down when arriving on station. The bottle was rinsed two times with seawater before taking the sample. Samples were then filtered using an acid-washed polysulfone filtration unit. It was found during the ulterior *CROZEX* cruise that surrounding surface waters around the ship could be contaminated by iron while on station, and that operations such as washing the anchor may also result in the release of iron into surface waters. It is therefore crucial to plan the surface water sampling carefully considering the ship's operations.

IV.4.1.2. Sample processing

Risks of contamination are also high during sample handling and pre-treatment. Scientists going to sea to study trace metals in seawater nowadays have a separate working environment, a trace-metal clean container where the air is filtered as in a clean room. The walls are coved and lined with plastic, and exposed metallic components are minimised through choice of materials and appropriate coatings. Contamination problems may then be reduced during sample handling even though "accidents" may still occur such as the contamination of the quartz distilled acid used to acidify samples or whilst pouring the sample into a container for analysis. It is therefore important to minimise these handling steps, which can partially be achieved through use of flow-injection techniques coupled to an in-line sampling device such as an underway Fish sampler (Vink *et al.*, 2000; Bowie *et al.*, 2002a; Croot and Laan, 2002).

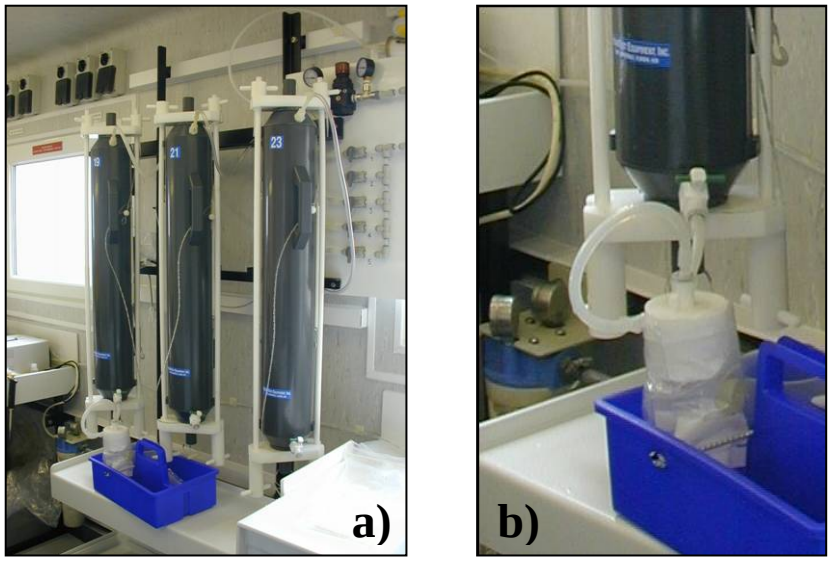

Figure IV.8: **a)** OTE bottles set up for filtration; **b)** Detail showing in-line filtration of sample.

Sample filtration may also potentially be a source of contamination. In the container the OTE bottles were held on a rack, a Teflon external frame was used to clamp top and bottom valves shut, and the bottles were pressurised using a filtered compressed nitrogen to about 0.9 atmospheres (Figure V.8a). Samples were filtered in-line using acid-washed silicone rubber tubing with Teflon connections and acid-washed Teflon filter holders and were directly poured in the storage bottle after rinsing with ample seawater (Figure V.8b).

All filters were acid-washed in a 10% quartz-distilled hydrochloric acid bath for several hours and then thoroughly rinsed with sub-boiled distilled water before use. During the *AMT-12* cruise, half of the filters used were Cyclopore® filters (Fisher Scientific) and half were PVP-free Poretics® filters (Poretics Ltd.). It was found during the cruise that the PVP-free Poretics® filters were actually hydrophobic, and had therefore to be wetted with few micro-litres of absolute 99% ethanol. When those filters were used, an additional rinsing step was carried out in order to ensure that all the ethanol was eliminated. During the *JR98* cruise, all filters were hydrophilic Cyclopore® (Fisher) to minimise potential risks of contamination during filtration.

IV.4.2. Storage of samples

Since it did not prove possible to analyse all samples directly on-board ship, they had to be preserved which raised the question of risks of contamination during the storage period. Samples for trace-metal analysis were stored in acid-washed low-density polyethylene (LDPE) bottles (Nalgene®, Fisher Scientific UK), which are low in trace metals and resistant to strong acids, and therefore can be thoroughly acid-washed to allow storage of open ocean waters (Moody and Lindstrom, 1977).

The standard procedure for acid washing the bottles was used (Moody and Lindstrom, 1977; Achterberg *et al.*, 2001). Low-density polyethylene bottles were first rinsed with reverse osmosis water and left three days in a 10% Micro® bath to dissolve greases that may remain after manufacture. They were then thoroughly rinsed with Milli-Q water and left for three days in a 50% hydrochloric acid bath. They were then rinsed again three times with Milli-Q water and left for three days in a 50% nitric bath. They were finally rinsed three times with Milli-Q water and then two more times with sub-boiled distilled water in a clean room, were left to dry and then were double zip-bagged. This

procedure was followed for all the new LDPE bottles received from the manufacture. As a large number of bottles had to be washed in a short period of time, the times for the acid-wash procedure normally used at the NOCS were reduced to three days in each bath instead of a week.

Most samples used for trace-metal analysis are acidified at pH ~ 2 in order to keep them in solution and avoid losses by adsorption onto the internal walls of the storage bottle (Moody, 1982). It is generally assumed that this procedure should not change the sample concentration in trace-metals for long-term storage. During this project, several LDPE bottles, which contained acidified samples collected during previous cruises, were recycled to store new samples collected during the *AMT-12* cruise. These bottles were emptied then thoroughly rinsed with Milli-Q water before going into the 50% hydrochloric acid bath as described above. It should be noted that "new" bottles and "recycled" bottles were kept separate during the procedure and had a different shape, so that they could be clearly identified.

More than a year after collection, a set of samples was analysed for dissolved iron. However some of the samples stored in "recycled" bottles showed abnormally high dissolved iron concentrations (Section IV.4.3). Despite uncertainties in some aspects of the quality of the analysis (Section IV.2 and IV.3), analytical problems were unlikely solely responsible for these unexpected results, therefore the quality of these stored samples was called into question, addressing an issue not in the literature regarding the "memory" of storage bottles. Given suspicion about some of the samples, some criteria were needed to evaluate whether samples were clearly contaminated or not. This was achieved by comparing the data obtained to high quality data and checking their oceanographic consistency.

IV.4.3. Oceanographic consistency of the AMT-12 data

The first *AMT-12* profile to be analysed was collected in the South Atlantic gyre (CTD 24, 20.5^{o}S, 25^{o}W; Figure IV.9). This region was assumed to be very low in dissolved iron as it is not supplied by any major dust storm and is far from any land (Duce and Tindale, 1991). Samples filtered through 0.4 μm membranes were stored in 1 L "recycled" LDPE bottles and 0.1 μm filtered samples were stored in 500 mL "recycled" LDPE bottles.

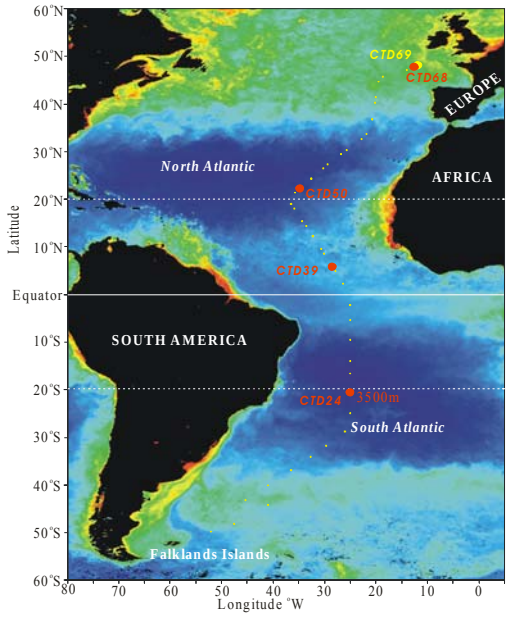

Figure IV.9: Location of profiles collected during the Atlantic Meridional Transect (*AMT-12*) cruise in May-June 2003 that were analysed for total dissolved iron.

During analysis of samples from CTD24, the signal detected saturated the PMT, and was estimated at more than 10 nM for 7 samples (Figure IV.10a). These levels of dissolved (DFe, < 0.4 µm) iron can be found in coastal waters where the major source of iron is sediment re-suspension (Hong and Kester, 1986; Bucciarelli *et al.*, 2001), but are highly unlikely in open ocean waters far from any land influence. In deep waters of open ocean profiles, total dissolved iron concentrations were reported to be 0.6 – 0.7 nM (Johnson *et al.*, 1997). However most of the deep samples here contained high dissolved Fe (≥ 1.5 nM) except at 3500 m and 3300 m depths where concentrations were plausible for both size fractions (Figure IV.10a). These results therefore suggest that these samples were contaminated for iron, and also for aluminium (Mahmoud, 2005, personal communication).

Contamination from OTE sampling bottles was unlikely since, for example, the 400 m and 1900 m depth samples were highly contaminated in iron in the < 0.4 µm fraction but not in the < 0.1 µm fraction whereas both size fractions were sampled from the same OTE bottle. The filters or filter holders may have been contaminated during the samples filtration. One Teflon® filter holder was used for the 0.4 µm filters and the other for 0.1 µm filters, as this latter filtration was much slower. Frits in the filter holders were checked for particles each time filters were changed in the laminar flow hood. Samples were filtered from the deepest to the shallowest, and filters were not always changed for each sample. However there was no sign in the data of contamination building up or of transfer of contamination from one sample to the other.

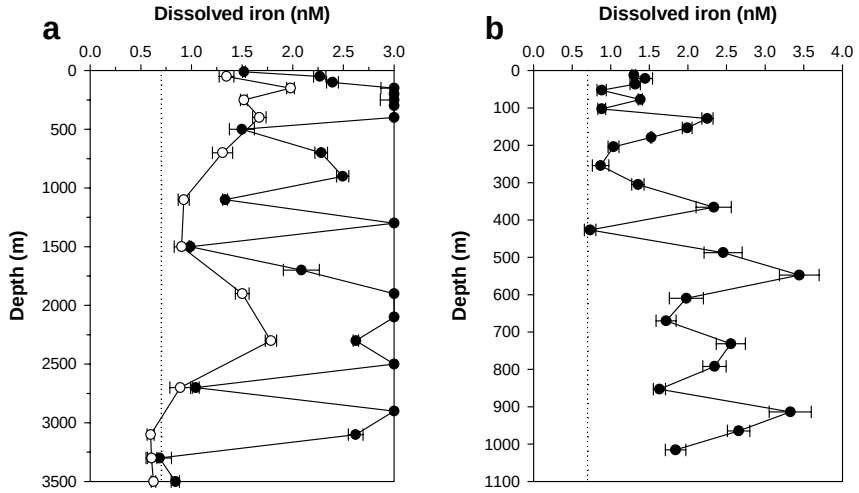

Figure IV.10: Dissolved iron (nM) concentration in < 0.4 μm (filled circles) and < 0.1 μm (open circles) size fractions in seawater samples collected at **a)** CTD24 (20.5°S, 25°W) in the South Atlantic Gyre (concentrations ≥ 3 nM are shown at 3 nM); and **b)** CTD69 (48°N, 12°W) in the Northeast Atlantic Ocean during the *AMT-12* cruise. The dotted lines (0.7 nM) indicate the average dissolved iron concentration found in deep waters of the open ocean (Johnson *et al.*, 1997).

The next step in sample processing was the sample acidification, which was carried out after all samples were filtered "on the assembly line". It was therefore unlikely that contamination occurred during this stage of the sample pre-treatment as it would be expected to affect all samples to the same degree, and not to be random if the acid was contaminated. Additionally samples from 3500 to 1300 m depth were analysed twice and showed both times that same samples were highly contaminated suggesting that contamination did not occur during analytical handling steps. At this stage, the only logical explanation was therefore that contamination of the samples occurred during storage in "recycled" bottles.

The profile from CTD69 was analysed earlier in the project (Figure IV.10b), using the Fe(II+III) FIA-CL system with the Obata *et al.* (1993) configuration (Appendix 6). This profile was not re-analysed using the finalised version of the analyser as it was already suspected of being contaminated because of the high variability of the data and elevated values of 0.9 nM to 3.4 nM (Figure IV.10b). The CTD69 profile was collected offshore and was therefore not under direct influence of the continental shelf system. In general, the reported DFe distribution in open ocean waters was found to be nutrient-like with a minimum at the chlorophyll *a* max, a sub-maximum of up to 1.4 nM at the oxygen minimum, stabilising to an average of about 0.7 nM in deep waters (Johnson *et al.*, 1997). The CTD69 DFe distribution did not show this pattern and concentrations were higher, although the distribution of dissolved aluminium did not appear subject to

contamination (Mahmoud, 2005, personal communication). Despite a small increase on beam attenuation between 320 and 730 m, the variability in DFe could not be correlated to any of the other oceanographic parameters (*i.e.* temperature, salinity, dissolved oxygen, fluorescence). These samples were stored in 500 mL "recycled" LDPE bottles, and were thus suspected of random contamination for iron from the storage bottles, although these bottles appeared significantly less contaminated than the 1 L bottles used to store samples from CTD24.

Three more profiles (CTD39, CTD50 and CTD68) from the *AMT-12* cruise that were stored in "recycled" LDPE bottles were analysed, as well as surface samples between the Equator and 40°N (see Figure IV.9). The DFe (< 0.4 μm and/or < 0.1 μm fractions) distributions for each of these profiles are shown in Figure IV.11**,** and the transect of surface samples is shown in Figure IV.12.

Profile CTD39 (6°N 28.5°W) was collected in the Equatorial Atlantic during the *AMT-12* cruise. It was located in the inter-tropical convergence zone well known for its intense rain events (as high as 2 $m.yr^{-1}$), which significantly influence the trace metal budget and chemistry of surface waters (Helmers and Schrems, 1995; Sarthou *et al.*, 2003). Profile CTD50 (22°N, 35°W) was collected in the Oligotrophic North Atlantic Gyre during the *AMT-12* cruise, in a region affected by episodic Sahara dust storms (Duce and Tindale, 1991). Reported data in the literature show that iron concentrations significantly increase when subject to such events (Bowie *et al.*, 2002b; Sarthou *et al.*, 2003).

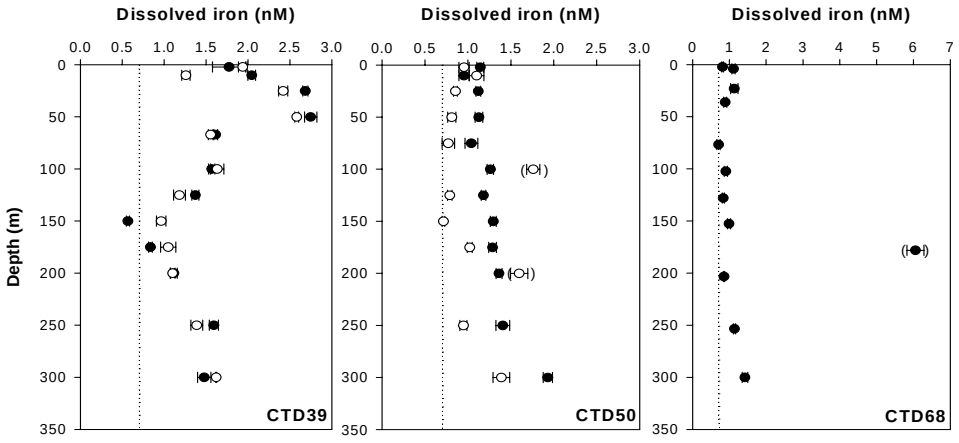

Figure IV.11: Dissolved iron (nM) distribution in the Equatorial Atlantic (CTD39, 6°N 28.5°W), the North Atlantic Gyre (CTD50, 22°N 35°W), Northeast Atlantic (CTD68, 47.7°N 12.7°W). Filled circles are < 0.4 μm fraction and open circles are < 0.1 μm fraction. Brackets indicate samples contaminated for iron.

Each of the profiles analysed was compared to the few high quality data published (Table IV.2). Bowie *et al.* (2002) suggested that in low-Suspended Particulate Material (SPM) waters, total dissolvable (TDFe) iron values were not significantly different from dissolved (< 0.2 μm) values. However, in high-SPM waters, TDFe concentrations could be much higher than that of the "dissolved" (< 0.2 μm) fraction (Bowie *et al.*, 2002b). Since published data included iron concentrations in different fractions, this information was used to facilitate the interpretation.

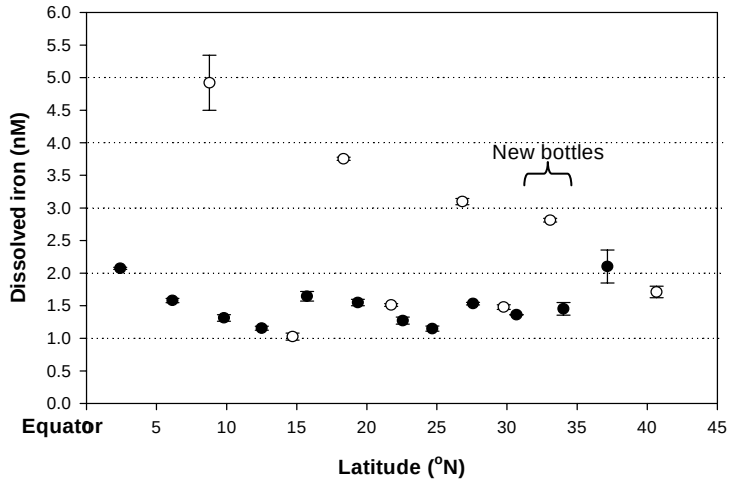

Figure IV.12: Dissolved iron (< 0.4 μm, nM) distribution in North Atlantic surface (2m) waters (0 to 40°N). Open circles indicate samples collected with the "dipper" as described in Chapter IV.

Variability in the iron data will also depend on which size fraction of the iron pool is studied (Table IV.3). In this study, the iron level in the < 0.1 μm fraction was found to be higher than the < 0.4 μm fraction at several depths of profiles CTD39 and CTD50 suggesting that these samples were subject to low levels of contamination (see Figure IV.11). In both profiles, the < 0.1 μm fraction iron signal seemed to follow the same trend as the < 0.4 μm fraction, representing respectively on average 90% and 70% of the < 0.4 μm fraction for CTD39 and CTD50 respectively, when contaminated samples were excluded, which is consistent with recent published results (Wu *et al.*, 2001). Additionally, recent analyses suggested that these samples were not subject to contamination for Al (Mahmoud, 2005, personal communication). Even though the < 0.4 μm data fell in the range of other reported data (see Table IV.3), it was difficult to confirm the overall quality of this data at this stage, as some samples from CTD24 stored in "recycled" bottles were clearly subject to random contamination for iron, as shown above.

Station Name Location	Size fraction	Depth (m)	[Fe] range *(mean)* (nM)	Reference
CTD39, 6°N, 28.5°W	**< 0.4 μm < 0.1 μm**	**2 – 300**	**0.6 – 2.7 *(1.6)* 0.9 – 2.6 *(1.5)***	***This study***
8°N, 45°W	< 0.4 μm	0 – 400	0.5 – 3.1 *(1.8)*	(de Baar and de Jong, 2001)
5°N, 24°W	Dissolvable	7 – 200	0.3 – 1.5 *(0.6)*	(Bowie *et al.*, 2002b)
CTD50 22°N, 35°W	**< 0.4 μm < 0.1 μm**	**2 – 300**	**0.9 – 1.9 *(1.2)* 0.7 – 1.8 *(1.0)***	***This study***
20°N, 20°W	Dissolvable	7 – 200	0.3 – 3.5 *(1.5)*	(Bowie *et al.*, 2002b)
CTD68 48°N, 13°W	**< 0.4 μm**	**2 – 300**	**0.7 – 1.4 *(1.0)*** ***excluding 6nM data***	***This study***
47°N, 20°W	< 0.4 μm	20 – 100 150 – 2900	0.07 – 0.2 *(0.16)* 0.3 – 0.6 *(0.5)*	(de Baar and de Jong, 2001)
45°N, 14°W	Dissolvable	7 – 100 250 – 1000	0.7 – 1.3 *(0.9)* 0.5 – 0.9 *(0.8)*	(Bowie *et al.*, 2002b)
0 – 40°N	**< 0.4 μm**	**0.5 – 2**	**1.0 – 4.9 *(1.9)***	***This study***
Off Africa 0 – 30°N	Dissolvable	0.5 – 1	0.5 – 10 *(4.0)*	(Powell *et al.*, 1995)
Off Africa 52°S – 50°N	Dissolvable	7	0.3 – 2.5 *(1.0)*	(Bowie *et al.*, 2002b)
Off Africa 15°S – 50°N	Dissolvable	7	0.4 – 2.2 *(1.0)*	(Bowie *et al.*, 2002b)
16°S – 5°N	< 0.2 μm	1	0.4 – 1.4 *(0.7)*	(Vink and Measures, 2001)
0 – 5°N	< 0.2 μm	1	0.3 – 0.7 *(0.55)*	(Powell and Donat, 2001)
Off Africa 5°N – 27°N	< 0.2 μm	1	0.2 – 1.1 *(0.4)*	(Sarthou *et al.*, 2003)

Table IV.3: Comparison of published iron concentrations with the *AMT-12* data from this study. Surface samples collected Off Africa (last part of Table) were taken close to the African continent.

Profile CTD68 (48°N, 13°W) was also collected in the Northeast Atlantic Ocean during the *AMT-12* cruise. The dissolved iron distribution was relatively homogeneous at *circa* 1 nM, except a spike of 6 nM at 175 m (Figure IV.11). This data was not significantly different from other published data (Table IV.3), and was consistent with low iron uptake in surface waters given that the biology was rather limited by macronutrients at that time of the year (M. Moore, 2004, personal communication). The spike corresponded to a SPM feature on the transmissometry plot, suggesting it may be real; however these samples were also stored in "recycled" bottles, so that contamination could not be ruled out.

The *AMT-12* surface seawater data between the Equator and 40°N also fell in the range of published data (Table IV.3). However high iron concentrations were all measured in samples collected with the “dipper” (Figure IV.12). Even though relatively low values

could also be obtained from samples collected with the “dipper” (Figure IV.12), this sampling technique was potentially more subject to contamination due to the additional handling steps. Only three of all surface samples were stored in "new" bottles, and their dissolved iron concentrations were found within the range of data of samples stored in "recycled" bottles.

In summary, there was a strong case for contamination for iron and aluminium of the CTD24 samples, and for iron only, to a lower extent, of CTD69 samples. However the majority of the DFe and DAl data appeared oceanographically consistent at other stations with only occasional contamination for iron. These results suggest that contamination for iron from the storage bottles probably depended on the origin of the samples previously stored in these bottles. The set of "recycled" bottles used for storage of CTD24 samples may have previously contained samples from waters affected by strong inputs of Al and Fe possibly originating from sediments. Additionally contamination may have also resulted from insufficient washing of the bottles as these had to soak in acid baths for three days instead of a week. Consequently, most of the *AMT-12* samples may well be of good enough quality to be used for trace metal analysis, including iron, after the rigorous evaluation discussed here.

Different sets of samples were then analysed and checked for their oceanographic consistency before interpretation using the criteria given above. This also allowed checking that the trace metal-clean techniques used were not contaminating the samples, as most of the following samples were stored in “new” LDPE bottles and those that were not could be clearly identified to the shape of the bottles.

IV.5. Evaluation of other data sets

IV.5.1. Data set from the JR98 cruise

Samples were collected and stored in "new" bottles (except for one sample with a high DFe value) during the *JR98* cruise in the Celtic Sea, where a transect of 9 CTD stations was carried out across the continental shelf break (Chapter V). Results were compared with the few published data available and checked for their oceanographic consistency, and the integrity of samples was evaluated using criteria given above.

As discussed above, a shift in the data on analysis event 13 was suspected, when samples from station N7 were analysed. Figure IV.11a displays data obtained with the

FIA-CL system with the Obata *et al.* (1993) configuration (Appendix 5) and with the finalised version of the analyser (Appendix 7). Results showed that data obtained with the two configurations (filled circles and inverted triangles) were very similar up to 900 m depth and above this depth new data (filled circles) was slightly higher (Figure IV.13a). Most of the samples from other profiles re-analysed gave concentrations about 1.5 nM on average lower than with the "Obata" configuration in the whole transect except at N7 (data not shown), suggesting that data was higher on analysis event 13. Moreover, DFe concentrations at N7 were on average 0.8 nM higher than at the surrounding stations (N6 and N8) without any other oceanographic data suggesting that dissolved iron could be higher at N7. However, after normalisation, background DFe concentrations at N7 were similar to those found at N6 and N8 (Figure IV.13b).

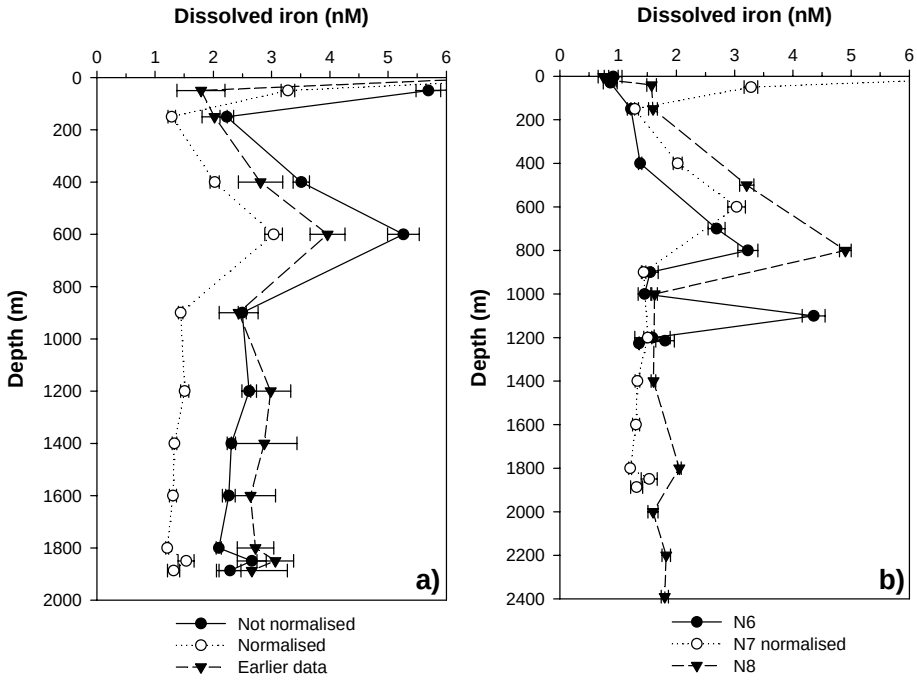

Figure IV.13: Dissolved (nM, < 0.4 μm) iron concentration distribution **a)** at N7 (48.4°N, 10.2°W) showing data obtained with the "Obata" configuration of the FIA-CL system (inverted triangles), data obtained with "Johnson" configuration not normalised (filled circles), and when normalised (open circles); and **b)** at Stations N6 (filled circles), N7 (open circles), and N8 (inverted triangles) in the Northeast Atlantic Ocean from a transect at the Celtic Sea shelf break.

It was thus decided that data from station N7 (analysis event 13) should be normalised to the LISW-IS mean value, given the evidences that: **i)** the NASS-5 value was exceptionally higher than other analysis events; **ii)** the LISW-IS values were also higher than the mean value; **iii)** concentrations between inter-batch measurements were generally found higher than during other analysis events and correlated better after normalisation; **iv)** prior to normalising, background concentrations at stations N7 were

higher than at surrounding stations without any obvious correlation with other oceanographic data; and **v)** this shift in the N7 data (0.8 nM) relative to adjacent stations was equivalent to the one observed of the LISW-IS value (0.7 nM) relative to the mean value. Despite the fact that normalisation of data is usually not suitable, and given that time did not allow re-analysis of this profile, this approach was felt well adapted to the situation.

Looking at the oceanographic consistency of the normalised data at Station N7, two surface data points (4 and 54 m depth) in the N7 profile were found to be much higher than expected (Figure IV.13a and b). The DFe concentration at 4 m depth was very high (7.93 ± 0.31 nM) for a surface sample, and was strongly suspected of contamination, as this sample was the only one stored in a "recycled" bottle (see Section IV.4.3). The concentration measured at 54 m (3.28 ± 0.12 nM) was also suspect as this depth corresponded to the chlorophyll *a* maximum where a significant fraction of dissolved iron is expected to be taken up by the biota resulting in a decrease in DFe concentrations down to sub-nanomolar levels as found at other stations of the transect (see Chapter V). Additionally, the DFe value was found to be significantly higher than when analysed initially with the "Obata" configuration (Figure IV.13a). These observations suggest that this sample was contaminated during analytical handling the first time it was analysed, and was therefore excluded from the data set as well as the surface sample at Station N7.

Additionally, elevated dissolved iron (4.90 ± 0.10 nM) was measured at 800 m depth at Station N8 (Figure IV.13b), with no particular feature in other parameters (*e.g.* enhanced SPM and nutrients) associated (data not shown). Dissolved iron (< 0.2 μm) was found at about 0.74 nM in waters at similar depths upstream in the Bay of Biscay (Laes *et al.*, 2003), which would likely still be significantly lower if that measurement was made in the < 0.4 μm fraction than the concentration measured here. These results therefore rule out the possibility for transport of iron-rich waters and for enhanced remineralisation, and imply that this sample may have been contaminated for iron. This sample was therefore excluded from the data set.

An additional sample from Station N1 at about 80 m depth was removed from the data set as it was suspected of contamination, since elevated dissolved iron (4.56 ± 0.19 nM) could not be explained oceanographically.

Station Name Location	Size fraction	Seafloor depth (m)	Depth (m)	[DFe] range *(mean)* (nM)	*Reference*
N1 48.6°N, 9.1°W	< 0.4 µm	157	2 – 145	0.6 – 5.4 *(2.6)*	*This study*
N2 48.6°N, 9.3°W	< 0.4 µm	165	2 – 157	0.2 – 0.7 *(0.4)*	*This study*
N3 48.5°N, 9.5°W	< 0.4 µm	250	35 – 236	0.2 – 0.7 *(0.4)*	*This study*
N4 48.5°N, 9.55°W	< 0.4 µm	365	2 – 345	0.6 – 1.7 *(1.0)*	*This study*
N5 48.5°N, 9.6°W	< 0.4 µm	542	2 – 520	0.3 – 2.5 *(0.9)*	*This study*
N6 48.45°N, 9.7°W	< 0.4 µm	1238	2 – 1227	0.9 – 4.4 *(1.9)*	*This study*
N7 48.4°N, 9.9°W	< 0.4 µm	1893	50 – 1887	1.2 – 3.0 *(1.6)*	*This study*
N8 48.35°N, 10.0°W	< 0.4 µm	2411	2 – 2390	0.7 – 4.9 *(1.9)*	*This study*
N9 48.3°N, 10.2°W	< 0.4 µm	2953	2 – 200	0.46 – 0.74 *(0.6)*	*This study*
52°N, 11-12°W	< 0.4 µm		0 – 800	< 1 – 4	(Muller *et al.*, 1994)
48 – 50.5°N	< 0.2 µm		2	0.7 – 1.9	(Boye *et al.*, 2003)

Table IV.4: Comparison of published iron concentrations with the *JR98* data from this study. Dissolved iron (nM) concentrations were normalised to the mean LISW-IS valued for profile N7 (see text).

After normalisation of Station N7 data and exclusion of samples at 4 and 54 m depth (N7), 800 m (N8), and 80 m (N1), all the data fell in the range of published data (Table IV.4), and showed consistency with other parameters such as temperature, salinity, chlorophyll *a*, transmission, and macro-nutrients concentration (see Chapter V).

IV.5.2. Data set from the JR80 cruise

An additional set of unfiltered samples were collected using a "pole sampler" during the *JR80* cruise in the Atlantic Sector of the Southern Ocean between the Falkland Islands and South Georgia (see Chapter V). The quality of the analysis carried out on day 10 was satisfactory (Table IV.1), even though the sensitivity was found to increase with time during analysis and the NASS-5 value was high (see above). Correcting the data using the slope given by the increasing peak area for the LISW-IS with time proved to give relatively good agreement with inter-batch data. The data was also consistent with total dissolvable iron measurements in open ocean and shelf waters published in the literature (Chapter V).

IV.6. Identification of high quality data

Given that the quality of data obtained for the *JR98* cruise was satisfactory in terms of the quality of the analysis and samples, these results also show that the sampling and handling procedures used at the National Oceanography Centre, Southampton allowed collection of good quality samples and confirmed that storage of samples in "recycled" bottles was potentially a source of random contamination for iron.

The "recycled" storage bottles were used previously for samples from a wide variety of locations varying from the open ocean to possibly metal-laden Black Sea waters, and hydrothermal vents. Results shown here have significant implications for carry-over of samples in plastic bottles. Fluctuations in the amount of contamination may therefore depend on the origin of the sample previously stored in these bottles. Iron is known to diffuse out of the bottle walls using acid washes since this is how storage bottles are cleaned before use; however, acidification of samples was thought to prevent trace-metal diffusion into bottle walls. Presumably iron (and possibly aluminium) also diffuses out of plastic therefore potentially influencing the sample concentration. It is therefore important to know the metal content of the previous sample before recycling storage bottles. Moreover, in the future only new bottles will be used for storage of open ocean samples, after rigorous cleaning and long-term leaching of internal walls with acidified Milli-Q solutions.

IV.7. Summary

Independent data checks showed that the Fe(II)+(III) FIA-CL system developed in this project was able to accurately determine inorganic Fe(II) *plus* Fe(III) at sub-nanomolar concentrations in samples stored acidified for a long time (> 1 year). It gave linear calibrations to up to 6 nM with good precision (often < 5%). The blank and limit of detection were fluctuating due to the quality of the rinsing water used (Milli-Q water) and should thus be improved in the future. However these figures of merit were adequate for the analysis of samples collected in the Atlantic Ocean (*AMT-12* cruise), at the Celtic Sea shelf break (*JR98* cruise), and between the Falkland Islands and South Georgia (*JR80* cruise).

The NASS-5 iron value was found to be significantly higher than the certified value during most of the analyses. The most likely reason was random contamination either

during handling or by leaching iron from the system itself caused by the lower pH of this solution relative to other samples and standards. The frequent analysis of low-iron seawater (mean concentration of 0.98 ± 0.17 nM) acidified to the same extent as the collected samples, allowed its use as an internal standard. The response of the system to this internal standard was relatively reproducible except on one day when the sensitivity increased with time and on another day when a shift in all the data was observed. No relationship was found between the NASS-5 values and the LISW-IS values which supported the hypothesis that there was pH-linked random contamination of the NASS-5 seawater. Reproducibility of inter-batch measurements was satisfactory after correction of the data when sensitivity or a shift in the response of the analyser was observed. The ability of the analyser to give reproducible values for samples, the reproducibility in the LISW-IS value, and the NASS-5 typically in line with those expected at the beginning and towards the end of the development phase, demonstrated the reliability and accuracy of the response of the technique.

After a detailed assessment of sources of contamination, there was a clear suspicion of variable and random contamination of samples during storage in “recycled” LDPE bottles. After comparison with published data and checking oceanographic consistency, it was concluded that some of the *AMT-12* data analysed was subject to random contamination for iron during storage from the bottles. However trace metals including iron could be determined in a significant number of the *AMT-12* samples stored in "recycled" bottles providing rigorous filtering of the data as applied here. Despite use of all the usual procedures for trace metal work at the National Oceanography Centre, Southampton, there was evidence of significant contamination of samples from storage bottles. Only new acid-cleaned LDPE bottles should therefore be used to store open ocean samples when working on iron.

Whilst the performance of the analysis was not optimal throughout, the data set produced for the *JR98* samples from the Celtic Sea continental margin and for the *JR80* samples from the North Scotia Ridge is of adequate quality to allow the study of processes such as benthic inputs of dissolved iron to the water column, and the influence of transport and of the water column biota on its distribution (see Chapter V). Those samples below the limit of detection have been excluded from the discussion other than giving a maximum possible concentration for these samples.

CHAPTER V.

PROCESSES INFLUENCING DISSOLVED IRON DISTRIBUTIONS AT THE OCEAN – SHELF INTERFACE: CELTIC SEA SHELF BREAK (NORTHEAST ATLANTIC) AND SOUTH GEORGIA (SOUTHERN OCEAN)

V.1. Introduction

The distribution of dissolved iron in the water column is influenced by inputs, removal, and recycling processes. In remote areas of the oceans where inputs are low, dissolved iron distributions are reported to be nutrient-like as they are strongly influenced by biological uptake in the surface mixed layer, and iron is recycled deeper (Johnson *et al.*, 1997). However the metal's distribution can be strongly modified by major inputs such as that from the atmosphere (Jickells and Spokes, 2001; Guieu *et al.*, 2002; Statham and Hart, 2005), and sediments in coastal shelf regions (Hong and Kester, 1986; Martin and Gordon, 1988; Muller *et al.*, 1994; Wu and Luther III, 1996; Croot and Hunter, 1998; Johnson *et al.*, 1999; Bucciarelli *et al.*, 2001; Bowie *et al.*, 2002b).

A multitude of sources, removal, and transport processes have been identified for dissolved iron in shelf environments (Santschi *et al.*, 1990). However little is known concerning the details of these mechanisms, and their relative contribution to iron biogeochemistry (de Baar and de Jong, 2001). The different processes influencing iron in coastal / shelf waters are shown in Figure V.1.

Dissolved iron may be released into near-bottom waters by: **i)** oxidation of particulate organic matter (Berelson *et al.*, 2003; Elrod *et al.*, 2004); and **ii)** pore water diffusion or advection by bio-irrigation (Santschi *et al.*, 1990; Elrod *et al.*, 2004). Episodic resuspension events may enhance release of iron-rich pore waters close to the sediment-water interface into overlying waters (Santschi *et al.*, 1990). The question as to whether iron may be released by dissolution from lithogenic material resuspended from sediments in seawater is as yet unaddressed but it is thought to be thermodynamically unlikely (Kuma *et al.*, 1992). In surface waters, dissolved iron may be released from particulate phases through biological processes (Hutchins *et al.*, 1993; Bowie *et al.*, 2001), and by dissolution of aerosols into seawater (Zhuang *et al.*, 1990; Jickells and Spokes, 2001; Bonnet and Guieu, 2004).

Removal of dissolved Fe may occur by: **i)** adsorption onto particles (Wells and Goldberg, 1993; Johnson *et al.*, 1997); **ii)** precipitation (Elrod *et al.*, 2004); and **iii)** uptake by the biota (Geider, 1999). Thus in productive shelf systems with high particle concentrations, there are a complex range of processes influencing sources and removal of dissolved iron.

Waters at the ocean – shelf interface are highly dynamic environments as regards water mass movement; therefore transport mechanisms also complicate iron

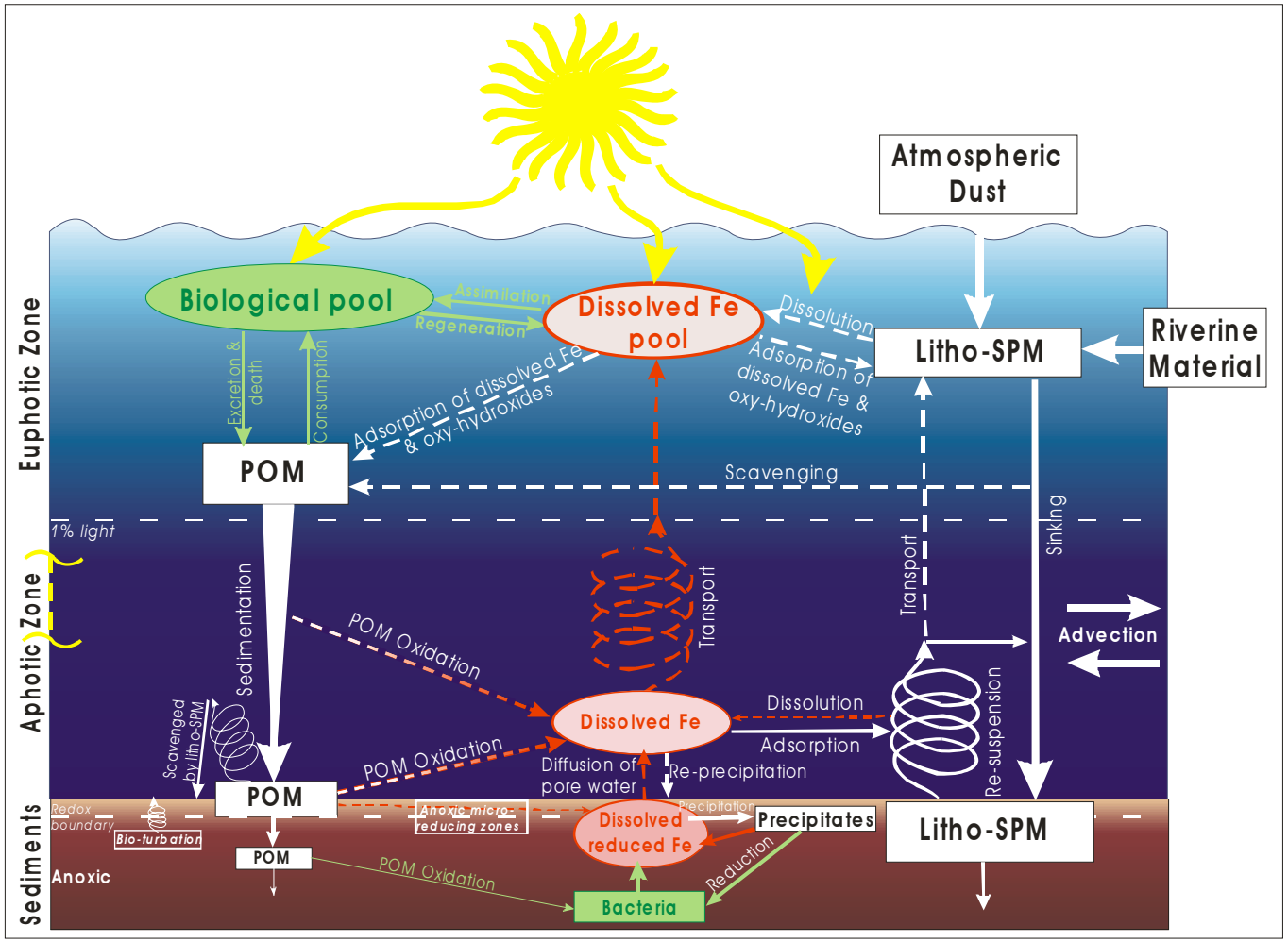

Figure V.1: Conceptual model of the iron cycle in shelf waters. Dashed arrows show uncertainty in the occurrence of processes. White arrows represent physicochemical processes; Green arrows, biologically driven processes; Red arrows, inputs of dissolved iron. Litho-SPM = lithogenic suspended particulate material; Bio-SPM = biogenic suspended particulate material; POM = particulate organic matter.

distributions. These processes include: **i)** wind-stress thickening the mixed-layer (Huthnance *et al.*, 2001); **ii)** diapycnal mixing by internal tides and "meddies" (Arhan and King, 1995; Huthnance *et al.*, 2001); **iii)** advection along isopycnals (Arhan and King, 1995; McCave *et al.*, 2001); and **iv)** in specific regions wind-driven upwelling (Johnson *et al.*, 1999). The distribution of dissolved iron in these systems is therefore difficult to study since it is a reflection of all the different processes occurring at that time, most of which are not well known and are variable in space and time (Wu and Luther III, 1996; Elrod *et al.*, 2004).

Shelf breaks have generally been considered as sinks for dissolved iron as the element is mainly lost from solution by adsorption onto particles (Hong and Kester, 1986; Muller *et al.*, 1994), which are abundant in these environments (McCave *et al.*, 2001; Weinstein and Moran, 2004). However, enrichment in dissolved iron in open ocean deep water masses, where atmospheric deposition was not likely to generate the observed concentrations, gave evidence that export of dissolved iron off-shelf is possible (Coale *et al.*, 1996a; Wu and Luther III, 1996; Gordon *et al.*, 1997; Mackey *et al.*, 2002; Laes *et al.*, 2003; Croot *et al.*, 2004a). At the European shelf break region, major re-suspension of particulate material from the sediments and lateral transport along isopycnals as intermediate nepheloid layers (INLs) have been observed (Dickson and McCave, 1986; Thorpe and White, 1988; McCave *et al.*, 2001). High dissolved iron concentrations (5 – 9 nM) have been measured in such INLs where dissolved oxygen concentrations exceeded 100 μM (Martin and Gordon, 1988), suggesting that dissolved iron may be exported off-shelf in such features. However, little is known about the mechanisms sustaining high dissolved iron concentrations in these INLs including the possibility of stabilisation of iron in colloids (Moran *et al.*, 1996).

Biological interactions are also important in influencing dissolved iron concentrations in the upper ocean. In summer, nutrients are generally low in surface waters due to intense uptake by the biota during the spring bloom and one or more may become limiting when supply is not sufficient to sustain high biological activity. Iron (co-) limitation or stress was reported from other shelf environments due to low Fe inputs by upwelling (*e.g.* (Bruland *et al.*, 2001; Bruland *et al.*, 2005), and from open ocean regions episodically supplied by atmospheric inputs (*e.g.* (Blain *et al.*, 2004; Mills *et al.*, 2004), but the potential for Fe limitation at the Celtic Sea shelf break has not as yet been investigated.

In the present study dissolved iron was determined in samples collected during a transect across the Northwest European continental margin. The European margin is characterised by a broad continental shelf (the Celtic Sea), and is limited westward by a steep slope down to 4000 m. European shelf waters are highly dynamic environments where wind-, tide- and wave-forced currents, and the topography of the shelf edge promote diapycnal mixing between water masses (van Aken, 2000), and potentially vertical transport of nutrients (Pingree *et al.*, 1986). Studies on iron in European coastal environments have mainly focussed on its behaviour on the shelf (*e.g.* (Dehairs *et al.*, 1989; Millward *et al.*, 1998). A few transects have been carried out across the Celtic Sea shelf edge (Kremling, 1983; Muller *et al.*, 1994; Boye *et al.*, 2003), including work in the OMEX programme (Le Gall *et al.*, 1999; Cotté-Krief *et al.*, 2002). The work presented here describes dissolved iron concentrations in the most detailed two-dimensional transect down to the deep seafloor across shelf break presently available, and the data are used to investigate processes affecting dissolved iron distribution in the whole water column. This study therefore additionally helps to provide a conceptual framework for discussing these processes and other iron data for such systems.

A consequence of effective iron supply from benthic sources in shallow waters may be the relief of iron-limitation for phytoplankton growth in waters surrounding islands in HNLC areas; an outcome also called the "island mass effect". This hypothesis has been proposed around South Georgia in the Atlantic sector of the Southern Ocean, where a persistent phytoplankton bloom is annually observed in satellite images taken during the austral spring to the northwest of the island, whereas surrounding HNLC waters do not show any enhanced primary production (Korb *et al.*, 2004) (see also Chapter I). To help understanding the contrast between these productive and non-productive waters, variations in phytoplankton photo-physiology and total dissolvable iron concentrations in seawater were examined across a transect between the Falkland Islands and South Georgia.

V.2. Sampling and analysis

V.2.1. Sampling

Samples were collected during the *RRS James Clark Ross* cruise *JR98*, July-August 2003, during an offshore transect across the Celtic Sea shelf break (Figure V.2). Nine stations (N1 – N9) were occupied across the continental slope and samples collected for

iron determination. Profiles extended from a few metres above the seafloor up to the surface except at Station N9, which extended down to only 200 m (Table V.1).

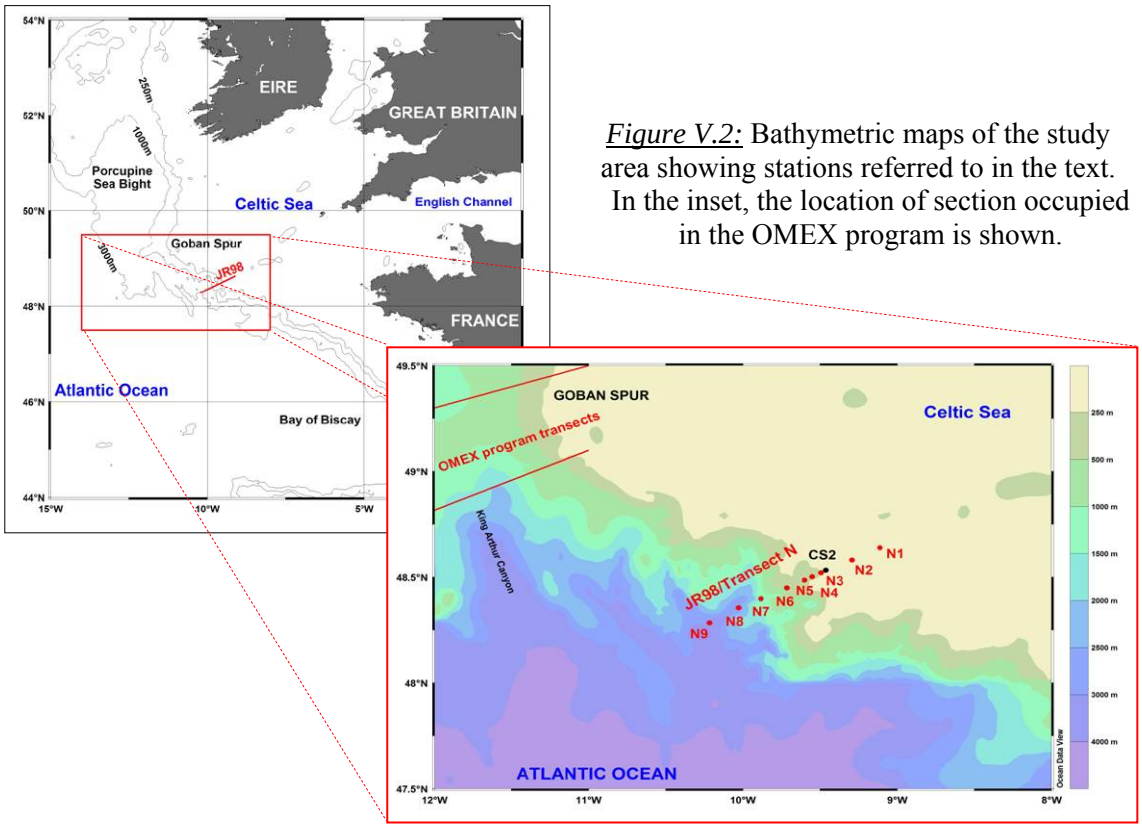

Figure V.2: Bathymetric maps of the study area showing stations referred to in the text. In the inset, the location of section occupied in the OMEX program is shown.

Sampling was carried out using a titanium CTD-rosette system fitted with trace metal clean sampling bottles, with filtration and acidification carried out as described in Chapter IV, in a trace-metal clean container laboratory. Samples were acidified with 1 µL of quartz distilled hydrochloric acid per mL of sample in a laminar flow hood, and double zip-bagged (polythene) for storage.

	Latitude (°N)	Longitude (°W)	Bottom depth (m)	Distance from bottom of deepest sample (m)	Distance between stations (km)
N1	48.638	9.112	157	10	
N2	48.580	9.292	165	11	12.8
N3	48.520	9.493	250	12	12.0
N4	48.502	9.550	365	18	3.8
N5	48.485	9.600	542	19	3.7
N6	48.448	9.715	1238	5	8.5
N7	48.397	9.883	1903	6	11.5
N8	48.355	10.027	2411	9	10.5
N9	48.283	10.217	2953	Only down to 200 m	13.3
CS2	48.532	9.463	198	12	

Table V.1: Stations sampled during the transect across the Celtic Sea shelf edge.
Total distance between N1 and N9 = 74 km.
Station CS2 was not sampled as part of the transect.

Temperature, salinity, and dissolved oxygen data were logged from the Seabird 911 CTD sensors. The beam attenuation signal derived from transmission obtained with the CTD ALPHA^{tracka} transmissometer was used as an indicator of SPM concentrations since they are linearly correlated, and as a calibration was not available (Chelsea Technologies Group) (McCave *et al.*, 2001). Samples for nutrients and chlorophyll *a* measurements were collected from duplicate sampling bottles closed at each Fe bottle sampling depth.

V.2.2. Analysis

Analyses were performed in a class-100 clean room in the Southampton laboratory, and critical steps were performed in a laminar flow hood. Samples were stored acidified for more than one year after collection, an approach that is reported to lead to measurement of all dissolved (< 0.4 μm) forms of iron (*i.e.* dissolved iron (DFe)) (Bowie *et al.*, 2004).

Dissolved iron was determined using a flow-injection analyser with chemiluminescence detection using luminol to detect Fe(II) and Fe(III) in seawater, after preconcentration (Obata *et al.*, 1997; Johnson *et al.*, 2003) (Chapter III). Data presented here went through a rigorous data quality check (Chapter IV). In the absence of a reliable calibration for one set of samples, data from profile N7 were normalised to the well characterised internal standard value (Chapter IV). Four outlier data points, one collected at the surface (8.01 ± 0.31 nM DFe), one in the chlorophyll *a* maximum (54 m-depth, 3.31 ± 0.12 nM DFe) at Station N7, one at Station N1 (80 m, 4.56 ± 0.19 nM), and one at Station N8 (800 m, 4.90 ± 0.10 nM DFe) were excluded from the data set as they were strongly suspected of contamination (Chapter IV). Additionally three data points were below the limit of detection (Station N3: 2 and 15 m depth, and Station N5: 20 m). These were the only data excluded for contamination out of a total of 80 values.

Nutrients were measured by Dr. David Hydes (National Oceanography Centre, Southampton) using a Skalar autoanalyser for nitrate plus nitrite (N), phosphate (P) and dissolved silicon (DSi). Total chlorophyll *a* measurements in acetone extractions were made using the fluorometric method of Welschmeyer (1994) after filtration onto Whatman GF/F (pore-size 0.7 μm) filters. Size-fractionated chlorophyll *a* measurements were carried out following the size categories of Sieburth *et al.* (1979) as < 5 μm and > 5 μm, after filtration onto 5 μm polycarbonate filters (Poretics), and were made using a fluorometer. Finally pigments of chlorophyll *a* were analysed following the method of

Barlow *et al.* (1993) by High Performance Liquid Chromatography (HPLC) after filtration on Whatman GF/F filters. These analyses were carried out by Pr. Patrick Holligan and Young-Nam Kim (NOCS) (Kim, In preparation).

V.3. Results

V.3.1. Horizontal distribution of dissolved iron across the shelf edge

The range of surface (~ 3 m depth) dissolved iron concentrations varied from a value below the limit of detection (< 0.16 nM) to 0.91 ± 0.15 nM at Stations N3 and N6 respectively, and did not show any clear trend of increasing concentrations from oceanic waters (Station N9) to shelf waters (Station N1) (Figure V.3). Highest DFe concentrations were found at Stations N4, N5, and N6 on the upper slope (500 – 1250 m) and lowest DFe levels were measured at the shelf break (Stations N2 and N3).

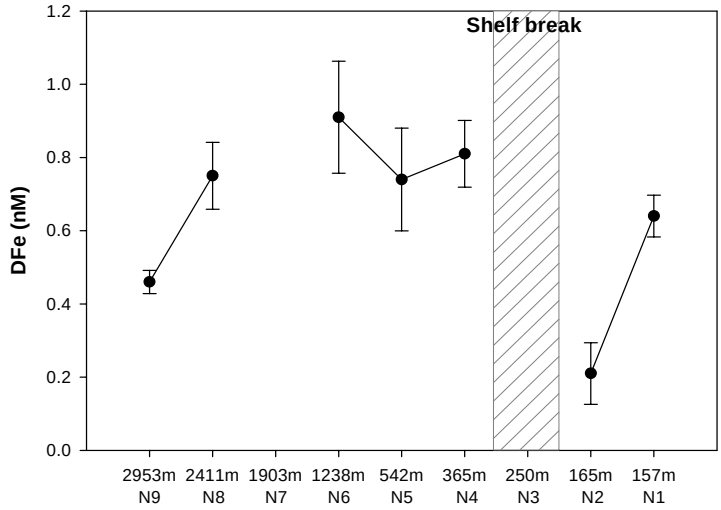

Figure V.3: Surface dissolved iron (nM) at *circa* 3 m-depth across the Celtic Sea shelf break. Stations number and seafloor depths are indicated as well as the approximate position of the shelf break. Error bars are ± 1 standard deviation. [DFe] at Station N3 below detection limit (< 0.16 nM).

Dissolved iron concentrations along this transect were comparable to published surface data from near the Porcupine Seabight (~ 51°N), and at about 48°N at the Celtic Sea shelf edge (Muller *et al.*, 1994; Boye *et al.*, 2003). Reported dissolved iron (< 0.4 μm) concentrations measured at 51°N increased from < 1 nM to > 3 nM in August 1984 (Muller *et al.*, 1994). In March 1998 at 48°N, DFe (< 0.2 μm) increased from about 0.7 nM in open ocean waters to about 1.1 nM at the shelf break (Boye *et al.*, 2003). Dissolved iron concentrations measured in the present study thus were slightly lower than those reported at 51°N, and were in the range found at 48°N even though the size fraction measured here was larger, and sampling was carried out in a different season, which can have a significant impact on DFe levels.

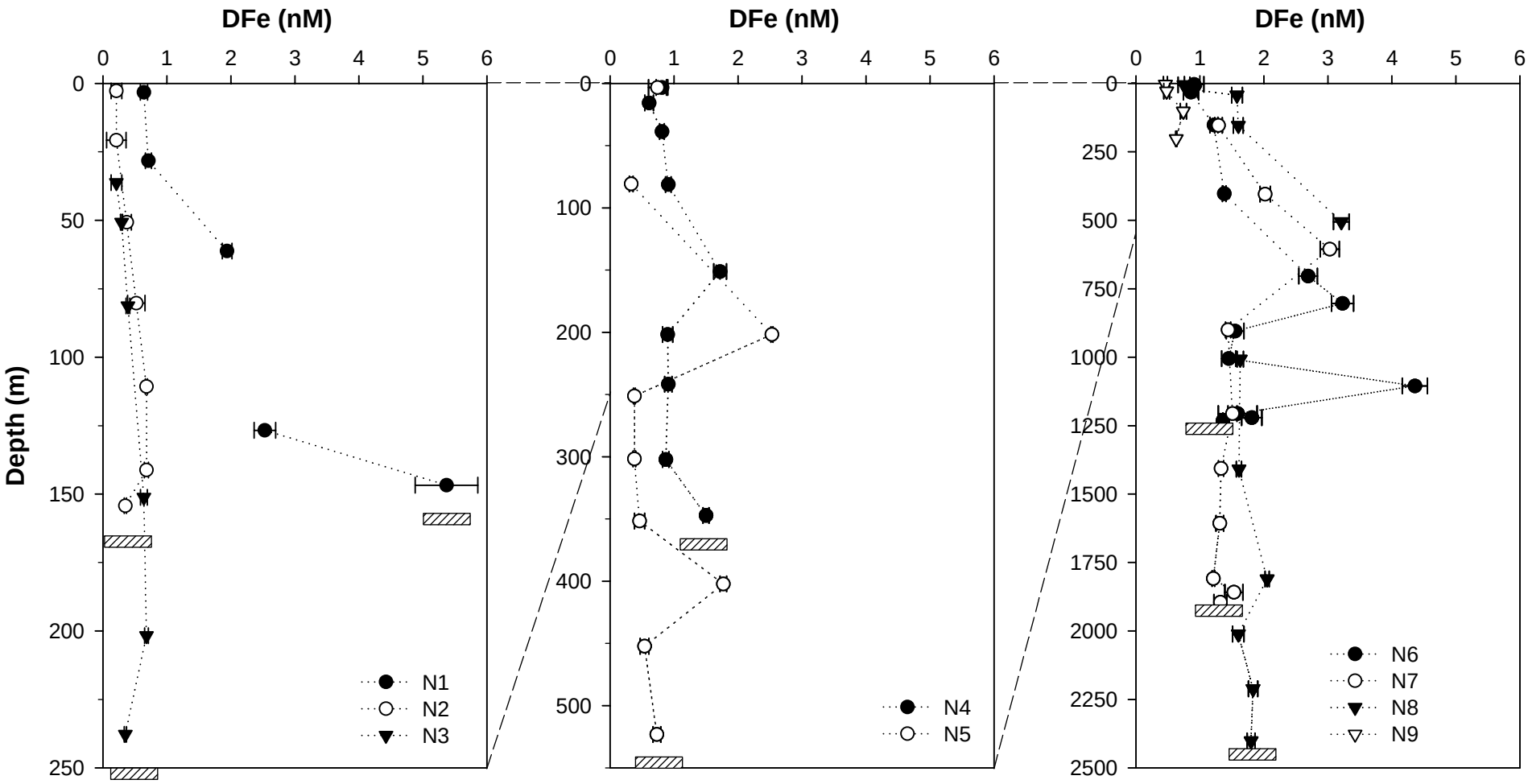

Figure V.4: Vertical distribution of dissolved iron (DFe) across the Celtic Sea shelf edge. Error bars are ± 1 standard deviation. Hatched boxes show bottom depth at each station except N9 (2953m-depth), which was sampled only down to 200m.

V.3.2. Vertical distribution of dissolved iron across the shelf edge

The distribution of dissolved iron across the Celtic Sea shelf edge did not present a clear trend of uniform increasing concentrations from oceanic to coastal waters, but had distinct spikes of high DFe at specific depths (Figure V.4). The presence of sub-nanomolar DFe at the shelf break (Stations N2, N3, N4 and N5) were surprising in that DFe concentrations have been reported to increase to up to several tens of nanomolar in shelf systems (Muller *et al.*, 1994; Wu and Luther III, 1996). High DFe concentrations (5.37 ± 0.49 nM ($n = 3$)) were measured near the seafloor at the shallowest Station N1 (Figure V.4). At the other stations, dissolved iron concentrations slowly increased with depth below 50 m, and were relatively homogeneous down to the seabed at Stations N2 and N3. This distribution is consistent with the relatively weak water column stratification at these stations relative to Station N1 (see Appendix 9 for CTD data). From Stations N4 to N8, DFe distributions in the water column were significantly perturbed by layers of high-DFe water at specific depths (Figure V.4). These spikes were not thought to be due to sample contamination as they corresponded to features in the water column (see Section V.4.2). No general increase in DFe concentration with proximity to the seafloor water was observed, and this feature was found at Stations N1, and N4 – N7 (Figure V.4).

V.4. Discussion

Dissolved iron and associated data (temperature, salinity, beam attenuation from the transmissometer, dissolved oxygen, macronutrients concentration, chlorophyll *a*, and pigments) were used to study three aspects of the iron cycle at the Celtic Sea shelf edge environment (see model, Figure V.1). Firstly an attempt was made to try and identify the sources of dissolved iron in near-bottom waters across the transect. The DFe distribution was then examined in the aphotic zone, focussing on mid- and upper water column transport. Finally, dissolved iron distributions were examined in the photic zone in relation to the biology.

V.4.1. Dissolved iron near the seafloor

The sediment-water interface is a highly dynamic environment, especially on continental margins. Modification of biogeochemical fluxes in bottom waters mainly depends on the nature of sediments, the degree of diagenetic reactions, and turbulence

leading to resuspension events (Aller, 2004). These processes affect directly the benthic nepheloid layer (BNL), the near bottom seawater showing higher SPM concentrations than clearer waters above due to resuspension. In this section, dissolved iron, oxygen, and nutrient data were used to help distinguish between the different potential benthic sources of iron at the seafloor. Also, the mechanisms by which DFe is removed and may be stabilised in the water column are considered.

V.4.1.1. Overview of benthic processes as potential dissolved iron sources

At the seafloor, iron in particulate phases can be found incorporated in biogenic detritus, within clay minerals or crystal lattices, adsorbed at particle surfaces, and as hydrogenous precipitates (de Baar and de Jong, 2001). Three main processes may release dissolved iron from these particles in seawater, and may be enhanced by episodic resuspension events: **i)** dissolution from lithogenic particles; **ii)** regeneration by POM oxidation at the seafloor; and **iii)** diffusion from pore waters through the sediment-water interface (see model Figure V.1) (Santschi *et al.*, 1990). However, other processes are expected to be operating to remove iron from solution and so the observed dissolved iron concentrations at any particular instant will be a balance of inputs and removal.

The surface sediments were studied at the Goban Spur near the sampling area (see Figure V.2), showing a marked change in composition and grain size, from predominantly terrigenous sandy shelf sediments on shelf to hemipelagic clayey silts on the abyssal plain (van Weering *et al.*, 1998). At the shelf edge, sediments presented a mixture of lithogenic and biogenic material, mostly of terrigenous origin (van Weering *et al.*, 1998). The average iron content of deep-sea clays and coastal mud are 6% and 6.5%, respectively (Chester, 1990). However iron contained within clays and more refractory oxide phases is not readily dissolved due to thermodynamic stability, and slow kinetics (Rich and Morel, 1990; Millero *et al.*, 1995b; Sulzberger and Laubscher, 1995).

Previous studies on the solubility of refractory alumino-silicates (clays) focussed on those deposited from the atmosphere. Incubation experiments showed that the solubility of alumino-silicates originating from Saharan dust was very low (0.001 to 1.6%), increasing with residence time in seawater and decreasing with particle load (Bonnet and Guieu, 2004). In the BNL clay and sand particles are expected to re-settle

shortly after resuspension due to their high settling velocity (Thomsen and van Weering, 1998; Huthnance *et al.*, 2002). If DFe were released, it is likely that it would be readily removed from seawater by adsorption and/or precipitation, unless it was released as colloids or quickly organically complexed.

Studies on the solubility of Fe oxy-hydroxides showed that the most refractory forms (hematite and goethite) were least soluble (Sulzberger and Laubscher, 1995), and that freshly precipitated iron (akageneite and ferrihydrite) were most soluble (Millero *et al.*, 1995b; Rose and Waite, 2003a). However, at seawater pH, if iron were released as Fe(II) it would quickly be oxidised to Fe(III) (Rose and Waite, 2002) unless stabilised by organic ligands, and Fe(III) is limited by its solubility to pico-molar levels (Millero *et al.*, 1995b; Rose and Waite, 2003a). Thus little, if any, iron is thermodynamically likely to be released from oxy-hydroxides in seawater, and it is expected to precipitate rapidly after release at seawater pH in oxic conditions. Dissolution of iron from lithogenic particles may be possible only if changes in pH and pE (*i.e.* lower pH increases iron solubility as in sediments (Canfield, 1989)), and light conditions (*i.e.* photo-reduction as in the photic zone, (Sulzberger and Laubscher, 1995; Borer *et al.*, 2005)) occur or if DFe is stabilised (Rose and Waite, 2003b).

An additional potential source of dissolved iron to bottom waters is its release from particulate organic matter (POM). In open ocean waters, most (> 95%) biogenic SPM (or POM) is slowly remineralised whilst sinking from surface waters so that very little reaches the seafloor (Wollast and Chou, 2001). However, in shallow shelf waters more POM reaches the sediments due to generally higher production in surface waters, and shorter time before arrival at the seabed (van Weering *et al.*, 2001), so that rates of benthic POM remineralisation significantly decrease ocean-ward (Jahnke *et al.*, 1990). Increased amounts of organic matter at the seafloor may promote DFe release from POM oxidation on shelf relative to deeper waters, as observed in the North Pacific Ocean (Berelson *et al.*, 2003; Elrod *et al.*, 2004).

According to the Redfield-Richards equation of respiration in oxic waters, POM remineralisation consumes oxygen and releases phosphate, carbon dioxide, sulphate, and ammonium which is quickly oxidised to nitrate, following the ratio $C:O_2:N:P$ of 106:138:16:1 (Redfield *et al.*, 1963). Several studies have been carried out to determine the iron requirement for growth for a range of phytoplankton species from both coastal and oceanic environments (Sunda and Huntsman, 1995, 1997; Ho *et al.*, 2003; Price, 2005). These experiments showed that the Fe:C ratio varied between about 10 to 50

μmol/mol for coastal species and that the ratio increased with iron availability (Sunda and Huntsman, 1995; Ho *et al.*, 2003; Price, 2005). This particulate iron is also expected to be largely released on oxidation of the POM. Concentrations of dissolved oxygen, macro-nutrients, and DFe thus have the potential to be used to investigate the importance of POM remineralisation as a source of dissolved iron in the BNL.

Finally, POM respiration at the sediment-water interface and within sediments consumes oxygen and may create sub-oxic reducing zones. In oxygen under-saturated conditions, reductive dissolution of iron from marine sediments takes place by reaction of Fe oxides with dissolved sulphide, or iron oxides are used as electron acceptors in POM respiration by bacteria in anaerobic conditions (Canfield, 1989; Santschi *et al.*, 1990). Dissolved iron concentrations in pore water can be as high as several tens of micro-molar (Elrod *et al.*, 2004), and are found mainly as Fe(II) in these reducing conditions (Canfield, 1989; Lohse *et al.*, 1998; Berelson *et al.*, 2003). As the redox boundary gets shallower in the sediments due to intense oxygen consumption during POM oxidation, diffusion of iron(II)-rich pore waters may lead to increased dissolved iron concentrations in overlying bottom waters (Dehairs *et al.*, 1989). When oxic conditions are restored in bottom waters, dissolved iron(II) in pore waters diffusing upward precipitates at the redox boundary (Dehairs *et al.*, 1989). Diffusion of iron-rich pore waters may only be possible in shallow waters, where the redox boundary may be shallower within the sediments due to increased fluxes of POM to the seafloor. Any diffusive flux of dissolved iron in pore water would however be expected to be limited to on-shelf stations, and if any, it would also be expected to be rapidly removed. The only way diffusion of pore water may be significant as a source of DFe under oxic conditions, is if iron is in colloidal or organically complexed forms. Bio-turbation and bio-irrigation are other mechanisms that may increase fluxes of dissolved iron into bottom waters and vary seasonally and spatially (Lohse *et al.*, 1998; Berelson *et al.*, 2003; Elrod *et al.*, 2004). Major resuspension events may also inject any surface sediment pore water DFe into the overlying waters, and lead to high dissolved iron concentrations in bottom waters, if fluxes of POM to the seafloor are high, and iron is stabilised.

V.4.1.2. Sediment resuspension across the Celtic Sea shelf edge

The beam attenuation signal was used as an indicator of SPM concentrations without giving information on the nature (*i.e.* biogenic, lithogenic, inorganic precipitates) of

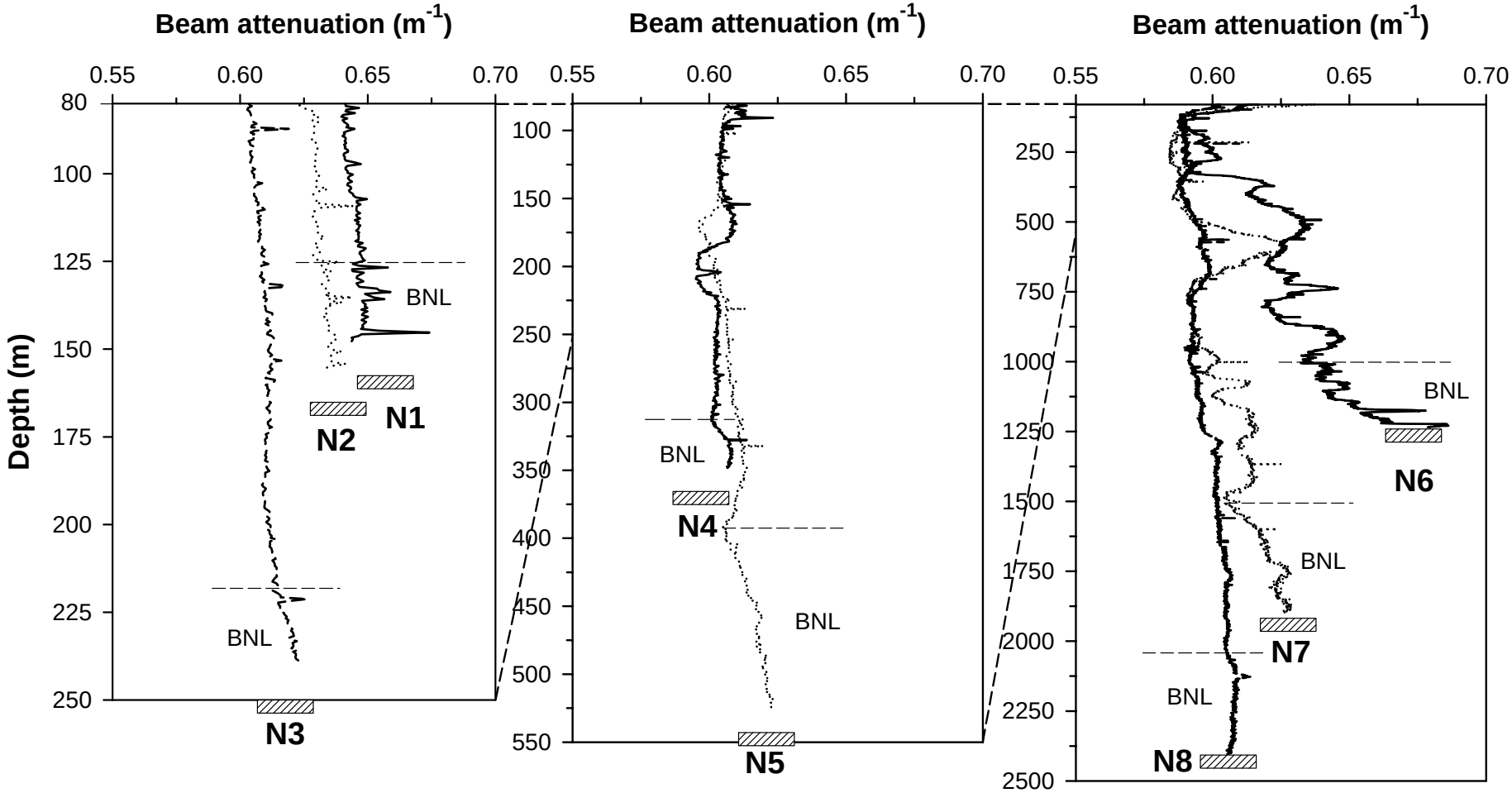

Figure V.5: a) Beam attenuation (m^{-1}) profiles from 80 m depth to bottom depth across the Celtic Sea shelf edge (N1 to N8). For clarity the upper 80 m are shown separately in b) for information, because of the high signal due to biological activity. Hatched rectangles show bottom depth and dashed horizontal lines the estimated upper limit of the benthic boundary nepheloid layer (BNL). The beam attenuation signal is linearly proportional to the SPM concentration and the attenuation in pure water is 0.364 m^{-1} (manufacturer Chelsea Technologies Group).

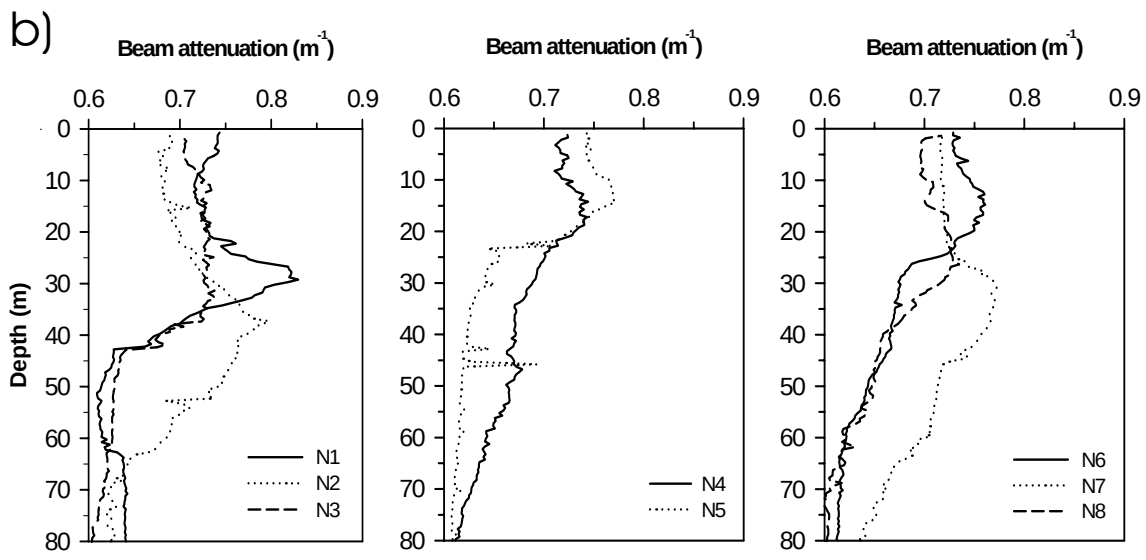

these particles. All beam attenuation profiles showed very high SPM concentrations in the mixed layer (< 80 m) due to biological activity (Section V.4.2.1). For clarity, the upper 80 m were shown in Figure V.5b to allow a suitable x-axis range to observe changes in the deeper waters in Figure V.5a.

To demarcate the zone influenced by benthic resuspension, the depth range of the BNL was estimated from beam attenuation data, where SPM increased towards the seafloor (Figure V.5). The highest near-bottom SPM (= highest beam attenuation) concentrations were observed at Station N6. This result may reflect the CTD at this station approaching closer to the seafloor than at Stations N1 to N5 (see Table V.1), where the core of the BNL may have been missed. Lower SPM at the deepest station (N8) is consistent with findings that the concentration of SPM in the BNL tends to decrease with increasing water column depth (McCave *et al.*, 2001; van Weering *et al.*, 2001).

Stations could be classified into four categories based on their beam attenuation signal: **1)** high SPM, and sharp features near bottom (Station N1); **2)** homogeneous beam attenuation, and a few features (Stations N2, N3, N4 and N5) likely due to weaker water column stratification (Section V.4.2.2); **3)** similar beam attenuation as the most off-slope stations just below the mixed layer, with very high SPM concentrations below 300 m (Station N6); and **4)** low beam attenuation signal, slightly increasing towards the seafloor with a few features (Stations N7 and N8) (Figure V.5). These results suggest that resuspension events were very localised, and are likely to be episodic as reported at Goban Spur (McCave *et al.*, 2001). The transect was carried out at neap tide when currents are generally weaker (J. Sharples, personal communication), which may

explain the observed low SPM at the upper slope stations (N3 to N5), as the heaviest particles may already have settled back to the seafloor (Jago *et al.*, 2002). Given the spatial and temporal variability of resuspension across the shelf, the relative importance of potential sources, and resulting inputs of dissolved iron to bottom waters, may thus significantly vary between stations.

V.4.1.3. Identification of benthic sources of dissolved iron near the seafloor

Elrod et al. (2004) suggested that POM oxidation from sediments is likely to be the major benthic source of dissolved iron on shelves. During the OMEX programme, fluxes of POM at the Goban Spur were of similar magnitude during spring and summer, with a difference in composition as fluxes were dominated by opal containing material in spring relative to summer (Antia *et al.*, 2001). Additionally it was estimated that 37 to 60% of carbon fixed by photosynthesis in the euphotic zone was not remineralised in the surface mixed layer (Joint *et al.*, 2001), and more than 90% of organic carbon mineralisation at the sediment-water interface was driven by oxygen (van Weering *et al.*, 1998). Finally, it was demonstrated that, at present, the North West European continental margin is not a carbon depocenter with a carbon burial efficiency of only 0.8 to 2.3% suggesting that most POM that was deposited yearly was remineralised (Lohse *et al.*, 1998; Wollast and Chou, 2001). These earlier studies therefore suggest that highly degradable POM is expected at the seafloor at the time of the cruise, and thus will provide a reservoir of biogenic iron that can be remineralised.

Waters below the euphotic zone are generally under-saturated with dissolved oxygen as it is consumed by mid-water column POM oxidation by heterotrophic bacteria. The observed apparent oxygen utilisation (AOU) concentration along a shelf/slope system will therefore be the result of mixing with waters with preformed AOU, and *in situ* oxygen consumption. Additionally, major resuspension events of anoxic/suboxic sediments may eventually decrease slightly dissolved oxygen concentrations in near-bottom waters of productive stations. The relationship between the AOU and the beam attenuation signal in the BNL at each station was thus examined in order to investigate the presence of oxygen consuming processes associated with resuspended particulate matter near the seafloor.

The data show three types of behaviour (Figure V.6): **i)** shallow stations influenced by water column mixing (N1, N2, and N3), showing low to moderately high

AOU with increasing SPM towards the seafloor; **ii)** stations showing possible *in situ* remineralisation of POM (N4 and N5) with a linear (R^2 = 0.95) relationship between beam attenuation and AOU; and **iii)** stations where any *in situ* AOU signal was diluted by the strong preformed AOU in adjacent water masses (N6, N7, and N8), and there was high AOU with increasing SPM towards the seafloor.

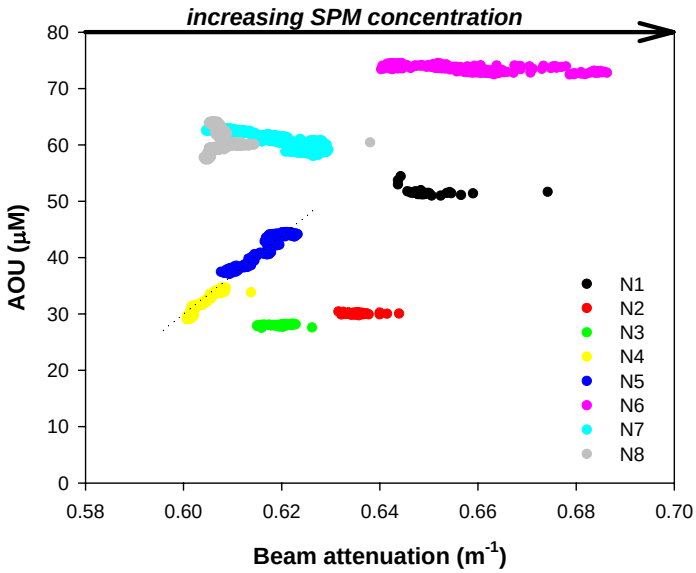

Figure V.6: Apparent oxygen utilisation (AOU, µM) *vs.* beam attenuation (m^{-1}) in the benthic nepheloid layer across the Celtic Sea shelf edge.

The most on-shelf station (N1) had a higher AOU than Stations N2 and N3 (Figure V.6), suggesting that at N1 there had been more POM remineralisation. The observed AOU signals in deeper waters at these stations therefore presumably reflect remineralisation of POM during the early part of the year.

The relationship of increasing AOU with increasing SPM near bottom at Stations N4 and N5 (Figure V.6), suggests that the high SPM was influencing AOU and was probably a recent feature. Sediments were found to be slightly sub-oxic, but not anoxic down to the redox boundary, which deepened from 1 cm at 210 m water column depth, to 2.5 cm at 1000 m, down to 5 cm at 2200 m across the shelf at Goban Spur during the OMEX programme (Lohse *et al.*, 1998). A resuspension event would thus have to be very important to induce such an increase in AOU (+ 7.3 µM at N4 and + 10.4 µM at N5 between the top and bottom of the BNL; Table V.2), which is not obvious from the beam attenuation profiles (Figure V.5). It was therefore most likely that the AOU reflected *in situ* remineralisation of the POM fraction within the resuspended material.

Despite high particle concentrations at Station N6 (Figure V.5), the AOU did not increase with increasing SPM in the BNL (~ 1200 m depth) (Figure V.6). Detecting a small AOU signal here is difficult because any in situ AOU signal would be diluted by the strong influence of low-oxygen waters at about 1000 m depth (Appendix 9). The

deep Stations N7 and N8 were also influenced by oceanic water masses (see Section V.4.2.3) with their own significant AOU signatures. The observed AOU signal at Stations N6, N7, and N8 was therefore dominated by the preformed AOU signals in the water masses that had accumulated during their transport.

The amount of dissolved iron released from POM oxidation in the BNL at each station can be estimated based on AOU values, and assuming that the Redfield-Richards ratio can be applied in these waters, and values for algal Fe:C ratio are known (Section V.4.1.1). The consumption of carbon was estimated from the difference in AOU between the top and bottom of the BNL, and using the Redfield-Richards ratio (C:AOU = 106:138). At Station N1, the estimated amount of carbon consumed was small (2.8 μM) and would only result in a maximum release of 0.14 nM DFe (Table V.2), with the maximum Fe:C ratio of 50 μmol/mol suggested in the literature (see above). The increase in DFe near the seafloor (Figure V.4) therefore cannot be explained by POM oxidation only, implying a contribution from an additional source (*e.g.* pore water diffusion or mixing through bio-turbation or resuspension).

Station	Depth (m)	AOU (μM)	ΔAOU (μM)	ΔC (μM)	Estimated ΔDFe (nM)	ΔDFe measured (nM)
N1	127 (top BNL)	47.8	3.7	2.8	0.03 – 0.14	2.84
	147 (bottom)	51.5				
N4	302 (top BNL)	26.8	7.3	5.6	0.06 – 0.28	0.63
	347 (bottom)	34.1				
N5	402 (top BNL)	33.5	10.4	8.0	0.08 – 0.40	0.19
	524 (bottom)	43.9				
	452 (mid-BNL)	40.7	3.2	2.4	0.02 – 0.12	
	524 (bottom)	43.9				

Table V.2: Estimation of carbon consumption and release of dissolved iron relative to measurements at Stations N1, N4, and N5 across the Celtic Sea shelf edge.
AOU = Apparent Oxygen Utilisation; Δ = difference between two values. ΔC calculated using the Redfield ratio (C:AOU = 106:138). Estimated ΔDFe calculated using published Fe:C ratios = 10 to 50 μmol/mol.

At Stations N4 and N5, the release of dissolved iron was estimated from carbon consumption as for Station N1 (see above). Much carbon was estimated to be remineralised at Stations N4 and N5 than at N1 (5.6 μM and 8.0 μM, respectively), and these values corresponded to a maximum release of 0.28 and 0.40 nM DFe, respectively (Table V.2). These estimates were not significantly different from the released DFe present in excess of background values at these stations (0.63 and 0.19 nM,

respectively). Whilst these calculations were based on assumptions of the carbon consumed and DFe released using the Redfield-Richard ratios, and that some removal may have been occurring simultaneously, these results are nonetheless consistent with the DFe being released from POM oxidation at Stations N4 and N5.

In contrast to Stations N1, N4, and N5, concentrations of dissolved iron were low at Stations N2 and N3, varying from 0.68 ± 0.03 nM at the top of the BNL and decreasing to 0.35 ± 0.02 nM in the bottom sample (Figure V.4). These generally low DFe, AOU, and SPM concentrations in the water column relative to N1 suggest that inputs of POM and DFe to bottom waters at these stations were less than at the other stations sampled. Decreasing DFe concentrations near the seafloor suggest that removal processes were more important than inputs at these stations, resulting in a significant loss (~ 40%) in DFe relative to background values, presumably as a result of adsorption onto particles.

Using the available data, it was thus possible to infer that *in situ* POM remineralisation was likely the major process releasing dissolved iron in the BNL at two upper-slope stations. It was also clear that dissolved iron was released in the BNL from other sources in addition to POM oxidation at the most on-shelf station; iron-rich pore water was the most likely based on our current knowledge of benthic processes. Removal processes were likely occurring in the BNL at all stations, and particularly at Stations N2 and N3. Mechanisms of DFe removal from seawater and DFe stabilisation in seawater are considered below.

V.4.1.4. Removal / stabilisation of dissolved iron in seawater near the seafloor

Dissolved iron is limited by its solubility to about 0.1-0.2 nM in seawater at pH 8.1 (Wu *et al.*, 2001). Excess dissolved iron should therefore precipitate quickly in oxic seawater (Rose and Waite, 2003a). Release processes of free iron (Fe(II) or Fe(III)) should therefore be quickly balanced by removal through precipitation or adsorption onto particles. However a significant fraction of DFe remains in solution despite thermodynamics constraints, and this may be due to organic complexation (Johnson *et al.*, 1997; Rose and Waite, 2003b), formation of colloidal species included in the measured "dissolved" (conventionally < 0.4-μm) fraction, or possibly kinetics constraints. Measured DFe concentrations therefore reflect the balance of input/removal/stabilisation processes at each station (Parekh *et al.*, 2004), and are dependent on the time since DFe release.

Precipitation of dissolved inorganic iron at the pH of oxic seawater is fast (Rose and Waite, 2003b), and therefore precipitation of pore water Fe(II) after oxidation to Fe(III) upon mixing with oxic seawater, is expected to take place before even reaching the sediment-water interface, unless it is stabilised (see below). The scavenging of dissolved iron onto particles is likely proportional to DFe and SPM concentrations (S_{Fe} = k [DFe] x [SPM], with k the scavenging rate constant) (de Baar and de Jong, 2001). Adsorption of dissolved iron onto particles will therefore be greater for waters with high SPM and high DFe, and if this were the only removal process, a linear relationship of decreasing dissolved iron with increasing SPM concentrations would be expected in the BNL.

Results (Figure V.7) reflected the complexity of the system as only a weak (r^2 = 0.38) relationship was found between DFe and beam attenuation for the upper shelf stations (N2 to N5), and DFe concentrations were similar at Stations N6 to N8 over a wide range of SPM levels. Very high DFe, associated with high SPM at Station N1 (Figure V.7) may result from resuspension of sediments containing DFe-rich pore waters or their advection or diffusion into overlying waters, where DFe may be organically complexed, or without time for the material to re-settle, and limited dissolved iron removal at the time of sampling. This result may be due to the efficiency of scavenging, which may vary with particle size. Small particles with a high surface area to volume ratio will also have a longer residence time that bigger particles, however particle size cannot be distinguished in the beam attenuation measurements. Temporal variability in inputs and removal and particle characteristics were thus likely controlling the measured DFe concentrations and stabilisation processes likely "buffered" the removal of DFe.

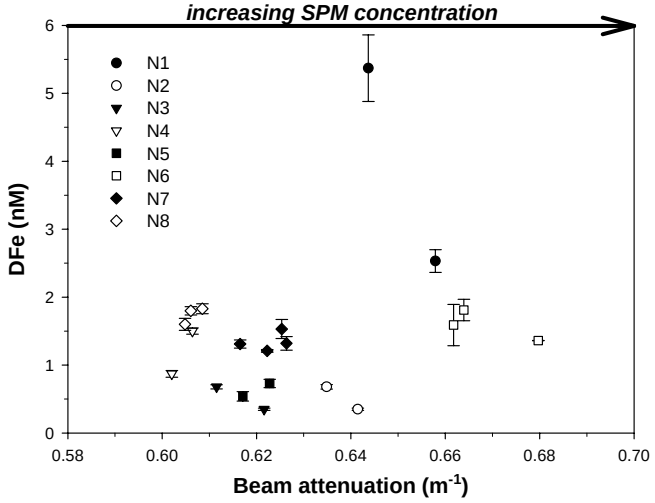

Figure V.7: Dissolved iron (nM) *vs.* beam attenuation (m^{-1}) in the benthic nepheloid layer across the Celtic Sea shelf edge.

Stabilisation of dissolved iron present in shelf waters may therefore be an important process that may allow iron export into the ocean (Mackey *et al.*, 2002; Laes *et al.*, 2003). The solubility of Fe(III) hydroxides in seawater depends on temperature, salinity, pH and organic ligands concentration (Liu and Millero, 2002). Solubility of Fe(III) hydroxides in seawater was calculated at all stations across the Celtic Sea shelf edge using the equation determined by Liu *et al.* (2002) which is valid for seawater with about 0.4 – 0.5 nM of unknown organic ligands:

$$Log[Fe(III)] = -10.53 + 322.5/T - 2.524I^{0.5} + 2.921I$$

with temperature T in Kelvin, and the ionic strength $I = 19.922S/(1000\text{-}1.005S)$ with the salinity S. Using this equation, the average Fe(III) hydroxides solubility across the transect was calculated to be 0.38 ± 0.01 nM (n = 80), which was generally lower than measured DFe concentrations (see Figure V.4). Liu *et al.* (2002) mentioned that changes in organic ligand concentrations will change the absolute value of iron solubility, and Boye *et al.* (2003) measured approximately 2 to 3 nM of iron complexing organic ligands in surface waters at the European continental slope. These concentrations of ligands are high enough to complex most of the iron measured in this study. One possible explanation to the increased concentrations of dissolved iron is therefore that organic ligands stabilised released DFe from benthic processes described above.

Dissolved (< 0.2 μm) iron, Fe(II) and iron-binding organic ligands were found to linearly increase in surface waters across the Celtic Sea shelf edge, indicating a common source (Boye *et al.*, 2003). Release of these ligands as a biological response to iron inputs by vertical mixing was considered unlikely due to the low cell numbers in these waters (Boye *et al.*, 2003). The authors therefore suggested that the ligands source must have been from admixed bottom waters implying that DFe was organically complexed before reaching surface waters (Boye *et al.*, 2003). Experiments performed with terrestrial natural organic matter (NOM) showed that iron formed Fe^{III}-NOM complexes as strong as the iron binding ligands produced by the biota in the open ocean (Rose and Waite, 2003b). Organic complexation between Fe and terrigenous NOM may therefore have an important effect on iron solubility in coastal waters (Rose and Waite, 2003b), and allow DFe transport to adjacent waters. However, export of DFe complexed to NOM far off-shelf would be limited when diluted in oceanic waters as these complexes would be thermodynamically less stable than oxy-hydroxides, with a half-life of several hours (Rose and Waite, 2003b).

Sediments are potentially an important source of Fe(II) to bottom waters depending on their redox conditions (Hong and Kester, 1986), and are also a source of dissolved organic carbon to bottom waters at Goban Spur (Otto and Balzer, 1998). Furthermore fluxes of copper-complexing ligands from estuarine sediments in excess by 3 to 40-fold to the dissolved copper concentration were reported (Skrabal *et al.*, 2000). Soluble species of Fe^{3+} complexed by natural organic ligands have recently been detected in coastal marine sediments (Carey and Taillefert, 2005). The possibility for the diffusion / advection of these iron organic complexes out of sediments has not yet been thoroughly investigated. Elderfield (1981) showed that 80% of iron was associated with colloidal organic matter of *in situ* origin, and likely of humic nature in pore waters from upper anoxic sediments. Whilst his calculations on diffusive transport of complexed dissolved iron indicated such sources would be negligible, advection due to bio-turbation might be significant (Elderfield, 1981). Further studies are clearly needed in order to determine whether sediments may be able to supply organic ligands, and organically complexed Fe(II) to bottom waters in oxic or sub-oxic conditions.

Recent studies on the speciation of iron in seawater showed that the operationally defined "dissolved" fraction (< 0.4 – 0.45 μm) included a substantial fraction of iron in the colloidal range (~ 0.01 to ~ 1.0 μm) (Moran *et al.*, 1996; Nishioka *et al.*, 2001; Wu *et al.*, 2001). Since more than 99% of dissolved iron is organically complexed (Gledhill and van den Berg, 1995), most of the colloidal iron is thus likely to be bound to organic ligands (Wu *et al.*, 2001). Sources of colloidal matter are numerous, and include sediment resuspension (Wells and Goldberg, 1994), although the release of colloidal iron from sediments has not yet been studied.

In summary, near-seafloor data were interpreted in terms of sources, removal, and stabilisation of dissolved iron across the shelf break. The main benthic source of dissolved iron appeared to be through remineralisation of POM at two upper slope, and possibly pore water release in bottom waters at the shallowest station. Release of dissolved iron near the seafloor will in part be balanced by removal; however a significant fraction of DFe remained in bottom seawater possibly as a result of organic complexation. Transport of dissolved iron to adjacent waters may thus be possible; therefore the influence of hydrodynamics at the shelf break on its distribution was examined.

V.4.2. Dissolved iron below the euphotic zone

The distribution of dissolved iron will also be influenced by the circulation (*i.e.* water masses and currents) at shelf break environments. Intermediate waters of the Northeast Atlantic Ocean near the European continental margin include three main water masses, which are flowing in opposite directions. Additionally, a permanent current is flowing pole-ward along slope (Pingree and Le Cann, 1989), and may promote resuspension events and horizontal transport along-shelf. In this section, iron data are used in association with physical parameters to investigate the role of circulation in promoting the transport of dissolved iron into the ocean's interior and towards surface waters.

V.4.2.1. Hydrography

The transect at the continental margin was examined in three-dimensions since the water masses and currents may influence the distribution of dissolved iron in all directions. The hydrography in the Northeast Atlantic is well characterised regarding water masses and their respective temperature, salinity, and preformed nutrient signatures (Tsuchiya *et al.*, 1992; Perez *et al.*, 1993; Pollard *et al.*, 1996; van Aken, 2000), and was thus interpreted accordingly with additional help (J. Read, 2005, personal communication). Surface waters are delimited by the seasonal thermocline (~ 50 – 100 m). Beneath, there is the Eastern North Atlantic Central Water (ENACW) originating from the advection of the sub-polar mode water formed by winter deep convection in the northern North Atlantic (Pollard *et al.*, 1996). ENACW is characterised by saline (~ 35.63) waters in its upper part (~ 100 to 300 m depth, ~ 27.00 < σ_t, kg/m^3 < 27.15), and a small salinity minimum (~ 35.53) in its lower part (300 to 600 m, ~ 27.15 < σ_t, kg/m^3 < 27.30) likely due to the influence of Sub-Arctic Intermediate Water (Figure V.8). ENACW overlies the saline Mediterranean Outflow Water (MOW) that flows northward along the continental slope from the Strait of Gibraltar (Arhan and King, 1995). It is found between about 600 m and 1300 m (27.30 < σ_t, kg/m^3 < 27.74) with its saline core at ~ 1000 m (Figure V.8). Beneath the MOW is the fresher and colder North East Atlantic Deep Water (NEADW, σ_t > 27.81 kg/m^3) (Figure V.8). NEADW results from the mixing of Iceland-Scotland Overflow Water, Labrador Sea Water (LSW) which is formed by deep convection in winter in the Labrador Sea (Paillet *et al.*, 1998), MOW, and the underlying Lower Deep Water influenced by Antarctic Bottom Water (van Aken, 2000). Diapycnal mixing is particularly strong along the continental slope and thus lead to a stronger modification

of the NEADW (van Aken, 2000). A small minimum in salinity at about 1800 m depth can be found in the eastern North Atlantic due to the LSW flowing south-eastwards (Talley and McCartney, 1982; Paillet *et al.*, 1998). However the LSW signature was not obvious here, presumably because of the close proximity of the stations to the shelf (Paillet *et al.*, 1998).

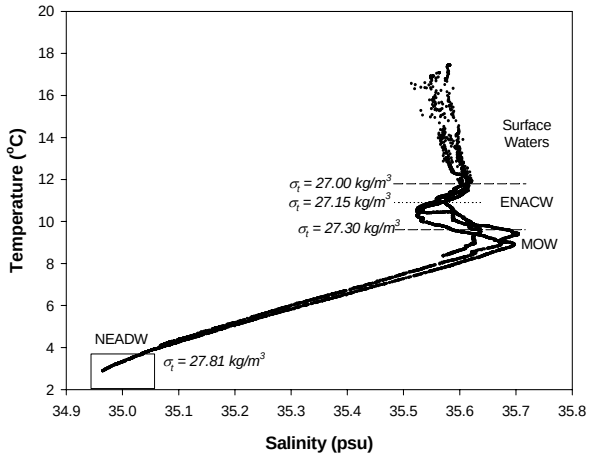

Figure V.8: T/S plot of Stations N6, N7, and N8 at the Celtic Sea shelf break, Northeast Atlantic. Main isopycnals (σ_t) are indicated. ENACW = Eastern North Atlantic Central Water; MOW = Mediterranean Outflow Water; NEADW = North East Atlantic Deep Water.

Macro-nutrient concentrations below 100 m (Stations N6 to N8) were similar to those reported in early summer at Goban Spur during the OMEX programme (Cotté-Krief *et al.*, 2002) (Table V.3). Nutrient levels were slightly lower in surface waters showing a more advanced state of depletion in August relative to values in June (Cotté-Krief *et al.*, 2002). Below the photic zone, little variation was observed between the data sets, as noted by Hydes *et al.* (2001). Dissolved silicon concentrations were high below 2000 m likely because of the stronger influence of Antarctic bottom water than during the OMEX programme (D. Hydes, personal communication).

	Surface < 100 m	ENACW 101-500 m	MOW 501-1250 m	NEADW 1251-3000 m
n	7 *27*	5 *18*	14 *30*	10 *22*
Nitrate (μM)	1.7 ± 2.0 *4.1 ± 3.4*	10.8 ± 1.5 *11.1 ± 1.6*	17.5 ± 1.3 *16.9 ± 1.4*	19.1 ± 0.6 *18.7 ± 1.1*
Phosphate (μM)	0.15 ± 0.11 *0.20 ± 0.13*	0.66 ± 0.10 *0.52 ± 0.10*	1.09 ± 0.12 *0.88 ± 0.14*	1.29 ± 0.05 *1.03 ± 0.10*
Dissolved Silicon (μM)	0.7 ± 0.6 *1.1 ± 0.9*	4.1 ± 1.1 *4.1 ± 0.9*	10.9 ± 1.9 *9.1 ± 1.8*	21.7 ± 4.8 *18.1 ± 7.9*

Table V.3: Macro-nutrient concentrations in the main water masses at the Celtic Sea shelf break (Stations N6 to N8) compared with data from Goban Spur in early summer (*in italic*) (Cotté-Krief *et al.*, 2002). ENACW = Eastern North Atlantic Central Water; MOW = Mediterranean Outflow Water; NEADW = North East Atlantic Deep Water.

A pole-ward current flowing along-slope at about 500 m depth was reported at the eastern North Atlantic boundary (Pingree and Le Cann, 1989; Pingree *et al.*, 1999; Souza *et al.*, 2001). It was observed here along the transect using geostrophic velocity calculated from the density gradients of temperature and salinity by the software Ocean Data View (reference at 2400 m depth) (Schlitzer, 2002). The main flow of this density-driven current was northwards with a small westwards component at N4, N5, N6 and N7 (Figure V.9). Geostrophic velocity was greatest between N5 and N6 with a down-slope component extending to about 1500 m between N6 and N7. The geostrophic flow sharpening in its core speed and its component offshore towards N7 possibly originated from mixing caused by internal tides which steepened the local gradients of the isopycnals (J. Sharples, 2004, personal communication), as also suggested by Pingree *et al.* (1989). The frictional stress at the benthic boundary layer by the slope current is likely of importance in that it will tend to induce a down-slope component of the flow with potential transport of benthic material down- and along-slope (Souza *et al.*, 2001; Huthnance *et al.*, 2002).

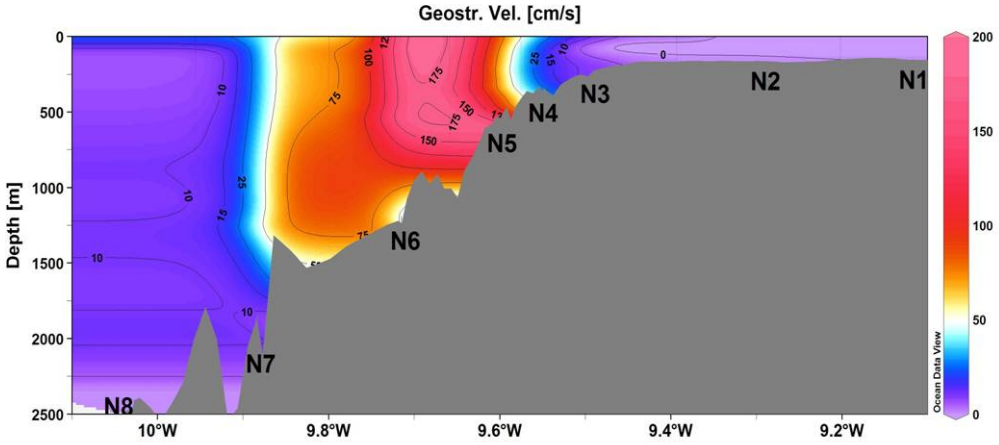

Figure V.9: Geostrophic velocity (cm/s) and contour lines along the transect at the Celtic Sea shelf break. Calculated from hydrographic data using the software Ocean Data View at the reference level 2400 m (Schlitzer, 2002). Bathymetry obtained from ship data and stations location, are indicated.

V.4.2.2. Lateral transport of dissolved iron

One approach to determining the influence of water circulation on the transport of shelf material at continental margins is to examine the distribution of particulate matter in the water column. Three types of nepheloid layers may be found at shelf breaks: **i)** surface nepheloid layers (SNL), mainly composed of biogenic material; **ii)** benthic nepheloid layers (BNL), formed by resuspension of sediments including a mixture of coarse, and

fine biogenic and lithogenic material; and **iii)** intermediate nepheloid layers (INL), defined as turbid waters distinct from the BNL by a layer of less turbid waters and likely composed of relatively fine biogenic, and lithogenic material (Dickson and McCave, 1986; McCave *et al.*, 2001).

The distribution of SPM across the shelf edge showed that all types of nepheloid layers were present at the time of the *JR98* cruise (Figure V.10). An intense BNL developed between Stations N5 and N7, and was most intense at Station N6 (Figure V.10), which also corresponded well to the zone of influence of the pole-ward flowing current (Figure V.9) (Pingree *et al.*, 1999). The likely sources of this major resuspension event on the upper slope were either the internal tide generating strong near-bead currents (Heathershaw *et al.*, 1987), or the friction due to the down-slope component of the pole-ward current (Souza *et al.*, 2001; Huthnance *et al.*, 2002).

The lowest beam attenuation values (lowest SPM) were found within the ENACW and MOW (Figure V.10) indicating that these water masses did not transport significant SPM in their core. Higher SPM concentrations were present below 1500 m depth (Figure V.10).

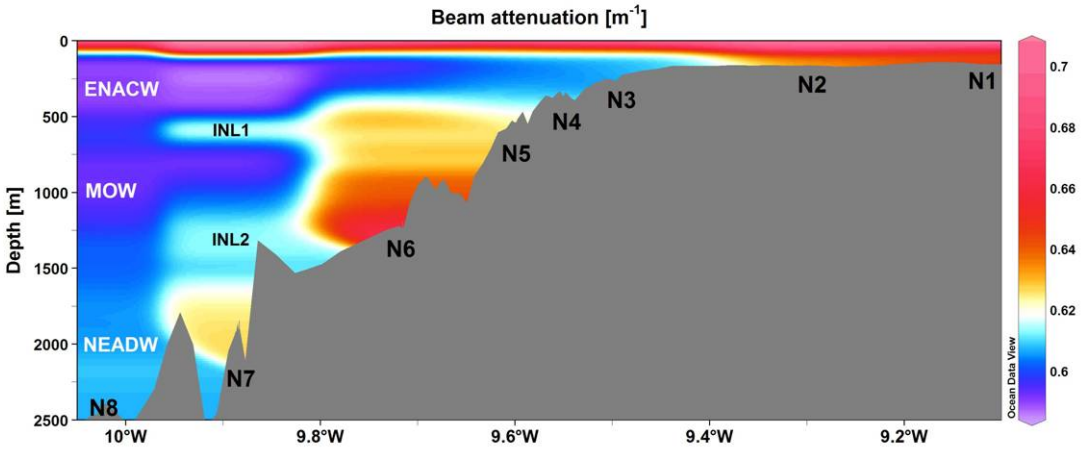

Figure V.10: Full depth beam attenuation signal (m^{-1}) across the Celtic Sea shelf edge. Bathymetry was obtained from the ship and main water masses are indicated. ENACW = Eastern North Atlantic Central Water, MOW = Mediterranean Outflow Water, NEADW = North East Atlantic Deep Water.

Two distinct INLs were detected at Stations N6 and N7 between 400 and 700 m depth (INL1, core at 600 m), and between 1000 and 1500 m (INL2, core at about 1300 m). These INLs could be formed from accumulation on density surfaces of biogenic particles settling from surface waters, or by detachment of an intense BNL (Dickson and

McCave, 1986). Given the strong SPM concentration in the BNL at Station N6, and that this feature followed the same isopycnals, BNL detachment was the most likely source.

The beam attenuation signal was stronger in the well-defined INL1 than in the broad INL2 at Station N7 (Figure V.10 and V.11). It was difficult to determine whether this difference in the intensity of those INLs was due to a variation in the magnitude of the resuspension event or in the time at which they were observed since creation, given that it was not possible to determine when those INLs were formed, and the transmissometer did not allow any distinction between particle sizes.

The INLs closely corresponded to the main water mass boundaries (Figure V.10), and their cores propagated along isopycnals at 27.30 kg/m^3 and 27.70 kg/m^3 for INL1 and INL2, respectively (Figure V.11), indicating the SPM advected along density surfaces between water masses. The beam attenuation signal of these INLs was relatively low at Station N8 (Figure V.10) suggesting that they may not propagate much further than Station N8, 22 km from Station N6, although along slope transport is also possible (Thorpe and White, 1988).

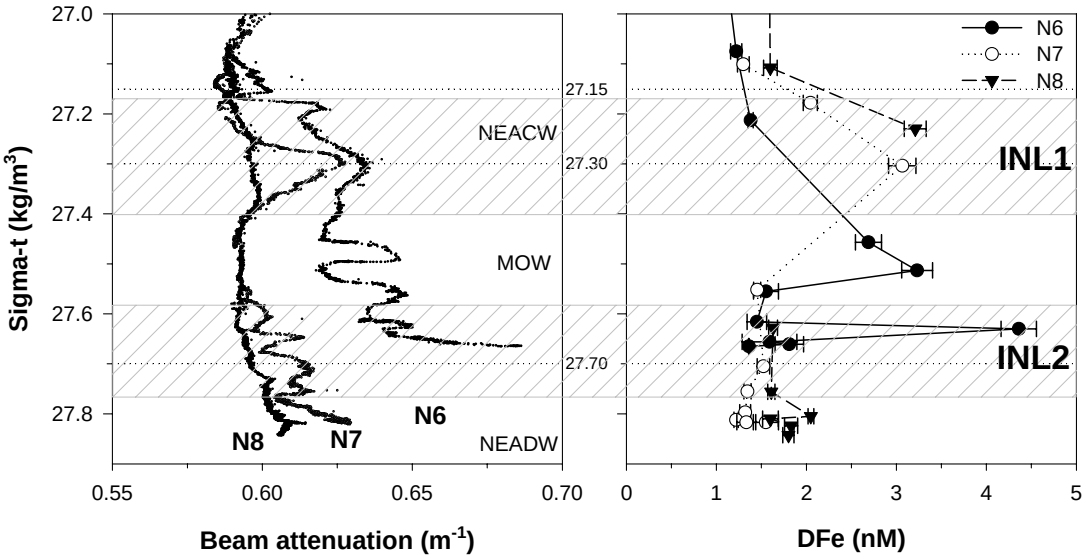

Figure V.11: Beam attenuation (m^{-1}) and dissolved iron (nM) distributions along density surfaces (σ_t kg/m^3) below the mixed layer at the deepest stations (N6 to N8) at the Celtic Sea shelf edge. Isopycnals separating the identified water masses (dotted lines) and INLs' zones of influence (grey hatched areas) are also indicated. ENACW = Eastern North Atlantic Central Water, MOW = Mediterranean Outflow Water, NEADW = North East Atlantic Deep Water.

Several studies suggested that dissolved iron was probably transported laterally offshore by local currents/water masses/eddies in order to explain enhanced DFe levels in the water column at different locations (*e.g.* Northeast Atlantic Ocean (Martin *et al.*, 1993;

Laes *et al.*, 2003), Equatorial Pacific (Gordon *et al.*, 1997; Mackey *et al.*, 2002), Southern Ocean (Croot *et al.*, 2004a), and Gulf of Alaska (Johnson *et al.*, 2005)). A plume of iron-rich waters was observed even at the most off-shelf stations below surface waters (σ_t > 27.0 kg/m^3) (Figure V.11). These DFe levels (~ 3.2 nM) were lower than those (5 – 9 nmol/kg) measured in association with turbidity plumes, and enhanced Al, Mn and Co levels within the Monterey Canyon (Martin and Gordon, 1988). High DFe levels coincided relatively well with INL1, and with a plume of relatively high beam attenuation deeper at Station N6, despite the relatively poor sampling resolution which did not properly constrain the SPM plumes (Figure V.11). By contrast, no DFe increase was found in association with INL2 at Stations N7 and N8 (further off-shelf) except in the BNL at Station N6 (Figure V.11).

High dissolved iron within INLs may originate from enhanced *in situ* remineralisation or from transport of DFe released from benthic processes within the BNL (see Section V.4.1). If DFe were to be remineralised *in situ* from POM by bacterial communities, elevated DFe concentrations would be associated with increased nitrate and phosphate and lower dissolved oxygen concentrations. However, N, P, and AOU were similar between Stations N6, N7, and N8 (Figure V.12), suggesting that enhanced *in situ* remineralisation was unlikely within INLs, and therefore that DFe was transported from its source near the seafloor.

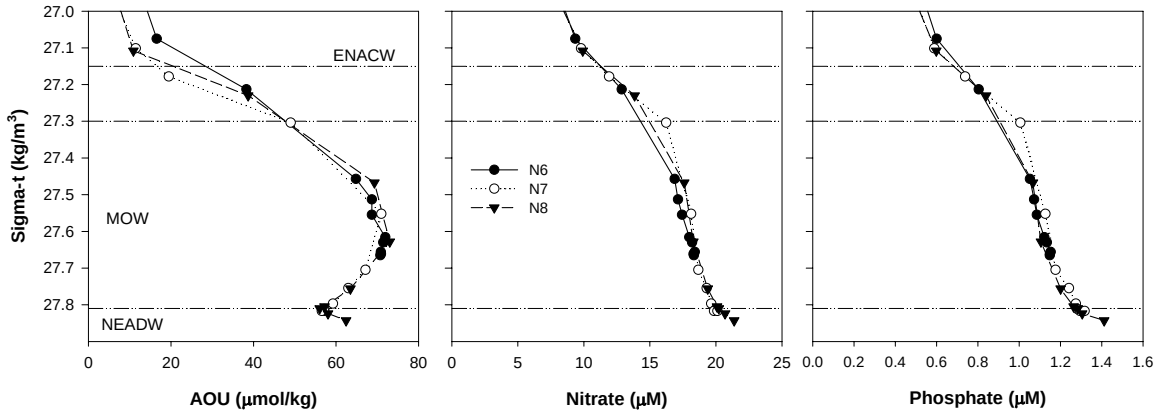

Figure V.12: Apparent Oxygen Utilisation (AOU), Nitrate, and Phosphate concentrations along density surfaces below the mixed layer at the deepest stations at the Celtic Sea shelf edge. Isopycnals separating main water masses are indicated by – ·· – lines.

Assuming that the INL was created from a single resuspension event, and DFe was transported from the BNL, DFe concentrations would be expected to be higher within INL1 at the most inshore station (N6), before significant reduction in

concentrations through mixing and removal processes occur. However, no clear DFe gradient in concentration was observed along the transect (Figure V.11), and the data may reflect the three-dimensional nature of the system, with INL1 and associated elevated dissolved iron concentrations formed to the south of this transect .

A further factor complicating interpretation is that intermediate nepheloid layers are common but intermittent events, which occur at specific depths at the Celtic Sea shelf edge as defined by the slope, and the amplitude of internal waves, as shown during the OMEX programme and in earlier studies (Dickson and McCave, 1986; Thorpe and White, 1988; McCave *et al.*, 2001). High DFe (~ 3.2 nM) was observed at the most offshore Station N8 at the same depth as INL1 (Figure V.11 and Figure V.13), however it was associated with only a weak increase in beam attenuation relative to surrounding waters. This high DFe signal suggests decoupling of dissolved iron from particles, so that most particles are lost but high DFe remains, and thus some form of DFe can survive particle scavenging.

No elevated DFe levels were observed within INL2 compared to within INL1 (Figure V.11 and Figure V.13), presumably reflecting the balance between inputs (depending on their source and intensity), and removal processes, which depend on particle characteristics (*e.g.* size, type) and concentration in these systems. Smaller particles will have a longer residence time due to their low settling velocity, and thus have more time to scavenge DFe.

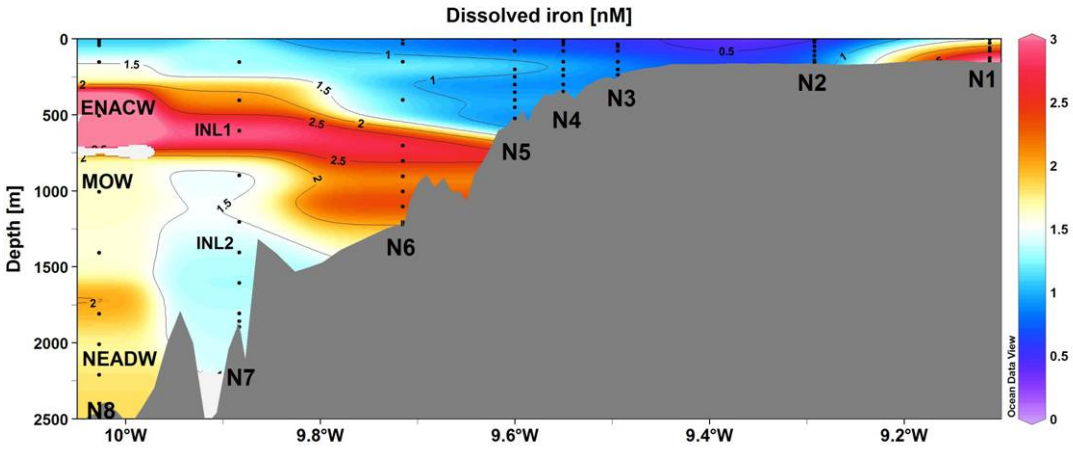

Figure V.13: Dissolved iron (nM) distribution across the Celtic Sea shelf break. Location of stations and of the cores of main water masses and intermediate nepheloid layers are indicated.

Mid-water column plumes of relatively high dissolved iron (about 1.8 nM) were observed at about 150 – 200 m at Stations N4 and N5 (Figure V.13). These features

were found at the depth of the ENACW, and also corresponded to the zone influenced by the along-slope current (see Figure V.9). Enhanced trace metal concentrations were found associated with the along-slope current at Goban Spur without any increase in beam attenuation (Le Gall *et al.*, 1999). It was hypothesised that this enrichment could occur when the current changed direction, and went over the shelf by infusion of trace metal rich waters near seafloor (Le Gall *et al.*, 1999). This theory may thus be valid here given that the current was relatively strong during the transect (see above). Finally dissolved iron was found to be higher (2.05 ± 0.03 nM) at 1800 m depth at Station N8 (Figure V.13 and 15), which corresponded to the depth at which LSW flows in the Northeast Atlantic Ocean (Paillet *et al.*, 1998).

The dissolved iron distribution below the euphotic zone was thus interpreted in terms of horizontal transport with the northward flowing current and with a fraction propagating along isopycnals, as was suggested by Dickson *et al.* (1986) for SPM transport. The possibility of enrichment of surface waters in dissolved iron by vertical mixing was then examined.

V.4.2.3. Vertical transport of dissolved iron

Macro-nutrient concentrations were very low in surface waters, however increased chlorophyll *a*, dissolved iron, nitrate, and phosphate were observed at the shelf break front (N3, N4, N5 and N6), and were strongest at Station N4 (Figure V.14). Low nutrient concentrations are common during summer at the Celtic Sea shelf break as winter stocks are consumed during the spring bloom (Hydes *et al.*, 2001). Surface dissolved silicon was not completely depleted across the shelf edge (Figure V.14), and was probably residual rather than regenerated (Hydes *et al.*, 2001).

The increase in dissolved iron across the shelf edge corresponded well with the trace metal fronts at the Celtic Sea shelf edge previously reported in the literature (Kremling, 1983; Muller *et al.*, 1994; Le Gall *et al.*, 1999; Cotté-Krief *et al.*, 2002; Boye *et al.*, 2003). The Northeast Atlantic Ocean is also under the influence of episodic Saharan dust plume events (Blain *et al.*, 2004), and may contribute to the surface DFe measured. However such a localised increase in all parameters is more likely due to vertical mixing of waters underlying the thermocline, and nitrate and phosphate were likely taken up by the biota as they were supplied to surface waters.

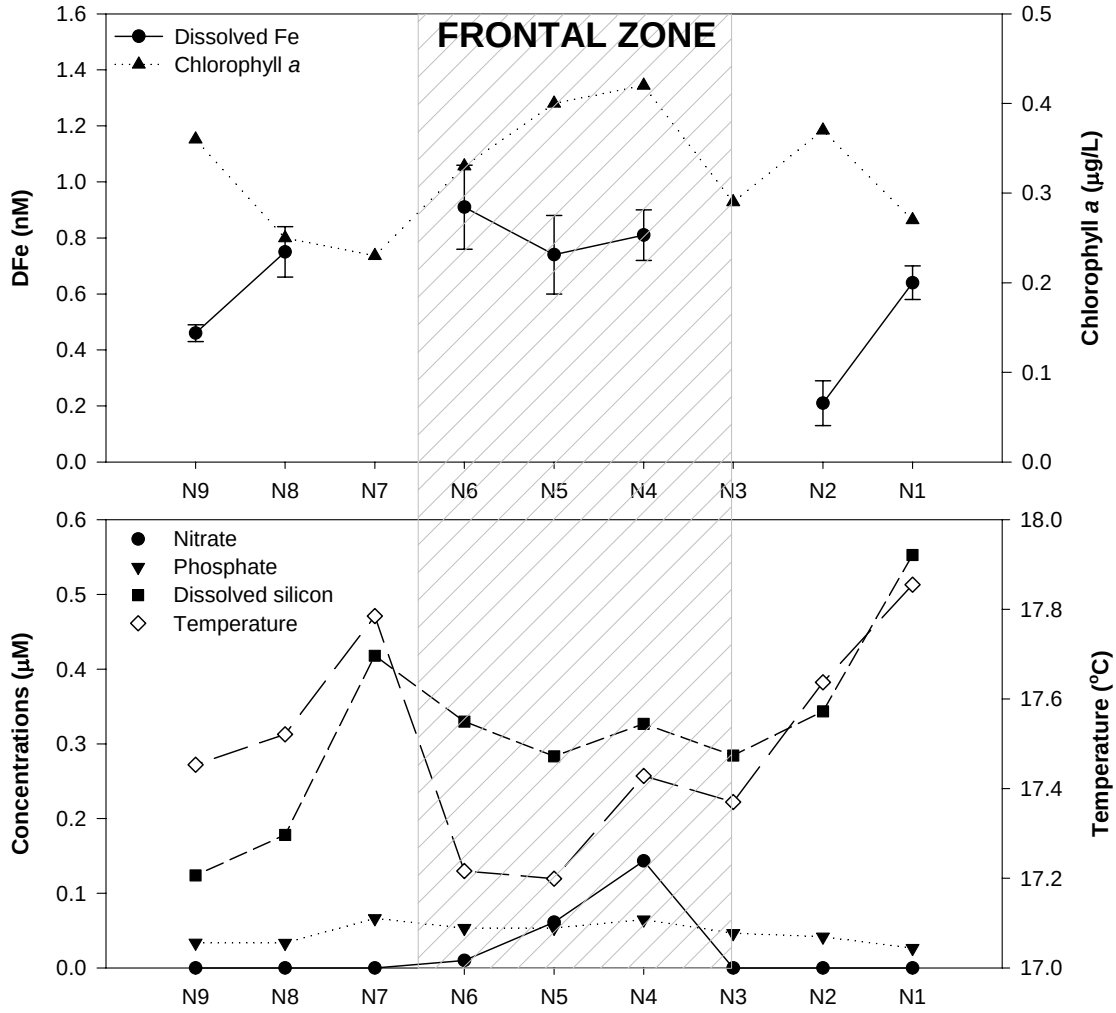

Figure V.14: Dissolved iron, chlorophyll *a*, macro-nutrient concentrations and temperature in surface waters (3 – 4 m) across the Celtic Sea shelf break. Shaded area highlights the location of the shelf break front. [DFe] in surface waters at Station N3 was below the limit of detection.

Evidence for vertical mixing at the Celtic Sea shelf break was given by the presence of a cool thermal front during summer months (~ 1°C cooler than surrounding waters; Figure V.15a) (Dickson and Gurbutt, 1980; Pingree *et al.*, 1986). Decreasing surface water temperatures (17.9°C to 16.9°C) showed that the front was located between Stations N3 and N6 (Figure V.15b), and corresponded well to the area of increased dissolved iron in surface waters (Figure V.14). This thermal front is due to the combination of sudden shallowing of waters across the continental shelf, and by the change in current speed across the shelf, which is likely induced by tidal exchange (Pingree *et al.*, 1986).

Surface waters were thus likely supplied in nutrients from waters underlying the thermocline vertically mixed. Dissolved iron concentrations below the thermocline were similar or higher than in surface waters (see Figure V.4), and thus vertical mixing of these waters could be sufficient to support measured DFe in surface waters.

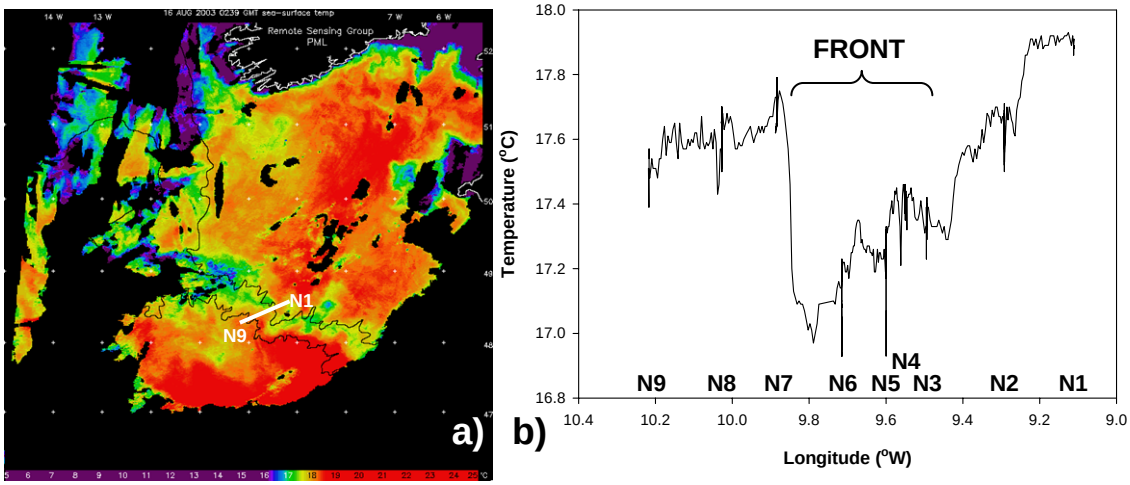

Figure V.15: Sea surface temperature at the Celtic Sea shelf edge at the end of the *JR98* cruise. **a)** Satellite picture provided by the Remote Sensing Group, Plymouth Marine Laboratory; and **b)** data from the ship's underway sampling system.

In summary, transport of dissolved iron by advection both horizontally and vertically was evident at the Celtic Sea shelf edge. Vertical mixing will thus have a significant impact on the primary production in surface waters, and since dissolved iron is an essential micro-nutrient to living organisms, its distribution in surface waters was examined in relation to the biology.

V.4.3. Dissolved iron in the euphotic zone

Shelf break systems mark the boundary between the biologically productive shelf waters and less productive oceanic waters. Changes of stratification across the shelf edge, and consequent vertical advection of nutrient-rich waters are likely to influence the biota but vertical mixing did not occur at all stations across the transect (see above). Given that iron is essential for phytoplankton development, biota are likely to influence dissolved iron distributions in surface waters. Here available data on the biology at the time of the cruise (courtesy of Y.-N. Kim) are firstly examined to give a biological context to this study. Then the distribution of nitrate and dissolved iron are studied in relation to the biomass in order to determine the degree of nutrient uptake. Finally the possibility of iron limitation of phytoplankton is investigated.

V.4.3.1. Biology in the euphotic zone across the transect

Data from Station CS2 (see Table V.1 for coordinates, sampled 8 days prior the transect during the cruise) was used to give information about the biology at the shelf break as

this station was very close to the position of Station N3 (Figure V.2), and detailed biological data was otherwise available only at Stations N1 and N9 across the transect.

Chlorophyll *a* concentrations were low (< 1 μg/L) at all stations across the shelf edge (including CS2; see Figure V.14) as expected during summer after winter nutrient stocks were used during the Spring bloom, and as supply of nutrients to surface waters was likely episodic (Hydes *et al.*, 2001; Cotté-Krief *et al.*, 2002). A sub-surface chlorophyll *a* maximum between 20 to 30 m depth was also observed (see Appendix 9), as reported previously at the Celtic Sea shelf (Sharples *et al.*, 2001). As nutrients become depleted in surface waters during summer, phytoplankton develops where nutrients are more available, *i.e.* at the base of the thermocline (Kremling, 1983; Sharples *et al.*, 2001).

At Stations N1 and CS2, chlorophyll *a* size fractions (< 5 μm and > 5 μm) were similar (~50% of chlorophyll *a* (chl*a*)) at the chlorophyll *a* maximum depth whereas Station N9 had slightly more (~60% chl*a*) small cells (Y.-N. Kim, 2005, personal communication).

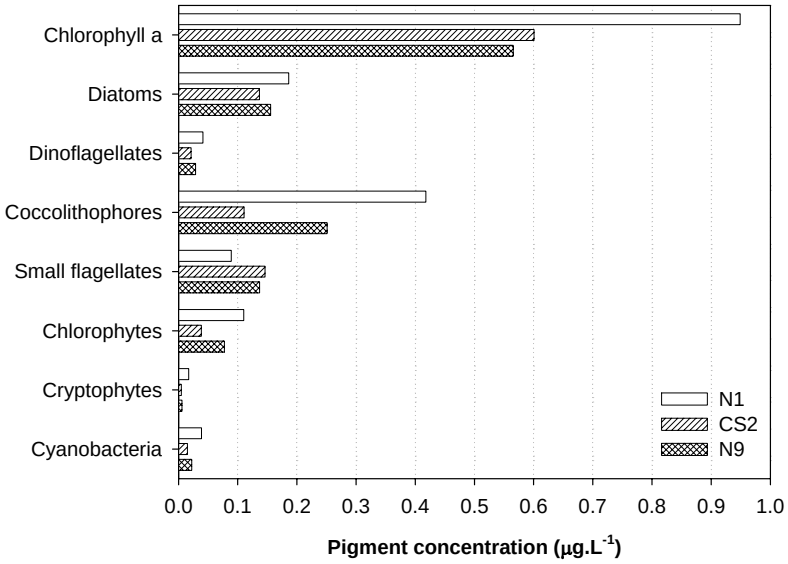

Figure V.16: Marker pigment concentrations at three stations across the Celtic Sea shelf edge. While chlorophyll *a* is used as a convenient proxy of phytoplankton biomass, many other phytoplankton pigments exhibit chemotaxonomic associations, which may be exploited to map the oceanographic distribution and composition of phytoplankton assemblages. Pigments and likely group: Fucoxanthin (as for diatoms); Peridinin (as for dinoflagellates), 19'-hexanoyloxygucoxanthin (as for Prymnesiophytes (coccolithophores)), 19'-butanoyloxyfucoxanthin (as for Chrysophytes (small flagellates)), chlorophyll *b* (as for Chlorophytes), alloxanthin (as for Cryptophytes), and zeaxanthin (as for Cyanobacteria) (Wright and Jeffrey, 1987; Bjornland and Liaaen-Jensen, 1989; Wright *et al.*, 1991; Barlow *et al.*, 1993). Data from Y.-N. Kim (*in preparation*).

Pigment HPLC analyses showed that the chlorophyll *a* maximum at Stations N1 and N9 were dominated (~44% chla_{HPLC}) by coccolithophores followed by diatoms (~20% and 27.5% chla_{HPLC} respectively), and small flagellates, which were less abundant at N1 (~9.5% chla_{HPLC}) than N9 (~24% chla_{HPLC}) (Figure V.16). In contrast, small flagellates, diatoms and coccolithophores were almost equally (~20% chla_{HPLC}) present at the shelf edge station (CS2) (Figure V.16). The stronger presence of coccolithophores at Stations N1 and N9 likely reflect their stronger water column stratification than Station CS2 (N3), which is affected by vertical mixing (see above). No other major difference was observed in the phytoplankton species composition.

V.4.3.2. Dissolved iron distribution in the euphotic zone

As iron is an essential nutrient for phytoplankton as well as nitrate and phosphate, a relationship showing the uptake of dissolved iron and macro-nutrients in response to increasing primary production (chlorophyll *a*) in the euphotic zone (< 50 m depth) might be expected if the system is not "saturated" with iron.

The relationship between nitrate and total chlorophyll *a* concentrations was consistent with the cycle of nutrient supply - biological uptake - nutrient depletion in the euphotic zone (< 50 m depth) (Figure V.17a). When nutrients were supplied to surface waters (N4, N5, and N6), phytoplankton developed and utilised macro-nutrients (N3, N9, and N1), and when one or more nutrient became depleted the bloom faded (N4, N8 and surface samples) (see arrows on Figure V.17a).

A reduction in dissolved iron in the euphotic zone (< 50 m depth) relative to deeper waters, presumably reflecting uptake at the chlorophyll *a* maximum, was observed only at Station N4 and likely N5 (Figure V.17b), which had the highest chlorophyll *a* concentration (Figure V.14). Reasons for the lack of correlation of DFe and total chlorophyll *a* at other stations may be that: **i)** samples were not always collected precisely at the chlorophyll maximum (*e.g.* Stations N1 and N6, see Appendix 9) so that the DFe minimum may have been missed; **ii)** there may be a time lag between iron input and biological response; **iii)** the biomass may have been controlled by nitrate uptake resulting in a restricted uptake of iron as nitrate was depleted; or **iv)** the phytoplankton species present had lower iron requirements.

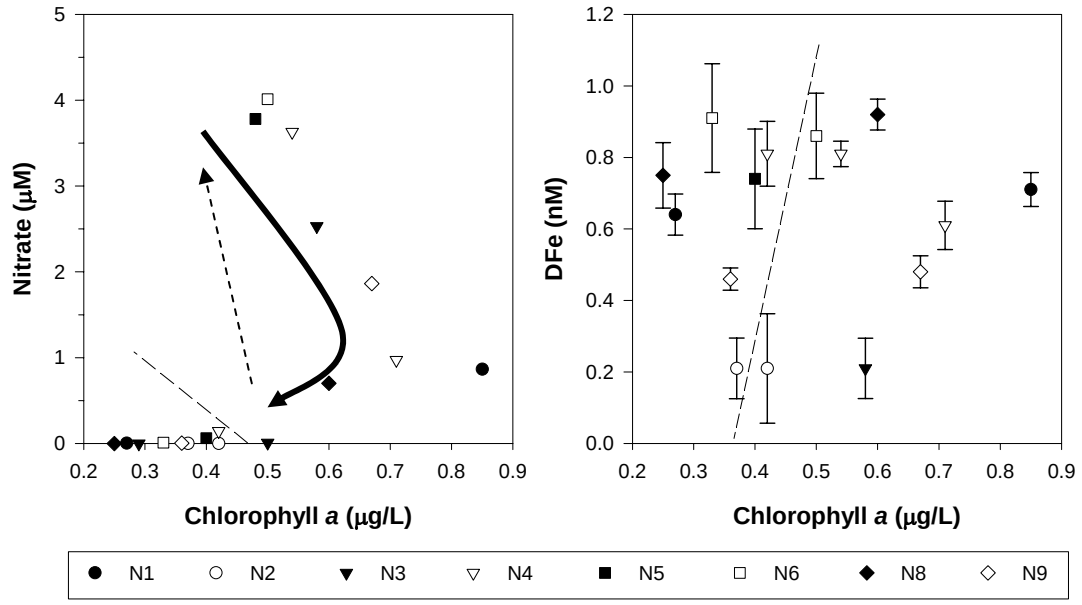

Figure V.17: Plots of **a)** nitrate and **b)** dissolved iron *vs.* chlorophyll *a* in surface waters (left hand side of dashed line) and at the chlorophyll *a* maximum (right hand side of dashed line) (< 50 m depth) across the transect at the Celtic Sea shelf edge. Dashed line separates data from surface waters (left hand side) and taken at the chlorophyll *a* maximum (right hand side). Plain arrow and dashed arrow on plot a) represents uptake and supply cycle of nitrate respectively. Three data points were below the detection limit (< 0.16 nM) at 2 and 15 m at N3 and at 20 m at N5 and are thus not shown in this figure.

One result of the mesoscale iron fertilisation experiments carried out in high-nutrient low-chlorophyll regions was that changes in algal stocks occurred a few (3 – 4) days after fertilisation with dissolved iron (*e.g.* (Martin *et al.*, 1994; Coale *et al.*, 1996b; Boyd *et al.*, 2000)). Thus supply of dissolved iron to surface waters by vertical mixing may not have induced an immediate biological response (*i.e.* increase in chlorophyll *a*), which may give an explanation as to why no direct relationship between DFe and total chlorophyll *a* was found.

Vertical mixing of nutrient-rich waters to the surface was observed at three of the stations (N4 to N6) (see above). However levels of dissolved iron were relatively low (sub-nanomolar) for shelf waters, especially at Stations N2 and N3. Since chlorophyll *a* was also found to be low across the transect, the possibility of iron limitation at the Celtic Sea shelf edge was examined.

V.4.3.3. Iron limitation at the Celtic Sea shelf break ?

Several iron fertilisation experiments showed that iron limitation was evident for phytoplankton in high-nutrient low-chlorophyll regions of the open ocean (Martin *et al.*,

1994; Coale *et al.*, 1996b; Boyd *et al.*, 2000). Phytoplankton was also found to be iron-stressed between supply of iron in regions affected by episodic natural iron inputs, even though dissolved iron concentrations were not very low, as in the Californian coastal upwelling (Hutchins and Bruland, 1998; Bruland *et al.*, 2001; Fitzwater *et al.*, 2003), or in waters influenced by atmospheric dust deposition (Sarthou and Jeandel, 2001; Blain *et al.*, 2004; Mills *et al.*, 2004). Shelf break regions are intermediate environments between generally productive shelf waters, and poorly productive oceanic waters. The shelf break front and geostrophic current act as barriers between these end-member waters. Additionally seasonal stratification acts as a barrier separating surface waters from deeper waters. This zonation may thus create water domains where some form of nutrient limitation may develop due to limited supply of dissolved iron when aeolian inputs are also small.

Hutchins *et al.* (1998) demonstrated that Fe limitation can be important in regions other than the traditional Fe-limited oceanic regimes (HNLC areas). The authors described four zones in a coastal environment generally replete in macro-nutrients: **1) Fe-replete**, with almost complete depletion of macro-nutrients after an extensive bloom of large diatoms; **2) Fe-stressed**, where iron limits growth of large diatoms only; **3) moderately Fe-limited**, where iron limitation controls species composition; and **4) severely Fe-limited**, where iron controls N and DSi drawdown, POC production, and limits biomass growth (Hutchins *et al.*, 1998). This classification shows that the concept of iron limitation of primary production is complex as it depends on many factors including the speciation of iron (Sunda, 2001; Chen *et al.*, 2003), the species composition and their iron growth requirement (Sunda and Huntsman, 1995), the supply and removal or iron (de Baar and de Jong, 2001), and its recycling (Hutchins and Bruland, 1994). Therefore new forms of iron limitation (or co-limitation) may be found in the future.

The approach adopted here to investigate on the possibility of iron limitation at the Celtic Sea shelf break was to examine the Fe:N ratio in the seasonal thermocline waters (< 50 m). It was assumed that, to achieve minimum growth, phytoplankton take up at least 10 μmol Fe/mol C (Fe:N = 0.07 nM/μM using the Redfield-Richards ratio), which corresponds to the approximate minimum growth rate for non-nutrient limited coastal phytoplankton, and particularly diatoms (Sunda and Huntsman, 1995) (see Section V.4.1). Therefore, when N is not depleted, lower Fe:N ratios would indicate that

phytoplankton were possibly iron-stressed, eventually leading to iron limitation if Fe was not re-supplied.

Results (Figure V.18) showed that the data could be divided into three groups.

In Group 1, nitrate was depleted in surface waters at all stations across the transect and below ~ 10 m at Stations N2 and N9 (Figure V.10 and Appendix 9). In this group, dissolved iron concentrations ranged between 0.21 nM up to 0.91 nM suggesting that nitrate was depleted before iron in surface waters.

In Group 2, both nitrate and DFe concentrations were high (Stations N4, N6 and N8) (Figure V.18) at the base of the thermocline, suggesting that supply of nutrients from below by vertical mixing recently occurred (see above).

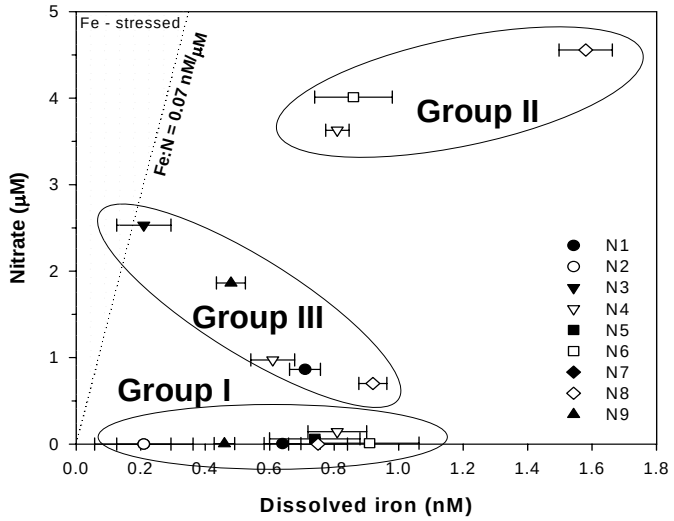

Figure V.18: Nitrate (µM) vs. dissolved iron (nM) in the seasonal thermocline (< 50 m) across the Celtic Sea shelf edge.

Finally the third group included waters collected at the chlorophyll *a* maximum depth at Stations N1, N3, N4, N8 and N9. Stations N3 and N9 had high-nitrate and relatively low-iron waters, and Stations N1, N4 and N8 had relatively low nitrate and relatively high dissolved iron (Figure V.18). At the latter stations, the seasonal thermocline may have recently been supplied in nutrients, and the input of DFe may have supplied nitrate thus allowing faster N uptake and increasing the Fe:N ratio (0.82, 0.22 and 1.31 nM/µM for N1, N4 and N8 respectively). Waters at Station N9 had low Fe:N ratios (0.26 nM/µM), and the Fe:N ratio was lowest (0.08 nM/µM) at Station N3 (Figure V.18). Phytoplankton were thus not limited at these stations since a maximum in chlorophyll *a* was found, but they may be iron-stressed particularly at Station N3, and may subsequently become iron limited if nutrients are not re-supplied.

These results indicate no signs of iron limitation when considering nutrient concentrations in surface waters only, except possible Fe-stress at Station N3. However, according to the study of Hutchins *et al.* (1998), these data are not sufficient to determine the state of possible nutrient-stress of the bloom, and bottle incubation experiments should be carried out. The possibility of iron limitation at the Celtic Sea shelf break cannot thus be ruled out based on the present data. An additional state of iron limitation was recently suggested, based on the observation that iron limitation may not only depend on Fe concentrations in the euphotic zone, but that phytoplankton may become iron limited as a result of low levels of macronutrients, and nitrate particularly (Wang and Dei, 2001). Nitrate-starved diatoms may thus not be able to take up iron using their N-enriched membrane proteins for Fe acquisition, resulting in N and Fe co-limitation (Wang and Dei, 2001). Additional studies are thus needed to investigate further the possibility of iron limitation of the biota at the Celtic Sea shelf edge during summer when waters are stratified. The role of grazers should also be considered given their potentially important contribution in the export or regeneration of iron in surface waters (Hutchins and Bruland, 1994).

In summary, conditions were typical of summer time with a weak sub-surface chlorophyll *a* maximum, and low macro-nutrient concentrations in the seasonal thermocline. Phytoplankton was likely limited by nitrate at all stations, although the possibility for iron-stress or iron co-limitation could not be ruled out. From this study at the Celtic Sea shelf edge, it appears that in addition to vertical mixing, Fe may be supplied to phytoplankton in surface waters by advection of shelf waters to surrounding areas. The case of the bloom observed in the HNLC waters surrounding South Georgia in the Southern Ocean and the possibility that benthic supply of iron may naturally fertilise those waters is now examined.

V.5. The « island mass effect » around South Georgia, Southern Ocean

The Southern Ocean was long thought to be a biological desert. However, thanks to satellite SeaWiFS observations, a few “oases” have been observed. Extensive phytoplankton blooms are reported in the vicinity of the main islands of the Southern Ocean: Crozet and Kerguelen (Indian sector), and South Georgia (Atlantic sector) (Figure V.19).

It was postulated that these blooms resulted from the enrichment of HNLC waters with dissolved iron through the resuspension and advection/diffusion of benthic inputs in shallow waters surrounding the islands. This hypothesis has been recently confirmed at the Kerguelen island where high dissolved iron concentrations were measured in association with enhanced biological activity around the island (Blain *et al.*, 2001; Bucciarelli *et al.*, 2001), and is under investigation at the Crozet archipelago (*CROZEX* project 2004 - 2005), but has not yet been studied at South Georgia.

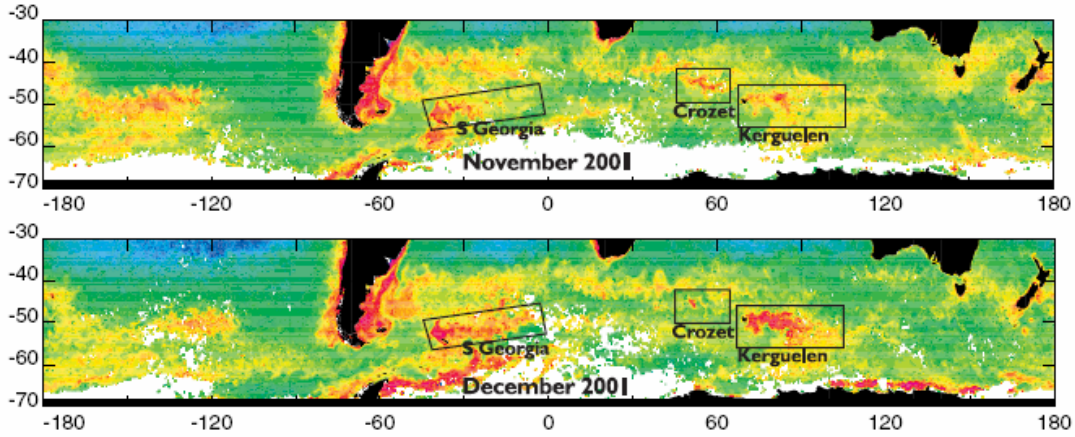

Figure V.19: Satellite SeaWiFS picture of surface chlorophyll a concentrations in November and December 2001 in the Southern Ocean from (Pollard, 2004). The main islands and their associated bloom are framed in rectangles. Blue = < 0.1 $\mu g.L^{-1}$, Green = 0.1-0.4 $\mu g.L^{-1}$, Yellow ~ 0.4-1.0 $\mu g.L^{-1}$, Red > 1.0 $\mu g.L^{-1}$.

A transect along the North Scotia Ridge (53-54°S) was organised between the Falkland Islands and South Georgia (58-33°W) in Austral autumn 2003. The aim of this study was to explore the possibility that the contrast between these areas of high-chlorophyll and surrounding HNLC areas is associated with variations in phytoplankton photo-physiology, and that the potential iron stress may be alleviated in phytoplankton populations near South Georgia (Holeton *et al.*, 2005). The iron analyses for this work were done as part of the present study. A set of unfiltered surface (~ 1 m depth) seawater samples were collected using a "pole sampler" (see Chapter IV), and were analysed for total dissolvable iron using the FIA-CL developed in this project (see Chapter III and IV) (Holeton *et al.*, 2005). These data were used to augment data on phytoplankton photo-physiology and community structure acquired at the same time.

Total dissolvable iron (TDFe, including both dissolved and particulate iron leachable at pH 2) concentrations varied between 0.9 to 13.6 nM (Figure V.20), which compared favourably to dissolved (< 0.4 µm) iron levels measured in the wake of Kerguelen

Islands (Bucciarelli *et al.*, 2001). The highest TDFe concentrations along the transect were found localised at the shallow South Georgia shelf (Figure V.20), suggesting that iron may have been supplied through benthic processes with subsequent transport to surface waters (Holeton *et al.*, 2005). This increase in TDFe near South Georgia was associated with enhancement of nitrate and dissolved silicon levels, chlorophyll *a*, and dark-adapted maximum photo-chemical quantum efficiency (F_v/F_m), relative to waters east of 46°W (Holeton *et al.*, 2005). Chlorophyll *a* pigments analyses by HPLC also showed a shift in species composition as the shelf waters of South Georgia contained the highest index of diatom-dominance (Holeton *et al.*, 2005).

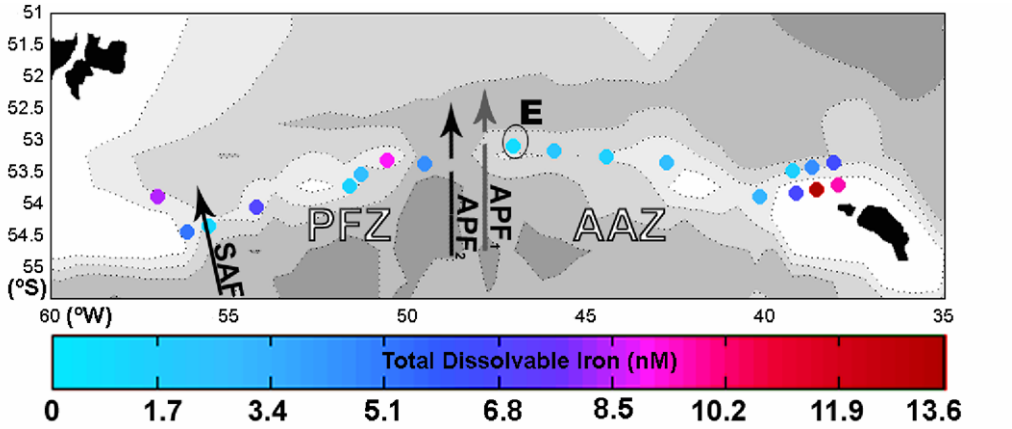

Figure V.20: Total dissolvable iron concentrations in surface (~ 1 m depth) waters along the transect between the Falkland Islands (top left) and South Georgia (bottom right). Indications of the hydrography are shown: SAF = Sub-Antarctic Front; APF1 and APF2 = Antarctic Polar Front on the eastward (1) and westward (2) transect; PFZ = Polar Frontal Zone; AAZ = Antarctic Zone; E = eddy (Holeton *et al.*, 2005).

It was suggested that species composition, and particularly cell sizes, might have affected measurements of F_v/F_m of bulk community, however another factor was more likely to induce the observed shift in photo-physiology at 46°W (Holeton *et al.*, 2005). It was hypothesised that currents flowing over the South Georgia shelf may naturally fertilise downstream waters with iron of benthic origin (Holeton *et al.*, 2005), as previously proposed (Korb and Whitehouse, 2004). Additionally it was suggested that the contrast between photo-physiological parameters in populations east and west of 46°W along the North Scotia Ridge represented a transition from iron-replete to iron-limited populations (Holeton *et al.*, 2005). The iron data included particulate iron that may not be bio-available, and thus dissolved iron (including small colloidal iron) may only represent a small fraction of the total dissolvable iron concentrations measured (Sunda, 2001).

This study therefore suggests that benthic supply of iron to surface waters potentially have important consequences on the phytoplankton population providing that macro-nutrients are not depleted. These results also imply that transport of bio-available iron was possible showing that this process should not be underestimated in the iron biogeochemical cycle. Additional studies are clearly needed at South Georgia in order to better understand this region, which provides important fisheries stocks, and to explain how increased dissolved iron concentrations were measured in the Antarctic Circumpolar Current thousands of kilometers eastward of the island (Loscher *et al.*, 1997; Croot *et al.*, 2004a).

V.6. Conclusions

The shelf break is a highly dynamic environment where oceanic and coastal waters meet; therefore the dissolved iron distribution was expected to be influenced by a multitude of processes induced by these two different environments.

Results are consistent with the main source of dissolved iron near seafloor being POM remineralisation, but other processes including mixing and removal complicated the interpretation. Dissolved iron concentrations were highest (5.4 nM) on shelf, and pore water resuspension was likely an additional source of iron to these bottom waters. Transport of dissolved iron was evident. Horizontal advection of dissolved iron (~ 3.2 nM) associated with an intermediate nepheloid layer propagating along an isopycnal was identified, and dissolved iron was possibly also transported within the along-slope pole-ward flowing current. A second weaker deeper INL did not show enhanced dissolved iron concentrations relative to background values (~ 1.3 nM), which may be due to variations in the scavenging efficiency or in the magnitude of the sources of dissolved iron. There was also evidence of vertical advection of nutrient-rich waters underlying the thermocline to the surface at the shelf break front, driven by the internal tide and shallowing topography. In the seasonal thermocline, the biology and nutrient distributions were typical of summertime in the northern hemisphere, and dissolved iron uptake was suggested at the chlorophyll *a* maximum at two stations on the upper slope. Nitrate appeared to be limiting phytoplankton growth in most of the seasonal thermocline; however, the phytoplankton population may become iron-stressed at some upper slope stations. Other forms of iron limitation, stress, or co-limitation were considered, and should be further investigated in the future.

Potential consequences of enrichment of shallow waters with dissolved iron were examined along an additional transect at the North Scotia Ridge between the Falkland Islands and South Georgia in the Southern Ocean. It was suggested that benthic sources may alleviate iron-limitation downstream of South Georgia, and lead to increased biological activity and photo-physiological efficiency. These results therefore support the theory of the "island mass effect" in HNLC waters of the Southern Ocean as already shown at the Kerguelen Islands (Blain *et al.*, 2001), and is under investigation at the Crozet islands.

Implications of these results reside in the improvement in our understanding of the iron cycle in shelf break environments (see model Figure V.1). Initially dissolved iron, nitrate, phosphate, and silicon for diatoms are taken up by phytoplankton in the nutrient-rich surface waters during the spring bloom. Sinking POM is then partially remineralised below the thermocline releasing nutrients. These shallow nutrient-rich waters may then be advected vertically, especially at the shelf break front, and fertilise nutrient-depleted surface waters. This recycling likely sustains a bloom at the shelf edge and allows growth of larger cells. When reaching the seafloor, the remaining fraction of POM is remineralised releasing dissolved iron and nutrients. On shelf, POM remineralisation in sediments will intensify if more detritus reaches the seafloor, and this may lead to micro-reducing zones where iron oxides could be dissolved through this bacterial respiration. Resuspension of sediments or mixing through bio-turbation may then release dissolved iron from pore waters into bottom waters in addition to that released by POM oxidation. Dissolved iron is likely organically complexed or colloidal when released from sediments therefore stabilising it when entering oxic waters, but a significant portion is eventually lost from solution by precipitation and/or adsorption onto particles. Iron- and SPM-enriched bottom waters may then be transported laterally as intermediate nepheloid layers or within the along-slope current. During wintertime, the mixed layer deepens towards the seafloor leading to enrichment of surface waters in iron and macro-nutrients, which are then consumed during the spring bloom.

As the aim of this work was to give a conceptual framework for discussing processes, several questions are raised, which could not be answered in the scope of this study given the limited data, but they do provide a basis for future work:

1. Sources of dissolved iron to bottom waters

We clearly need a better understanding of release processes near the seafloor in order to determine fluxes of dissolved iron from benthic sources, and fluxes that actually reach surface waters, and thus allow them to be included in the global budget of oceanic iron (Elrod *et al.*, 2004). Additionally, it is still unknown whether dissolved iron is organically complexed when released from pore waters or from POM oxidation. This point is important in understanding how high dissolved iron concentrations may be sustained in oxic shelf waters and possibly transported offshore. The source and stability of these organic ligands also remains unknown and could potentially be of biological or terrestrial origin. The importance of inorganic colloids in the dissolved iron fraction and their role in the iron cycle is also still largely unclear. Hong *et al.* (1986) showed that a significant fraction of iron released from sediments was Fe(II) at the Peru upwelling system. No additional studies were carried out in non-upwelling systems so that the fate of dissolved Fe(II) in oxic waters such as the Celtic Sea shelf edge is unknown. If dissolved Fe(II) were to be transported in oxic waters, it should be stabilised by organic complexation before its oxidation to Fe(III). Additionally if it were to reach the euphotic zone its almost immediate removal by biological uptake would be expected.

2. Transport / export of dissolved iron

In this study, high dissolved iron concentrations were measured only within one of the two observed intermediate nepheloid layers. This result implies that dissolved iron can survive particle scavenging in some conditions, and that it can be decoupled from particles, and therefore clearly needs to be investigated further. Additionally, since dissolved iron can potentially be transported within intermediate nepheloid layers, it would be interesting to determine how far offshore enhanced dissolved iron concentrations can be measured, as this would give an indication of removal kinetics within these layers providing that the velocity and mixing of these waters can be established. However, following an intermediate nepheloid layer may be a real challenge (R. Lampitt, 2005, personal communication).

Vertical advection of dissolved iron was also observed in this study. Since this mixing was likely induced by internal tide propagation, it would be interesting to monitor dissolved iron concentrations and its speciation for several tidal cycles at stations with different degree of stratification. This experiment may allow determination

of a vertical flux of dissolved iron, and its fate, but may be difficult to study due to the dynamics of the system, and the work load involved.

3. Biological influence on dissolved iron distribution in surface waters

Additional studies are needed at the shelf break front to determine the potential for iron stress, limitation, or co-limitation of phytoplankton. Incubation experiments could be carried out at stations with different water column stratification (*i.e.* on shelf, at the shelf break, at the upper slope, and offshore), with iron and/or other nutrients additions while monitoring physiological parameters, species composition, and zooplankton grazing. This limitation would be expected to occur only at the end of the summer when recycling may not be sufficient to provide nutrients in the Fe:N ratio required for minimum growth of coastal species.

The role of the zooplankton community could also be examined in terms of their participation in recycling or export of dissolved iron from the euphotic zone, which potentially can increase the iron stress for the phytoplankton population (Wang and Dei, 2001).

CHAPTER VI.

CONCLUSIONS AND FUTURE WORK

VI.1. Initial objectives

The aim of this project was to improve our understanding of the marine iron cycle by investigating the processes influencing dissolved iron distributions in different environments. The two major objectives were: **1)** to develop an analytical method to determine dissolved iron in seawater at sub-nanomolar concentrations, and to ensure the quality of the data obtained; and **2)** to use this method to determine dissolved iron in samples collected in different environments: the Celtic Sea shelf and shelf edge, and the open Atlantic Ocean.

The implementation of the analytical method using recent published methods proved difficult, and was not a trivial exercise. Given the difficulties in optimising the initial method chosen (see Chapter II), an alternative technique was developed, which also proved difficult but was in the end successfully used (see Chapter III). The quality of the analyses of main samples was found satisfactory for specific samples based on current means of assessment (see Chapter IV). A summary of main findings during this analytical exercise, and comments on future work are given in Section VI.2.

Two sets of samples were collected using careful trace metal techniques, as contamination risks are high when sampling for iron (see Chapter IV). Unfortunately despite all precautions, one set of samples was contaminated apparently through diffusion of iron from the walls of the storage bottles into some of the samples analysed from the *AMT-12* cruise in the open Atlantic Ocean (see Chapter IV and Section VI.2). Despite uncertainties in the quality of the analysis, samples collected during the *JR98* cruise at the Celtic Sea shelf edge were generally of good quality (see Chapter IV), and the data was interpreted in terms of processes (*i.e.* sources, removal, and transport) influencing dissolved iron distribution at the Atlantic Ocean – Celtic Sea shelf edge. This data was used in association with ancillary information to provide a conceptual framework for future studies in these highly dynamic environments (see Chapter V). An additional set of samples from the North Scotia Ridge between the Falkland Islands and South Georgia (Atlantic sector of the Southern Ocean, not collected within this project) was analysed using the newly developed technique for total dissolvable iron (see Chapter V). This additional study gave insights into the importance of benthic sources of iron for enhancing primary production and the physiological impact on algal cells of the alleviation of iron-stress in regions of the ocean where atmospheric inputs are low.

A summary of main findings from the study of the Celtic Sea samples and Southern Ocean samples, and suggestions for future work are given in Section VI.3.

VI.2. Objective 1: Analysis of dissolved iron; and future work

The choice of a flow-injection (FI) system to develop was based on the criteria of using the technique while at sea, allowing measurements of iron in Fe-depleted open ocean waters, and requiring very little sample handling and rapid sample throughput for near real-time measurements. Two types of detection methods for FI techniques for Fe are currently used worldwide for the determination of iron in seawater: **i)** the chemiluminescence (CL) reaction with commercially available luminol, with two versions to detect Fe(II) (or Fe(II+III) after reduction), or Fe(II)+Fe(III) directly (see Chapter II); and **ii)** the catalytic spectrophotometric reaction with commercially available N,N-dimethyl-p-phenylenediamine (DPD) to determine Fe(II+III) after oxidation of Fe(II) to Fe(III) (see (Measures *et al.*, 1995)). Initially the method chosen here was the Fe(II) FI-CL system based on the technique of Bowie *et al.* (1998), as its advantage over the other FI-CL and DPD methods, was to allow the direct determination of Fe(II) (and of Fe(II+III) after reduction). This technique thus had the potential of giving a direct measurement of the most bio-available form of iron in the ocean.

VI.2.1. Implementation of an technique to determine very low concentrations of dissolved iron in seawater

The Fe(II) FI-CL system was relatively simple to assemble; however problems arose during optimisation including mainly the lack of sensitivity and of reproducibility of replicate peaks, and the unreliability of the calibration. Despite designing and executing an extensive number of experiments to help identify and solve them, these problems remained, and it was decided to compare the system with the Fe(II) FI-CL technique developed at the University of Plymouth. Results from this comparison exercise showed that the resins prepared within this project were responsible for the lack of sensitivity and reproducibility of the signal. However problems remained with the calibration so that, due to project time constraints, the analyser was modified to the other version of the FI-CL method for Fe(II)+Fe(III) determination based on the method of Obata *et al.* (1993). After optimisation of numerous parameters, the system showed good

calibrations and sensitivity, and allowed analysis of a selection of samples collected during this project.

The complications encountered during the development were thus caused by the mis-behaviour of the preconcentration resins prepared, and also likely to the batch of luminol used for the chemiluminescence reaction.

VI.2.1.1. Preconcentration step

Many issues were encountered with the preconcentration step (see Chapter II):

1. The preparation of the 8-hydroxiquinoline (8-HQ) immobilised on TSK-Fractogel resin following the protocol of Dierssen *et al.* (2001) did not appear immediately successful, and failures were also reported when using the protocol of Landing *et al.* (1986) (S. Ussher, personal communication, and (Dierssen *et al.*, 2001)). The chemistry involved in the preparation of 8-HQ Fractogel resins therefore may not be fully understood, and factors influencing the reaction should be better constrained.

2. The 8-HQ was found to significantly “bleed” from the TSK resin in the “Dierssen resins” prepared within this project; even though these resins were washed before use until “bleeding” appeared to stop. The "Landing resin" was also found to slowly discolour with use. Potential release of 8-HQ in the system may have consequences on the overall sensitivity of the system, as 8-HQ was recently found to mask the Fe(II) CL signal (Ussher *et al.*, 2005).

3. The fine 8-HQ resin was found to pack with time, and therefore needed changing regularly to avoid the formation of channels within the resin where sample solutions would pass through without all Fe binding the 8-HQ. Increasing the bead size of the resin or decreasing the amount of resin packed in the preconcentration column minimised this effect, and thus increased the column’s lifetime.

4. The “Dierssen resins” prepared within this project had a much lower sensitivity towards Fe than the “Landing resin” later used (courtesy of S. Ussher). In addition to the lack of sensitivity, the “Dierssen resins” were thus also found responsible for the lack of reproducibility of replicate peaks as good reproducibility was obtained when using the “Landing resin”.

VI.2.1.2. Chemiluminescence reaction

Obtaining reliable calibrations proved to be a major problem with the technique used as the sensitivity and curvature varied subsentially between batches of reagents. Differences between calibrations executed immediately one after the other using the "old" and "new" luminol were not significant. However the fact that all calibrations carried out using the "new" luminol with the Fe(II)+Fe(III) technique were linear or positively curved, whereas calibrations were often found negatively curved with the Fe(II) technique and "old" luminol, strongly suggests that the quality of the first batch of luminol used was questionable. The results obtained here suggest that there is likely substantial variability between commercial luminol batches that potentially give variable responses during the chemiluminescence reaction. Furthermore, given the photo-sensitivity of the product, one may wonder how the reagent will evolve/degrade whilst ageing. The different colours observed for the two luminol products used in this project suggest that the initial reagent may have degraded with time by exposure to light and/or oxygen. Additionally it was found by word to mouth that there may be "bad batches" of luminol. All of the above point to the fact that the first batch purchased was possibly probably of poor quality and led to many of the problems observed.

In addition to the uncertainty about the quality of luminol, the chemiluminescence reaction was found to be very complex (see Chapter II). Previous work demonstrated that the chemiluminescence of luminol is a reaction indirectly related to the iron concentration, and that several secondary reactions occur simultaneously (Chapter II). The CL reaction thus does not seem to be fully understood mechanistically.

In summary, FI-CL systems using luminol are difficult to optimise given the numerous factors influencing the response of the technique, and there are remaining uncertainties about the two main analytical steps involved. Moreover it seemed that the technique was not completely reliable as difficulties were encountered in re-optimising the system after moving the analyser for use at sea. However despite all the problems encountered, the Fe(II)+Fe(III) technique worked for a period of time during which some of the samples collected during this project and elsewhere were analysed.

VI.2.2. Quality of the data

The quality of the analysis was assessed using a standard approach examining the correlation of the calibration, precision of measurements, levels of blanks and limit of detection, values obtained for a certified reference material or internal seawater standard, and inter-batch data comparisons (see Chapter IV). The quality of the data was then examined by comparison with published data, and by their oceanographic consistency.

The analytical performance of the optimised analyser were generally satisfactory despite difficulties in keeping the blank levels low, and dissolved iron could be analysed in samples from most oceanic environments. A few problems were encountered when checking the accuracy of the technique using a certified seawater reference material (NASS-5), and high values were assumed to result from low-level contamination likely from containers due to the high acidity of the NASS-5. The use of a low-iron seawater sample as an internal standard gave confidence in the data, and allowed identifying data that were influenced by increasing sensitivity, or affected by a positive shift. Agreement in the inter-batch measurements and the oceanographic consistency when these data were normalised gave confidence in their quality.

High dissolved iron concentrations (and also aluminium in one profile) in some of the samples from the *AMT-12* cruise were ascribed to diffusion of iron from the walls of "recycled" storage bottles. Given the suspicion of contamination in some of the data, and since most of the *AMT-12* samples were stored in "recycled" bottles, these data were not used for interpretation. Overall, only 2 profiles from the whole *AMT-12* cruise were stored in new bottles, and may not be contaminated for iron but are not yet analysed due to time constraints. Most of the samples collected during the *JR98* cruise were stored in new bottles, and their dissolved iron concentrations fell in the range of published data. Similarly, total dissolvable concentrations measured in the set of samples collected independently from this project at the North Scotia Ridge (Southern Ocean) fell within the range of concentrations expected for this size fraction of iron in open and coastal waters.

The assessment of the quality of the analysis therefore showed that during that period, the analyser allowed obtaining relatively good quality data for samples from most oceanic environments. These results have implications for sample storage and for the

conventional wisdom that acid washes will readily clean plastic bottles, which may require more than the conventional 1 + 1 week to remove trace metals from "recycled" bottles containing samples collected in metal laden waters.

VI.2.3. Future analytical work

VI.2.3.1. Future analytical work for the determination of iron in seawater

The problems encountered using the 8-HQ resins prepared during this project show that more attention should be brought to characterise this type of preconcentration resin given their importance in the success of the overall development of the technique. Additionally unexplained failures in the preparation of 8-HQ resins bring up a factor of "luck" in the success of the preparation, which should not be tolerated in analytical chemistry.

A possible solution to these limitations may exist through the use of a new, commercially available resin, the Nitriloacetic Acid (NTA) Superflow resin. This resin showed good recovery for iron(III) (100%) and of copper (80%) at pH 1.7, and strong synthetic organic ligands did not show any significant effect on iron recovery (Lohan *et al.*, 2005). This resin therefore presents many advantages: **i)** resin preparation failures and "bleeding" would be avoided; **ii)** samples can be directly preconcentrated onto the resin without increasing the pH with a buffer therefore potentially lowering the blank; and **iii)** at pH 1.7, iron is rapidly released from complexes thus avoiding the addition of an additional step (Lohan *et al.*, 2005). However, this resin does not allow collection of Fe(II) at pH 1.7, as it is collected at pH > 5. Hydrogen peroxide must thus be added and allowed to react for 10min before preconcentration to allow determination of total dissolved iron in samples (Lohan *et al.*, 2005), thus increasing the analysis time and potentially increasing the blank. Nevertheless the main advantages are that this commercial resin would avoid problems associated with the preparation of the resin, and can potentially allow better inter-comparison of iron data if it is used by several laboratories.

Problems encountered with getting reliable calibrations using the Fe(II) FI-CL technique were ascribed to the quality of the commercial luminol used, and thus there was an element of chance, depending upon which luminol was used. In the implementation of the analyser in this project, many parameters were tested prior the luminol (no reference to problems with batches of luminol was found in the literature),

and resulting in significant loss of time during the project. Additionally the CL reaction appears to be complex and not well understood.

The final version of the Fe(II)+Fe(III) FI-CL system worked well with good sensitivity and precision allowing determination of iron in seawater from most oceanic environments, and could be further optimised to lower the blanks and limit of detection. However the technique appeared not as reliable as in the laboratory when used at sea. The analyst may thus want to consider using an alternative analytical technique with similar sensitivity but with a reaction for the detection of the analyte that is better known and constrained. A possible choice is the catalytic spectrophotometric method of Measures *et al.* (1995) using DPD, which has been used with good sensitivity to determine iron in different regions of the ocean (Sedwick *et al.*, 2000; Vink *et al.*, 2000; Weeks and Bruland, 2002). This method could be used with the NTA resin presented above, providing an analyser that has the potential to overcome most of the analytical problems encountered in this project.

VI.2.3.2. Future work to ensure the quality of the iron data

During this project, problems were encountered to check the accuracy of the analysis when using the current certified seawater standard (NASS-5), which appeared to be related to its higher acidity, and relatively high concentration (3.71 ± 0.63 nM) compared to the levels measured in open ocean samples (< 1 nM). It would therefore be preferable to have a new certified seawater reference material with acidity and concentration similar to the samples analysed in most laboratories, as recently suggested by other authors (Bowie *et al.*, 2004).

Significant contamination was observed in samples stored for more than a year in acid-washed bottles that previously contained acidified samples from different origins. This result suggests that LDPE storage bottles potentially have a "memory" of the samples previously stored despite the low acidification. It is therefore important to keep a record on which samples were stored in the bottles before recycling them, to prioritise the use of new bottles when samples are to be collected in iron deplete open ocean waters, and ensure the use of efficient cleaning methods.

Despite the numerous analytical problems encountered during this project, two sets of samples were analysed for iron, and were thus interpreted to improve our understanding of the iron cycle at the ocean – shelf interface.

VI.3. Objective 2: Dissolved iron distribution at the ocean – shelf interface; Future work

VI.3.1. Processes at the Celtic Sea – ocean interface

Main findings during the interpretation of dissolved iron data at the shelf edge were:

1. Near seafloor (~ 5-10 m above bottom), oxic degradation of particulate organic matter was likely the largest source of dissolved iron at two upper slope stations. An additional source likely supplied dissolved iron at the most shallow station, presumably by recent remobilisation of sediment pore water. The balance between inputs and removal processes was in favour of removal near the seafloor at two other upper slope stations as seen by a decrease in dissolved iron when approaching the seafloor. Residual dissolved iron concentrations were thought to be stabilised in seawater through inorganic colloidal formation or organic complexation.

2. Intense resuspension occurred on the upper slope at ~ 1000 m depth where a component of the geostrophic current was found to flow northward. A significant fraction of this material was thus probably transported along shelf by this current. A small fraction of this material was also found to propagate in intermediate nepheloid layers along two isopycnals demarcating the main water masses. However enhanced dissolved iron concentrations were only found associated with the shallowest and strongest of the two intermediate nepheloid layers. This result may be explained by variations in the intensity of scavenging and of the source of iron.

3. Vertical mixing of deeper waters induced by the internal tide was also observed across the transect with increased dissolved iron concentrations associated with cooler temperatures in surface waters. Nutrients supplied through this mechanism are likely rapidly utilised by primary production resulting in depletion of nitrate in surface waters relative to other nutrients.

4. Finally little obvious uptake of dissolved iron was observed in surface waters relative to deeper waters, whereas nitrate was depleted at most stations in the euphotic zone. Low nitrate concentrations in seawater thus suggested that primary production was limited by this nutrient at the time of the cruise. However, given that supply of dissolved iron in surface waters may be limited by stratification, and that mixing between oceanic and coastal waters is limited by the geostrophic current, different

degree of iron (co-)limitation, stress for phytoplankton may potentially occur at different times of the year at the Celtic Sea shelf edge.

VI.3.2. The "island mass effect" near South Georgia (Southern Ocean)

The Southern Ocean is mostly an iron-limited HNLC area due to the lack of source of dissolved iron, however a few "oasis" were observed by satellite images around main islands (*i.e.* Crozet, Kerguelen, and South Georgia). Blooms last for months in the surrounding former HNLC waters around these islands that have presumably been naturally fertilised with iron, suggesting alleviation of iron-stress in the phytoplankton population. In the published study presented here, total dissolvable iron concentrations increased significantly near South Georgia, suggesting that the island shallow waters were fertilised in iron presumably by benthic sources. Additionally changes in the photo-physiology of algal cells were found near South Georgia, and in waters downstream of the island. Changes in these parameters were likely related to the supply of iron, which is consistent with the fact that iron is an essential element in the mechanism of photosynthesis. This study thus reported the first iron data supporting the "island mass effect" hypothesis around South Georgia.

VI.3.3. Implications

Some authors have suggested that iron may be released in surface waters by photo-reduction of particulate iron transported from the benthic boundary layer (*e.g.* (Chase *et al.*, 2005)). However the present work suggests that a significant fraction may actually be supplied in the dissolved (< 0.4 μm) form, although an important portion may be found as inorganic colloids or organic complexes. This source of iron therefore can potentially be directly available to the phytoplankton population without additional transformation. The release of potentially bioavailable iron supplied from benthic sources would have important consequences on severely iron-stressed algal cells as found around islands of the Southern Ocean, assuming that scavenging remains limited, and that transport mechanisms rapidly bring dissolved iron to the surface.

Remineralisation by oxic degradation of particulate organic matter (POM) settled onto the seafloor appeared to be the main benthic source of dissolved iron in this shelf break environments. Shelf waters are generally productive areas in spring, which is followed by an intense export of POM that is oxidised by heterotrophic respiration during

summer months. Therefore POM oxidation is potentially an important source of dissolved iron in most of the world's shelf waters. This source term should thus be included in the global oceanic iron budget, providing that a significant fraction of this regenerated dissolved iron can be transported to surface waters, as previously suggested by Elrod *et al.* (2004).

From this work, it was evident that dissolved iron was transported both horizontally and vertically at the ocean-shelf interface. Vertical mixing is not specific to the northwest European margin, and is strong in regions affected by wind-driven upwelling of deep waters (*e.g.* off Bengal, off California, Southern Ocean). However intermediate nepheloid layers (INLs) were only observed at the Celtic Sea margin, and the northeast Pacific (Dickson and McCave, 1986; Martin and Gordon, 1988; Thorpe and White, 1988). One may wonder whether these intermittent INLs propagating into the ocean's interior may be a more worldwide spread phenomenon, and could therefore provide an additional but occasional transport mechanism for particulate and/or dissolved iron off shelf, as recently found with eddy propagation (Johnson *et al.*, 2005). Even though a large fraction of dissolved released by benthic sources is presumably trapped at continental shelves, the remaining fraction may be exported off shelves; a flux that should be included in the estimates of the global oceanic iron budget.

The concept of iron limitation of phytoplankton communities is relatively recent and experiments gave evidence of this limitation in the extreme HNLC environments where macro-nutrients are replete. The Iron Theory helped scientists to better understand the contrasting distribution of primary production in the world's ocean. Recent studies suggest that iron limitation may also occur in episodically naturally fertilised areas including in the open North Atlantic ocean subject to dust storm deposition (Blain *et al.*, 2004; Mills *et al.*, 2004), and the California upwelling system (Firme *et al.*, 2003). Hutchins *et al.* (1998) also recently revealed that different forms of iron limitation may occur in coastal environments. The concept of iron limitation should thus be revisited by investigating regions such as the Celtic Sea shelf edge in space and time, as sub-nanomolar concentrations of dissolved iron were measured here in waters assumed to be iron-rich due to their proximity with benthic sources. Given that nitrate concentrations were depleted in surface waters and were very low in the seasonal thermocline, co-limitation of nitrate and iron may be more likely during summer.

VI.3.4. Future work on aspects of iron biogeochemistry

The aim of this work was to give a conceptual framework for discussing processes. Several aspects of the iron cycle in these systems could not be addressed in the scope of this study but provide a basis for future work (see details end of Chapter V).

In order to better understand the "island mass effect" around Antarctic islands for example, good process studies are necessary to improve our understanding of the proposed mechanisms involved in the supply / removal / transport of dissolved iron from shelf waters to the ocean. New studies should focus on release processes of iron from sediments, and the balance of input and removal of iron. Determining the speciation of dissolved iron is also crucial to explain how high DFe concentrations are maintained in these waters that can potentially be transported offshore. Intermediate nepheloid layers can be a possible transport mechanism for dissolved iron to the ocean interior, however this process implies that, in some conditions, DFe could survive particle scavenging, which clearly needs investigating. A further important component of these systems to study is surface biology, as, apart from other factors, it is the major supplier of carbon to the seafloor. Monitoring the effect of vertical mixing on dissolved iron and nitrate distributions may thus allow the study of bloom dynamics at shelf breaks. Given that different degrees of iron limitation may exist even in coastal waters, and given the relatively low iron concentrations in surface waters observed here, the possibility of iron limitation or co-limitation should be investigated. Additionally the role of zooplankton grazing in the recycling of dissolved iron should be studied as stratification may not allow regular supply from deeper waters.

This study of dissolved iron distributions at the Celtic Sea shelf edge therefore highlights our relatively poor understanding of processes governing the release, removal, stabilisation, transport and biological uptake of iron at oceanic-shelf interface environments. A non-exhaustive series of suggestions for process studies have been made here for future work to improve our understanding of the iron cycle in these generally highly productive environments, which are also important in terms of fisheries and as potential carbon sinks.

APPENDICES

APPENDIX 1.

DESCRIPTION OF THE FIA-CL SYSTEM TO DETECT Fe(II) IN DE-IONISED WATER

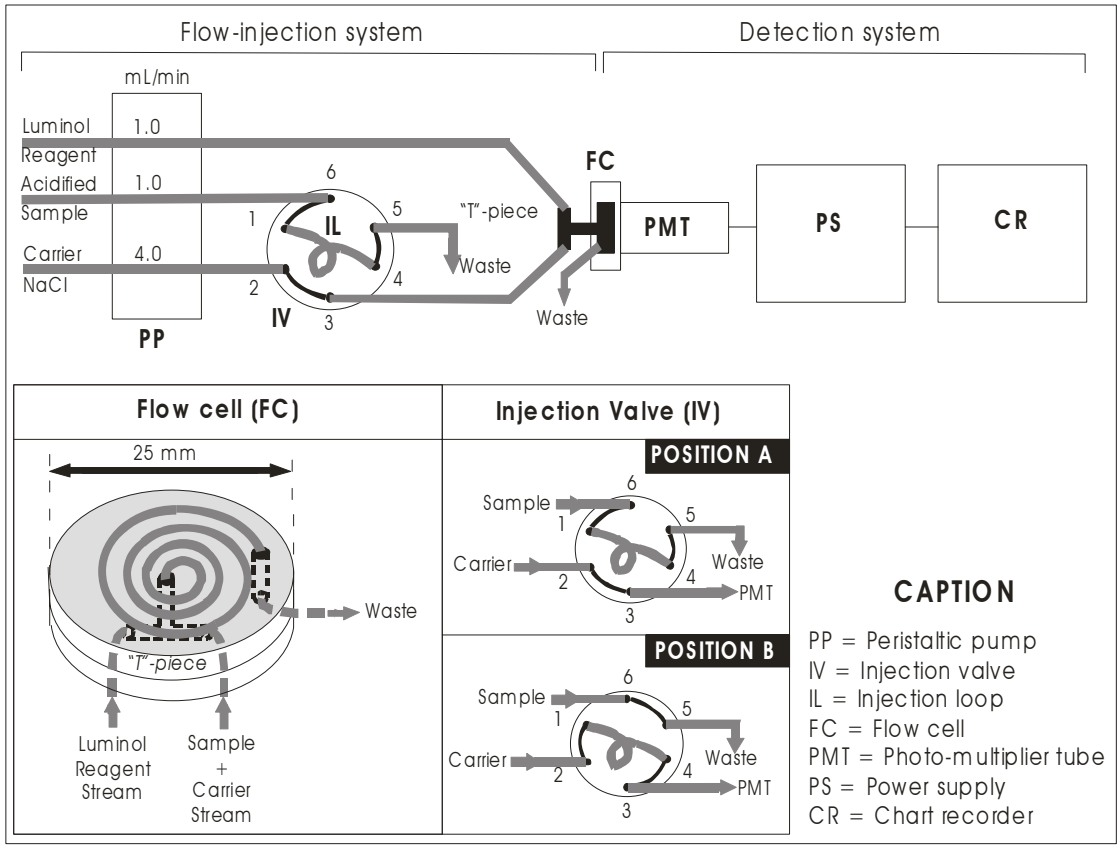

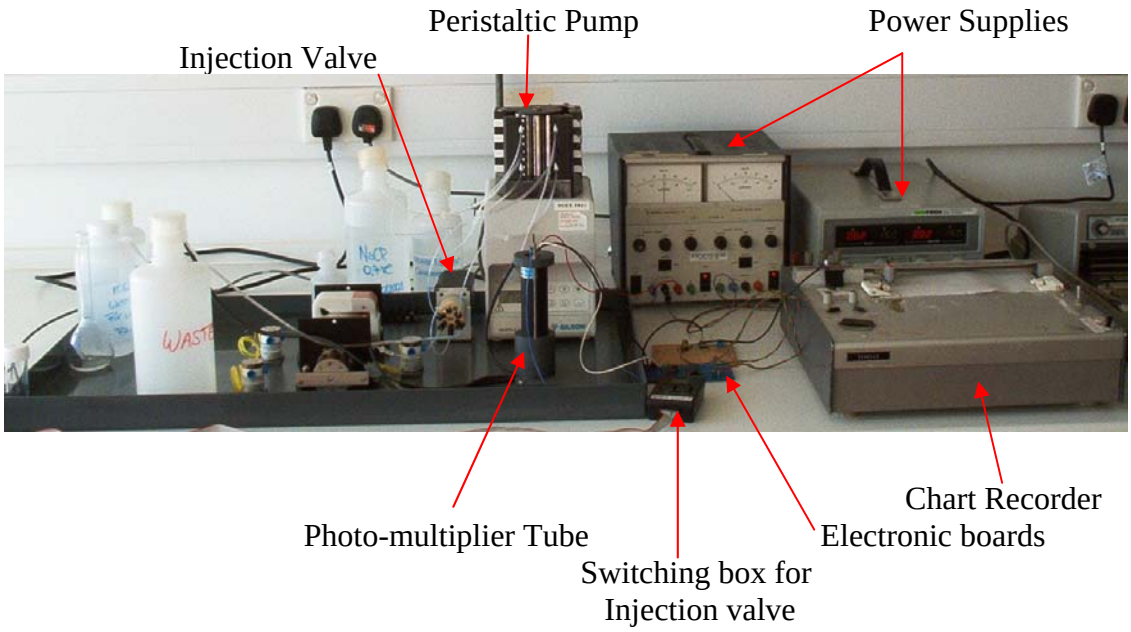

INSTRUMENTATION

Peristaltic Pump (PP)	Gilson Minipuls 3, 8 channels (Anachem Ltd., #F155013)
Injection Valve (IV)	6-port Cheminert low-pressure valve model C22 with micro-electric 2-position actuator and ¼-28 fittings switched manually (VICI Valco Inst. Co., Thames Restek, C22-3186EH)
Flow Cell (FC)	1-mm i.d. transparent PVC tubing coil with aluminium foil to optimise light detection and mounted on the PMT window
Photo-Multiplier Tube (PMT)	End-on photo-counting head incorporating a low-noise PMT and internal high voltage supply, with low voltage (5Vdc) source from main control unit (Hamamatsu Photonics, H84443)
Power Supplies (PS)	Iso-tech laboratory dc power supply, dual tracking with 5V fixed, model IPS 2303DD
Chart Recorder (CR)	Servoscribe
Tubing	0.8-mm i.d. PTFE tubing for the manifold Flow-rated PVC peristaltic pump tubing (Altec)

REAGENTS using Milli-Q water (18.2 MΩ.cm), according to King *et al.* (1995)

Luminol Reagent	500μM luminol reagent (3-aminophthalhydrazide, > 98%, Fluka # 09253) buffered with 0.02M sodium tetraborate (Analytical grade, Sigma-Aldrich, # S9640) and adjusted to pH 11.5 with 2M NaOH (Analytical grade, Fisher Scientific, # S4920)
Carrier solution	0.7M NaCl (Analytical grade, Fisher Scientific, # S3160)
Fe(II) stock solution	250μM standard stock solution of Fe(II) was prepared monthly by dissolving 0.0098g of ammonium ferrous sulphate (Fisher Scientific, # A4880) in 100mL 0.2M HCl (Fisher Scientific, # H1100)
Fe(II) working standard	prepared daily by serial dilution of Fe(II) stock solution, in 0.7M NaCl

ANALYTICAL SEQUENCE

The luminol reagent stream was continuously pumped during the analysis and went directly to the "T"-piece at the flow cell. When the injection valve was in the loading position (position A, see diagram above), the standard was pumped through the manifold, loaded in the injection loop, and excess went directly to waste. When the loop was filled, the valve was switched to the elution position (position B) to allow the standard solution in the loop to be carried by the sodium chloride carrier stream to the flow cell. A "T"-piece allowed the luminol reagent stream and the carrier stream to meet at the entrance of the flow cell. The resultant stream passed through the flow cell coil in front of the photo-multiplier tube to allow the reaction to be complete and emitted light detected; after the flow cell the solution went to waste.

APPENDIX 2.

PREPARATION AND TESTING OF THE 8-HYDROXYQUINOLINE RESIN

REAGENTS

The Toyopearl SEC HW-65F resin (94% between 30-60μm particle sizes, fine, Anachem) was washed three times with Milli-Q water and the supernatant removed to rinse away the preservative. The 8-hydroxyquinoline (8-HQ, 5-amino-8-hydroxyquinoline, dihydrochloride 95%, Sigma-Aldrich) and 1-chloro-2,3-epoxypropane (epichlorohydrin, 99+%, Fisher) were used as received. Two solutions of 10M and 0.5M NaOH were prepared by dissolving analytical grade NaOH pellets (Fisher) in Milli-Q water and 1M HCl was prepared by dilution of 32%w/v analytical grade HCl (Fisher) with Milli-Q water.

PROCEDURE

The first step in the protocol is the epoxy-activation of the resin with epichlorohydrin. 25mL of 10M NaOH were diluted with 37mL Milli-Q water and 38mL of epichlorohydrin. 5g of dried Toyopearl HW-65F resin were then added to the mixture which was left to react at 50^{o}C for 2h while stirring slowly to avoid damaging the particles. The epoxy-activated resin was then rinsed thoroughly with Milli-Q water using a vacuum filtration system whilst supported on an acid washed fine glass fibre filter (GF/F, Whatman). The resin was air dried and stored in a plastic vial.

The second step in the protocol is the coupling of the 8-HQ to the epoxy-activated resin. As a significant loss of 8-HQ from the resin after preparation has been reported (S. Severmann, personal communication), therefore half the quantity of 8-HQ suggested in the "Dierssen protocol" was used. 2.5g of 8-HQ were thus dissolved in 25mL Milli-Q water and adjusted to pH 11.5-12.0 with 10M NaOH. 2.5g of epoxy-activated resin were then added to the mixture and was left to react at 80^{o}C for 6h while stirring slowly. Using a vacuum filtration system, the resin was collected on a 0.45-μm acid washed cellulose nitrate filter, and the resin was rinsed with: 2 x 25mL 0.5M NaOH, 3 x 25mL Milli-Q water, 2 x 25mL 1M HCl and 3 x 25mL Milli-Q water. Rinses following this sequence were carried out until major "bleeding" of the 8-HQ from the resin was ceased. The 8-HQ resin was then stored under Milli-Q water.

DETERMINING METAL COLLECTION CAPACITY OF THE RESIN

In order to check complexing capacity of the prepared resin, an experiment was performed with copper, which has a similar behaviour to iron as regards 8-HQ and this experiment also allowed comparison with the results reported by Dierssen *et al.* (2001).

Reagents were prepared as follows. Ammonium acetate buffer was prepared by diluting 115μL glacial acetic acid (certified, Fisher) to 100mL with Milli-Q water and adjusted to pH 5.5 with 25% ammonia (sp. gr. 0.91, BDH chemicals). To elute copper from the resin, 2% HNO_3 was prepared by diluting 70% HNO_3 (trace analysis, sp. gr. 1.42, Fisher) in Milli-Q water. The 3.15 μM Cu(II) standard solution was prepared by diluting 10mL of 15.7 μM Cu(II) (for AAS, Fisher) to 50mL with Milli-Q water and was adjusted to pH 5 with 25% ammonia.

The experiment was carried out as follows. 100mg of dried 8-HQ resin were suspended in 5mL of Milli-Q water to make a slurry which was then loaded into an acid-washed (in 10%w/v HCl) plastic column (10 cm^3). The 8-HQ resin was conditioned with 10mL of ammonium acetate buffer to convert it into ammonium form. 10mL of 3.15 μM Cu(II) standard solution were then loaded. The resin was then rinsed with 10mL ammonium acetate buffer to remove any non-bound copper, and finally eluted with 10mL 2% HNO_3. A blank was performed following the same procedure but loading 10mL of ammonium acetate buffer instead of the Cu(II) standard. The eluted acid solution was then analysed using a Varian Spectra AA55 atomic absorption spectrometer. A calibration curve was made using standards: 0 (2% HNO_3 only), 15.7, 78.7, and 157.4 $\mu mol.L^{-1}$.

Four experiments were performed which were in good agreement with the results given by Dierssen *et al.* (2001) for a batch experiment, since the blank corrected values obtained in this study were 100.1 ± 9.7 μmol Cu/g of resin (n = 4).

APPENDIX 3.

MANUALLY CONTROLLED FIA-CL WITH PRECONCENTRATION STEP TO DETECT Fe(II) IN SEAWATER

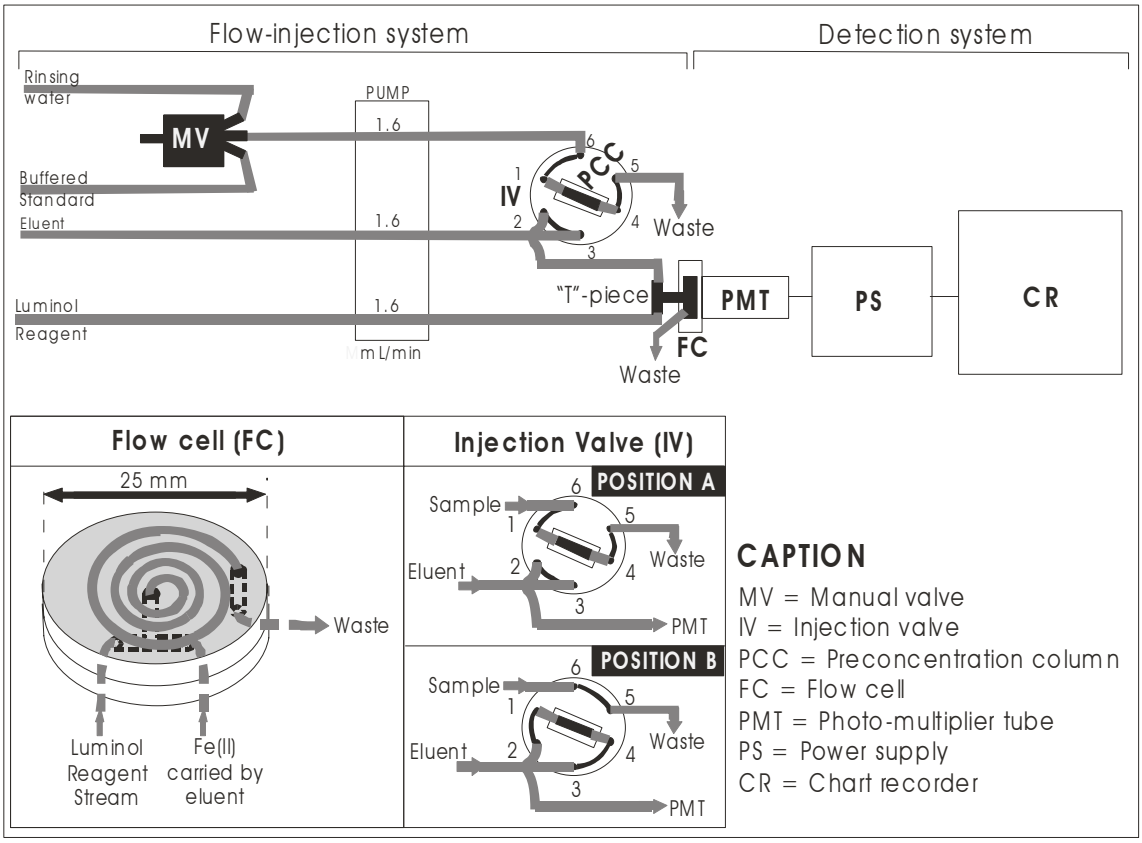

INSTRUMENTATION

Peristaltic Pump (PP)	Gilson Minipuls 3, 8 channels (Anachem Ltd. #F155013)
Injection Valve (IV)	6-port Cheminert low-pressure valve model C22 with micro-electric 2-position actuator and ¼-28 fittings (VICI Valco Inst. Co., Thames Restek, C22-3186EH)
Flow Cell (FC)	1-mm i.d. transparent PVC tubing coil with aluminium foil to optimise light detection and mounted on the PMT window
Photo-Multiplier Tube (PMT)	End-on photo-counting head incorporated a low-noise PMT and internal high voltage supply, with low voltage (5Vdc) source from main control unit (Hamamatsu Photonics, H84443)
Power Supplies (PS)	Iso-Tech Laboratory dc Power Supply, dual tracking with 5V fixed, model IPS 2303DD
Chart Recorder (CR)	Servoscribe
Tubing	0.8-mm i.d. PTFE tubing for the manifold Flow-rated PVC peristaltic pump tubing (Altec)

REAGENTS prepared in Milli-Q water, according to Bowie *et al.* (1998)

Luminol Reagent	10μM luminol reagent (3-aminophthalhydrazide, Fluka, # 09253) buffered with 0.1M sodium carbonate (Analytical Grade, Fisher Scientific, #S/2920/53) and adjusted to pH 12.4 with 5M NaOH
Eluent	0.09M quartz distilled HCl (Q-HCl) in Milli-Q water
0.4M NH_4OAc buffer	Dilution of 20mL of 2M NH_4OAc stock solution (dilution of 90mL 6M ammonia and 22.2mL glacial acetic acid to 200mL with Milli-Q water) to 100mL with Milli-Q water adjusted to pH 5.5 with 5M acetic acid
Fe(II) stock solution	250μM standard stock solution of Fe(II) was prepared monthly by dilution of 2.5mM Fe(II) stock (0.0098g of ammonium ferrous sulphate (Fisher Scientific, # A4880) dissolved in 100mL 0.1M Q-HCl) in 100mL 0.01M Q-HCl
Fe(II) working standard	prepared daily by serial dilution of the 250μM stock in 0.01M Q-HCl

PROCEDURE

The luminol reagent was continuously pumped through the analyser and was mixing with the eluent at the entrance of the flow cell. When the injection valve was in loading position (position A, see diagram above and Table below), the standard was first loaded onto the preconcentration column. The manual valve was then switched to allow the resin to be rinsed with Milli-Q water. The injection valve was then manually switched to the elution position (position B) to allow the eluent to go through the preconcentration column and elute iron which was carried to the flow cell where it reacted with the luminol reagent. At the end of the elution, the injection valve was manually switched back to position A to allow the preconcentration column to be rinsed with Milli-Q water to remove any remaining acid. The manual valve was then switched back to allow the standard to be loaded onto the column for a new cycle.

Time	Manual valve position	Injection valve position	Process
60s	1	A	Loading Fe(II) onto 8HQ resin
30s	2	A	Rinsing column with Milli-Q water
60s	2	B	Elution of Fe(II) from the 8-HQ resin
30s	2	A	Rinsing column with Milli-Q water

Timing sequence of 4 minutes used with the manual iron analyser.
Manual Valve: Position 1 = Sample (or standard); Position 2 = Milli-Q water
Injection Valve: Position A = Loading; Position B = Eluting

APPENDIX 4.

AUTOMATED FIA-CL WITH PRECONCENTRATION STEP TO DETECT Fe(II) IN SEA WATER

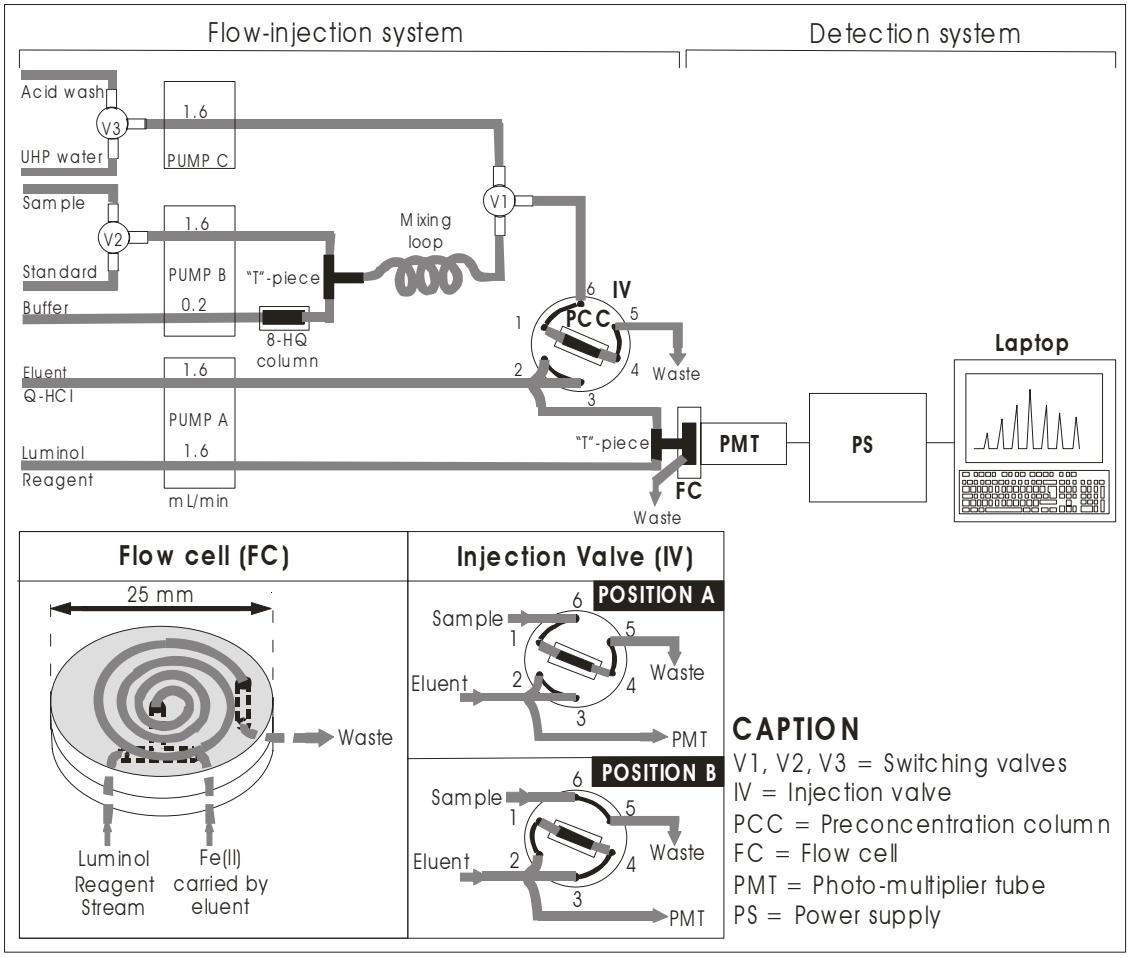

View from above:

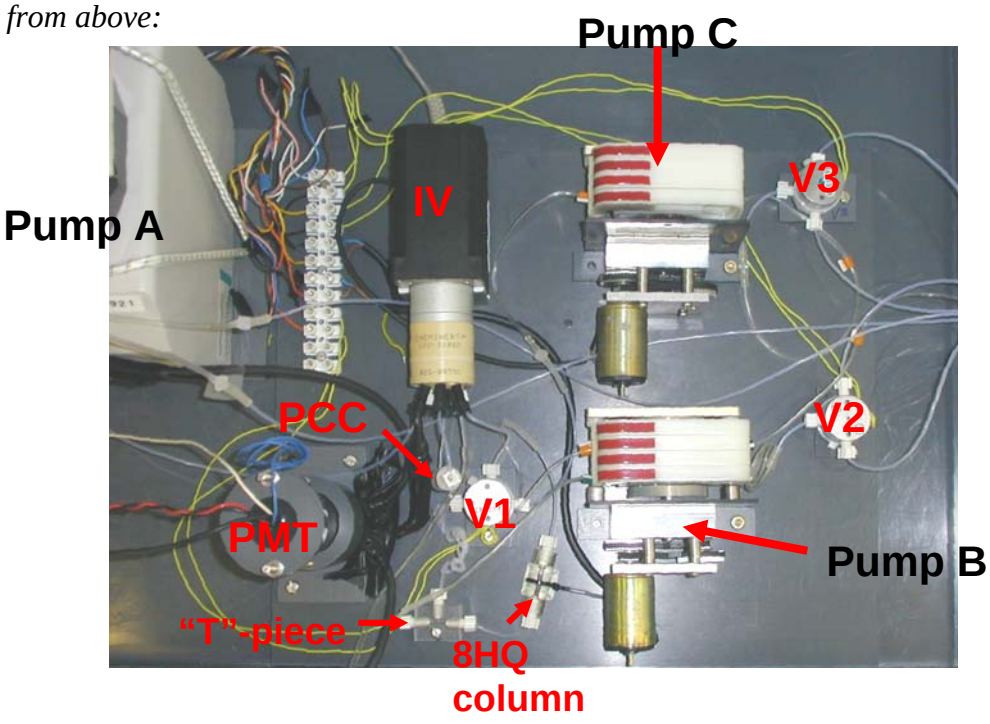

INSTRUMENTATION

Peristaltic Pump (Pump A)	Gilson Minipuls 3, 8 channels (Anachem Ltd. #F155013)
Low-Voltage pumps (B&C)	4 channels, panel mounted 12Vdc Ismatec pumps
Injection Valve (IV)	6-port Cheminert valve model C22 with micro-electric 2-position actuator and ¼-28 fittings (VICI Valco Inst. Co., Thames Restek UK Ltd., C22-3186EH)
Switching valves (V1, V2 & V3)	12Vdc 3-way electronic switching valves, 2-position solenoid valves containing PTFE wetted parts and zero dead volume (Cole-Parmer Inst. Company Ltd., UK# EW-01367-72)
Flow Cell (FC)	1-mm i.d. transparent PVC tubing coil with aluminium foil to optimise light reflection and mounted on the PMT window
Photo-Multiplier Tube (PMT)	End-on photo-counting head incorporated a low-noise PMT and internal high voltage supply, with low voltage (5Vdc) source from main control unit (Hamamatsu Photonics UK Ltd., H84443)
Power Supply (PS)	Designed & constructed by Dr Matt Mowlem (OED, SOC)
Instrument control card	National Instruments DAQPad-6020E card, 16 inputs, 100kS/s, 12-bit Multifunction input/output (I/O) card
Signal acquisition card	National Instruments DAQPad-6507, 96-bit Digital I/O for USB
Laptop	Toshiba satellite Pro
"T"- piece	Constructed from Perspex
Mixing loop	0.8 mm i.d. PTFE tubing knitted coil (~0.5m)
Tubing	0.8-mm i.d. PTFE tubing for the manifold Flow-rated PVC peristaltic pump tubing (Altec)
Communication software	Software written in LabVIEW 6.1 (National Instruments Corp.) by Dr. Matt Mowlem (OED, SOC) (see Appendix 5)
Data processing	Software written in LabVIEW 6.1 (National Instruments Corp.) by F. Nédélec (see Appendix 5)

REAGENTS (according to Bowie *et al.* (1998))

Luminol Reagent	10μM luminol reagent (3-aminophthalhydrazide, Fluka, # 09253) buffered with 0.1M sodium carbonate (Analytical grade, Fisher Scientific, S/2920/53), adjusted to pH 12.4 with 5M NaOH and purified through 8-HQ resin and kept in the dark for 24h before use
Eluent	0.08M quartz distilled HCl (Q-HCl) in sub-boiled distilled (SBD) water
0.4M NH_4OAc buffer	Dilution of 20mL of 2M NH_4OAc stock solution (dilution of 90mL isothermally distilled (ITD) ammonia and 22.2mL Q-acetic acid to 200mL with SBD water) to 100mL with SBD water, adjusted to pH 7 with ITD-NH_3 and purified off-line with a 8-HQ column
Acid wash	0.5M Q-HCl in SBD water
Reducing agent	0.1g sodium sulphite (Analytical grade, Fisher Scientific, #S/6850/53) dissolved in 15mL Milli-Q water, 5mL of 0.4M NH_4OAc buffer added and purified through two sequential 8-HQ columns
Fe(II) stock solution	10μM standard stock solution of Fe(II) prepared weekly by dilution of 10mM Fe(II) stock solution (0.3921g of ammonium ferrous sulphate (Fisher Scientific, # A4880) in 100mL 0.1M Q-HCl with 250μL of reducing agent) in 100mL 0.1M Q-HCl with 250μL of reducing agent
Fe(II) working standard	500nM stock prepared daily by dilution of 10mM stock in 0.01M Q-HCl with reducing agent then standards prepared by serial dilution of 500nM Fe stock in seawater

PROCEDURE

The luminol reagent was continuously pumped and was mixing with the eluent at the entrance of the flow cell. When the injection valve was in the loading position (position A, see Table below), the standard was first loaded onto the preconcentration column. The 8-HQ column was then rinsed with Milli-Q water to remove sea-salts. The injection valve was then switched to the elution position (position B) to allow the eluent to go through the preconcentration column and elute iron which was carried to the flow cell where it reacted with the luminol reagent. At the end of the elution, the injection valve was switched back to position A to allow the preconcentration column to be rinsed with Milli-Q water to remove any remaining acid. At the same time the buffered sample/standard solution was pumped to flush the tubing and minimise the carry-over or dilution effect for the first peak when analysing a new solution. An analytical cycle was thus performed in about 3 minutes.

Time	**Valves**		**Pumps**			**IV**	**Procedure**
	V1	**V2**	**A**	**B**	**C**		
60s	**ON**	OFF	**ON**	**ON**	OFF	A	Loading onto 8-HQ resin
30s	OFF	OFF	**ON**	OFF	**ON**	A	Rinsing of 8-HQ resin
60s	OFF	OFF	**ON**	OFF	**ON**	B	Elution of Fe from 8-HQ resin
50s	OFF	**ON**	**ON**	**ON**	**ON**	A	Rinsing of 8-HQ resin & pumping

Timing sequence used with the automated Fe(II) FIA-CL system

V1 ⇔ Loading = ON & Rinsing, Washing = OFF
V2 ⇔ Pumping new buffered sample = ON & Loading = OFF
A ⇔ Gilson Minipuls 3 pumping the luminol reagent and eluent
B ⇔ Ismatec pump delivering buffer & sample/standard
C ⇔ Ismatec pump delivering rinsing water
IV ⇔ Injection Valve: Position A = Loading & Position B = Eluting

Notes: When doing replicates, the last rinsing step is set up at 30sec but when a new solution is analysed it is set up at 50sec to minimise any carry-over / dilution effect on the first peak.

APPENDIX 5.

DATA ACQUISITION AND PROCESSING WITH LABVIEW 6.1 AND DIAGRAMS FOR THE ELECTRONICS

LIST OF CONTENT


IronIIItotal.vi
File Edit Operate Tools Browse Window Help
valve setup
main panel
transposed waveform chart
first channel
input device (1)
scan rate (1000 scans/sec)
buffer size (4000 scans)
scans to read at a time (1000)
scan backlog
input channels (0)
input limits
high limit
low limit
interchannel delay in secs (-1 : hw default)
pmt gain channel (0)
transposed waveform chart
first channel
PMT reading
2.31
PMT gain
6
Run sequence
STOP
Time in loop
225803
Save File as
C:\Documents
log to file
Tab Control
Start
LabVIEW
IronIIItotal.vi

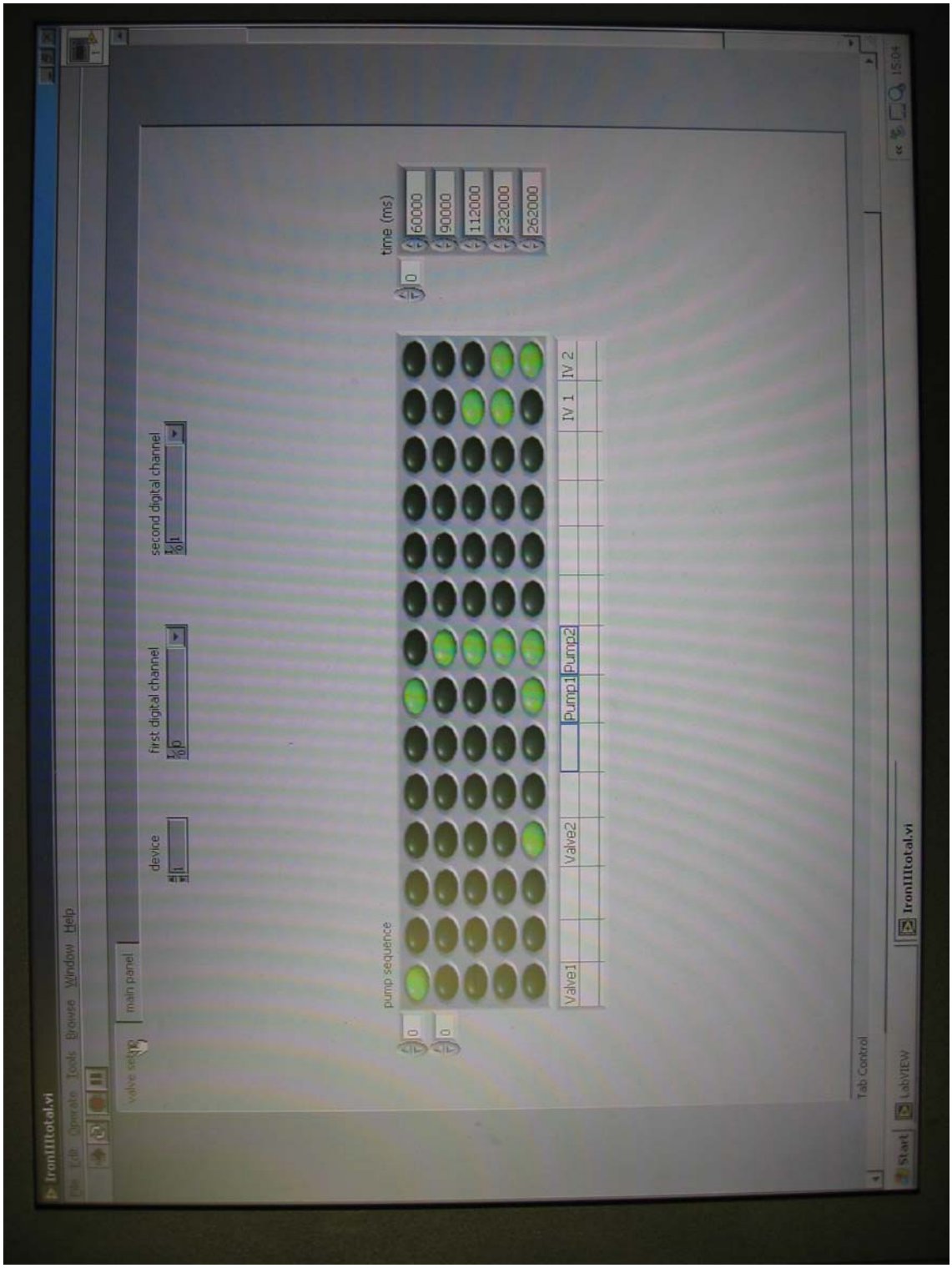
IronIItotal.vi
File Edit Operate Tools Browse Window Help
valve setup
main panel
device
first digital channel
second digital channel
time (ms)
60000
90000
112000
232000
262000
pump sequence
Valve1
Valve2
Pump1
Pump2
IV 1
IV 2
Tab Control
Start
LabVIEW
IronIItotal.vi
15:04

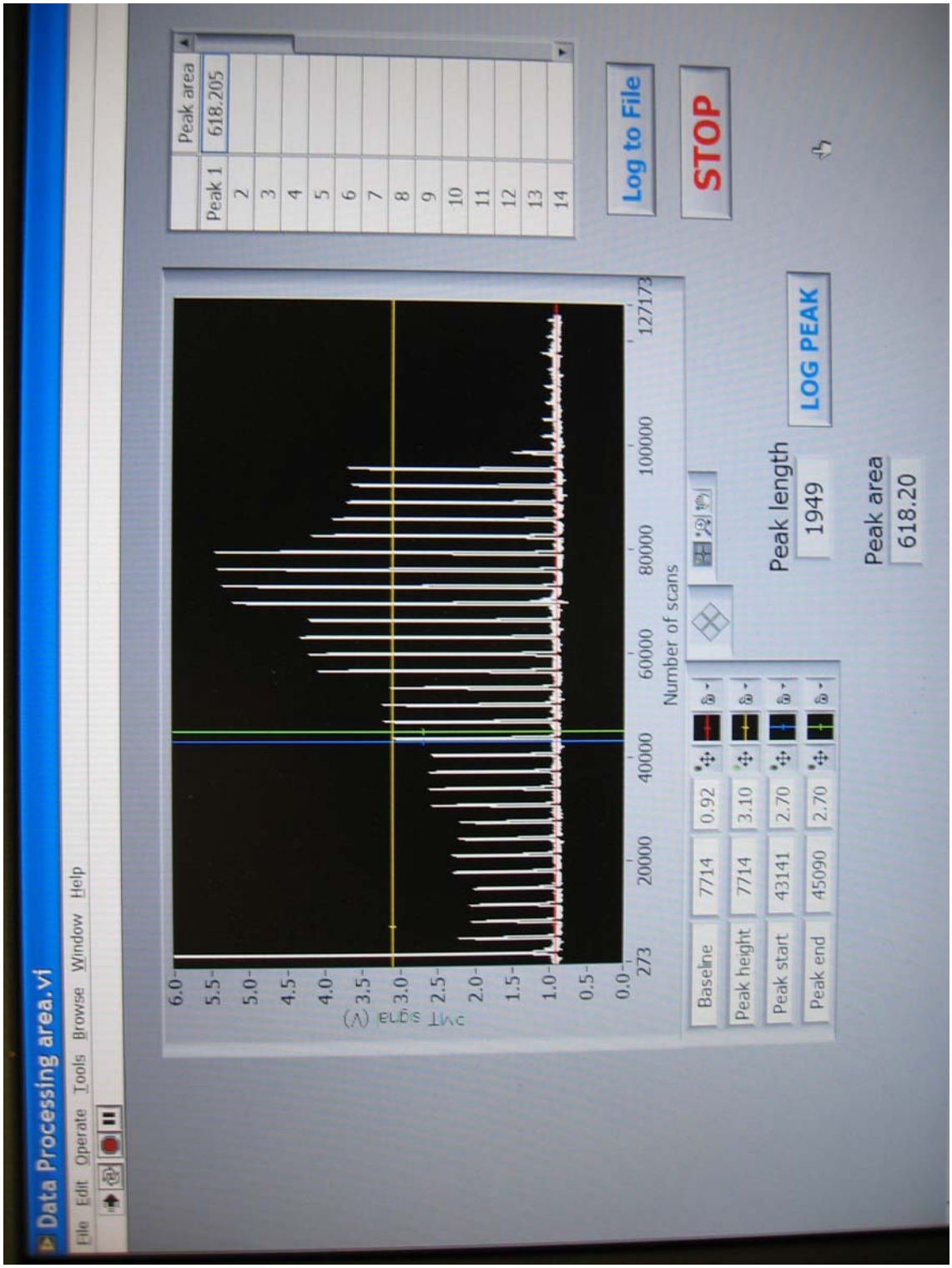
Data Processing area.vi
File Edit Operate Tools Browse Window Help
Peak area
Peak 1 618.205
2
3
4
5
6
7
8
9
10
11
12
13
14
Log to File
STOP
Number of scans
Baseline 7714 0.92
Peak height 7714 3.10
Peak start 43141 2.70
Peak end 45090 2.70
Peak length
1949
LOG PEAK
Peak area
618.20

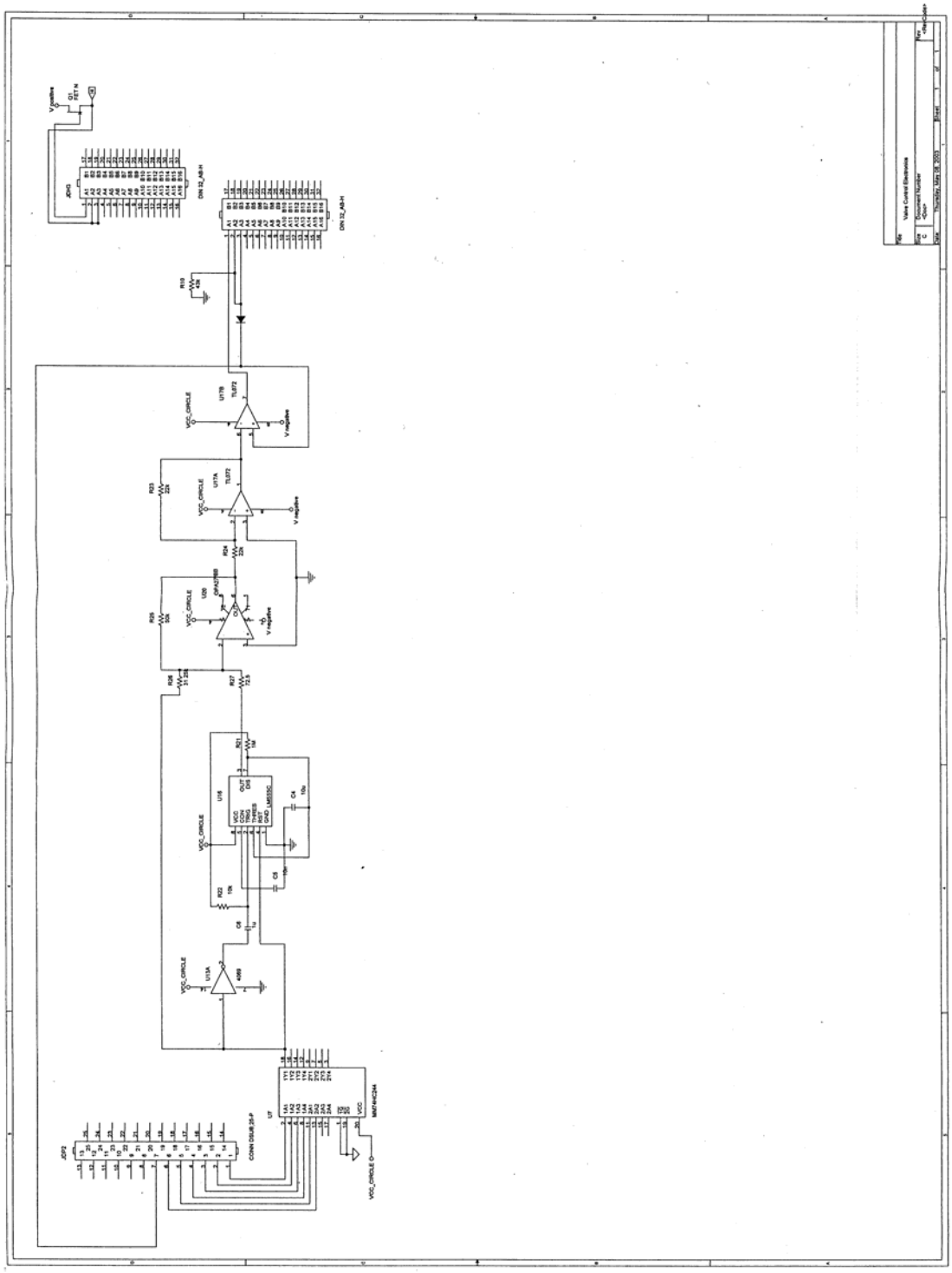

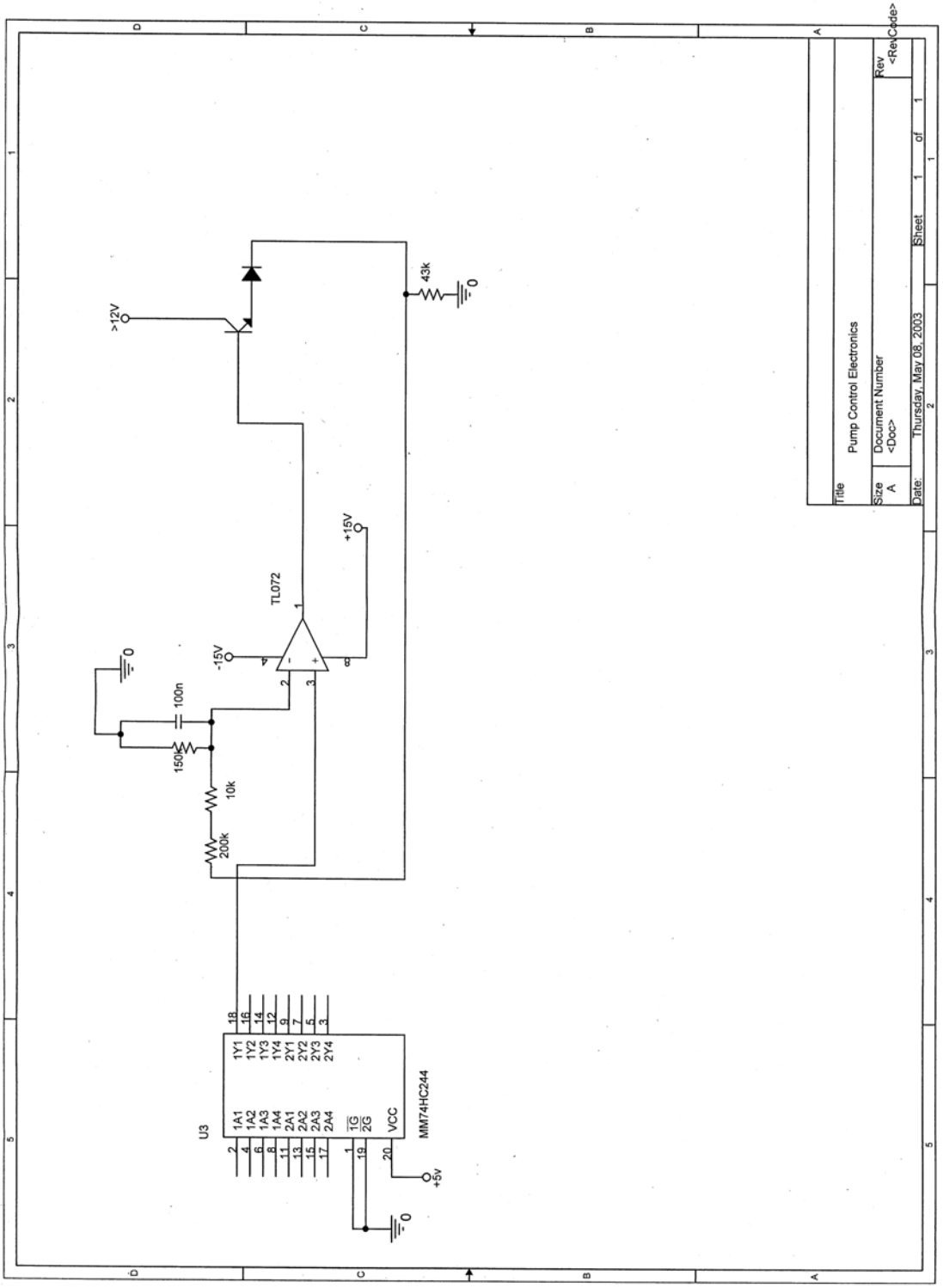
Title
Pump Control Electronics
Size
A
Document Number
<Doc>
Rev
<RevCode>
Date:
Thursday, May 08, 2003
Sheet
1
of
1
>12V
43k
0
+15V
TL072
-15V
100n
150k
10k
200k
U3
MM74HC244
1A1
1A2
1A3
1A4
2A1
2A2
2A3
2A4
1Y1
1Y2
1Y3
1Y4
2Y1
2Y2
2Y3
2Y4
1G
2G
VCC
+5v

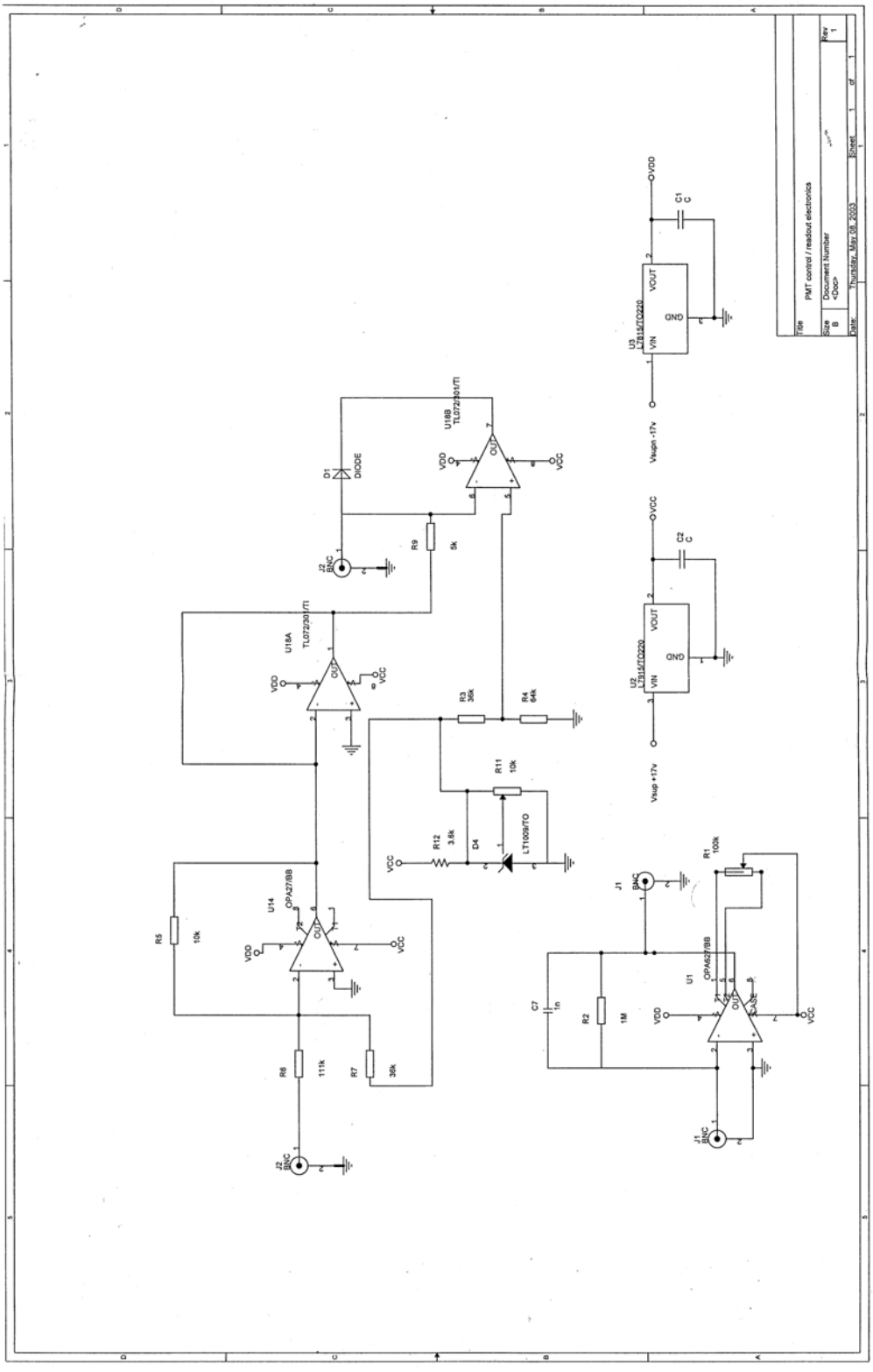
Title
PMT control / readout electronics
Size
B
Document Number
<Doc>
Rev
1
Date:
Thursday, May 08, 2003
Sheet
1
of
1
U18B
TL072/301/TI
U18A
TL072/301/TI
U14
OPA27/8B
U1
OPA627/8B
U2
LT315/TO220
U3
LT315/TO220
D1
DIODE
D4
LT1009/TO
J1
BNC
J2
BNC
R1
100k
R2
1M
R3
36k
R4
64k
R5
10k
R6
111k
R7
39k
R9
5k
R11
10k
R12
3.6k
C1
C
C2
C
C7
1n
VDD
VCC
VOUT
GND
VIN
Vsupp -17v
Vsup +17v

APPENDIX 6.

AUTOMATED FIA-CL WITH PRECONCENTRATION STEP TO DETECT Fe(II)+(III) IN SEAWATER

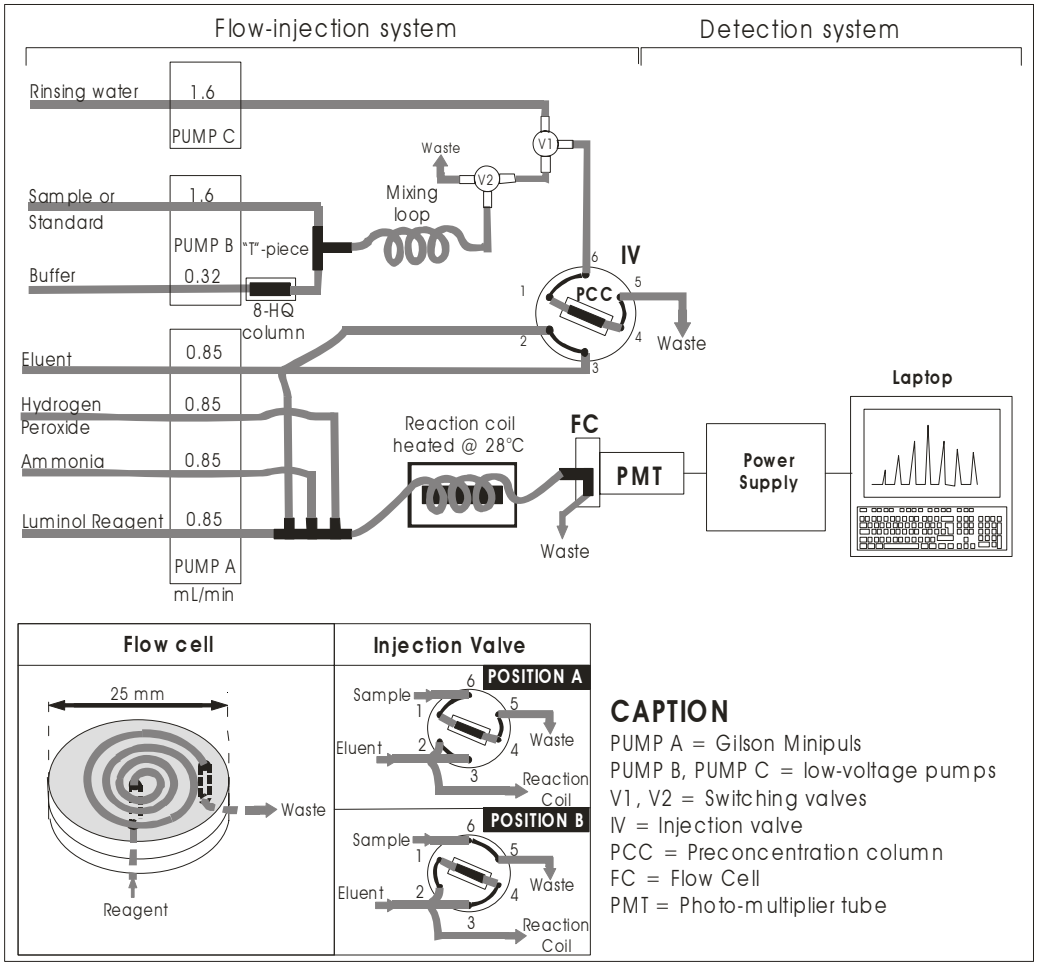

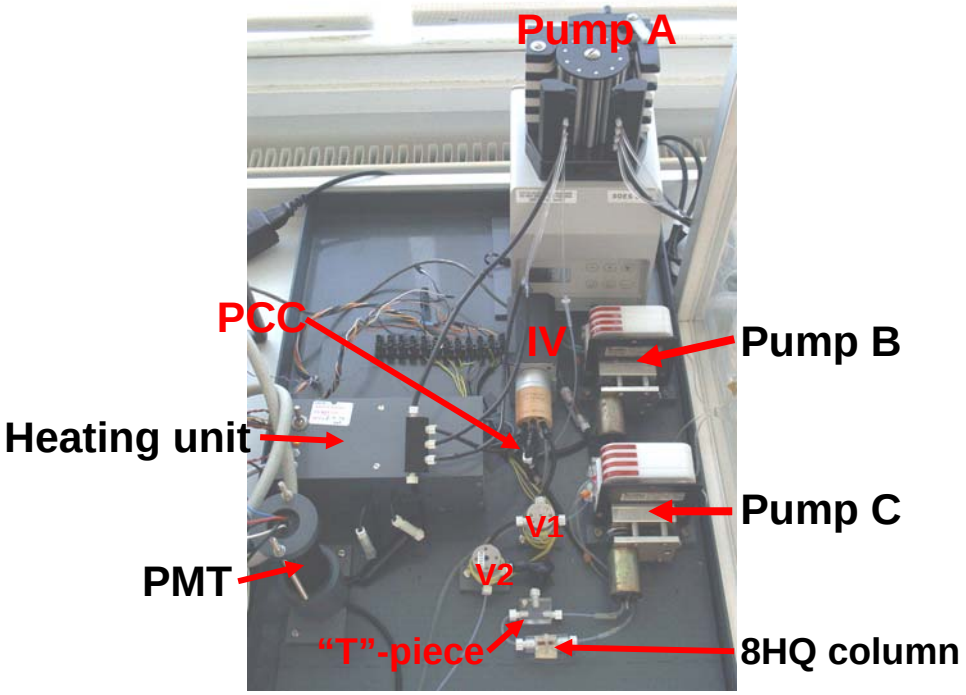

INSTRUMENTATION

Peristaltic Pump (Pump A)	Gilson Minipuls 3, 8 channels (Anachem Ltd. #F155013)
Low-voltage pumps (B&C)	4 channels, panel mounted 12Vdc Ismatec pumps
Injection Valve (IV)	6-port Cheminert low-pressure valve model C22 with micro-electric 2-position actuator and ¼-28 fittings (VICI Valco Inst. Co., Thames Restek UK Ltd., C22-3186EH)
Switching valves (V1 & V2)	12Vdc 3-way electronic switching valves, 2-position direct lift solenoid valves containing PTFE wetted parts and zero dead volume (Cole-Parmer Inst. Company Ltd., UK# EW-01367-72)
"T"- piece & 5-way piece	Constructed from Perspex
Mixing loop	0.8 mm i.d. PTFE tubing knitted coil (~0.5m)
Tubing	0.8-mm i.d. PTFE tubing for the manifold Flow-rated PVC peristaltic pump tubing (Altec)
Reaction coil	0.8 mm i.d. PTFE tubing coiled around the thermostated heating (~ 1.8m)
Heating unit	Laboratory-made thermostated at 28^{o}C
Flow Cell (FC)	1-mm i.d. transparent PVC tubing coil with aluminium foil to optimise light reflection and mounted on the PMT window
Photo-Multiplier Tube (PMT)	End-on photo-counting head incorporated a low-noise PMT and internal high voltage supply, with low voltage (5Vdc) source from main control unit (Hamamatsu Photonics UK Ltd., H84443)
Power Supply (PS)	Designed & constructed by Dr Matt Mowlem (OED, SOC)
Instrument control card	National Instruments DAQPad-6020E card, 16 inputs, 100kS/s, 12-bit Multifunction input/output (I/O) card
Signal acquisition card	National Instruments DAQPad-6507, 96-bit Digital I/O for USB
Laptop	Toshiba satellite Pro
Communication software	Software written in LabVIEW 6.1 (National Instruments Corp.) by Dr. Matt Mowlem (OED, SOC) (see Appendix 5)
Data processing	Software written in LabVIEW 6.1 (National Instruments Corp.) by F. Nédélec (see Appendix 5)

REAGENTS (according to Obata *et al.* (1993))

Luminol stock solution 0.01 M	177mg of luminol dissolved in 0.04M sodium carbonate buffer
Luminol Reagent 100µM	Dilution of 10mL 0.01 M luminol stock solution in 0.04M sodium carbonate (Analytical grade, Fisher), with 75 µL of 60% TETA (triethylenetetramine, Technical grade, Sigma-Aldrich), purified through 8-HQ resin and kept in the dark for 24h before use
Eluent	Concentrated quartz distilled HCl (Q-HCl) diluted to 0.3 M
Ammonia buffer	35% Primar ammonia (Fisher) diluted to 0.55 M
Hydrogen peroxide	30%w/v Aristar H_2O_2 (Merk) diluted to 0.4 M
2 M NH_4OAc stock solution	Dilution of 23mL Q-acetic acid (~ 17.5 M) and 22mL 35% Primar ammonia to 200mL with sub-boiled distilled (SBD) water
0.2M NH_4OAc buffer	Dilution of 10mL of 2M NH_4OAc stock solution to 100mL with SBD water, adjusted to pH 7 with 5 M NH_3 and purified off-line with three 8-HQ columns in series
Fe stock solution	10µM standard stock solution of Fe(II) prepared by dilution of 1000ppm Fe AAS standard (Z-Tek) in 0.1M Q-HCl
Fe working standard	Prepared daily by dilution of 10µM stock in 0.01M Q-HCl

PROCEDURE

The luminol reagent was continuously pumped and was mixing with the eluent at the entrance of the flow cell. When the injection valve was in the loading position (position A, see Table below), the standard was first loaded onto the preconcentration column. The 8-HQ column was then rinsed with Milli-Q water to remove sea-salts. The injection valve was then switched to the elution position (position B) to allow the eluent to go through the preconcentration column and elute iron. The iron aliquot then mixed successively with the luminol reagent, the ammonia buffer, and hydrogen peroxide. The mixture was then heated to *circa* 30^{o}C in an *in-line* reaction coil and was carried to the flow cell for detection. At the end of the elution, the injection valve was switched back to position A to allow the preconcentration column to be rinsed with Milli-Q water to remove any remaining acid. At the same time the buffered sample/standard solution was pumped to flush the tubing and avoid a carry-over or dilution effect for the first peak when analysing a new solution. An analytical cycle was thus performed in about 4.5 minutes.

Time	**Valves**		**Pumps**			**IV**	**Procedure**
	V1	**V2**	**A**	**B**	**C**		
60s	**ON**	OFF	**ON**	**ON**	OFF	A	Loading of buffered sample onto 8HQ resin
30s	OFF	OFF	**ON**	OFF	**ON**	A	Rinsing of 8HQ resin
150s	OFF	OFF	**ON**	OFF	**ON**	B	Elution of Fe from 8HQ resin
30s	OFF	**ON**	**ON**	**ON**	**ON**	A	Rinsing of 8HQ resin & pumping of new buffered sample

Timing sequence used with the automated Fe(II) FIA-CL system

V1 ⇔ Loading = ON & Rinsing, Washing = OFF
V2 ⇔ Pumping new buffered sample = ON & Loading = OFF
A ⇔ Gilson Minipuls 3 pumping the CL reagents
B ⇔ Ismatec pump delivering buffer & sample/standard
C ⇔ Ismatec pump delivering rinsing water
IV ⇔ Injection Valve: Position A = Loading & Position B = Eluting

APPENDIX 7.

AUTOMATED FIA-CL WITH JOHNSON CONFIGURATION TO DETECT Fe(II)+(III) IN SEAWATER AND INSTRUCTIONS FOR USE

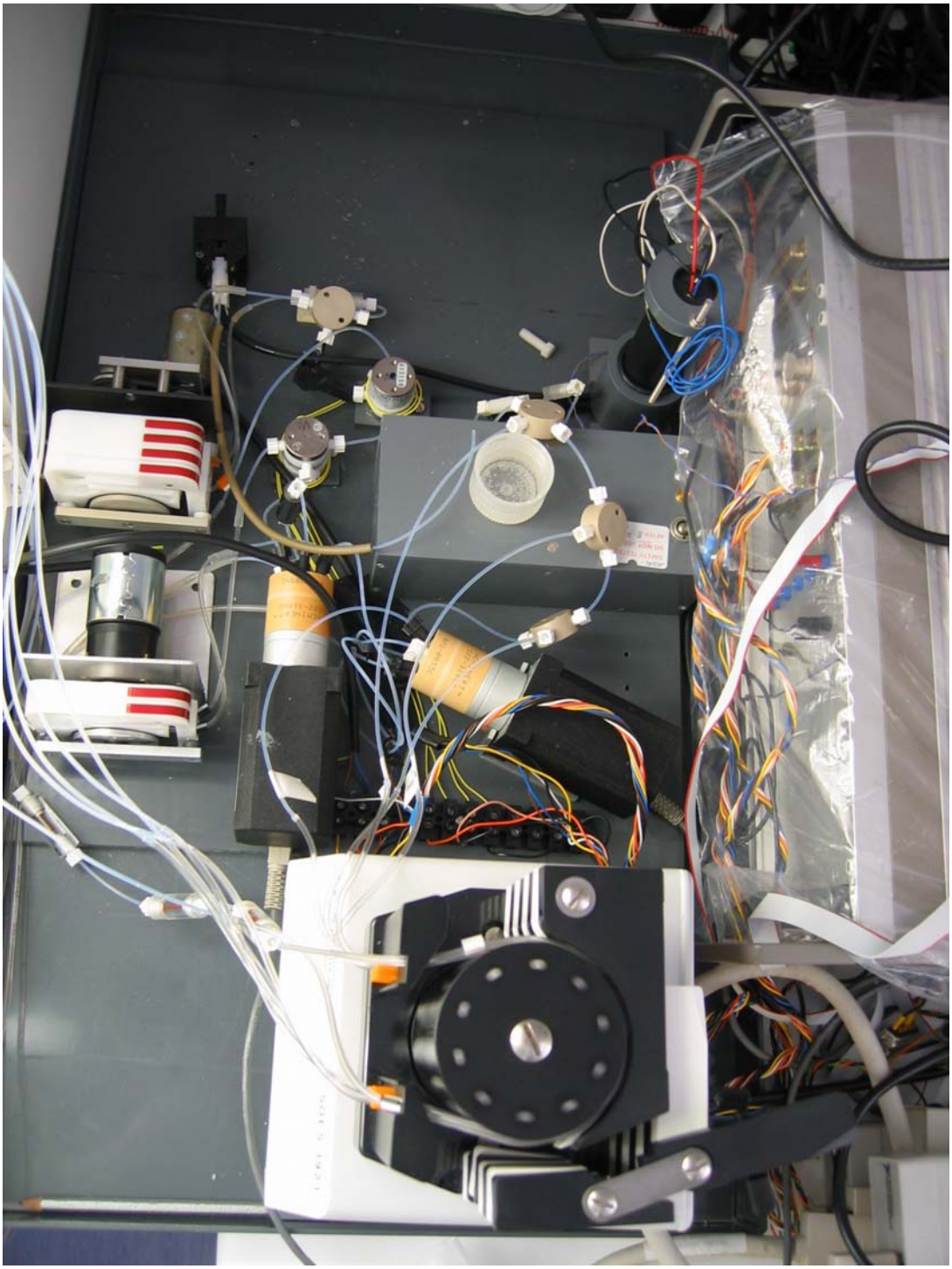

INSTRUMENTATION

Peristaltic Pump (Pump A)	Gilson Minipuls 3, 8 channels (Anachem)
Low-Voltage pumps (B & C)	4 channels, panel mounted 12 Vdc Ismatec pumps
2 Injection Valves (IV1 & IV2)	6-port Cheminert low-pressure valves model C22 with micro-electric 2-position actuator and ¼-28 fittings (VICI Valco Instruments, Thames Restek)
Switching valves (V1, V2 & V3)	12 Vdc 3-way electronic switching valves, 2-position direct lift solenoid valves containing PTFE wetted parts and zero dead volume (Cole-Parmer)
3 Tee-pieces	Peek 3-way junctions
Elution loop	0.5 m 0.8 mm i.d. PTFE tubing
Reaction coil	1.8 m 0.8 mm i.d. PTFE tubing
Heating unit	Laboratory made thermostated heating system (at 28 ± 1^{o}C)
8-HQ columns (PCC)	Made in Perspex (1.6 mm long, 2 mm i.d.) packed with HW-75F 8-hydroxyquinoline resin prepared following the protocol of Landing *et al.* (1986) (courtesy of S. Ussher)
Tubing	0.8 mm i.d. PTFE tubing for the manifold Flow-rated PVC peristaltic pump tubing (Altec)
Flow Cell (FC)	0.8 mm i.d. PTFE tubing coil backed with aluminium foil to optimise light reflection and mounted on the PMT window
Photo-Multiplier Tube (PMT)	End-on photo-counting head incorporated a low-noise PMT and internal high voltage supply, with low voltage (5 Vdc) source from main control unit (Hamamatsu Photonics)
Power Supply (PS)	Designed & constructed by Dr Matt Mowlem (OED, NOCS)
Instrument control card	National Instruments DAQPad-6020E card, 16 inputs, 100 kS/s, 12-bit Multifunction input/output (I/O) card
Signal acquisition card	National Instruments DAQPad-6507, 96-bit Digital I/O card
Laptop	Toshiba satellite Pro
Communication software	Software written in LabVIEW 6.1 (National Instruments Corp.) by Dr. Matt Mowlem (OED, NOCS) (Appendix 5)
Data processing	Software written in LabVIEW 6.1 (National Instruments Corp.) by F. Nédélec (Appendix 5)

ANALYTICAL PROCEDURE

Calibrations were carried out by standard additions to low-iron seawater (see Chapter II) and signal size was calculated using peak area (see below).

The blank was defined as the signal recorded for the loading of the ammonium acetate buffer only, applying the same loading time as for standards and samples by blocking the sample/standard line at the tee-piece with an acid washed nylon screw. It therefore included contributions from: **i)** the CL reagents (*i.e.* luminol reagent, eluent, ammonia, and hydrogen peroxide); **ii)** the preconcentration column and any perturbation in the baseline caused by the injection valve switching; **iii)** the rinsing water (*i.e.* Milli-Q water) potentially remaining in the elution loop despite adjusting the timing to remove

it; **iv)** the ammonium acetate buffer used to buffer the sample; and **v)** any contamination from the components of the system.

An analytical cycle was as follows. Buffered sample at *ca.* pH 5.5 first passed through the preconcentration column (Figure III.11). Valve (V1) then switched to allow the column to be rinsed with Milli-Q water to remove sea-salts. When the injection valve IV-1 switched, the eluent passed through the column in reverse flow direction to release iron and fill the elution loop. As soon as the elution loop was filled, the injection valve IV-2 switched to allow the acid eluent to carry the iron aliquot to meet other CL reagents and flow to the PMT flow cell for detection. Whilst the light from the CL reaction was being measured, IV-1 switched to allow Milli-Q water to remove the remaining eluent from the column and the new standard/sample was pumped in to flush out any previous solution from valve V2. An analytical cycle took 202 s plus loading time.

A batch of reagents lasted about 18 hours, so that a new batch was used approximately every day of analysis. Each solution was determined using three replicates after the signal stabilised. The full analytical procedure was as follows:

1. The system was left to stabilise for a minimum of 30 min. The baseline usually stabilised to its background level, and meanwhile the pH in the flow cell (CL pH) was checked and eventually adjusted to the optimum at pH 9.5.
2. The blank signal was then determined with a minimum of 4 replicates after the signal had stabilised.
3. The low-iron seawater (LISW) used as an internal standard (LISW-IS) (see Chapter IV) was then analysed for about 5 cycles.
4. The calibration was then carried out from the lowest concentration to the highest using standards prepared by standard addition to LISW.
5. The NASS-5 certified seawater standard was then analysed if the calibration range chosen covered its high concentration.
6. The LISW-IS was then re-analysed in order to check that the sensitivity of the analyser did not change with time, and was re-analysed every 2 hours during sample measurements.
7. Samples were then analysed with a minimum of 3 replicates.
8. The LISW-IS was analysed after all samples.
9. The analysis finished with a blank determination.

REAGENTS

- **Luminol Reagent (LR)**

  - **Monthly:** 0.01M luminol stock — Dissolve 1.06g Na_2CO_3 in 100mL MQW
    Dissolve 177mg luminol in 100mL 0.1M Na_2CO_3
    Good shake & let dissolve overnight in the dark

  - **24h in advance:** 100µM luminol reagent / 0.3mM TETA in 0.04M Na_2CO_3
    Dissolve 425mg Na_2CO_3 in 1L MQW
    Let dissolve a couple of hours
    Add 75µL of 60% TETA
    Add 10mL 0.01M luminol stock solution
    Condition 8HQ resin with 10mL of 0.04M Na_2CO_3
    Rinse 8HQ resin with 10mL of luminol reagent (LR)
    Pass LR through 8HQ resin (~ 8h)
    Wash 8HQ resin with 0.3M HCl (6 x column)
    Rinse 8HQ resin with SBDW (1 x column)
    Keep LR 24h in the dark

- **Eluent (E)** (0.3M Q-HCl) — Add 60mL Q-HCl concentrated to 1.94L of MQW (using tube)
  Can be prepared just before analysis — ***(2 lines of tubing in this bottle: Eluent & Eluent2)***

- **Ammonia (NH3)** (0.55M) — Add 30mL Primar-NH_3 (35%) to 0.97L of MQW (using tube)
  Should be prepared 12h in advance

- **Hydrogen Peroxide (H2O2)** (0.4M) — Add 40mL Aristar-H_2O_2 (~30%) to 0.96L MQW (using tube)
  Should be prepared just before analysis

- **Ammonium Acetate buffer (Sample buffer)**

  - 2M NH_4OAc stock — Dilute 110mL P-NH_3 (35%) and 115mL Q-acetic acid (~17.5M) to 1L with SBDW
    (✋ Exothermic reaction + fumes)

  - 0.2M NH_4OAc buffer — Add 10mL 2M NH_4OAc stock to 90mL of SBDW
    To prepare in advance — *Adjust pH to ~ 7.5 with 5M P-NH_3 if necessary*
    Purify through 3 in-line 8HQ columns (~ 2h), first 30 drops to waste !
    Wash columns with 0.3M Q-HCl for ~ 30min
    Rinse briefly columns with SBDW (~ 1mL)

- **Rinsing Water (RW)** SBDW water or freshly taken Milli-Q water if ran out *(Quality crucial to blank)*
  (Let flush minimum 1L first from MilliQ system)

- **Iron standards**

  - 10µM Fe stock solution in 0.1M Q-HCl in SBDW
    Add 200µL Q-HCl to 19.8mL of SBDW in a PS tube
    Add 11µL of 1000ppm Fe(III)
  - 600nM Fe stock solution in 0.01M Q-HCl in SBDW
    Add 25µL of Q-HCl to 25mL of SBDW
    Add 600µL 10µM Fe to 9.4mL of 0.01M Q-HCl
  - **Daily:** Fe addition just prior to analysis *(ASW = Acidified filtered Sea Water)*

  To prepare in Teflon pots directly, always the same for same concentration.
  If internal standard is used as a matrix, do not pipette directly from the bottle but first pore in a PS tube.
  Microwave 2 x 10s before adding Fe and allow to cool (at least 30min)

Solutions	Teflon pot nb	Volume of Seawater	Vol. 600nM Fe(III) (µL)	Vol. 0.01M Q-HCl (µL)
ASW "blank"	13	30mL	0	200
ASW + 0.25nM		30mL	12.5	187.5
ASW + 0.5nM	14	30mL	25	175
ASW + 1nM		30mL	50	150
ASW + 2nM	15	30mL	100	100
ASW + 2.5nM		30mL	125	75
ASW + 4nM	16	30mL	200	0

SOFTWARE PREPARATION

- ☐ Plug the two USB cables to the laptop (green lights appear on NI cards when ON)
- ☐ Click on the icon "**LabView7.1**" then on the arrow next to the button "OPEN" and select the destination finishing with "**Iron(III)total2.vi**"
- ☐ **The LabView window opens on the "Main panel"**
- ☐ Before doing anything, click on the horizontal white arrow icon (⇨ "run", in the menu) which turns black *(allows you to change parameters without modifying the program)*
- ☐ Click on the "**Timing sequence**" tab

The analytical sequence is set up as follows:

Time (s)	Valves		Pumps		IV1	IV2	Procedure
	V1	V2	P1	P2			
0-60	**ON**	OFF	**ON**	OFF	A	A	Load buffered sample onto 8HQ resin (**60s**)
60-90	OFF	OFF	OFF	**ON**	A	A	Rinse of 8HQ resin to remove sea salts (**30s**)
90-112	OFF	OFF	OFF	**ON**	B	A	Elute the 8HQ resin to fill elution loop (**22s**)
112-232	OFF	OFF	OFF	**ON**	B	B	Elution aliquot carried to flow cell (**120s**)
232-262	OFF	**ON**	**ON**	**ON**	A	B	End of detection, rinse 8HQ resin & pump buffered sample (**30s**)

V1 ⇔ Loading = ON & Rinsing = OFF
V2 ⇔ Pumping new buffered sample = ON & Loading = OFF
P1 ⇔ Ismatec pump delivering buffer & sample/standard
P2 ⇔ Ismatec pump pumping rinsing water & eluent
IV ⇔ Injection Valve: Position A = Green ; Position B = No colour
SV ⇔ Selection Valve which is not used at the moment

Time is written in milliseconds in the column on the right! Check number of zeros!

Time at the end of a line is the ENDING time for the sequence described on the line.

Times are ADDED between lines, if loading time is changed, all the values must be changed.

The table should look like that (timing can change)

■						■								0	60000
							■							0	90000
							■					■		0	112000
							■					■	■	0	232000
			■			■	■						■	0	262000
V1			V2	V3		P1	P2					IV1	IV2	SV	Time

Here is an idea on how to choose the appropriate timing sequence :

Conditions	**Coastal waters**	**Shelf waters**	**Shelf break**	**Open ocean waters**	**HNLC**
Range stds	**1 - 10nM**	**0.5 - 5nM**	**0.25 - 3nM**	**0.1 - 2nM**	**0.05 - 1nM**
Loading time	**30s**	**1min**	**2min**	**4min**	**6min**
Line 1	30000	60000	120000	240000	360000
Line 2	60000	90000	150000	270000	390000
Line 3	82000	112000	172000	292000	412000
Line 4	202000	232000	292000	412000	532000
Line 5	232000	262000	322000	442000	562000

BEFORE STARTING, CHECK THAT NUMBER OF ZEROS IS CORRECT !!!

- **Still in the "Timing sequence" tab**, give a name to the file recording the time stamp. The date and time when V1 is switched ON is saved in a separate file. This time corresponds at the time when the sample was taken for analysis. *(compulsory to avoid error messages during analysis, even when time stamp not needed)*

  Files will be named as: Timing*_[date]*, e.g. **Timing_1211**

- **On the "Main panel"**,

  1. Select the gain needed (with up/down arrows) which will remain the same over the whole analysis. *(A gain of 6 is a good compromise, unless the baseline is too high, in that case reduce it to 4 but this will loose sensitivity)*

  2. Click on 🗁, select the folder where the file will be saved (/CROZEX/leg1 or leg 2).
     For a calibration, files will be named as:
     Calib[*range*]_[*matrix*]_[*Gain*]_[*Date*]

     Ex.: A calibration from 0.5 to 5nM prepared with the internal standard (IS), with a gain of 6 on the 12th November, will be: Calib0.5-5nM_IS_G6_1211

     For samples, files will be named as: **Samples[*location*]_[*Gain*]_[*Date*]**

     Ex.: Samples from the transect J to M4 analysed with a gain of 6 on the 12th November, will be: SamplesJ-M4_G6_1211

  3. Click on ☐ to log the data in the file (if ■, data is being logged)
  4. Press Ctrl + S to ensure all changes are saved

ANALYTICAL PROCEDURE IN PRACTICE

- Switch ON the white extension lead which will turn ON all the equipment
- Switch ON the reaction coil heating unit in advance (minimum **30min**)
- **Empty the waste bottle !!!**
- Switch ON the Gilson pump after putting the tension on the PVC tubing after checking if they got flatter, in that case change them
- Place all PTFE tubing in their respective reagent bottle one by one in order to avoid any reflux into the bottles, checking that they are pumped properly, adjust one by one the pressure on the tubing if necessary *(especially if were changed)*
- Close the reagents bottle plastic bag to avoid contamination
- **Let system to stabilise for 30min - 1h**, meanwhile, check the **baseline level and CL pH** *(write on analysis log sheet, see troubleshooting (p5) if baseline high (>2V, gain 6))*

To check the CL pH, rinse a PS tube with MQW and dry, disconnect the PMT waste tubing and collect the waste flow in the tube. Wait for the waste solution to cool to ambient temperature before reading the CL pH.

- ❑ **Prepare file name, and click on "log data" square** *(as explained in section above)*

- ❑ **Start the analyses with a blank** defined as the signal obtained for the loading time used of the buffer only. For this, leave the sample line to pump air (**~ 10 blank values**) (*NB: the first peak may be very high & may take some time to stabilise. Wait to obtain 3 reproducible replicates. Blanks are considered "too high" when higher than 2V added to the baseline level*). **Click on the START button when ready. Prepare the standards meanwhile !!**

- ❑ Analyse the **internal standard**, which has been micro-waved for 2 x 10s before and allowed to cool ~ 30min, until its signal is stabilised (**~ 5 replicates**)

Solutions must be switched before the last 30sec of the analytical cycle !!

- ❑ Analyse the **standards** (3 good replicates each) to draw the calibration curve, from the less concentrated to the more concentrated, additions of Fe should be made at the last minute if possible, and standards should be vigorously shaken.

- ❑ Check the accuracy of the system with **NASS certified seawater** if appropriate to the range of concentrations

- ❑ Check the signal for the **internal standard** and wait for its stabilisation. It should be re-analysed regularly (**every ~ 2h** to check for any drift of sensitivity)

- ❑ **Change file name** as explained above, to start analysing samples. Files should **not exceed 100,000 data points** (number given at the x-axis of the charts) to limit the file size and avoid crashing the NI card. Therefore change the file name every 2h or so.

- ❑ Analyse **samples** (**2 replicates** for a first analysis, unless one peak is strongly perturbed with bubbles. When doing final analysis of samples, 3 replications should be done)

- ❑ Finish the analyses with **the internal standard** and **blank** (as above) until it stabilises

- ❑ Stop the system clicking **firstly** on the **"START"** button and **then** on the **"STOP"** button **at the end of a cycle** (262s with 60s loading time sequence)!

- ❑ If continuous analysis is made, when a batch of reagent is finished, stop the program and Gilson pump. Change the CL reagents bottle and start Gilson, and start the whole procedure again.

End of analysis

- ❑ Wash the **whole** system with **0.3M Q-HCl** for minimum **5minutes.** For this, put **ALL** the tubing in the acid wash bottle and run cycles as when doing analyses.

- **Release the pressure on all the peristaltic pump tubes** after removing the tubing from the reagent bottle

- **Switch off everything (Gilson, heating, white extension lead, laptop)**

DURING THE ANALYSIS

1. Prepare new sample buffer (purification of 100mL takes about 2h) if more is prepared, wash columns after every 100mL as described in sample preparation
2. Dissolve sodium carbonate for luminol reagent, leave to dissolve about 2h
3. Prepare luminol reagent, purify immediately (purification of 1L takes about 8h)
4. Prepare eluent, ammonia, hydrogen peroxide reagents (keep luminol reagent and hydrogen hydroxide away from light)

TROUBLESHOOTING

PROBLEM OBSERVED	ACTIONS
One (or both) National Instruments card(s) crashed = no green light at the front or green light flashing Symptoms: Low voltage pumps not working when due to Injection valves not switching when due to = NI card 2 (instrument control) On software, acquisition of data stopped even if time in loop did not = NI card 1 (data acquisition)	1. Stop iron2 program 2. Do not stop Gilson pumping CL reagents if crashed during analysis 3. Close and Exit Labview 4. Shut down both cards and switch back ON (switches are behind cards) 5. Start iron2 6. Continue analysis with **new file name** 7. If crashed again, try again 1-6 with restarting laptop! 8. If crashed again, switch USB connections at back of laptop 9. If still crashes, leave for a while and try again later!
Baseline is high (> 2V, Gain 6) (it seems that with MQW on board, signal is high, 3V, gain 6 anyway)	1. Check that no CL reagents was contaminated by changing one by one each reagent. 2. Check that Luminol Reagent (LR) had time to age 3. Check that CL reagents are properly pumped (tubing not twisted, low pulsing …) 4. Check CL pH (should be at pH 9.5) ➢ If too high (9.7), add ca. 20mL of MQW to NH_3 ➢ If too low (9.4), add ca. 5mL of 5M NH_3 to NH_3 (if 9.15 ⇔ + 17mL 5M NH_3 gives 9.37)
No peak is observed at the normal time (20-25sec after IV2 switched to B)	1. Check that cards did not crash (see previous) 2. Check that sample tubing in container is

	pumping liquid 3. Check that injection valves properly connected electronically 4. Check loading pH
Peaks are not as high as expected	1. Check that heating unit is ON 2. Check loading pH 3. Fe added to standard ? 4. Check for leaks in the manifold
One peak was much higher than other replicates	1. Check immediately in waste for abnormal number of bubbles 2. Add a replicate to analysis 3. Check loading pH
If one low-voltage pump does not pump properly	1. Grease junctions 2. Change pump with spare

DATA PROCESSING

There are 3 categories of data files saved during analyses: Timing files, Calibration files and Samples files. All files generated by the LabView program are **text files**. These files can easily be imported in Excel.

1. **Timing files** will only be used when samples will be analysed in-line the underway fish system.

   They give the time at which V1 was switched ON, which therefore corresponds at the time at which the sample was taken up for analysis from the underway sampling device.

   The time for the sample to arrive at V1 will have to be added to this time stamp to know when the sample was pumped by the fish system. It will then be possible to retrieve the position of the ship at that time using the GPS data from the ship.

   It will be crucial to synchronize everyday or so the time on the laptop to ship time !!

2. **Calibration and samples files** will be processed the same way. Raw data files produced during analyses are 1-column data files, where the first column is the PMT signal (in Volts). Because we use a relatively high scan rate for the PMT readings (a lower scan rate would slow down the program), these files can be very big and would have to be split in several files before being imported in Excel as Excel spreadsheets are limited in the number of rows. We will therefore use in the first place another LabView software to calculate the peak area before being imported in Excel.

a. Determination of peak area

i. Calculations

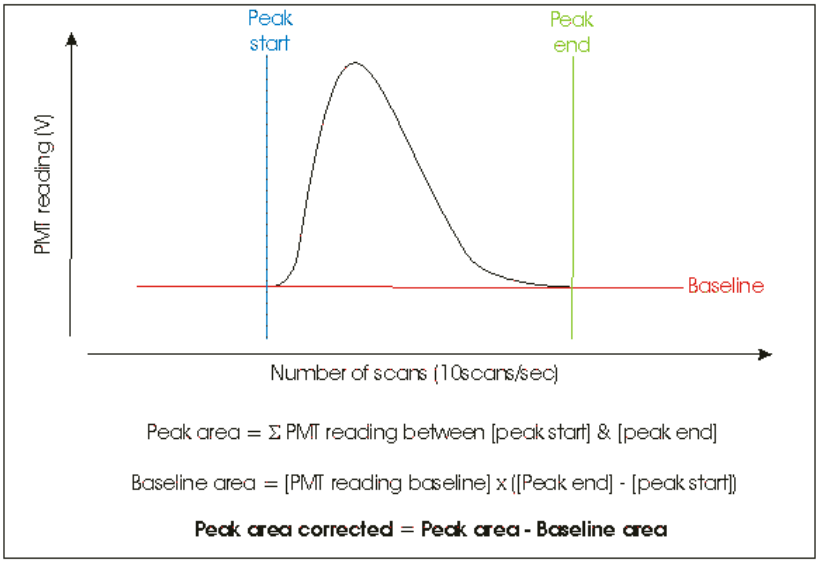

ii. Procedure to determine peak area

a) Open **"Data processing area"** from the desktop (in LabView 6.1 !)

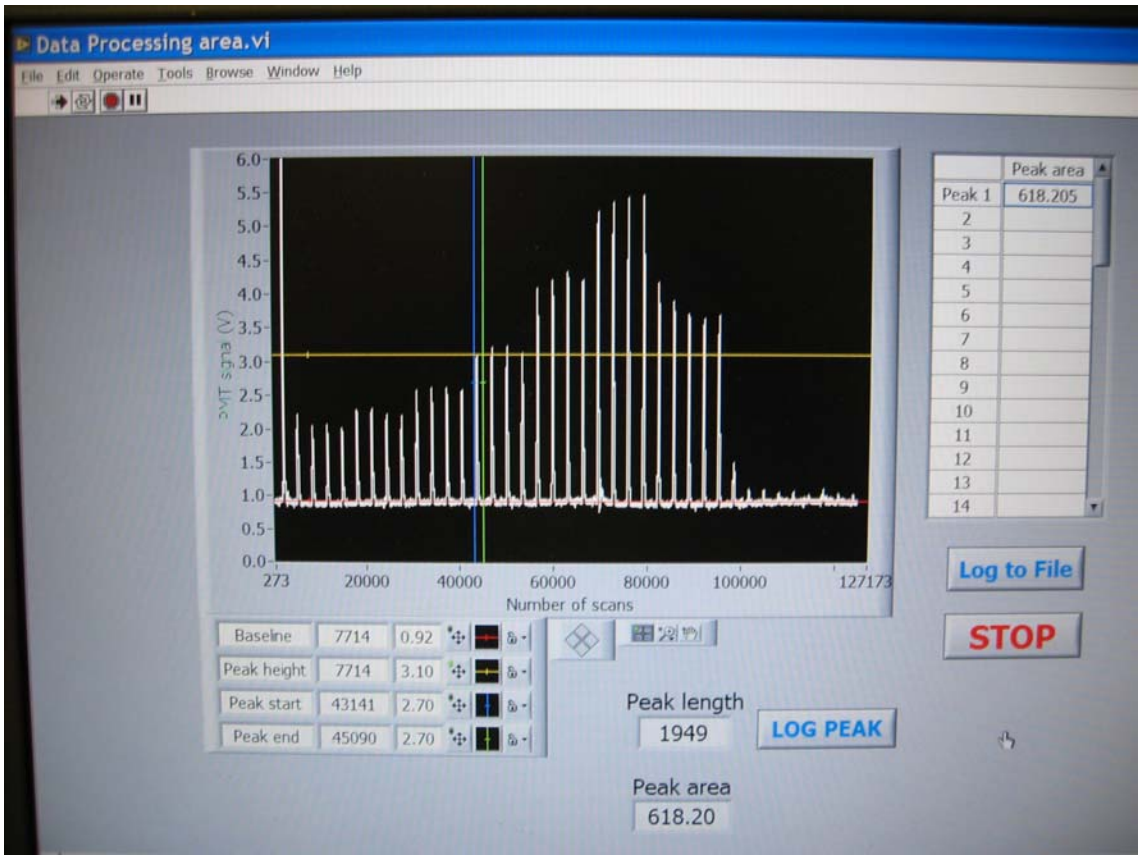

Description of the screen:

- The chart is empty when opening this program.

- Bottom left of the chart are the readings of the different axes where 2nd column = x; 3rd column = y = PMT signal (V) :
  Red line ⇔ Baseline
  Yellow line ⇔ Peak height
  Blue line ⇔ Peak start
  Green line ⇔ Peak end
- Under the chart is a small display of the different options :
  The cross + is to drag the axis to the position wanted
  The middle one is a zoom function
  The hand ✋ is to go from one peak to another by dragging the chart
- Bottom middle of the screen are: "**peak length**" corresponding to the number of scans between [peak start] and [peak end]; the instant reading of "**peak area**"; a button to "**LOG PEAK**" in a table when axis are placed properly on the chart.
- Top right of the screen is the table where logged peaks are displayed
- Under the table are: the button to save the table in a file ("**Log To File**"); and to stop the program when finished ("**STOP**")

b) Click on the white arrow on top-right of the screen (⇨), a window opens asking which file to open, select a file, click OK, the data is plotted on the chart

c) Click on the middle button of the chart options to zoom on one peak (*only the base of the peak is needed*)

d) Click on the cross icon to be able to drag the axis. If the axis is not shown after zooming, call it: left-click on the cross of the axis wanted <u>in the chart caption</u> and select "**bring to center**"

e) Drag the axis at their position :

- the baseline (red) at the baseline level <u>after</u> the peak;
- the peak start (blue) where the signal increases from the baseline level;
- the peak end (green) where the signal comes back to the baseline level.

f) The **peak length** should **not exceed 1200** (end of detection) and it is preferable to avoid taking in account bubbles shown in the baseline after the peak and take the **end of the peak <u>before</u> the bubble** if the signal was already back to the baseline level.

g) When axes are positioned, click on the "**LOG PEAK**" button **ONCE** to record the peak area measured in the table. The value saved is then shown for peak 1 in the table.

!! *There is **no way** but starting from the beginning or taking notes that peak 23 = peak 24 if the value was logged by mistake twice or if the wrong peak was measured* **!!**

h) Click then on the "hand ✋" icon to drag the chart to the next peak and start again from point **d).**

i) When all peaks have been logged in the table, click on the "**Log To File**" button. A window will appear asking where to save the file. The file should be named as: **Calib*[date]*ToExcel** for a calibration, and **Samples*[location]*ToExcel** for samples

j) It is possible to open a new file afterwards, but the table needs to be emptied before logging new peaks otherwise new data will be logged on the same file. To empty the table, left-click on the table and select "**Empty Table**". Then start logging peaks from point **c).**

k) When finished, press the "**STOP**" button and close the program.

The new file is a text file of 1 column with peak areas which can be imported in Excel.

b. Plotting the calibration curve and calculating concentrations

i. Open **Excel** and the file "**Calib_spreadsheet.xls**" or "**UnderwaySamples_spreadsheet.xls**" or "**CTDSamples_spreadsheet.xls**" (My documents/CROZEX/data/)

ii. Open the file prepared as "**Calib*[date]*ToExcel**" or "**Samples*[location]*ToExcel**" (Select "All files" for "Files of Type:"). Press "**Finish**" at the Text Import Wizard.

iii. Copy the column of data of the imported file in column A of the spreadsheet.

iv. Then using the notes taken during analysis, copy and paste the peak area to the right solution analysed.

v. For the calibration, also check that the standards concentrations are right and the calibration will be drawn automatically.

vi. Don't forget to save the file with a name as: Calib*[range]_[sw matrix]_[gain]_[Date]*, i.e. Calib0.5-5nM_IS_G6_1211; or (Underway or CTD) Samples*[location]_[gain]_[Date]* i.e. (Underway or CTD)SamplesJ-M4_G6_1211

APPENDIX 8

INTER-BATCH DATA CHECK – DATA TABLE

Sample's label Cruise/CTD station/bottle number	**Location in water column (depth, m)**	**Determination 1**		**Determination 2**	
		Day	**DFe (nM)**	**Day**	**DFe (nM)**
JR98/N9/7	Chlorophyll *a* max (27m)	12	0.48 *(±0.04)*	14	0.45 *(±0.01)*
JR98/N8/23	Surface (2m)	12	0.75 *(±0.09)*	13	0.81[*] *(±0.03)*
JR80/SG/051unfiltered	Surface with pole sampler (1m)	10	0.98[**] *(±0.02)*	11	1.12 *(±0.03)*
AMT12/CTD68/7	Top water column (175m)	11	6.04 *(±0.23)*	12	6.25 *(±0.15)*
AMT12/CTD68/19	Chlorophyll *a* max (23m)	11	1.12 *(±0.10)*	13	1.05[*] *(±0.09)*
AMT12/CTD24/2	Deep waters (3300m)	2	0.69 *(±0.12)*	6	0.73 *(±0.04)*
AMT12/CTD24/2/0.1-µm	Deep waters (3300m)	6	0.79 *(±0.01)*	5	0.92 *(±0.22)*
AMT12/CTD24/10	Deep waters (1700m)	2	2.09 *(±0.18)*	5	2.13 *(±0.14)*
AMT12/CTD24/16	Top water column (500m)	2	1.26 *(±0.12)*	5	1.04 *(±0.02)*
AMT12/CTD39/9	Top water column (150m)	7	0.77 *(±0.02)*	6	0.69 *(±0.05)*
AMT12/CTD39/9/0.1-µm	Top water column (150m)	6	0.96 *(±0.06)*	7	0.98 *(±0.08)*
AMT12/CTD39/23	Surface (2m)	5	1.77 *(±0.20)*	9	1.58 *(±0.03)*
AMT12/CTD50/15	Shallow waters (75m)	7	1.04 *(±0.07)*	8	1.11 *(±0.04)*
AMT12/CTD50/23	Surface (2m)	1	1.18 *(±0.08)*	7	1.14 *(±0.04)*
AMT12/CTD62/23	Surface (2m)	11	2.10 *(±0.25)*	13	1.83[*] *(±0.10)*

By default, all samples were filtered through a 0.4-µm filter pore size, unless stated otherwise in the sample label.

[*] Samples from analysis day 13 that were normalized using the low-iron seawater internal standard average value (see Chapter IV).

[**] Samples from analysis day 10 that were corrected from a shift in sensitivity using the equation found with LISW-IS value changes with time.

APPENDIX 9.

CTD, CHLOROPHYLL *a* AND NUTRIENT DATA AT EACH OF THE STATIONS OF THE TRANSECT AT THE CELTIC SEA SHELF EDGE (*JR98* CRUISE)

CONTENT

CAPTION

(LoD = Limit of Detection)

Plot A
- Temperature (^{o}C) ——
- Salinity (psu) ——

Plot B
- Beam attenuation (m^{-1}) ——
- Dissolved oxygen (μM) ——

Plot C
- Dissolved iron (nM) ●
- Chlorophyll *a* (μg/L) (measured) △
- Fluorescence (μg/L) (CTD) ——

Plot D
- Nitrate (μM) ○
- Dissolved silicon (μM) ▽
- Phosphate (μM) ◇

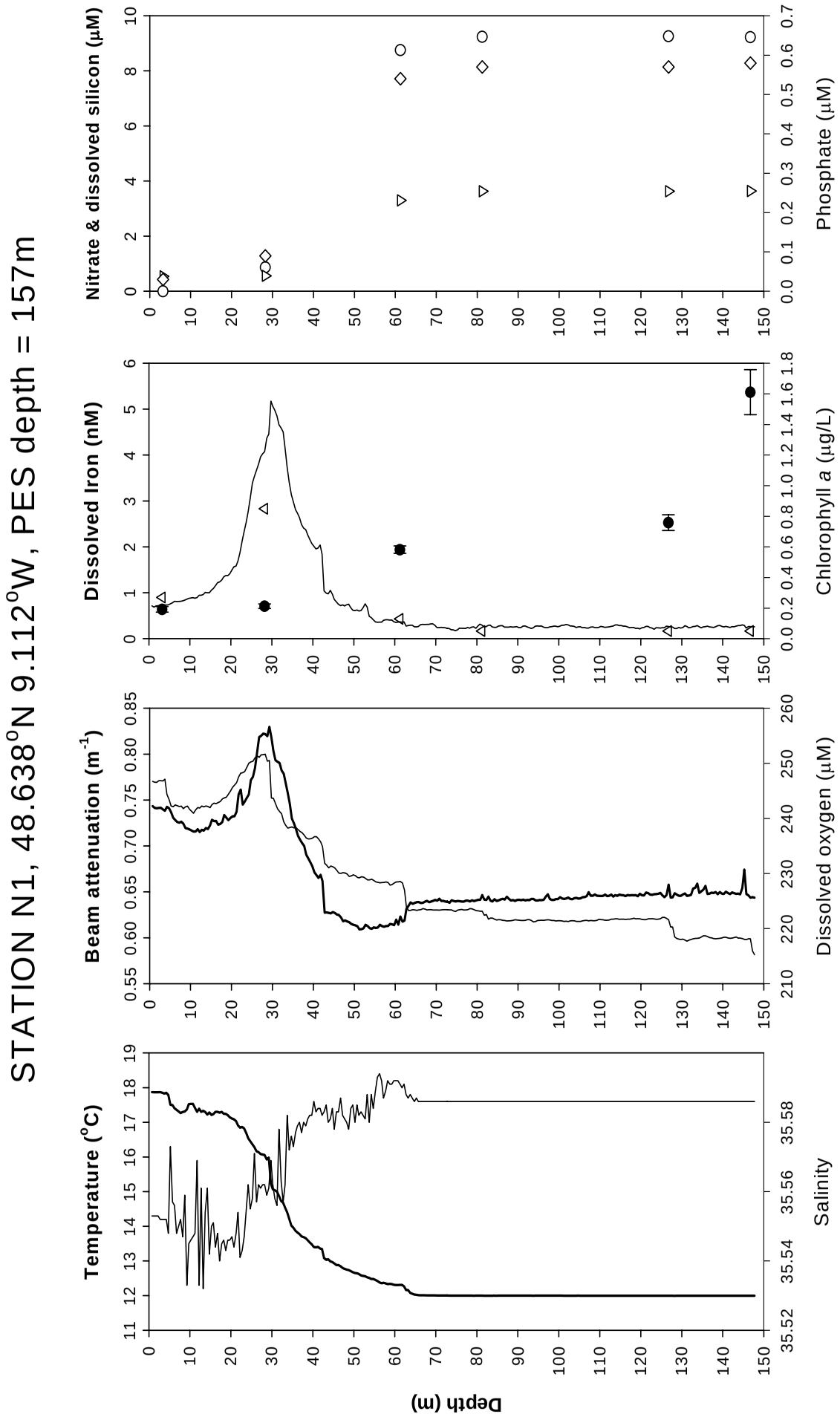
STATION N1, 48.638°N 9.112°W, PES depth = 157m
Temperature (°C)
Beam attenuation (m-1)
Dissolved Iron (nM)
Nitrate & dissolved silicon (µM)
Salinity
Dissolved oxygen (µM)
Chlorophyll a (µg/L)
Phosphate (µM)
Depth (m)

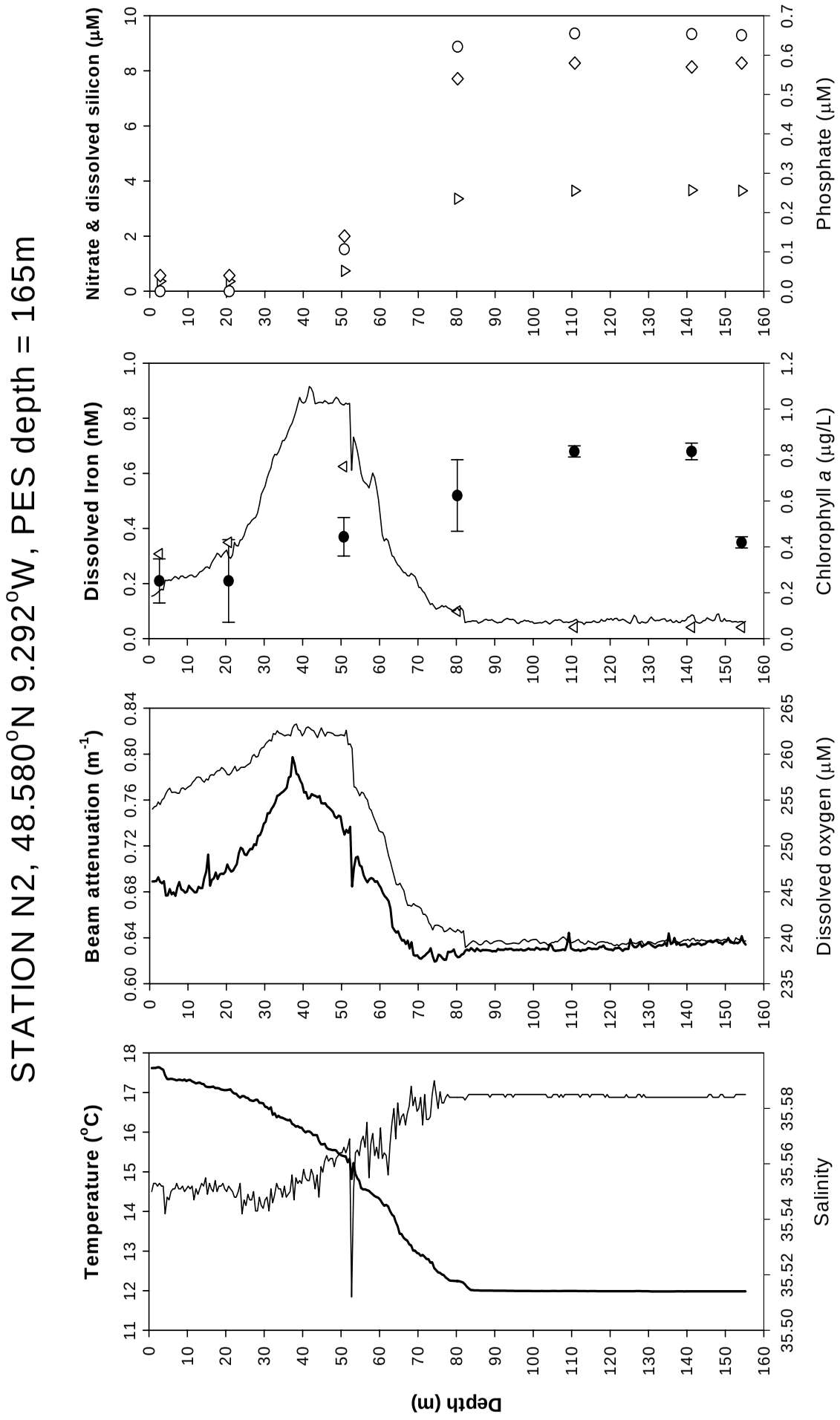
STATION N2, 48.580°N 9.292°W, PES depth = 165m
Temperature (°C)
Beam attenuation (m-1)
Dissolved Iron (nM)
Nitrate & dissolved silicon (µM)
Salinity
Dissolved oxygen (µM)
Chlorophyll a (µg/L)
Phosphate (µM)
Depth (m)

STATION N3, 48.520°N 9.493°W, PES depth = 250m

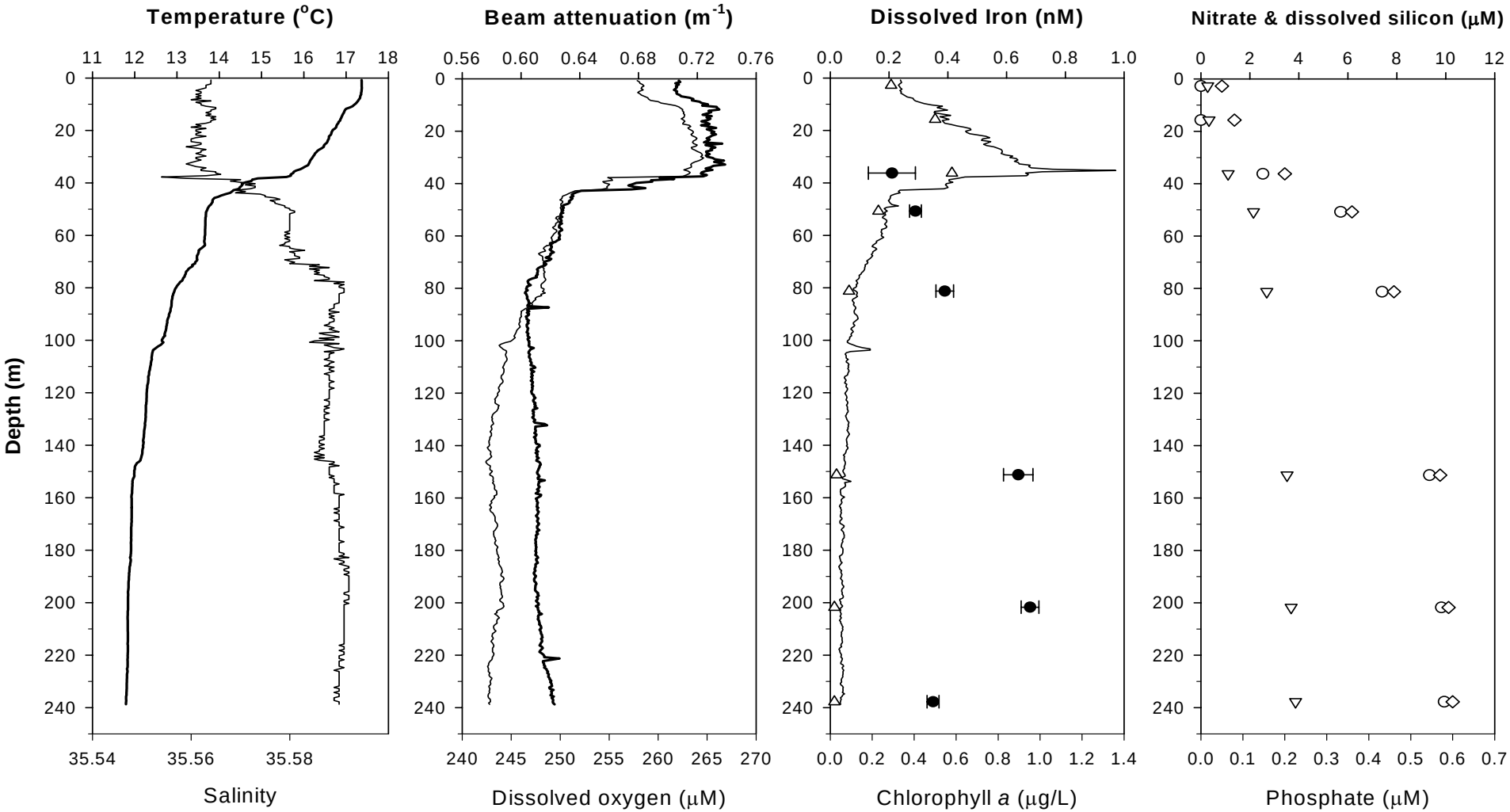

STATION N4, 48.502°N 9.550°W, PES depth = 365m

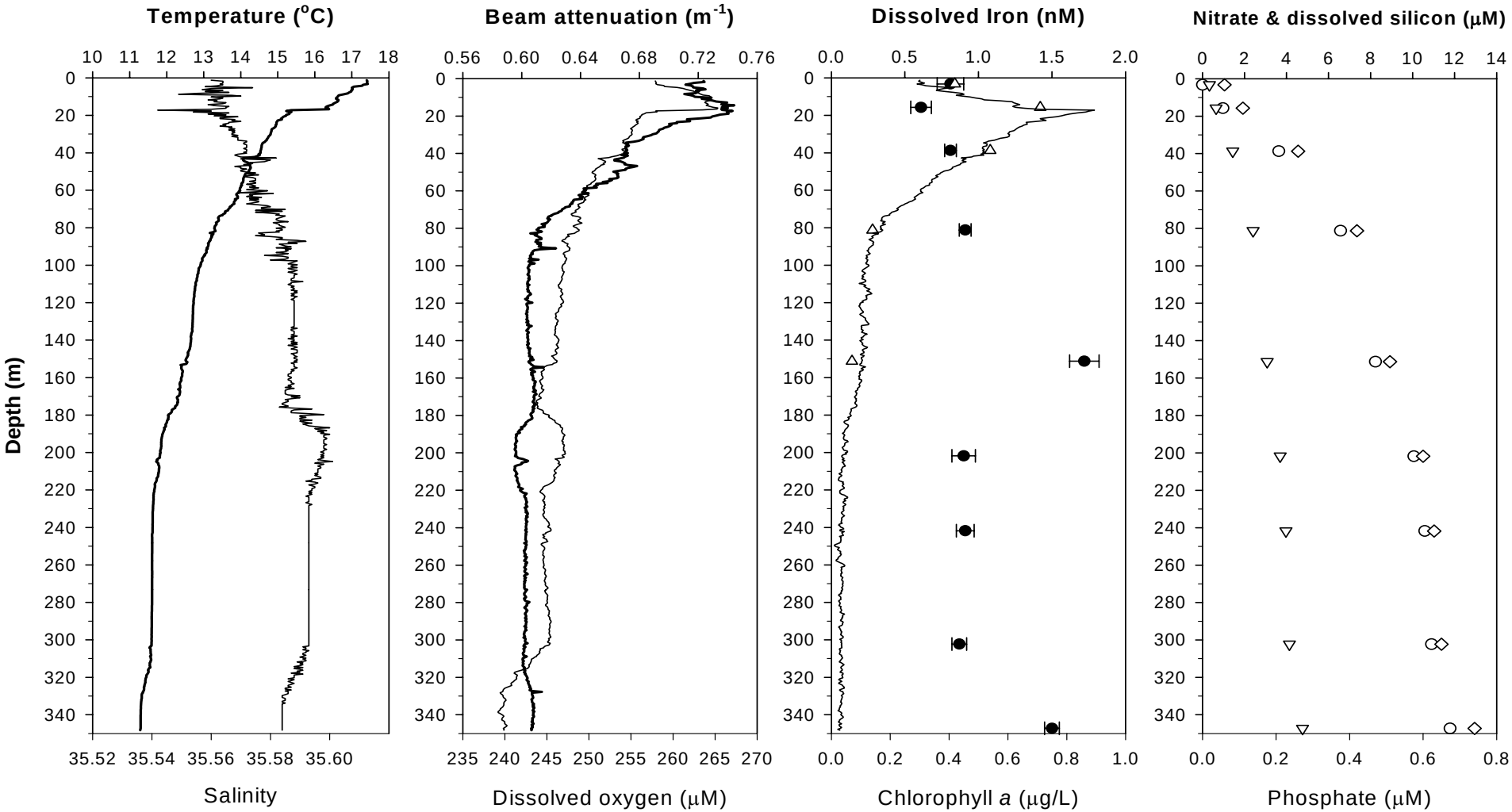

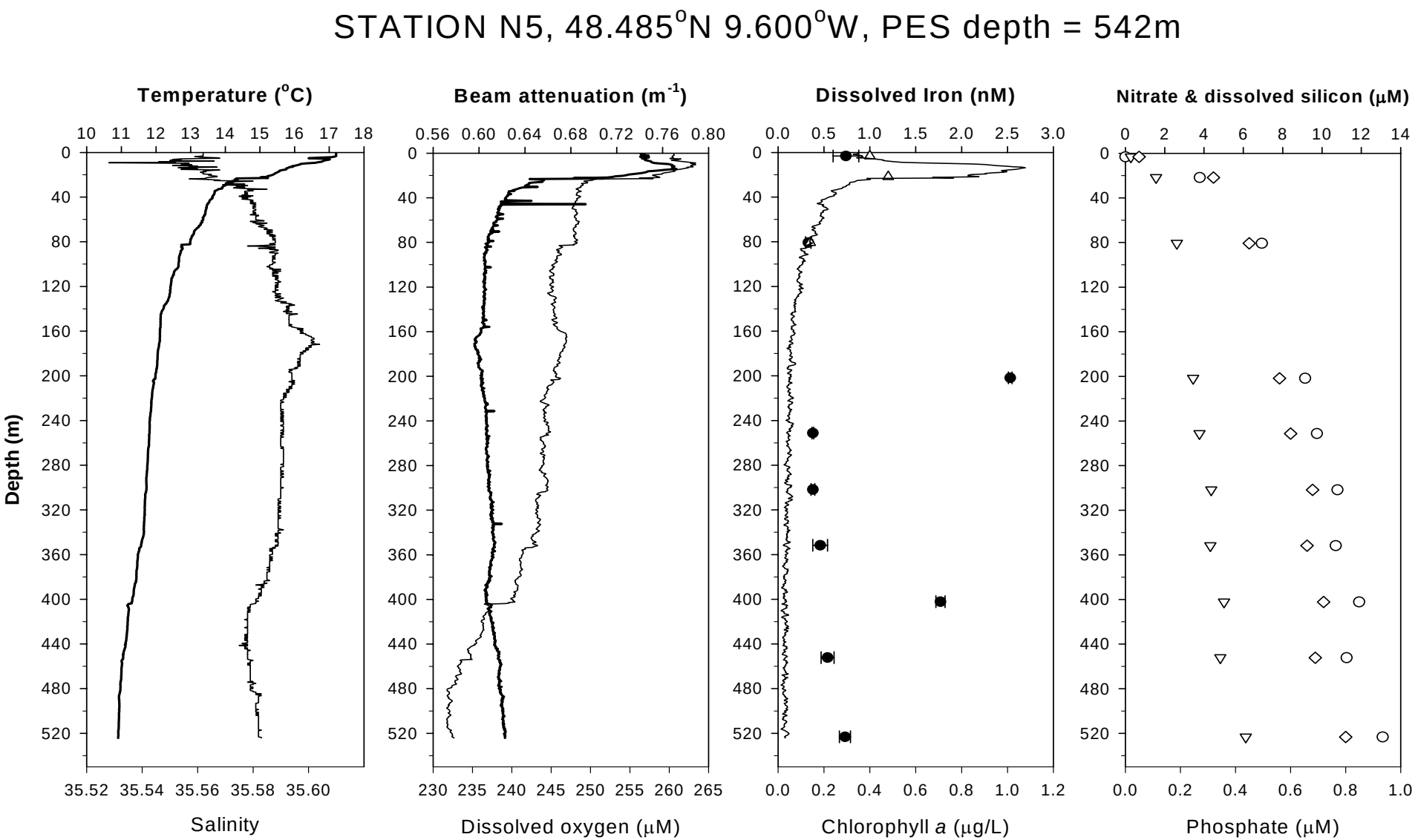
STATION N5, 48.485°N 9.600°W, PES depth = 542m
Temperature (°C)
Beam attenuation (m-1)
Dissolved Iron (nM)
Nitrate & dissolved silicon (μM)
Depth (m)
Salinity
Dissolved oxygen (μM)
Chlorophyll a (μg/L)
Phosphate (μM)

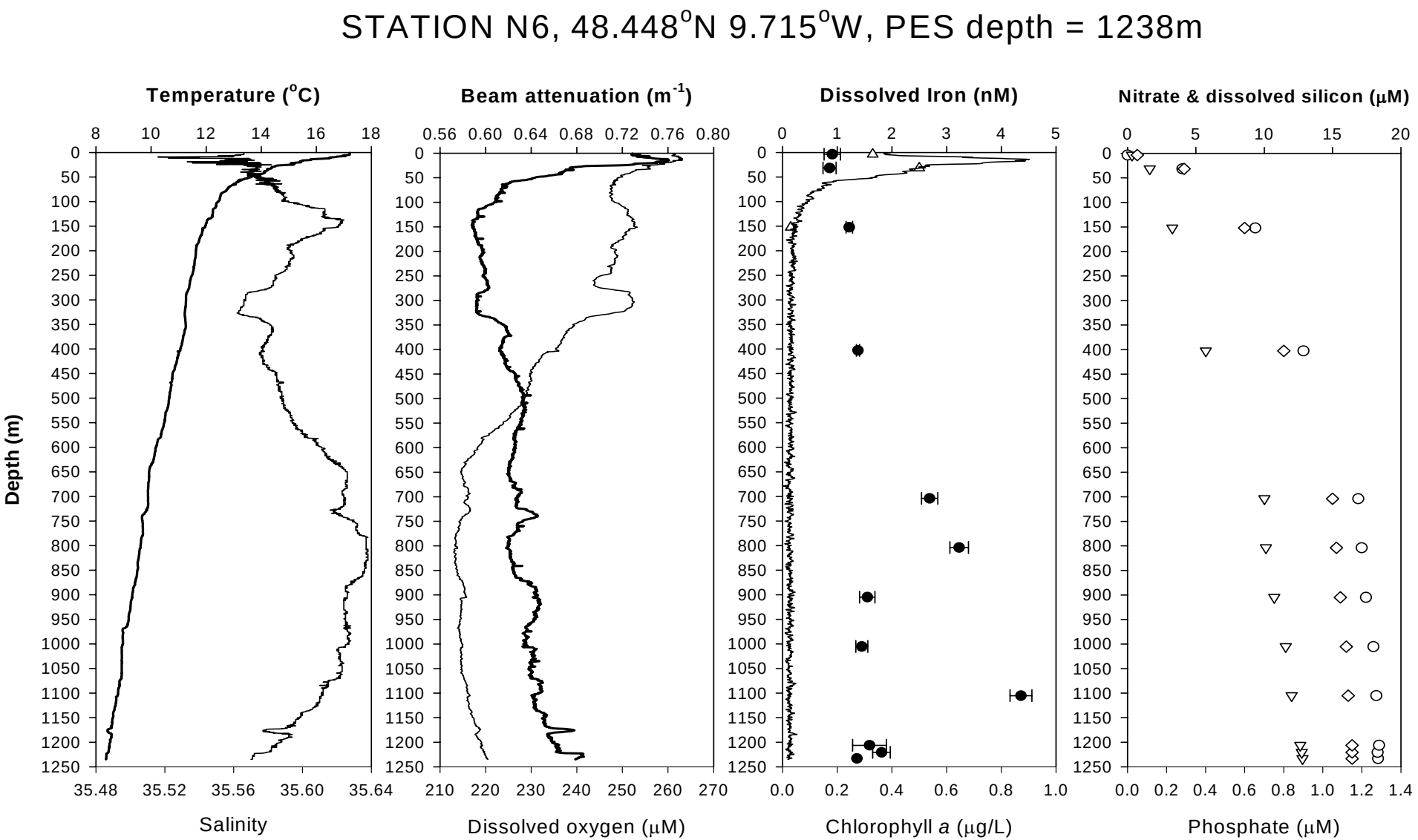
STATION N6, 48.448°N 9.715°W, PES depth = 1238m
Temperature (°C)
Beam attenuation (m-1)
Dissolved Iron (nM)
Nitrate & dissolved silicon (µM)
Depth (m)
Salinity
Dissolved oxygen (µM)
Chlorophyll a (µg/L)
Phosphate (µM)

STATION N7, 48.397°N 9.883°W, PES depth = 1903m

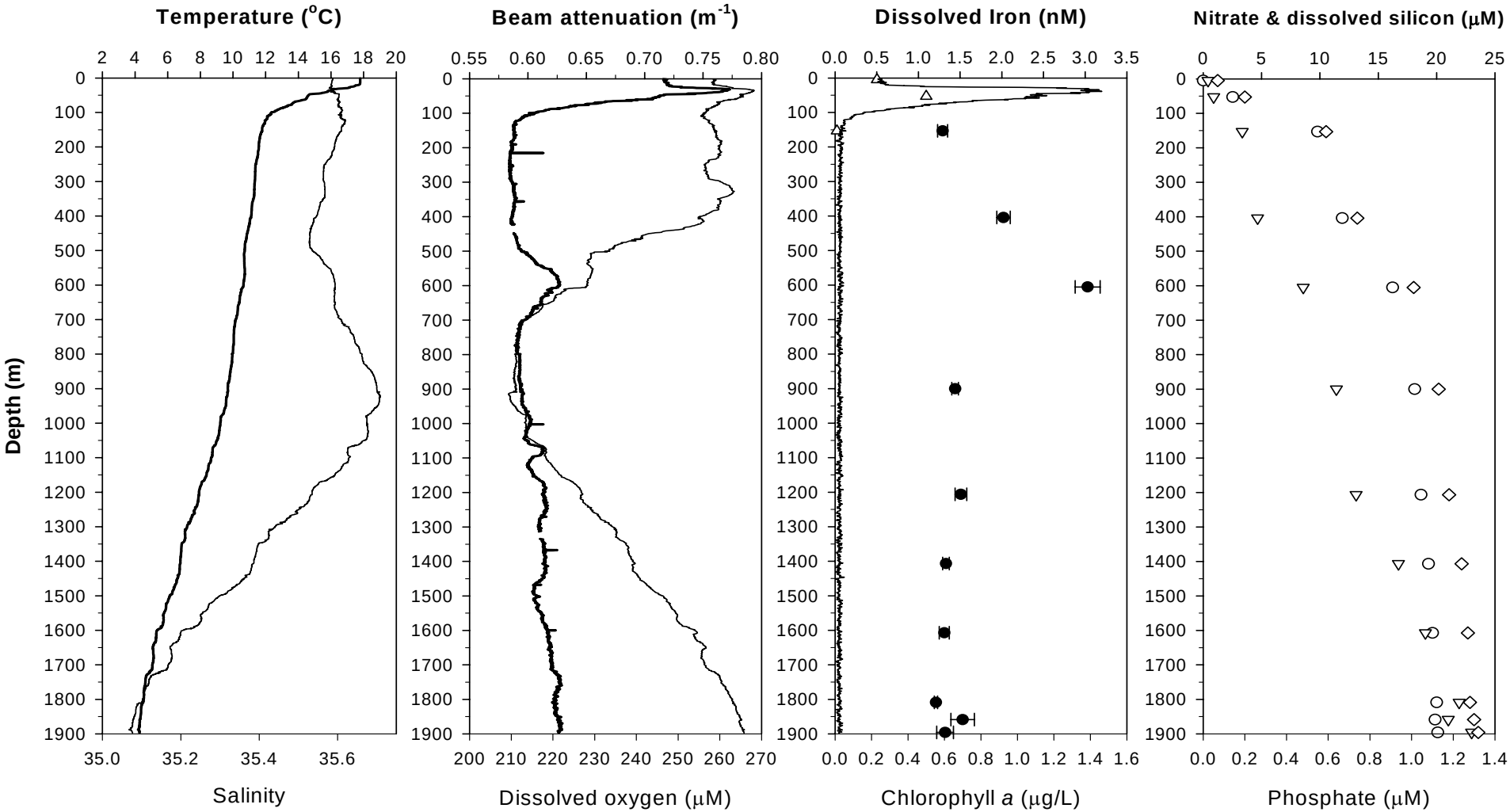

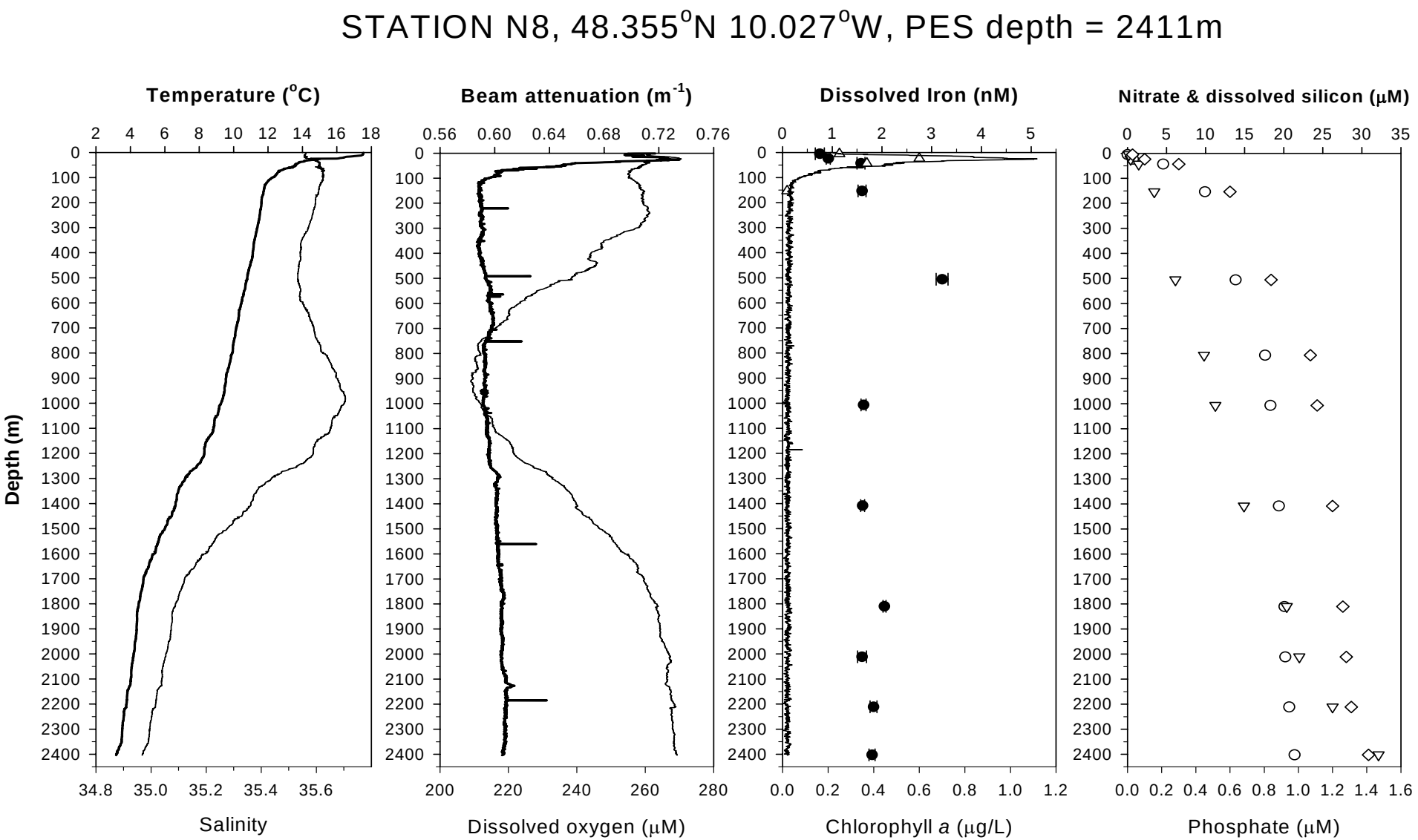
STATION N8, 48.355°N 10.027°W, PES depth = 2411m
Temperature (°C)
Beam attenuation (m-1)
Dissolved Iron (nM)
Nitrate & dissolved silicon (μM)
Depth (m)
Salinity
Dissolved oxygen (μM)
Chlorophyll a (μg/L)
Phosphate (μM)

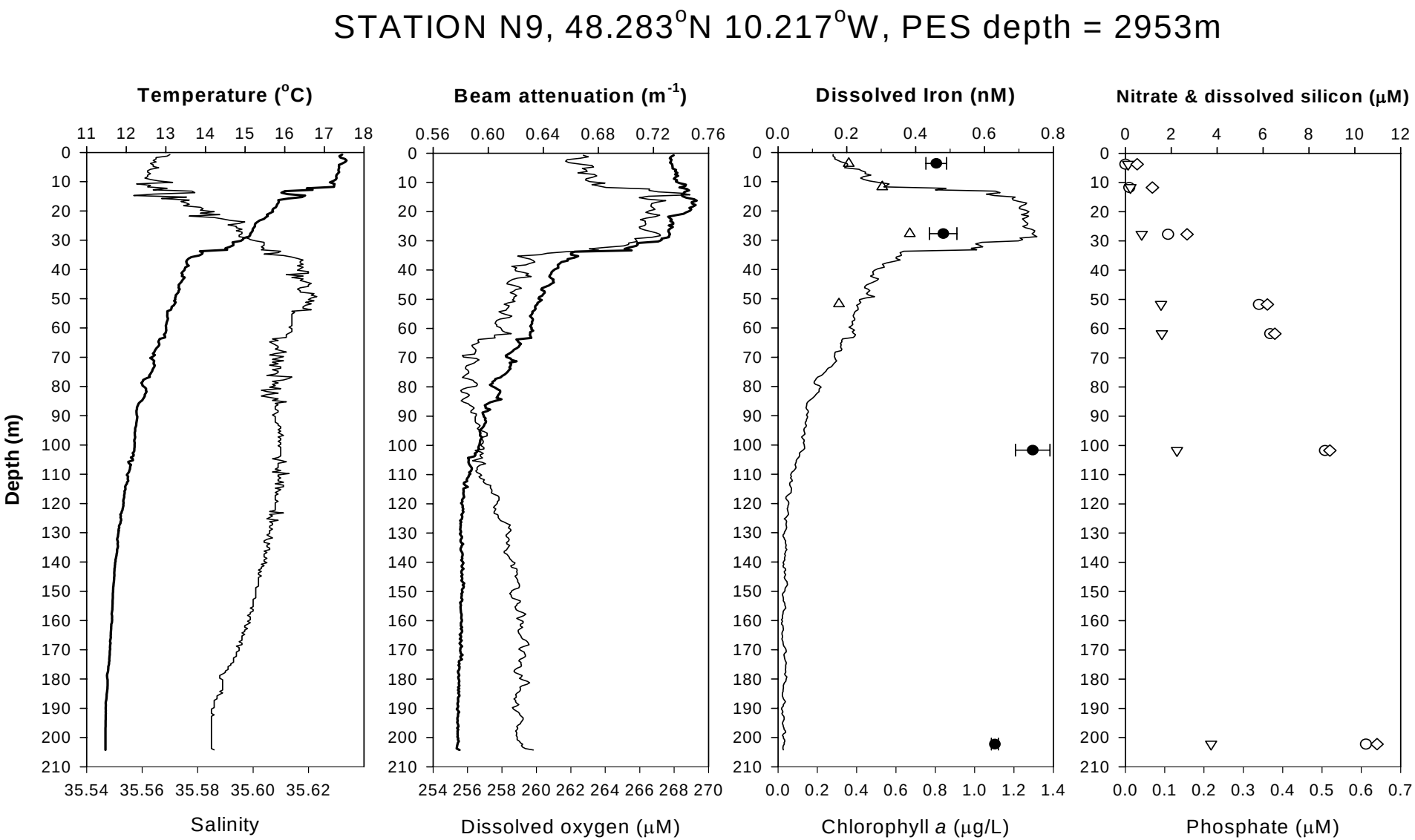
STATION N9, 48.283°N 10.217°W, PES depth = 2953m
Temperature (°C)
Beam attenuation (m-1)
Dissolved Iron (nM)
Nitrate & dissolved silicon (µM)
Depth (m)
Salinity
Dissolved oxygen (µM)
Chlorophyll a (µg/L)
Phosphate (µM)

Station (water depth)	Depth (m)	Temperature (°C)	Salinity	Chlorophyll *a* (μg/L)	Dissolved oxygen (μM)	AOU (μM)	Nitrate (μM)	Phosphate (μM)	Dissolved silicon (μM)	Dissolved iron (nM)
N1 (157 m)	3	17.8	35.55	0.27	246.8	-7.4	0	0.027	0.55	0.64 ± 0.06
	28	16.0	35.56	0.85	251.7	-3.7	0.87	0.092	0.56	0.71 ± 0.05
	61	12.3	35.59	0.13	228.5	39.3	8.76	0.542	3.30	1.94 ± 0.07
	81	12.0	35.58	0.05	223.2	46.4	9.24	0.571	3.63	---
	127	12.0	35.58	0.05	221.6	48.1	9.26	0.572	3.63	2.53 ± 0.17
	147	12.0	35.58	0.05	218.2	51.5	9.23	0.578	3.64	5.37 ± 0.49
N2 (165 m)	3	17.6	35.55	0.37	254.5	-14.1	0	0.042	0.34	0.21 ± 0.08
	21	17.1	35.55	0.42	257.7	-14.7	0	0.045	0.36	0.21 ± 0.15
	51	15.4	35.57	0.75	262.0	-10.7	1.53	0.136	0.74	0.37 ± 0.07
	80	12.2	35.58	0.12	240.9	27.3	8.88	0.542	3.36	0.52 ± 0.13
	111	12.0	35.58	0.05	239.6	30.1	9.36	0.576	3.65	0.68 ± 0.01
	141	12.0	35.58	0.05	239.9	29.9	9.34	0.570	3.67	0.68 ± 0.03
	154	12.0	35.58	0.05	239.7	30.0	9.30	0.581	3.65	0.35 ± 0.02
N3 (250 m)	3	17.4	35.56	0.29	258.5	-16.9	0	0.046	0.28	< LoD
	16	17.9	35.56	0.50	262.6	-18.6	0.01	0.081	0.33	< LoD
	36	15.7	35.56	0.58	263.2	-13.7	2.53	0.200	1.11	0.21 ± 0.08
	51	13.7	35.58	0.23	250.1	10.0	5.71	0.365	2.15	0.29 ± 0.02
	81	12.9	35.59	0.09	248.2	16.1	7.40	0.458	2.69	0.39 ± 0.03
	151	11.9	35.59	0.03	242.8	26.9	9.34	0.567	3.52	0.64 ± 0.05
	202	11.8	35.59	0.02	244.2	26.4	9.82	0.592	3.69	0.68 ± 0.03
	238	11.8	35.59	0.02	242.9	28.0	9.94	0.598	3.87	0.35 ± 0.02
N4 (365 m)	3	17.4	35.56	0.42	258.1	-16.8	0.14	0.064	0.33	0.81 ± 0.09
	16	16.3	35.56	0.71	265.3	-18.5	0.97	0.110	0.65	0.61 ± 0.07
	39	14.5	35.57	0.54	254.3	1.4	3.63	0.262	1.44	0.81 ± 0.03
	81	13.3	35.58	0.14	248.8	13.5	6.57	0.416	2.41	0.91 ± 0.04
	151	12.5	35.59	0.07	246.2	20.5	8.23	0.515	3.08	1.72 ± 0.10
	202	11.8	35.59		246.9	23.9	10.06	0.601	3.70	0.90 ± 0.08
	241	11.6	35.59		245.4	26.5	10.58	0.626	3.97	0.91 ± 0.06
	302	11.6	35.59		245.3	26.8	10.90	0.648	4.14	0.87 ± 0.05

	347	11.3	35.58		239.8	34.1	11.78	0.738	4.76	1.50 ± 0.04
N5 (542 m)	3	17.2	35.56	0.40	260.4	-18.0	0.06	0.054	0.28	0.74 ± 0.14
	22	15.2	35.57	0.48	258.8	-6.7	3.78	0.318	1.56	< LoD
	81	12.9	35.59	0.14	248.2	15.8	6.94	0.448	2.62	0.33 ± 0.03
	202	11.9	35.59		246.2	23.5	9.14	0.563	3.45	2.53 ± 0.01
	251	11.8	35.59		244.4	26.4	9.74	0.601	3.77	~ LoD
	302	11.7	35.59		244.5	26.8	10.78	0.675	4.37	0.38 ± 0.02
	352	11.6	35.59		243.3	28.9	10.70	0.662	4.32	0.46 ± 0.08
	402	11.3	35.58		240.4	33.5	11.89	0.723	5.02	1.77 ± 0.05
	452	11.0	35.58		234.8	40.7	11.25	0.688	4.83	0.54 ± 0.07
	523	10.9	35.58		232.4	43.8	13.08	0.800	6.12	0.73 ± 0.06
N6 (1238 m)	4	17.2	35.57	0.33	261.5	-19.2	0	0.053	0.33	0.91 ± 0.15
	32	14.4	35.57	0.50	256.0	0.5	4.01	0.295	1.63	0.86 ± 0.12
	152	11.9	35.62	0.03	252.8	16.9	9.35	0.600	3.28	1.22 ± 0.06
	403	11.0	35.58		236.1	39.3	12.87	0.804	5.73	1.38 ± 0.03
	704	9.9	35.62		216.0	66.6	16.88	1.052	10.01	2.69 ± 0.14
	804	9.6	35.64		213.9	70.6	17.13	1.073	10.13	3.23 ± 0.17
	905	9.3	35.63		215.9	70.6	17.44	1.085	10.74	1.55 ± 0.14
	1005	8.9	35.62		215.0	73.9	17.99	1.122	11.57	1.45 ± 0.11
	1105	8.8	35.61		216.6	73.4	18.20	1.135	12.00	4.36 ± 0.19
	1206	8.5	35.58		219.3	72.7	18.40	1.153	12.63	1.59 ± 0.30
	1221	8.4	35.58		219.6	72.8	18.30	1.149	12.75	1.81 ± 0.16
	1233	8.4	35.57		220.3	72.6	18.32	1.149	12.80	1.36 ± 0.00
N7 (1893 m)	4	17.8	35.59	0.23	259.0	-19.3	0.01	0.066	0.42	---
	53	14.6	35.60	0.50	265.7	-10.2	2.53	0.196	0.90	---
	153	11.8	35.61	0.01	259.1	11.8	9.79	0.589	3.35	1.29 ± 0.06
	404	11.1	35.52		255.1	20.0	11.92	0.738	4.67	2.02 ± 0.08
	605	10.6	35.59		227.8	50.3	16.23	1.006	8.57	3.03 ± 0.15
	900	9.7	35.70		211.1	72.9	18.12	1.127	11.41	1.44 ± 0.04
	1206	7.9	35.53		227.0	68.9	18.67	1.176	13.11	1.51 ± 0.07
	1407	6.8	35.38		239.7	64.6	19.30	1.241	16.73	1.33 ± 0.04

	1607	5.3	35.20		254.6	60.9	19.65	1.274	19.04	1.31 ± 0.06
	1809	4.5	35.10		263.3	58.8	20.00	1.284	21.93	1.21 ± 0.02
	1859	4.3	35.08		265.1	58.7	19.86	1.295	21.00	1.53 ± 0.14
	1896	4.3	35.08		265.8	58.1	20.10	1.318	23.00	1.32 ± 0.10
	5	17.5	35.56	0.25	261.4	-20.5	0	0.033	0.18	0.75 ± 0.09
	24	16.1	35.56	0.60	270.4	-22.6	0.70	0.096	0.41	0.92 ± 0.04
	43	13.7	35.61	0.37	260.2	-0.3	4.56	0.302	1.43	1.58 ± 0.08
	154	11.7	35.61	0.02	259.9	11.2	9.92	0.598	3.43	1.60 ± 0.07
	506	10.8	35.53		237.5	39.7	13.85	0.840	6.14	3.21 ± 0.12
N8	807	9.9	35.63		211.6	71.2	17.60	1.067	9.80	---
(2411 m)	1007	9.2	35.69		212.1	75.0	18.29	1.106	11.25	1.63 ± 0.05
	1409	6.6	35.46		240.2	65.3	19.38	1.201	14.91	1.61 ± 0.04
	1810	4.5	35.09		263.5	58.8	20.09	1.264	20.38	2.05 ± 0.03
	2011	4.2	35.05		267.3	57.5	20.21	1.284	21.99	1.60 ± 0.09
	2211	4.8	35.02		268.7	59.7	20.70	1.306	26.25	1.83 ± 0.07
	2402	3.2	34.97		269.2	64.1	21.38	1.412	32.14	1.80 ± 0.06
	4	17.4	35.56	0.36	262.6	-21.3	0.01	0.034	0.12	0.46 ± 0.03
N9	29	15.1	35.59	0.67	266.7	-13.9	1.86	0.157	0.71	0.48 ± 0.04
(2953 m)	102	12.2	35.61		256.4	12.0	8.70	0.519	2.25	0.74 ± 0.05
	202	11.5	35.58		259.2	13.5	10.49	0.639	3.74	0.63 ± 0.01

APPENDIX 10.

COPY OF THE FIRST DRAFT OF THE SUBMITTED ARTICLE

"Processes influencing dissolved iron distributions below the surface at the Atlantic Ocean – Celtic Sea shelf edge"

Florence Nédélec, Peter J. Statham, and Matt Mowlem

Submitted to Marine Chemistry on the 30th October 2005

This copy will be revised considering the comments of the examiners of the thesis and of the reviewers.

Elsevier Editorial System(tm) for Marine Chemistry

Manuscript Draft

Manuscript Number:

Title: Processes influencing dissolved iron distributions below the surface at the Atlantic Ocean - Celtic Sea shelf edge

Article Type: Wollast Memorial Special Issue

Keywords: Particulate organic matter oxidation; Transport processes; Intermediate nepheloid layers; Vertical mixing; Northeast Atlantic; Celtic Sea shelf edge

Corresponding Author: Miss Florence Nédélec,

Corresponding Author's Institution: National Oceanography Centre, Southampton

First Author: Florence Nédélec

Order of Authors: Florence Nédélec; Peter J. Statham; Matt Mowlem

Abstract: ABSTRACT

Shelf break systems are highly dynamic environments. However little is known about the influence that benthic interactions and water mass mixing may have on vertical distributions of iron in these systems. Dissolved Fe (< 0.4 µm) concentrations were measured in samples from nine vertical profiles across the upper slope (150 - 2400 m water depth) at the Atlantic Ocean - Celtic Sea shelf break. Dissolved iron concentrations varied between 0.2 and 5.4 nM, and the resulting detailed section showed evidence of a range of processes influencing the Fe distributions. The near sea floor data was interpreted in terms of release and removal processes. The concentrations of dissolved Fe present in near seabed waters were consistent with release of Fe from in situ particulate organic matter remineralisation at two upper slope stations, and possibly of pore water release upon resuspension on shelf. Lateral transport of dissolved iron was evident from elevated Fe concentrations in an intermediate nepheloid layer and its advection along isopycnals. Surface waters at the shelf break also showed evidence of vertical mixing of deeper iron-rich

waters. These waters contained macronutrients that sustained primary productivity in these otherwise nutrient-depleted surface waters. The data also suggest some degree of stabilisation of relatively high concentrations of iron, presumably through ligand association or as colloids. This study supports the view that export of dissolved iron laterally to the ocean's interior from shelf and coastal zones and may have important implications for the global budget of oceanic iron.

George Deacon Division
National Oceanography Centre, Southampton
European Way
Southampton
SO14 3ZH
United Kingdom

30th September, 2005

Professor Millero,

Please find attached a copy of the manuscript entitled :

"Processes influencing dissolved iron distributions below the surface at the Atlantic Ocean – Celtic Sea shelf edge" (authors: F. Nédélec, P.J. Statham, and M. Mowlem)

that I submit for publication in the Wollast Memorial Special Issue.

We feel that this iron data from a detailed section of stations across the shelf break provides new information on this element's distribution in these systems, and begins to unravel the range of processes that influence iron in these environments. The paper therefore additionally helps to provide a conceptual framework for discussing these processes and other iron data for such systems. The work is therefore topical, and timely given the recent interest in understanding shelf break systems as a source of iron to the ocean interior.

We shall look forward to hearing from the journal about our paper,

Yours Sincerely,

Florence Nédélec

Processes influencing dissolved iron distributions below the surface at the Atlantic Ocean Celtic Sea shelf edge

Florence Nédélec[1*], Peter J. Statham[2], Matt Mowlem[3]

[1] George Deacon Division, National Oceanography Centre, Southampton, European Way, Southampton, Hampshire, SO14 3ZH, United Kingdom.
f.nedelec@noc.soton.ac.uk

[2] School of Ocean and Earth Sciences, National Oceanography Centre, Southampton, European Way, Southampton, Hampshire, SO14 3ZH, United Kingdom.
peter.j.statham@noc.soton.ac.uk

[3] Ocean Engineering Division, National Oceanography Centre, Southampton, European Way, Southampton, Hampshire, SO14 3ZH, United Kingdom.
matm@noc.soton.ac.uk

[*]Corresponding author : Florence Nédélec

George Deacon Division

National Oceanography Centre, Southampton

European Way

Southampton

Hampshire

SO14 3ZH

United Kingdom

f.nedelec@noc.soton.ac.uk

Phone number : 00 44 (0)23 8059 6016

Fax number : 00 44 (0)23 8059 6247

Running head : Dissolved iron at the Celtic Sea shelf break

Submitted to Marine Chemistry for Wollast Memorial Special Issue

ABSTRACT

Shelf break systems are highly dynamic environments. However little is known about the influence that benthic interactions and water mass mixing may have on vertical distributions of iron in these systems. Dissolved Fe (< 0.4 μm) concentrations were measured in samples from nine vertical profiles across the upper slope (150 – 2950 m water depth) at the Atlantic Ocean – Celtic Sea shelf break. Dissolved iron concentrations varied between 0.2 and 5.4 nM, and the resulting detailed section showed evidence of a range of processes influencing the Fe distributions. The near sea floor data was interpreted in terms of release and removal processes. The concentrations of dissolved Fe present in near seabed waters were consistent with release of Fe from *in situ* particulate organic matter remineralisation at two upper slope stations, and possibly of pore water release upon resuspension on shelf. Lateral transport of dissolved iron was evident from elevated Fe concentrations in an intermediate nepheloid layer and its advection along isopycnals. Surface waters at the shelf break also showed evidence of vertical mixing of deeper iron-rich waters. These waters contained macronutrients that sustained primary productivity in these otherwise nutrient-depleted surface waters. The data also suggest some degree of stabilisation of relatively high concentrations of iron, presumably through ligand association or as colloids. This study supports the view that export of dissolved iron laterally to the ocean's interior from shelf and coastal zones and may have important implications for the global budget of oceanic iron.

KEYWORDS

Dissolved iron; Particulate organic matter oxidation; Transport processes; Intermediate nepheloid layers; Vertical mixing; Northeast Atlantic; Celtic Sea shelf edge

1. Introduction

Shelf waters are generally rich in iron thanks to the proximity of many terrigenous sources including rivers, sediments, and transport *via* the atmosphere. The emphasis in most previous studies has been mainly on the behaviour of iron in coastal and shelf waters (*e.g.* Dehairs *et al.*, 1989; Tappin *et al.*, 1995; Millward *et al.*, 1998; Chase *et al.*, 2002; Berelson *et al.*, 2003; Weinstein *et al.*, 2004), and in the open ocean (*e.g.* Johnson *et al.*, 1997; Wu *et al.*, 2001). However, very few studies have examined the distribution of iron across the shelf break (Hong *et al.*, 1986; Muller *et al.*, 1994; Wu *et al.*, 1996; Boye *et al.*, 2003), or mechanisms of iron cycling and release in this zone (Elrod *et al.*, 2004). It is generally believed that dissolved iron is trapped on shelf by intense removal due to high concentrations of particles in the water column (Hong *et al.*, 1986), making shelf breaks sinks for dissolved iron. Transport mechanisms of dissolved iron from the shelf to the ocean were recently described (*e.g.* wind-driven upwelling (Johnson *et al.*, 1999), eddy formation and transport (Johnson *et al.*, 2005), and horizontal advection (Wu *et al.*, 1996; Gordon *et al.*, 1997; Laes *et al.*, 2003; Croot *et al.*, 2004)), suggesting that shelves may potentially act as sources of dissolved iron to the ocean (Elrod *et al.*, 2004). A consequence of export of dissolved iron from coastal to surrounding waters is the alleviation of iron-stress in phytoplankton in high-nutrient low-chlorophyll waters such as around Antarctic islands (*e.g.* Crozet (Pollard, 2004), Kerguelen (Blain *et al.*, 2001), and South Georgia (Holeton *et al.*, 2005)). In order to explain features such as blooms developing downstream of island systems, we clearly need a better understanding of processes governing dissolved iron distribution in shelf waters and potential mechanisms for its export into oceanic waters.

The nutrient-like distribution of dissolved iron in the oceanic water column can be strongly modified by inputs, removal, and transport processes. A multitude of these processes have been identified for dissolved iron in shelf environments (Santschi *et al.*, 1990). When far from any estuaries, particulate organic matter remineralisation and pore water diffusion / advection / resuspension are likely to be the main benthic sources (Santschi *et al.*, 1990; Berelson *et al.*, 2003; Elrod *et al.*, 2004), and main removal processes include adsorption onto particles (Wells *et al.*, 1993), precipitation (Rose *et al.*, 2003a), and biological uptake (Geider, 1999). Sustained high dissolved iron concentrations in shelf waters infer that a stabilisation mechanism (*e.g.* inorganic colloids or organic complexation) must maintain iron above its solubility limit. However little is known about the detail of these mechanisms, and their relative contribution to iron biogeochemistry (de Baar *et al.*, 2001).

The present study was carried out at the Northwest European continental margin, which is characterised by a broad continental shelf (the Celtic Sea), and is limited westward by a steep slope down to 4000m. European shelf waters are highly dynamic environments where wind-, tide- and wave-forced currents, and topography at the shelf edge promote diapycnal mixing between water masses (van Aken, 2000), and potentially vertical transport of nutrients (Pingree *et al.*, 1986). Sampling was carried out in proximity to Goban Spur where the *OMEX* (Ocean Margin EXchange) programme took place (Wollast *et al.*, 2001). Some water sampling transects have been carried out across the Celtic Sea shelf edge (Kremling, 1983; Muller *et al.*, 1994; Boye *et al.*, 2003), including work in the *OMEX* programme (Le Gall *et al.*, 1999; Cotté-Krief *et al.*, 2002). These studies reported trace metal distributions across the shelf, but

dissolved iron distributions were restricted to surface waters or upper slope (< 800 m water depth) only in two of these transects.

The work presented here describes dissolved iron concentrations in the most detailed two-dimensional transect down to the deep seafloor across shelf break that is presently available, and the data are used to investigate processes affecting dissolved iron distributions in the water column below the euphotic zone. Several aspects of the iron cycle are explored here including processes occurring in bottom waters (*i.e.* sources, removal, and stabilisation), and the lateral transport of dissolved iron, and the study also provides a conceptual framework for discussing processes and other iron data reported for such systems.

2. Sampling and analysis

2.1. Sampling

Samples were collected during the *R.R.S. James Clark Ross* cruise *JR98*, July-August 2003, during an offshore transect across the Celtic Sea shelf break (Figure 1). Nine stations (N1 – N9) were occupied across the continental slope and samples collected for iron determination. Profiles extended from a few metres above the seafloor up to the surface except at Station N9, which extended down to only 200 m (Table 1).

Figure 1

Table 1

Sampling was carried out using a CTD rosette built to minimise trace-metal contamination, and made from titanium and plastic, with the sensors all being housed in titanium cases without any zinc sacrificial electrodes. The rosette was fitted with trace

metal clean 10 L OTE (Ocean Technology Equipment) sampling bottles with external springs, and modified for trace metal work.

Filtration was performed in a trace-metal clean container laboratory. Storage bottle were acid cleaned following the standard procedures for trace metal work (Achterberg *et al.*, 2001). The OTE bottles were held on a rack, a Teflon external frame was used to clamp top and bottom valves shut, and the bottles were pressurised using filtered compressed nitrogen at about 0.8 atmospheres. Samples were filtered in-line through acid-washed all-Teflon filter holders (Morley *et al.*, 1993), fitted with acid-washed 0.4 µm Cyclopore® polycarbonate filters directly into the sample rinsed storage bottle. Samples were acidified with 1 µL of quartz distilled hydrochloric acid per mL of sample in a laminar flow hood, and double zip-bagged (polythene) for storage.

Temperature, salinity, and dissolved oxygen data were logged from the Seabird 911 CTD sensors. The beam attenuation signal derived from transmission obtained with the CTD ALPHA^{tracka} transmissometer was used as an indicator of SPM concentrations since they are linearly correlated, and as a calibration was not available (Chelsea Technologies Group) (McCave *et al.*, 2001). Samples for nutrients and chlorophyll *a* measurements were collected from duplicate sampling bottles closed at each Fe bottle sampling depth.

2.2. Analysis

Analyses were performed in a class-100 clean room in the Southampton laboratory, and critical steps were performed in a laminar flow hood. Samples were stored acidified for more than one year after collection, an approach that is reported to

lead to measurement of all dissolved (< 0.4 µm) forms of iron (*i.e.* dissolved iron (DFe)) (Bowie *et al.*, 2004).

Dissolved iron was determined using a flow-injection analyser with chemiluminescence detection using luminol to detect Fe(II) and Fe(III) in seawater, after preconcentration (Obata *et al.*, 1997; Johnson *et al.*, 2003). An analytical cycle consisted of preconcentration of iron onto 8-hydroxyquinoline immobilised on a Fractogel resin (Landing *et al.*, 1986), rinsing with Milli-Q water, elution and chemiluminescent detection. Calibrations by standard additions of iron to acidified seawater were linear, and precision on all measurements averaged approximately 5% *rsd*. Limit of detection (3*sd* of the blank) values reached 32pM thus allowing determination of iron in most oceanic environments. Accuracy of this analysis was routinely checked using a low-iron seawater internal standard with a concentration determined at 0.99 ± 0.17 nM (*i.e.* inter-batch precision of 17% *rsd*), and with a NASS-5 certified reference material (from the National Research Council of Canada) on several occasions. The NASS-5 value was found to be within the range of the certified value of 3.71 ± 0.63 nM. Data presented here has gone through a rigorous data quality check (Nédélec, *submitted*). Four outlier data points, one collected at the surface (8.01 ± 0.31 nM DFe), one in the chlorophyll *a* maximum (54 m depth, 3.31 ± 0.12 nM DFe) at Station N7, one at Station N1 (80 m, 4.56 ± 0.19 nM), and one at Station N8 (800 m, 4.90 ± 0.10 nM DFe), were excluded from the data set as they were strongly suspected of contamination (Nédélec, *submitted*). These were the only data excluded out of a total of 80 values.

Nutrients were measured using a Skalar autoanalyser for nitrate *plus* nitrite (N), phosphate (P) and dissolved silicon (DSi). Total chlorophyll *a* measurements in acetone

extractions were made using the fluorometric method of Welschmeyer (1994) after filtration onto Whatman GF/F (pore-size 0.7 μm) filters.

3. Results and discussion

3.1. Distribution of dissolved iron across the shelf edge

The distribution of dissolved iron across the Celtic Sea shelf edge did not present a clear trend of uniform increasing concentrations from oceanic to coastal waters, but had distinct spikes of high DFe at specific depths (Figure 2). The presence of sub-nanomolar DFe at the shelf break (Stations N2, N3, N4 and N5) were surprising in that DFe concentrations have been reported to increase to up to several tens of nanomolar in shelf systems (Muller *et al.*, 1994; Wu *et al.*, 1996; Table 2). High DFe concentrations (5.37 ± 0.49 nM ($n = 3$)) were measured near the seafloor at the most on-shelf Station N1 (Figure 2). At the other stations, dissolved iron concentrations slowly increased with depth below 50 m, and were relatively homogeneous down to the seabed at Stations N2 and N3. This distribution is consistent with the relatively weak water column stratification at these stations relative to Station N1. From Stations N4 to N8, DFe distributions in the water column were significantly perturbed by layers of high-DFe water at specific depths (Figure 2). These spikes were not thought to be due to sample contamination as they corresponded to features in the water column. No general increase in DFe concentration with proximity to the seafloor water was observed, and this feature was only found at Stations N1, N4 to N7 (Figure 2).

Figure 2

Table 2

The range of surface (~ 3 m depth) dissolved iron concentrations varied from 0.19 ± 0.06 nM to 0.91 ± 0.15 nM at Stations N3 and N6 respectively, and did not show any clear trend of increasing concentrations from oceanic waters (Station N9) to shelf waters (Station N1) (Figure 2). Highest DFe concentrations were found at Stations N4, N5 and N6 on the upper slope (500 – 1235 m water depth), and lowest DFe levels were measured at the shelf break (Stations N2 and N3). DFe concentrations along this transect were comparable to published surface data from near the Porcupine Seabight (~ 51°N), and at about 48°N at the Celtic Sea shelf edge (Muller *et al.*, 1994; Boye *et al.*, 2003). Reported dissolved iron (< 0.4 μm) concentrations measured at 51°N increased from < 1 nM to > 3 nM in August 1984 (Muller *et al.*, 1994). In March 1998 at 48°N, DFe (< 0.2 μm) increased from about 0.7 nM in open ocean waters to about 1.1 nM at the shelf break (Boye *et al.*, 2003). Dissolved iron concentrations measured in the present study thus were slightly lower than those reported at 51°N and were in the range found at 48°N even though the size fraction measured here was larger, and sampling was done in a different season, which can have a significant impact on DFe levels.

3.2. Sources of dissolved iron near the seafloor

Elrod *et al.* (2004) suggested that particulate organic matter (POM) oxidation from sediments is likely to be the major benthic source of dissolved iron on shelves. During the *OMEX* programme, fluxes of POM at the Goban Spur were of similar magnitude during Spring and Summer, with a difference in composition as fluxes were dominated by opal containing material in Spring relative to Summer (Antia *et al.*, 2001). Additionally it was estimated that 37 to 60% of carbon fixed by photosynthesis in the euphotic zone was not remineralised in the surface mixed layer (Joint *et al.*, 2001), and

that more than 90% of organic carbon mineralisation at the sediment-water interface is driven by oxygen (van Weering *et al.*, 1998). Finally, it was demonstrated that, at present, the North West European continental margin is not a carbon depocenter with a carbon burial efficiency of only 0.8 to 2.3% suggesting that most POM that was deposited yearly was remineralised (Lohse *et al.*, 1998). These earlier studies therefore suggest that highly degradable POM is expected at the seafloor at the time of the cruise, and thus will provide a reservoir of biogenic iron that can be remineralised.

Waters below the euphotic zone in the ocean are generally under-saturated with dissolved oxygen as it is consumed by mid-water column POM oxidation by heterotrophic bacteria. The observed apparent oxygen utilisation (AOU) concentration along a shelf/slope system will therefore be the result of mixing of waters with preformed AOU, and *in situ* oxygen consumption. Additionally, major resuspension events of any anoxic/suboxic sediments may slightly decrease dissolved oxygen concentrations in near-bottom waters. The relationship between the AOU and the beam attenuation signal in the benthic nepheloid layer (BNL; waters of high suspended particulate matter (SPM) near the seafloor) at each station was thus examined in order to investigate the presence of oxygen consuming processes associated with resuspended particulate matter near the seafloor.

The data show three types of behaviour (Figure 3): i) shallow stations influenced by water column mixing (N1, N2, and N3), showing low to moderately high AOU with increasing SPM towards the seafloor; ii) stations showing possible *in situ* remineralisation of POM (N4 and N5) with a linear (R^2 = 0.95) relationship between beam attenuation and AOU; and iii) stations where any *in situ* AOU signal was diluted

by the strong preformed AOU in adjacent water masses (N6, N7, and N8), and there was high AOU with increasing SPM towards the seafloor.

Figure 3

The most on-shelf station (N1) had a higher AOU than Stations N2 and N3 (Figure 3), suggesting that at N1, there had been more POM remineralisation. The observed AOU signals in deeper waters at these stations therefore presumably reflect remineralisation of POM during the early part of the year.

The relationship of increasing AOU with increasing SPM near bottom at Stations N4 and N5 (Figure 3), suggests that the high SPM was influencing AOU and was probably a recent feature. Sediments were found to be slightly sub-oxic, but not anoxic, until the iron redox boundary was reached, which deepened from 1 cm at 210 m water column depth, to 2.5 cm at 1000 m, down to 5 cm at 2200 m across the shelf at Goban Spur during the *OMEX* programme (Lohse *et al.*, 1998). A resuspension event would thus have to be very important to induce such an increase in AOU (+ 7.3 µM at N4 and + 10.4 µM at N5 between the top and bottom of the BNL; Table 2), which is not obvious from the beam attenuation profiles (Section 3.3.1). It was therefore most likely that the AOU reflected *in situ* remineralisation of the POM fraction within the resuspended material.

Despite high particle concentrations at Station N6 (Section 3.3.1), the AOU did not increase with increasing SPM in the BNL (~ 1200 m depth; Figure 3). Detecting a small AOU signal here is difficult because any *in situ* AOU signal would be diluted by the strong influence of low-oxygen waters at about 1000 m depth. The deep Stations N7 and N8 were also influenced by oceanic water masses (Section 3.3.1) with their own significant AOU signatures.

The amount of dissolved iron released from POM oxidation in the BNL at each station can be estimated based on AOU values, and assuming that the Redfield-Richards ratio can be applied in these waters, and values for algal Fe:C ratio are known (Sunda *et al.*, 1995).

The consumption of carbon was estimated from the difference in AOU between the top and bottom of the BNL, and using the Redfield-Richards ratio (C:AOU = 106:138). The estimated amount of carbon consumed was small (2.8 μM) and would only result in a release of 0.14 nM DFe (Table 3), using the maximum Fe:C ratio of 50 μmol/mol suggested in the literature (Sunda *et al.*, 1995). The increase in DFe near the seafloor (Figure 2) therefore cannot be explained by POM oxidation only, implying a contribution from an additional source (*e.g.* pore water diffusion or mixing through bio-turbation or resuspension).

Table 3

At Stations N4 and N5, the release of dissolved iron was estimated from carbon consumption as for Station N1. Much carbon was estimated to be remineralised at Stations N4 and N5 than at N1 (5.6 μM and 8.0 μM, respectively), and these values corresponded to a maximum release of 0.28 and 0.40 nM DFe, respectively (Table 3). These estimates were not significantly different from the DFe present in excess of background values at these stations (0.63 and 0.19 nM, respectively). Whilst these calculations are based on assumptions of the carbon consumed and DFe released using the Redfield-Richard ratios, and some removal may have been occurring simultaneously, these results are nonetheless consistent with DFe being released from POM oxidation at Stations N4 and N5.

In contrast to Stations N1, N4, and N5, concentrations of dissolved iron were low at Stations N2 and N3, varying from 0.78 ± 0.03 nM at the top of the BNL and decreasing to 0.45 ± 0.02 nM in the bottom sample (Figure 2). These generally low DFe, AOU, and SPM concentrations in the water column relative to N1 suggest that inputs of POM and iron to bottom waters at these stations were less than at the other stations sampled. Decreasing DFe concentrations near the seafloor suggest that removal processes were more important than inputs at these stations, resulting in a significant loss (~ 40%) in DFe relative to background values, presumably as a result of adsorption onto particles.

The form of DFe present in these shelf waters will have a major impact on the ultimate fate of iron in solution. Dissolved iron is limited by its solubility to about 0.1-0.2 nM in seawater at pH 8.1 (Wu *et al.*, 2001). Release processes of excess free iron (Fe(II) or Fe(III)) in oxic seawater should thus be quickly balanced by removal through precipitation (Rose *et al.*, 2003a), or adsorption onto particles (Johnson *et al.*, 1997). However a significant fraction of DFe remains in solution despite thermodynamics constraints, and this may be due to organic complexation, formation of colloidal species conventionally included in the measured "dissolved" (< 0.4 μm) fraction, or possibly kinetic constraints. Dissolved (< 0.2 μm) iron, Fe(II) and iron-binding organic ligands in excess of Fe were found to linearly increase in surface waters across the Celtic Sea shelf edge, indicating a common source of these ligands (Boye *et al.*, 2003). Experiments performed with terrestrial natural organic matter (NOM) showed that iron formed Fe^{III}-NOM complexes as strong as the iron binding ligands produced by the biota in the open ocean (Rose *et al.*, 2003b). Sediments are potentially an important

source of Fe(II) to bottom waters depending on their redox conditions ((Hong *et al.*, 1986), and S. Ussher, 2005, personal communication), and are also a source of dissolved organic carbon to bottom waters at Goban Spur (Otto *et al.*, 1998), and soluble species of Fe^{3+} complexed by natural organic ligands have recently been detected in coastal marine sediments (Carey *et al.*, 2005). Dissolved iron may thus already be organically complexed when supplied to bottom waters, providing a mechanism for its stabilisation in seawater, although the particle adsorption behaviour of these complexes is unknown. Additionally, sources of colloidal matter are numerous, and include sediment resuspension (Wells *et al.*, 1994). These processes clearly need further investigation given their importance to explaining how DFe may be maintained in solution and exported from shelf environments. Measured DFe concentrations therefore reflect the balance of input / removal / stabilisation processes at each station, and are dependent on the time since any DFe release.

3.3. Advection of dissolved iron

3.3.1. Horizontal advection

The distribution of SPM across the shelf edge showed that all types of nepheloid layers (*i.e.* surface nepheloid layer (SNL), benthic nepheloid layer (BNL), and intermediate nepheloid layer (INL; McCave *et al.*, 2001) were present at the time of the cruise (Figure 4). An intense BNL developed between Stations N5 and N7, and was most intense at Stations N5 and N6 (Figure 4), which also corresponded well to the zone of influence of the pole-ward flowing current in this area (Pingree *et al.*, 1999). The likely sources of this major resuspension event on the upper slope were either the internal tide generating strong near-bed currents (Heathershaw *et al.*, 1987), or the

friction due to the down-slope component of the pole-ward current (Souza *et al.*, 2001; Huthnance *et al.*, 2002).

Figure 4

The lowest beam attenuation values (lowest SPM) were found within the Eastern North Atlantic Central Water (ENACW) and Mediterranean Outflow Water (MOW) (Figure 4) indicating that these water masses did not transport significant SPM in their core. Higher SPM concentrations were present below 1500 m depth (Figure 4).

Two distinct INLs were detected at Stations N6 and N7 between 400 and 700 m depth (INL1, core at 600 m), and between 1000 and 1500 m (INL2, core at *ca.* 1300 m), and the beam attenuation signal was stronger in the well-defined INL1 than in the broad INL2 at Station N7 (Figure 4 and 5). These INLs could be formed from accumulation on density surfaces of biogenic particles settling from surface waters, or by detachment of an intense BNL (Dickson *et al.*, 1986). Given the strong SPM concentration in the BNL at Station N6, and that this feature followed the same isopycnals, BNL detachment was the most likely source.

The INLs closely corresponded to the main water mass boundaries (Figure 4), and their core propagated along isopycnals at 27.30 kg/m^3 and 27.70 kg/m^3 for INL1 and INL2 respectively (Figure 5), indicating the SPM advected along density surfaces between water masses. The beam attenuation signal of these INLs was relatively low at Station N8 (Figure 4), suggesting that they may not propagate much further than Station N8, 22 km from Station N6, although along slope transport is also possible (Thorpe *et al.*, 1988).

Figure 5

A plume of iron-rich waters was observed even at the most off-shelf stations below the euphotic zone ($\sigma_t > 27.0$ kg/m^3) (Figure 5). These DFe levels (~ 3.2 nM) were lower than those (5 – 9 nmol/kg) measured in association with turbidity plumes, and enhanced Al, Mn and Co levels within the Monterey Canyon (Martin *et al.*, 1988). High DFe levels coincided relatively well with INL1, and with a plume of relatively high beam attenuation deeper at Station N6, despite the relatively poor sampling resolution, which did not properly constrain the SPM plumes (Figure 5). By contrast, no DFe increase was found in association with INL2 at Stations N7 and N8 (further off-shelf) except in the BNL at Station N6 (Figure 5).

High dissolved iron within INLs may originate from enhanced *in situ* remineralisation or from transport of DFe released from benthic processes within the BNL. If DFe were to be remineralised *in situ* from POM by bacterial communities, elevated DFe concentrations would be associated with increased nitrate and phosphate and lower dissolved oxygen concentrations. However, N, P, and AOU were similar between stations, suggesting that enhanced *in situ* remineralisation was unlikely within INLs, and therefore that DFe was transported from its source near the seafloor.

Assuming that the INL was created from a single resuspension event, and DFe was transported from the BNL, DFe concentrations would be expected to be higher within INL1 at the most inshore station (N6), before significant reduction in concentrations through mixing and removal processes occur. However no clear DFe gradient in concentration was observed along the transect (Figure 5), and the data may reflect the three-dimensional nature of the system, with INL1 and associated elevated dissolved iron concentrations formed to the south of this transect.

A further factor complicating interpretation is that intermediate nepheloid layers are common but intermittent events, which occur at specific depths at the Celtic Sea shelf edge as defined by the slope, and the amplitude of internal waves, as shown during the *OMEX* programme and in earlier studies (Dickson *et al.*, 1986; Thorpe *et al.*, 1988; McCave *et al.*, 2001). High DFe (~ 3 nM) was observed at the most offshore Station N8 at the same depth as INL1 (Figure 5), however it was associated with only a weak increase in beam attenuation relative to surrounding waters. This high DFe signal implies decoupling of dissolved iron from particles so that most particles are lost but high DFe remains, and thus some form of DFe can survive particle scavenging.

No elevated DFe levels were observed within INL2 compared to within INL1 (Figure 4 and Figure 5), presumably reflecting the balance between inputs (depending on their source and intensity), and removal processes, which depend on particle characteristics (*e.g.* size, type) and concentration in these systems. Smaller particles will have a longer residence time due to their low settling velocity, and thus have more time to scavenge DFe.

3.3.2. Vertical advection

Macro-nutrient concentrations were generally very low in surface waters. However, increased chlorophyll *a*, dissolved iron, nitrate, and phosphate were observed at the shelf break front (N3, N4, N5 and N6), and were strongest at Station N4 (Figure 6). Low nutrient concentrations are common during Summer at the Celtic Sea shelf break as winter stocks are consumed during the Spring bloom (Hydes *et al.*, 2001). Surface dissolved silicon was not completely depleted across the shelf edge (Figure 6) and was probably residual rather than regenerated (Hydes *et al.*, 2001).

Figure 6

The increase in dissolved iron across the shelf edge corresponded well with the trace metal fronts at the Celtic Sea shelf edge previously reported in the literature (Kremling, 1983; Muller *et al.*, 1994; Le Gall *et al.*, 1999; Cotté-Krief *et al.*, 2002; Boye *et al.*, 2003). The Northeast Atlantic Ocean is also under the influence of episodic Saharan dust plume events (Blain *et al.*, 2004), and may contribute to the surface DFe measured. However such a localised increase in all parameters is more likely due to vertical mixing of waters underlying the thermocline, and nitrate and phosphate were likely to be taken up by the biota as they were supplied to surface waters.

Evidence for vertical mixing at the Celtic Sea shelf break was given by the presence of a cool thermal front during summer months (~ 1^{o}C cooler than surrounding waters) (Dickson *et al.*, 1980; Pingree *et al.*, 1986). Decreasing surface water temperatures (17.9^{o}C to 16.9^{o}C) showed that the front was located between Stations N3 and N6, and corresponded well to the area of increased dissolved iron in surface waters (Figure 6). This thermal front is due to the combination of sudden shallowing of waters across the continental shelf, and by the change in current speed across the shelf, which is likely induced by tidal exchange (Pingree *et al.*, 1986).

Surface waters thus appear to be supplied in nutrients from waters underlying the thermocline mixed up by propagation of the internal tide. Dissolved iron concentrations below the thermocline were similar to or higher than those in surface waters (Figure 2), and thus vertical mixing of these waters could be sufficient to support measured DFe in surface waters.

4. Conclusions

The shelf break is a highly dynamic environment where oceanic and coastal waters meet; therefore the dissolved iron distributions were expected to be influenced by a series of processes induced by these two different environments.

Results are consistent with the main source of dissolved iron near seafloor for at least two stations being POM remineralisation, but other processes including mixing and removal complicated the interpretation. Dissolved iron concentrations were highest (5.4 nM DFe) on shelf, and pore water resuspension was likely an additional source of iron to these bottom waters. Transport of dissolved iron was evident. Horizontal advection of dissolved iron (~ 3.2 nM DFe) associated with an intermediate nepheloid layer propagating along an isopycnal was identified and dissolved iron was possibly also transported within the along-slope pole-ward flowing current. A second weaker deeper INL did not show enhanced dissolved iron concentrations relative to background values (~ 1.3 nM), which may be due to variations in the scavenging efficiency or in the magnitude of the sources of dissolved iron. There was also evidence of vertical advection of iron-rich waters to the surface at the shelf break front, driven by the internal tide and shallowing topography.

It is clear that the behaviour of dissolved iron in this environment is very complex and will vary on relatively short time scales, and whilst advances in our knowledge are made here, there are remaining uncertainties regarding the mechanisms controlling dissolved iron. New studies should focus on release processes of iron from sediments, and the balance of input and removal of iron. Determining the speciation of dissolved iron is also crucial in order to explain how high DFe concentrations are maintained in these waters that can potentially be transported offshore. Intermediate nepheloid layers

can be a transport mechanism for dissolved iron to the ocean interior, however this process implies that, in some conditions, DFe could survive particle scavenging, which clearly needs investigating. A further important component of these systems to study is surface biology, as, apart from other factors, it is the major supplier of carbon to the seafloor. Monitoring the effect of vertical mixing on dissolved iron and nitrate distributions may thus allow the study of bloom dynamics at shelf breaks. Given that different degrees of iron limitation may exist even in coastal waters (Hutchins *et al.*, 1998), and given the relatively low iron concentrations in surface waters observed here, the possibility of iron limitation or co-limitation should be investigated.

This study of dissolved iron distributions at the Celtic Sea shelf edge therefore highlights our relatively poor understanding of processes governing the release, removal, stabilisation, and transport of iron at oceanic-shelf interface environments, and underlines the need for process studies.

Acknowledgements

Professor Roland Wollast is remembered by Peter J. Statham as an excellent and erudite researcher, who tempered his sharp logic with a human and endearing touch. It is an honour to be able to offer a contribution to this memorial volume.

The authors wish to thank Dr. D. Hydes for the nutrient data, Prof. P. Holligan, and Y.-N. Kim for the chlorophyll *a* information, and Dr. J. Sharples, the principal scientist officer, who ensured that this transect could take place, and for his support during the cruise. T. Edwards and J. Short are acknowledged for their support with the titanium CTD system, and S. Torres and Y.-N. Kim for helping carrying the CTD bottles to the trace metal clean container. Thanks to the officers and crew of the *R.R.S. James Clark Ross* for their assistance during cruise *JR98*. This work was supported by the George Deacon Division, National Oceanography Centre, Southampton, UK.

References

Achterberg, E.P., Holland, T.W., Bowie, A.R., Mantoura, R.F.C. and Worsfold, P.J., 2001. Determination of iron in seawater. Analytica Chimica Acta, 442(1): 1-14.

Antia, A.N., Maaβen, J., Herman, P., Voβ, M., Scholten, J., Groom, S. and Miller, P., 2001. Spatial and temporal variability of particle flux at the N. W. European continental margin. Deep-Sea Research II, 48: 3083-3106.

Berelson, W.M., McManus, J., Coale, K.H., Johnson, K.S., Burdige, D., Kilgore, T., Colodner, D., Chavez, F.P., Kudela, R.M. and Boucher, J., 2003. A time series of benthic flux measurements from Monterey Bay, CA. Continental Shelf Research, 23: 457-481.

Blain, S., Tréguer, P., Belviso, S., Bucciarelli, E., Denis, M., Desabre, S., Fiala, M., Jezequel, V.M., Le Fevre, J., Mayzaud, P., Marty, J.-C. and Razouls, S., 2001. A biogeochemical study of the island mass effect in the context of the iron hypothesis: Kerguelen Islands, Southern Ocean. Deep-Sea Research I, 48(1): 163-187.

Blain, S., Guieu, C., Claustre, H., Leblanc, K., Moutin, T., Quéguiner, B., Ras, J. and Sarthou, G., 2004. Availability of iron and major nutrients for phytoplankton in the northeast Atlantic Ocean. Limnology and Oceanography, 49(6): 2095-2104.

Bowie, A.R., Sedwick, P.N. and Worsfold, P.J., 2004. Analytical intercomparison between flow injection-chemiluminescence and flow injection-spectrophotometry for the determination of picomolar concentrations of iron in seawater. Limnology and Oceanography: Methods, 2: 42-54.

Boye, M., Aldrich, A.P., van den Berg, C.M.G., de Jong, J.T.M., Veldhuis, M.J.W. and de Baar, H.J.W., 2003. Horizontal gradient of the chemical speciation of iron in surface waters of the northeast Atlantic Ocean. Marine Chemistry, 80(2-3): 129-143.

Carey, E. and Taillefert, M., 2005. The role of soluble Fe(III) in the cycling of iron and sulfur in coastal marine sediments. Limnology and Oceanography, 50(4): 1129-1141.

Chase, Z., van Geen, A., Kosro, P.M., Marra, J. and Wheeler, P.A., 2002. Iron, nutrient, and phytoplankton distributions in Oregon coastal waters. Journal of Geophysical Research, 107(C10): 3174.

Cotté-Krief, M.-H., Thomas, A.J. and Martin, J.-M., 2002. Trace metal (Cd, Cu, Ni and Pb) cycling in the upper water column near the shelf edge of the European continental margin (Celtic Sea). Marine Chemistry, 79: 1-26.

Croot, P.L., Andersson, K., Öztürk, M. and Turner, D.R., 2004. The distribution and speciation of iron along 6°E in the Southern Ocean. Deep-Sea Research II, 51: 2857-2879.

de Baar, H.J.W. and de Jong, J.T.M., 2001. Distributions, sources and sinks of iron in seawater. In: D.R. Turner and K.A. Hunter (Eds.), The Biogeochemistry of Iron in Seawater. John Wiley & Sons, Chichester, pp. 123-253.

Dehairs, F., Baeyens, W. and van Gansbeke, D., 1989. Tight coupling between enrichment of iron and manganese in North Sea suspended matter and sedimentary redox processes: evidence for seasonal variability. Estuarine, Coastal and Shelf Science, 29: 457-471.

Dickson, R.R. and Gurbutt, P.A., 1980. Satellite evidence of enhanced upwelling along the European continental slope. Journal of Physical Oceanography, 10: 813-819.

Dickson, R.R. and McCave, I.N., 1986. Nepheloid layers on the continental slope west of Porcupine Bank. Deep-Sea Research I, 33(6): 791-818.

Elrod, V.A., Berelson, W.M., Coale, K.H. and Johnson, K.S., 2004. The flux of iron from continental shelf sediments: A missing source for global budgets. Geophysical Research Letters, 31(L12307): 1-4.

Geider, R.J., 1999. Complex lessons of iron uptake. Nature, 400(6747): 815-816.

Gordon, R.M., Coale, K.H. and Johnson, K.S., 1997. Iron distributions in the equatorial Pacific: Implications for new production. Limnology and Oceanography, 42(3): 419-431.

Heathershaw, A.D., New, A.L. and Edwards, P.D., 1987. Internal tides and sediment transport at the shelf break in the Celtic Sea. Continental Shelf Research, 7(5): 485-517.

Holeton, C.L., Nédélec, F., Sanders, R., Brown, L., Moore, M.C., Stevens, D.P., Heywood, K.J., Statham, P.J. and Lucas, C., 2005. Physiological state of phytoplankton communities from the Southwest Atlantic sector of the Southern Ocean, as measured by fast repetition rate fluorometry. Polar Biology, doi 10.1007/s00300-005-0028-y.

Hong, H. and Kester, D.R., 1986. Redox state of iron in the offshore waters of Peru. Limnology and Oceanography, 31(3): 512-524.

Hutchins, D.A., DiTullio, G.R., Zhang, Y. and Bruland, K.W., 1998. An iron limitation mosaic in the California upwelling regime. Limnology and Oceanography, 43(6): 1037-1057.

Huthnance, J.M., Humphery, J.D., Knight, P.J., Chatwin, P.G., Thomsen, L. and White, M., 2002. Near-bed turbulence measurements, stress estimates and sediment mobility at the continental shelf edge. Progress in Oceanography, 52: 171-194.

Hydes, D.J., Le Gall, A.C., Miller, A.E.J., Brockmann, U., Raabe, T., Holley, S.E., Alvarez-Salgado, X., Antia, A.N., Balzer, W., Chou, L., Elskens, M., Helder, W., Joint, I. and Orren, M., 2001. Supply and demand of nutrients and dissolved organic matter at and across the NW European shelf break in relation to hydrography and biogeochemical activity. Deep-Sea Research II, 48: 3023-3047.

Johnson, K.S., Gordon, R.M. and Coale, K.H., 1997. What controls dissolved iron concentrations in the world ocean ? Marine Chemistry, 57(3-4): 137-161.

Johnson, K.S., Chavez, F.P. and Friederich, G.E., 1999. Continental-shelf sediment as a primary source of iron for coastal phytoplankton. Nature, 398: 697-700.

Johnson, K.S., Elrod, V.A., Fitzwater, S.E., Plant, J.N., Chavez, F.P., Tanner, S.J., Gordon, R.M., Westphal, D.L., Perry, K.D., Wu, J. and Karl, D.M., 2003. Surface ocean-lower atmosphere interactions in the Northeast Pacific Ocean Gyre: Aerosols, iron, and the ecosystem response. Global Biogeochemical Cycles, 17(2): 32.

Johnson, W.K., Miller, L.A., Sutherland, N.E. and Wong, C.S., 2005. Iron transport by mesoscale Haida eddies in the Gulf of Alaska. Deep-Sea Research II, 52: 933-953.

Joint, I., Wollast, R., Chou, L., Batten, S., Elskens, M., Edwards, E., Hirst, A., Burkill, P., Groom, S., Gibb, S., Miller, A., Hydes, D., Dehairs, F., Antia, A., Barlow, R., Rees,

A., Pomroy, A., Brockmann, U., Cummings, D., Lampitt, R., Loijens, M., Mantoura, F., Miller, P., Raabe, T., Alvarez-Salgado, X., Stelfox, C. and Woolfenden, J., 2001. Pelagic production at the Celtic Sea shelf break. Deep-Sea Research II, 48: 3049-3081.

Kremling, K., 1983. Trace metal fronts in European shelf waters. Nature, 303: 225-227.

Laes, A., Blain, S., Laan, P., Achterberg, E.P., Sarthou, G. and de Baar, H.J.W., 2003. Deep dissolved iron profiles in the eastern North Atlantic in relation to water masses. Geophysical Research Letters, 30(17): 1902.

Landing, W.M., Haraldsson, C. and Paxeus, N., 1986. Vinyl polymer agglomerate based transition metal cation chelating ion-exchange resin containing the 8-hydroxyquinoline functional group. Analytical Chemistry, 58(14): 3031-3035.

Le Gall, A.C., Statham, P.J., Morley, N.H., Hydes, D.J. and Hunt, C.H., 1999. Processes influencing distributions and concentrations of Cd, Cu, Mn and Ni at the North West European shelf break. Marine Chemistry, 68: 97-115.

Lohse, L., Helder, W., Epping, E.H.G. and Balzer, W., 1998. Recycling of organic matter along a shelf-slope transect across the N.W. European Continental Margin (Goban Spur). Progress in Oceanography, 42: 77-110.

Martin, J.H. and Gordon, R.M., 1988. Northeast Pacific iron distributions in relation to phytoplankton productivity. Deep-Sea Research I, 35(2): 177-196.

McCave, I.N., Hall, I.R., Antia, A.N., Chou, L., Dehairs, F., Lampitt, R.S., Thomsen, L., van Weering, T.C.E. and Wollast, R., 2001. Distribution, composition and flux of particulate material over the European margin at 47^{o} - 50^{o}N. Deep-Sea Research II, 48(14-15): 3107-3139.

Millward, G.E., Morris, A.W. and Tappin, A.D., 1998. Trace metals at two sites in the southern North Sea: Results from a sediment resuspension study. Continental Shelf Research, 18: 1381-1400.

Morley, N.H., Statham, P.J. and Burton, J.D., 1993. Dissolved trace metals in the southwestern Indian Ocean. Deep Sea Research I, 40(5): 1043-1062.

Muller, F.L.L., Tappin, A.D., Statham, P.J., Burton, J.D. and Hydes, D.J., 1994. Trace metal fronts in waters of the Celtic Sea. Oceanologica Acta, 17(4): 383-396.

Nédélec, F., *submitted*. Implementation of a method to determine sub-nanomolar concentrations of iron in seawater and its application to the study of marine iron biogeochemistry at the ocean - shelf interface. PhD Thesis Thesis, University of Southampton, Southampton, 175 pp.

Obata, H., Karatani, H., Matsui, M. and Nakayama, E., 1997. Fundamental studies for chemical speciation of iron in seawater with an improved analytical method. Marine Chemistry, 56(1-2): 97-106.

Otto, S. and Balzer, W., 1998. Release of dissolved organic carbon (DOC) from sediments of the N.W. European Continental Margin (Goban Spur) and its significance for benthic carbon cycling. Progress in Oceanography, 42: 127-144.

Pingree, R.D., Mardell, G.T. and New, A.L., 1986. Propagation of internal tides from the upper slopes of the Bay of Biscay. Nature, 321: 154-158.

Pingree, R.D., Sinha, B. and Griffiths, C.R., 1999. Seasonality of the European slope current (Goban Spur) and ocean margin exchange. Continental Shelf Research, 19: 929-975.

Pollard, R.T., 2004. Iron rations. Planet Earth, Spring 2004: 19.

Rose, A.L. and Waite, T.D., 2003a. Kinetics of hydrolysis and precipitation of ferric iron in seawater. Environmental Science and Technology, 37: 3897-3903.

Rose, A.L. and Waite, T.D., 2003b. Kinetics of iron complexation by dissolved natural organic matter in coastal waters. Marine Chemistry, 84: 85-103.

Santschi, P.H., Höhener, P., Gaboury, B. and Buchholtz-ten Brink, M., 1990. Chemical processes at the sediment-water interface. Marine Chemistry, 30: 269-315.

Souza, A.J., Simpson, J.H., Harikrishnan, M. and Malarkey, J., 2001. Flow structure and seasonality in the Hebridean slope current. Oceanologica Acta, 24(S63-S76).

Sunda, W.G. and Huntsman, S.A., 1995. Iron uptake and growth limitation in oceanic and coastal phytoplankton. Marine Chemistry, 50(1-4): 189-206.

Tappin, A.D., Millward, G.E., Statham, P.J., Burton, J.D. and Morris, A.W., 1995. Trace metals in the central and southern North Sea. Estuarine, Coastal and Shelf Science, 41(3): 275-323.

Thorpe, S.A. and White, M., 1988. A deep intermediate nepheloid layer. Deep-Sea Research I, 35(9): 1665-1671.

van Aken, H.M., 2000. The hydrography of the mid-latitude Northeast Atlantic Ocean II : The intermediate water masses. Deep-Sea Research I, 47: 789-824.

van Weering, T.C.E., Hall, I.R., de Stigter, H.C., McCave, I.N. and Thomsen, L., 1998. Recent sediments, sediment accumulation and carbon burial at Goban Spur, N.W. European Continental Margin (47-50^{o}N). Progress in Oceanography, 42: 5-35.

Weinstein, S.E. and Moran, S.B., 2004. Distribution of size-fractionated particulate trace metals collected by bottles and in-situ pumps in the Gulf of Maine-Scotian shelf and Labrador Sea. Marine Chemistry, 87: 121-135.

Wells, M.L. and Goldberg, E.D., 1993. Colloid aggregation in seawater. Marine Chemistry, 41: 353-358.

Wells, M.L. and Goldberg, E.D., 1994. The distribution of colloids in the North Atlantic and Southern Oceans. Limnology and Oceanography, 39(2): 286-302.

Welschmeyer, N.A., 1994. Fluorometric analysis of chlorophyll-*a* in the presence of chlorophyll-*b* and phaeopigments. Limnology and Oceanography, 39: 1985-1992.

Wollast, R. and Chou, L., 2001. Ocean Margin EXchange in the Northern Gulf of Biscay: OMEX I. An introduction. Deep-Sea Research II, 48: 2971-2978.

Wu, J. and Luther III, G.W., 1996. Spatial and temporal distribution of iron in the surface water of the northwestern Atlantic Ocean. Geochimica et Cosmochimica Acta, 60(15): 2729-2741.

Wu, J., Boyle, E.A., Sunda, W.G. and Wen, L.-S., 2001. Soluble and colloidal iron in the oligotrophic North Atlantic and North Pacific. Science, 293(5531): 847-849.

Table 1. Stations sampled during the transect across the Celtic Sea shelf edge on *JR98* cruise. Total distance between N1 and N9 = 74 km. Station CS2 was not sampled as part of the transect.

Table 2. Data derived from the CTD sensors (*in situ* temperature, salinity, dissolved oxygen, and apparent oxygen utilisation (AOU)), and concentrations of chlorophyll *a*, nitrate, phosphate, dissolved silicon, and dissolved iron at all stations sampled across the Celtic Sea shelf edge.

Table 3. Estimation of carbon consumption and release of dissolved iron relative to measurements at Stations N1, N4, and N5 across the Celtic Sea shelf edge. AOU = Apparent Oxygen Utilisation; Δ = difference between two values. ΔC calculated using the Redfield ratio (C:AOU = 106:138). Estimated ΔDFe calculated using published Fe:C ratios = 10 to 50 µmol/mol.

Figure 1. Bathymetric maps of the study area with stations as referred to in the text.

Figure 2. Vertical distribution of dissolved iron (DFe) across the Celtic Sea shelf edge. Error bars are ± 1 standard deviation. Hatched boxes show bottom depth at each station except N9 (2953 m depth), which was sampled only down to 200 m.

Figure 3: Apparent oxygen utilisation (AOU, µM) *vs*. beam attenuation (m^{-1}) in the benthic nepheloid layer across the Celtic Sea shelf edge.

Figure 4: Full depth beam attenuation signal (m^{-1}) across the Celtic Sea shelf edge. Bathymetry was obtained from the ship and main water masses are indicated. ENACW = Eastern North Atlantic Central Water, MOW = Mediterranean Outflow Water, NEADW = North East Atlantic Deep Water.

Figure 5: Beam attenuation (m^{-1}) and dissolved iron (nM) distributions along density surfaces (σ_t kg/m^3) below the mixed layer at the deepest stations (N6 to N8) at the Celtic Sea shelf edge. Isopycnals separating the identified water masses (dotted lines) and INLs' zones of influence (grey hatched areas) are also indicated. ENACW = Eastern North Atlantic Central Water, MOW = Mediterranean Outflow Water, NEADW = North East Atlantic Deep Water.

Figure 6: Dissolved iron, chlorophyll *a*, macro-nutrient concentrations and temperature in surface waters (3 – 4 m) across the Celtic Sea shelf break. Shaded area highlights the location of the shelf break front.

Table 1. Stations location

Station	Latitude (°N)	Longitude (°W)	Bottom depth (m)	Distance from bottom of deepest sample (m)	Distance between stations (km)
N1	48.638	9.112	157	10	
N2	48.580	9.292	165	11	12.8
N3	48.520	9.493	250	12	12.0
N4	48.502	9.550	365	18	3.8
N5	48.485	9.600	542	19	3.7
N6	48.448	9.715	1238	5	8.5
N7	48.397	9.883	1903	6	11.5
N8	48.355	10.027	2411	9	10.5
N9	48.283	10.217	2953	Only down to 200 m	13.3

Table 2. All data

Station (water depth)	Depth (m)	Temp. (°C)	Salinity	Chlorophyll *a* (μg/L)	Dissolved oxygen (μM)	AOU (μM)	Nitrate (μM)	Phosphate (μM)	Dissolved silicon (μM)	Dissolved iron (nM)
N1 (157 m)	3	17.8	35.55	0.27	246.8	-7.4	0	0.027	0.55	0.64 ± 0.06
	28	16.0	35.56	0.85	251.7	-3.7	0.87	0.092	0.56	0.71 ± 0.05
	61	12.3	35.59	0.13	228.5	39.3	8.76	0.542	3.30	1.94 ± 0.07
	81	12.0	35.58	0.05	223.2	46.4	9.24	0.571	3.63	---
	127	12.0	35.58	0.05	221.6	48.1	9.26	0.572	3.63	2.53 ± 0.17
	147	12.0	35.58	0.05	218.2	51.5	9.23	0.578	3.64	5.37 ± 0.49
N2 (165 m)	3	17.6	35.55	0.37	254.5	-14.1	0	0.042	0.34	0.31 ± 0.08
	21	17.1	35.55	0.42	257.7	-14.7	0	0.045	0.36	0.31 ± 0.15
	51	15.4	35.57	0.75	262.0	-10.7	1.53	0.136	0.74	0.47 ± 0.07
	80	12.2	35.58	0.12	240.9	27.3	8.88	0.542	3.36	0.62 ± 0.13
	111	12.0	35.58	0.05	239.6	30.1	9.36	0.576	3.65	0.78 ± 0.01
	141	12.0	35.58	0.05	239.9	29.9	9.34	0.570	3.67	0.78 ± 0.03
	154	12.0	35.58	0.05	239.7	30.0	9.30	0.581	3.65	0.45 ± 0.02
N3 (250 m)	3	17.4	35.56	0.29	258.5	-16.9	0	0.046	0.28	0.19 ± 0.06
	16	17.9	35.56	0.50	262.6	-18.6	0.01	0.081	0.33	0.14 ± 0.02
	36	15.7	35.56	0.58	263.2	-13.7	2.53	0.200	1.11	0.31 ± 0.08
	51	13.7	35.58	0.23	250.1	10.0	5.71	0.365	2.15	0.39 ± 0.02
	81	12.9	35.59	0.09	248.2	16.1	7.40	0.458	2.69	0.49 ± 0.03
	151	11.9	35.59	0.03	242.8	26.9	9.34	0.567	3.52	0.74 ± 0.05
	202	11.8	35.59	0.02	244.2	26.4	9.82	0.592	3.69	0.78 ± 0.03
	238	11.8	35.59	0.02	242.9	28.0	9.94	0.598	3.87	0.45 ± 0.02
N4 (365 m)	3	17.4	35.56	0.42	258.1	-16.8	0.14	0.064	0.33	0.81 ± 0.09
	16	16.3	35.56	0.71	265.3	-18.5	0.97	0.110	0.65	0.61 ± 0.07
	39	14.5	35.57	0.54	254.3	1.4	3.63	0.262	1.44	0.81 ± 0.03
	81	13.3	35.58	0.14	248.8	13.5	6.57	0.416	2.41	0.91 ± 0.04
	151	12.5	35.59	0.07	246.2	20.5	8.23	0.515	3.08	1.72 ± 0.10
	202	11.8	35.59		246.9	23.9	10.06	0.601	3.70	0.90 ± 0.08
	241	11.6	35.59		245.4	26.5	10.58	0.626	3.97	0.91 ± 0.06
	302	11.6	35.59		245.3	26.8	10.90	0.648	4.14	0.87 ± 0.05
	347	11.3	35.58		239.8	34.1	11.78	0.738	4.76	1.50 ± 0.04
N5 (542 m)	3	17.2	35.56	0.40	260.4	-18.0	0.06	0.054	0.28	0.84 ± 0.14
	22	15.2	35.57	0.48	258.8	-6.7	3.78	0.318	1.56	0.16 ± 0.00
	81	12.9	35.59	0.14	248.2	15.8	6.94	0.448	2.62	0.43 ± 0.03
	202	11.9	35.59		246.2	23.5	9.14	0.563	3.45	2.63 ± 0.01
	251	11.8	35.59		244.4	26.4	9.74	0.601	3.77	0.46 ± 0.01
	302	11.7	35.59		244.5	26.8	10.78	0.675	4.37	0.48 ± 0.02
	352	11.6	35.59		243.3	28.9	10.70	0.662	4.32	0.56 ± 0.08
	402	11.3	35.58		240.4	33.5	11.89	0.723	5.02	1.87 ± 0.05
	452	11.0	35.58		234.8	40.7	11.25	0.688	4.83	0.64 ± 0.07
	523	10.9	35.58		232.4	43.8	13.08	0.800	6.12	0.83 ± 0.06
N6 (1238 m)	4	17.2	35.57	0.33	261.5	-19.2	0	0.053	0.33	0.91 ± 0.15
	32	14.4	35.57	0.50	256.0	0.5	4.01	0.295	1.63	0.86 ± 0.12
	152	11.9	35.62	0.03	252.8	16.9	9.35	0.600	3.28	1.22 ± 0.06
	403	11.0	35.58		236.1	39.3	12.87	0.804	5.73	1.38 ± 0.03
	704	9.9	35.62		216.0	66.6	16.88	1.052	10.01	2.69 ± 0.14
	804	9.6	35.64		213.9	70.6	17.13	1.073	10.13	3.23 ± 0.17
	905	9.3	35.63		215.9	70.6	17.44	1.085	10.74	1.55 ± 0.14
	1005	8.9	35.62		215.0	73.9	17.99	1.122	11.57	1.45 ± 0.11
	1105	8.8	35.61		216.6	73.4	18.20	1.135	12.00	4.36 ± 0.19
	1206	8.5	35.58		219.3	72.7	18.40	1.153	12.63	1.59 ± 0.30
	1221	8.4	35.58		219.6	72.8	18.30	1.149	12.75	1.81 ± 0.16
	1233	8.4	35.57		220.3	72.6	18.32	1.149	12.80	1.36 ± 0.00
N7 (1893 m)	4	17.8	35.59	0.23	259.0	-19.3	0.01	0.066	0.42	---
	53	14.6	35.60	0.50	265.7	-10.2	2.53	0.196	0.90	---
	153	11.8	35.61	0.01	259.1	11.8	9.79	0.589	3.35	1.30 ± 0.06
	404	11.1	35.52		255.1	20.0	11.92	0.738	4.67	2.04 ± 0.08
	605	10.6	35.59		227.8	50.3	16.23	1.006	8.57	3.07 ± 0.15
	900	9.7	35.70		211.1	72.9	18.12	1.127	11.41	1.45 ± 0.04
	1206	7.9	35.53		227.0	68.9	18.67	1.176	13.11	1.52 ± 0.07
	1407	6.8	35.38		239.7	64.6	19.30	1.241	16.73	1.35 ± 0.04
	1607	5.3	35.20		254.6	60.9	19.65	1.274	19.04	1.32 ± 0.06
	1809	4.5	35.10		263.3	58.8	20.00	1.284	21.93	1.22 ± 0.02
	1859	4.3	35.08		265.1	58.7	19.86	1.295	21.00	1.55 ± 0.14

	1896	4.3	35.08		265.8	58.1	20.10	1.318	23.00	1.33 ± 0.10
	5	17.5	35.56	0.25	261.4	-20.5	0	0.033	0.18	0.75 ± 0.09
	24	16.1	35.56	0.60	270.4	-22.6	0.70	0.096	0.41	0.92 ± 0.04
	43	13.7	35.61	0.37	260.2	-0.3	4.56	0.302	1.43	1.58 ± 0.08
	154	11.7	35.61	0.02	259.9	11.2	9.92	0.598	3.43	1.60 ± 0.07
	506	10.8	35.53		237.5	39.7	13.85	0.840	6.14	3.21 ± 0.12
N8	807	9.9	35.63		211.6	71.2	17.60	1.067	9.80	---
(2411 m)	1007	9.2	35.69		212.1	75.0	18.29	1.106	11.25	1.63 ± 0.05
	1409	6.6	35.46		240.2	65.3	19.38	1.201	14.91	1.61 ± 0.04
	1810	4.5	35.09		263.5	58.8	20.09	1.264	20.38	2.05 ± 0.03
	2011	4.2	35.05		267.3	57.5	20.21	1.284	21.99	1.60 ± 0.09
	2211	4.8	35.02		268.7	59.7	20.70	1.306	26.25	1.83 ± 0.07
	2402	3.2	34.97		269.2	64.1	21.38	1.412	32.14	1.80 ± 0.06
	4	17.4	35.56	0.36	262.6	-21.3	0.01	0.034	0.12	0.46 ± 0.03
N9	29	15.1	35.59	0.67	266.7	-13.9	1.86	0.157	0.71	0.48 ± 0.04
(2953 m)	102	12.2	35.61		256.4	12.0	8.70	0.519	2.25	0.74 ± 0.05
	202	11.5	35.58		259.2	13.5	10.49	0.639	3.74	0.63 ± 0.01

Table 3. DFe release

Station	Depth (m)	AOU (μM)	ΔAOU (μM)	ΔC (μM)	Estimated ΔDFe (nM)	ΔDFe measured (nM)
N1	127 (top BNL) 147 (bottom)	47.8 51.5	3.7	2.8	0.03 – 0.14	2.84
N4	302 (top BNL) 347 (bottom)	26.8 34.1	7.3	5.6	0.06 – 0.28	0.63
N5	402 (top BNL) 524 (bottom)	33.5 43.9	10.4	8.0	0.08 – 0.40	0.19
	452 (mid-BNL) 524 (bottom)	40.7 43.9	3.2	2.4	0.02 – 0.12	

Figure 1. Maps

Click here to download high resolution image

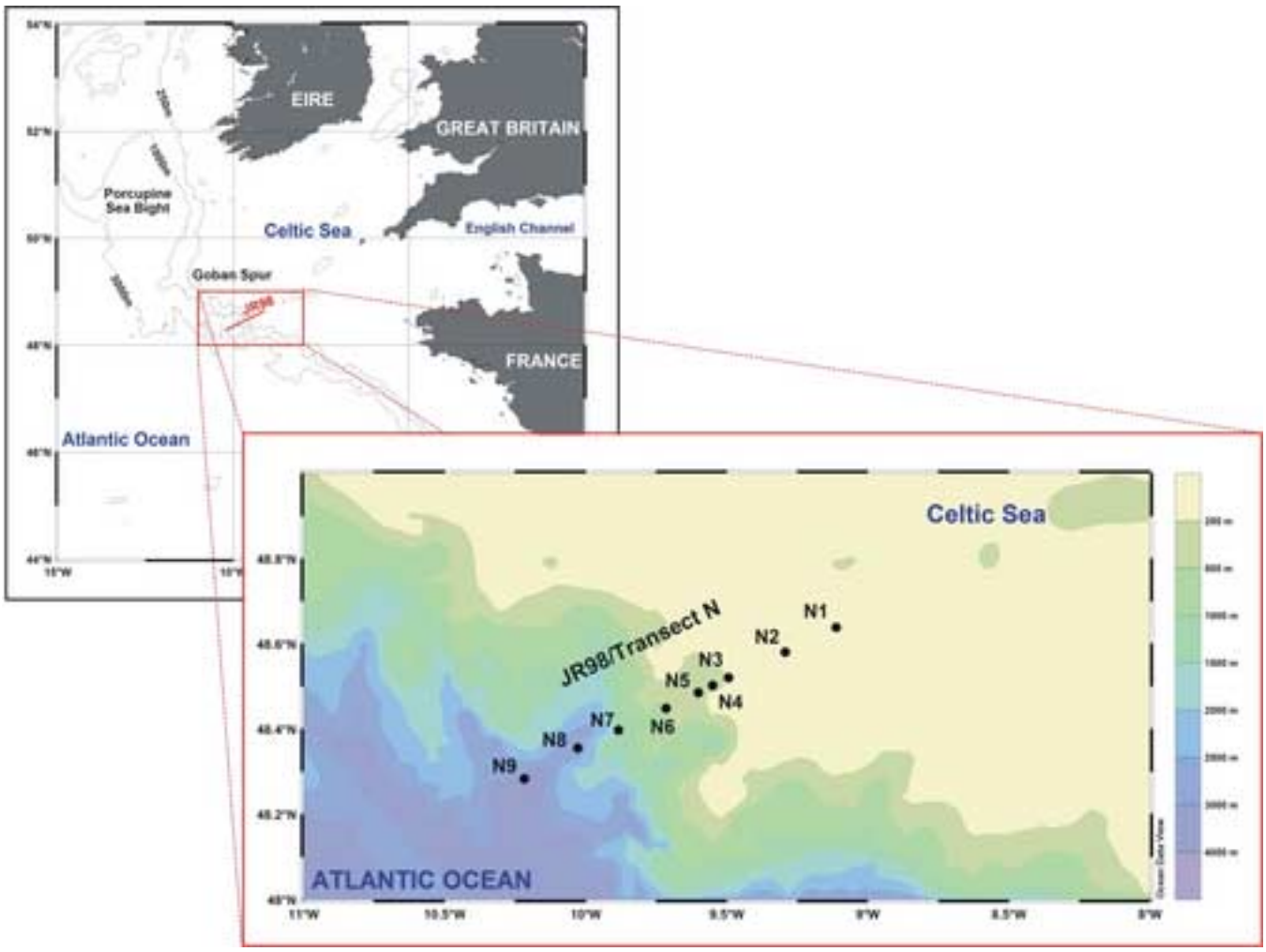

Figure 2. DFe distribution

Click here to download high resolution image

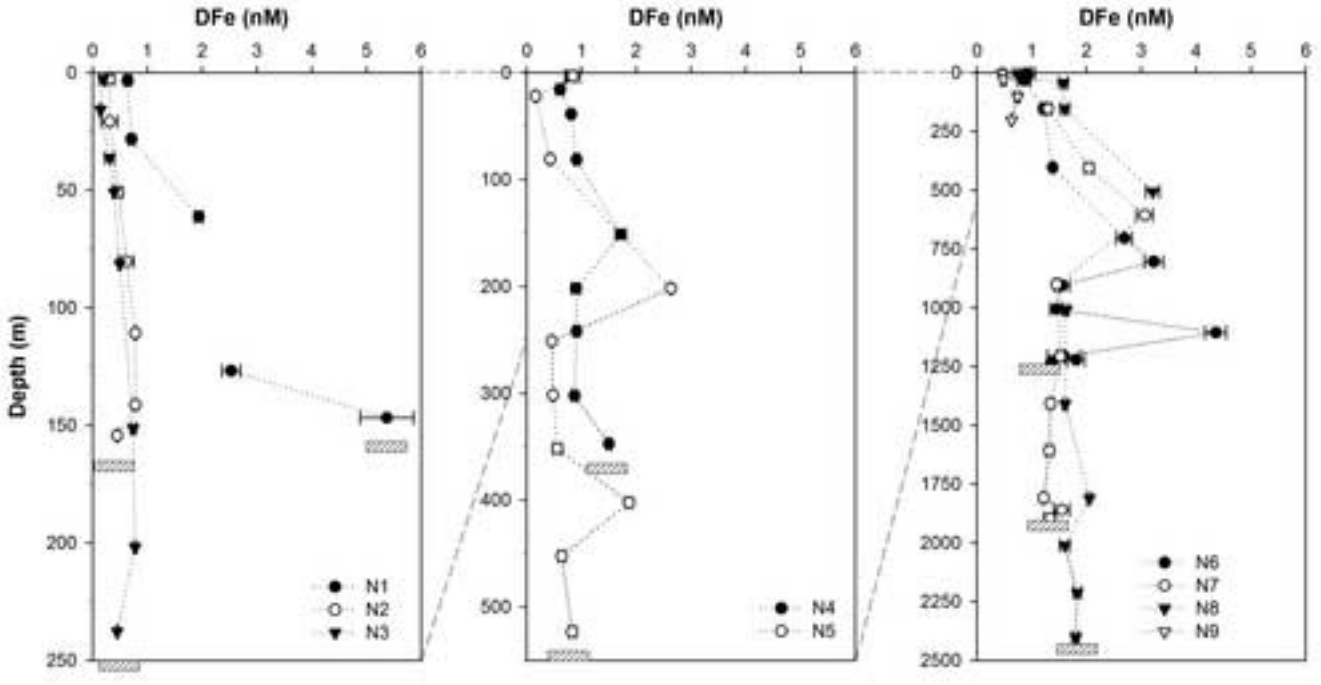

Figure 3. AOU vs Beam
Click here to download high resolution image

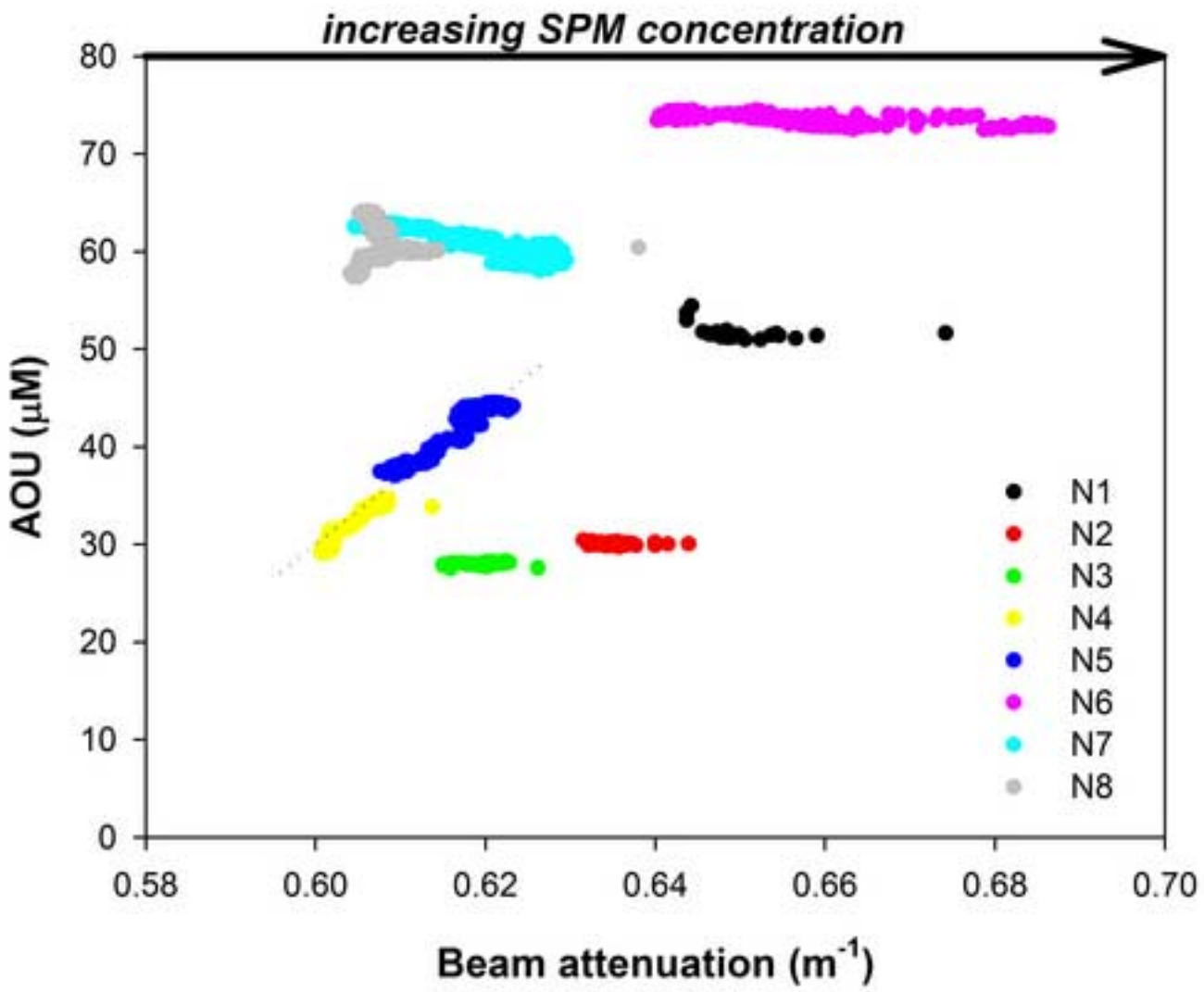

Figure 4. Beam section

Click here to download high resolution image

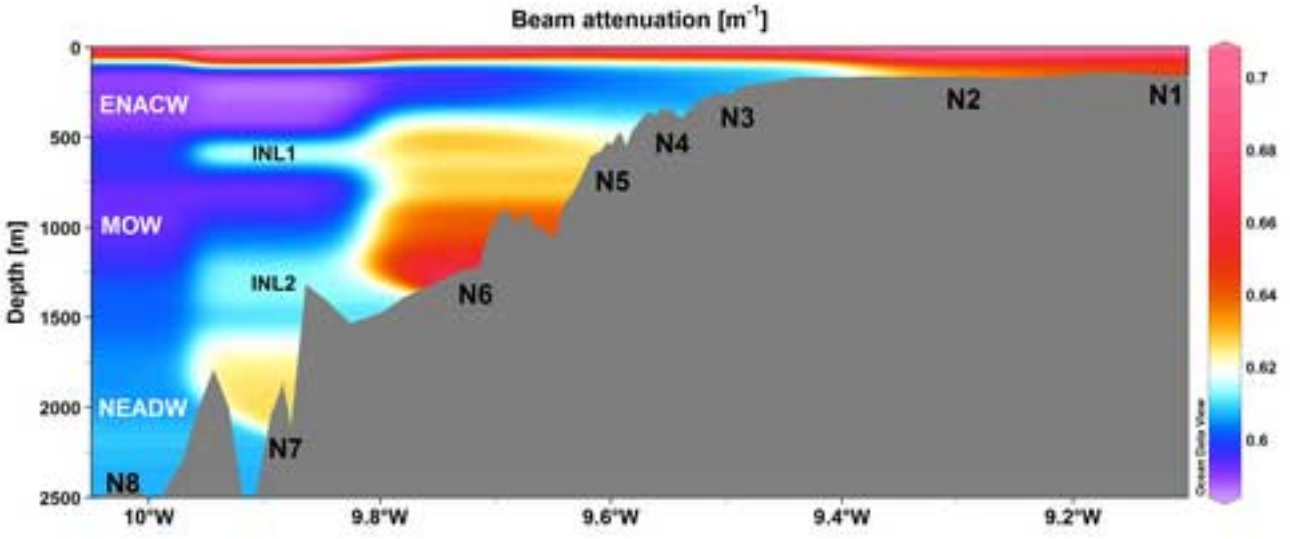

Figure 5. Beam & DFe vs SigT
Click here to download high resolution image

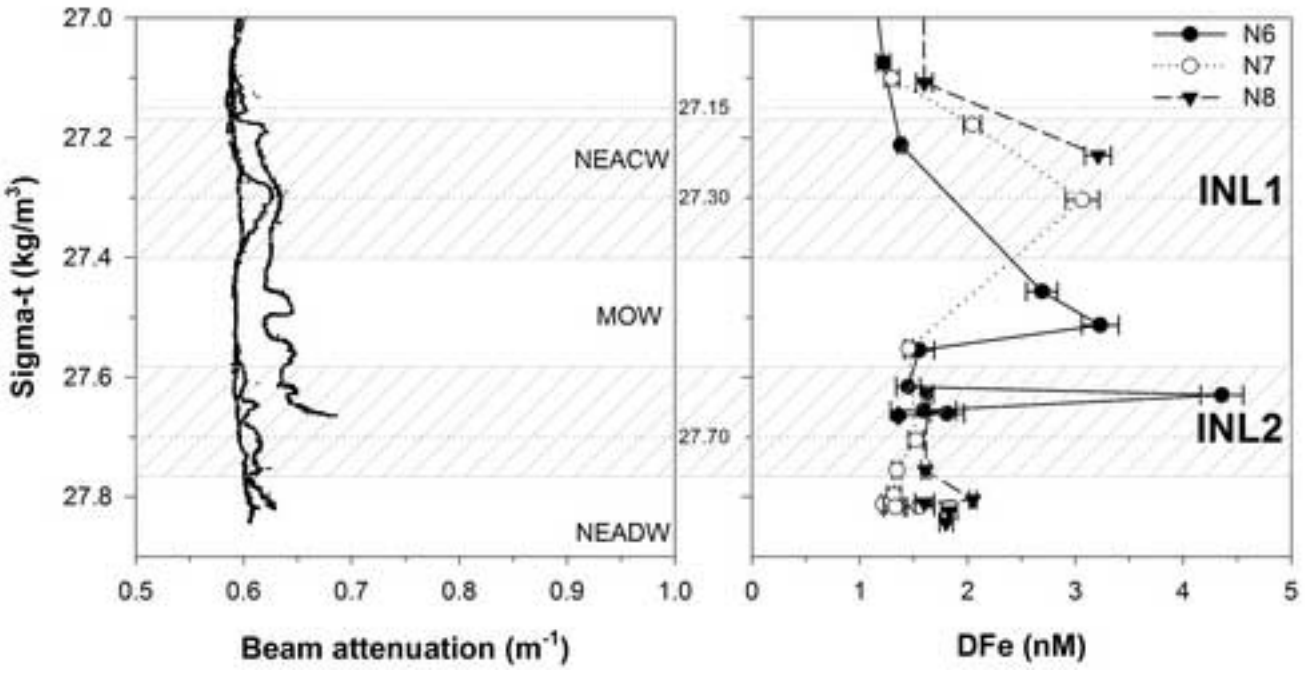

Figure 6. Surface data

Click here to download high resolution image

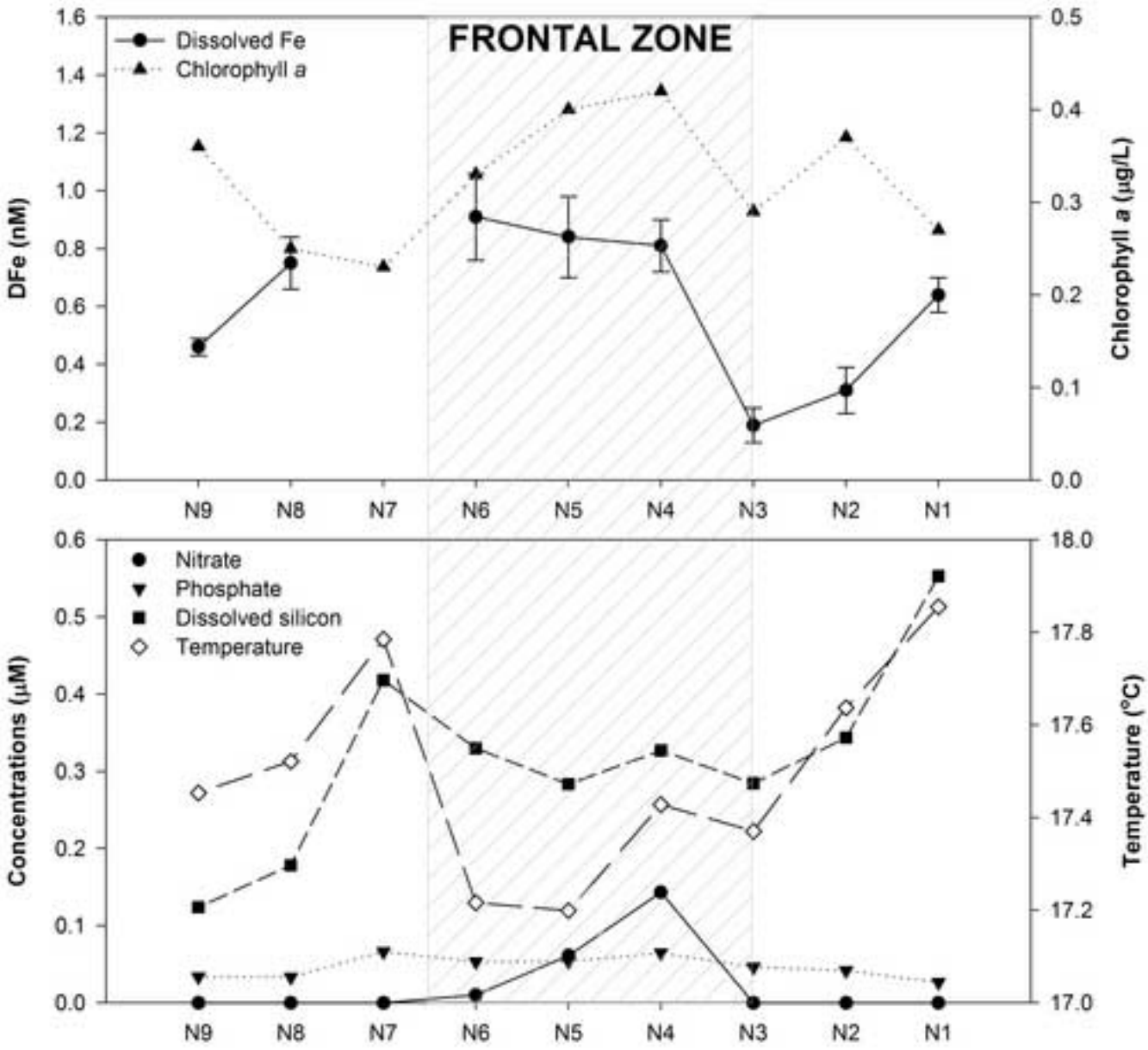

REFERENCES

REFERENCES

Achterberg E.P., Holland T.W., Bowie A.R., Mantoura R.F.C., and Worsfold P.J., **2001**. Determination of iron in seawater. *Analytica Chimica Acta*, **442**(1): 1-14.

Adams M.L., and Powell K.J., **2001**. Flow injection method for iron fractionation by reaction with oxine-derivatised Fractogel. *Analytica Chimica Acta*, **433**: 289-297.

Aller R.C., **2004**. Conceptual models of early diagenetic processes: The muddy seafloor as an unsteady, batch reactor. *Journal of Marine Research*, **62**: 815-835.

Antia A.N., Maaβen J., Herman P., Voβ M., Scholten J., Groom S., and Miller P., **2001**. Spatial and temporal variability of particle flux at the N. W. European continental margin. *Deep-Sea Research II*, **48**: 3083-3106.

Arhan M., and King B., **1995**. Lateral mixing of the Mediterranean Water in the eastern North Atlantic. *Journal of Marine Research*, **53**(6): 865-895.

Arhan M., Naveira Garabato A.C., Heywood K.J., and Stevens D.P., **2002**. The Antarctic Circumpolar Current between the Falkland Islands and South Georgia. *Journal of Physical Oceanography*, **32**: 1914-1931.

Atkinson A., Whitehouse M.J., Priddle J., C. C.G., Ward P., and Brandon M.A., **2001**. South Georgia, Antarctica: a productive, cold water, pelagic ecosystem. *Marine Ecology Progress Series*, **216**: 279-308.

Baker A.R., Jickells T.D., Witt M., and Linge K.L., **2006**. Trends in the solubility of iron, aluminium, manganese and phosphorus in aerosol collected over the Atlantic Ocean. *Marine Chemistry*, **98**: 43-58.

Barbeau K., Moffett J.W., Caron D.A., Croot P.L., and Erdner D.L., **1996**. Role of protozoan grazing in relieving iron limitation of phytoplankton. *Nature*, **380**: 61-64.

Barbeau K., Rue E.L., Bruland K.W., and Butler A., **2001**. Photochemical cycling of iron in the surface ocean mediated by microbial iron(III)-binding ligands. *Nature*, **413**: 409-413.

Barlow R.G., Mantoura R.F.C., Gough M.A., and Fileman T.W., **1993**. Pigment signatures of the phytoplankton composition in the northeastern Atlantic during the 1990 spring bloom. *Deep-Sea Research II*, **40**(1/2): 459-477.

Behra P., and Sigg L., **1990**. Evidence for redox cycling of iron in atmospheric water droplets. *Nature*, **344**: 419-421.

Berelson W.M., McManus J., Coale K.H., Johnson K.S., Burdige D., Kilgore T., Colodner D., Chavez F.P., Kudela R.M., and Boucher J., **2003**. A time series of benthic flux measurements from Monterey Bay, CA. *Continental Shelf Research*, **23**: 457-481.

Berman-Franck I., Cullen J.T., Shaked Y., Sherrell R.M., and Falkowski P.G., **2001**. Iron availability, cellular iron quotas, and nitrogen fixation in *Trichodesmium*. *Limnology and Oceanography*, **46**(6): 1249-1260.

Bjornland T., and Liaaen-Jensen S., **1989**. Distribution patterns of carotenoids in relation to chromophyte phylogeny and systematics. In: *The Chromophyte Algae: Problems and Perspectives*. Green J.C., Leadbeater B.S.C., and Diver W.L., Oxford, Clarendon Press.

Blain S., and Treguer P., **1995**. Iron(II) and iron(III) determination in sea water at the nanomolar level with selective on-line preconcentration and spectrophotometric determination. *Analytica Chimica Acta*, **308**(1-3): 425-432.

Blain S., Tréguer P., Belviso S., Bucciarelli E., Denis M., Desabre S., Fiala M., Jezequel V.M., Le Fevre J., Mayzaud P., Marty J.-C., and Razouls S., **2001**. A biogeochemical study of the island mass effect in the context of the iron hypothesis: Kerguelen Islands, Southern Ocean. *Deep-Sea Research I,* **48**(1): 163-187.

Blain S., Guieu C., Claustre H., Leblanc K., Moutin T., Quéguiner B., Ras J., and Sarthou G., **2004**. Availability of iron and major nutrients for phytoplankton in the northeast Atlantic Ocean. *Limnology and Oceanography*, **49**(6): 2095-2104.

Bonnet S., and Guieu C., **2004**. Dissolution of atmospheric iron in seawater. *Geophysical Research Letters*, **31**: L03303.

Borer P.M., Sulzberger B., Reichard P., and Kraemer S.M., **2005**. Effect of siderophores on the light-induced dissolution of colloidal iron(III) (hydr)oxides. *Marine Chemistry*, **93**: 179-193.

Bowie A.R., Achterberg E.P., Mantoura R.F.C., and Worsfold P.J., **1998**. Determination of sub-nanomolar levels of iron in seawater using flow injection with chemiluminescence detection. *Analytica Chimica Acta*, **361**(3): 189-200.

Bowie A.R., Maldonado M.T., Frew R.D., Croot P.L., Achterberg E.P., Mantoura R.F.C., Worsfold P.J., Law C.S., and Boyd P.W., **2001**. The fate of added iron during a mesoscale fertilisation experiment in the Southern Ocean. *Deep-Sea Research II*, **48**(11-12): 2703-2743.

Bowie A.R., Achterberg E.P., Ussher S., and Worsfold P.J., **2002a**. Real-time monitoring of picomolar concentrations of iron(II) in marine waters using automated flow injection-chemiluminescence instrumentation. *Environmental Science and Technology*, **36**(21): 4483-4706.

Bowie A.R., Whitworth D.J., Achterberg E.P., Mantoura R.F.C., and Worsfold P.J., **2002b**. Biogeochemistry of Fe and other trace elements (Al, Co, Ni) in the upper Atlantic Ocean. *Deep-Sea Research I,* **49**(4): 605-636.

Bowie A.R., Achterberg E.P., Blain S., Boye M., Croot P.L., de Baar H.J.W., Laan P., Sarthou G., and Worsfold P.J., **2003**. Shipboard analytical intercomparison of dissolved iron in surface waters along a north–south transect of the Atlantic Ocean. *Marine Chemistry*, **84**: 19-34.

Bowie A.R., Sedwick P.N., and Worsfold P.J., **2004**. Analytical intercomparison between flow injection-chemiluminescence and flow injection-spectrophotometry for the determination of picomolar concentrations of iron in seawater. *Limnology and Oceanography: Methods*, **2**: 42-54.

Boyd P.W., Watson A.J., Law C.S., Abraham E.R., Trull T., Murdoch R., Bakker D.C.E., Bowie A.R., Buesseler K.O., Chang H., Charette M.A., Croot P.L., Downing K., Frew R.D., Gall M., Hadfield M., Hall J.A., Harvey M., Jameson G., LaRoche J., Liddicoat M.I., Ling R., Maldonado M.T., McKay R.M., Nodder S., Pickmere S., Pridmore R., Rintoul S., Safi K.A., Sutton P., Strzepek R., Tanneberger K., Turner S., Waite A., and Zeldis J., **2000**. A mesoscale phytoplankton bloom in the polar Southern Ocean stimulated by iron fertilization. *Nature*, **407**: 695-702.

Boyd P.W., Law C.S., Wong C.S., Nojiri Y., Tsuda A., Levasseur M., Takeda S., Rivkin R., Harrison P.J., Strzepek R., Gower J., McKay R.M., Abraham E.R., Arychuk M., Barwell-Clarke J., Crawford W., Crawford D., Hale M., Harada K., Johnson K.S., Kiyosawa H., Kudo I., Marchetti A., Miller W.L., Needoba J., Nishioka J., Ogawa H., Page J., Robert M., Saito H., Sastri A., Sherry N., Soutar T., Sutherland N., Taira Y., Whitney F., Wong S.-K.E., and Yoshimura T., **2004**. The decline and fate of an iron-induced subarctic phytoplankton bloom. *Nature*, **428**: 549-553.

Boye M., van den Berg C.M.G., de Jong J.T.M., Leach H., Croot P.L., and de Baar H.J.W., **2001**. Organic complexation of iron in the Southern Ocean. *Deep-Sea Research I*, **48**(6): 1477-1497.

Boye M., Aldrich A.P., van den Berg C.M.G., de Jong J.T.M., Veldhuis M.J.W., and de Baar H.J.W., **2003**. Horizontal gradient of the chemical speciation of iron in surface waters of the northeast Atlantic Ocean. *Marine Chemistry*, **80**(2-3): 129-143.

Boyle E.A., Edmond J.M., and Sholkovitz E.R., **1977**. The mechanism of iron removal in estuaries. *Geochimica et Cosmochimica Acta*, **41**: 1313-1324.

Bruland K.W., Franks R.P., Knauer G.A., and Martin J.H., **1979**. Sampling and analytical methods for the determination of copper, cadmium, zinc, and nickel at the nanogram per liter level in sea water. *Analytica Chimica Acta*, **105**: 233-245.

Bruland K.W., and Rue E.L., **2001**. Analytical methods for the determination of concentrations and speciation of iron. In: *The Biogeochemistry of Iron in Seawater*. Turner D.R., and Hunter K.A., Chichester, John Wiley & Sons, **IUPAC 7:** 255-289.

Bruland K.W., Rue E.L., and Smith G.J., **2001**. Iron and macronutrients in California coastal upwelling regimes: Implications for diatom blooms. *Limnology and Oceanography*, **46**(7): 1661-1674.

Bruland K.W., Rue E.L., Smith G.J., and DiTullio G.R., **2005**. Iron, macronutrients and diatom blooms in the Peru upwelling regime: brown and blue waters of Peru. *Marine Chemistry*, **93**(1): 81-103.

Bucciarelli E., Blain S., and Tréguer P., **2001**. Iron and manganese in the wake of the Kerguelen Islands (Southern Ocean). *Marine Chemistry*, **73**(1): 21-36.

Buesseler K.O., and Boyd P.W., **2003**. Will ocean fertilization work ? *Science*, **300**: 67-68.

Buesseler K.O., Andrews J.E., Pike S.M., and Charette M.A., **2004**. The effects of iron fertilization on carbon sequestration in the Southern Ocean. *Science*, **304**: 414-417.

Canfield D.E., **1989**. Reactive iron in marine sediments. *Geochimica et Cosmochimica Acta*, **53**(3): 619-632.

Cannizzaro V., Bowie A.R., Sax A., Achterberg E.P., and Worsfold P.J., **2000**. Determination of cobalt and iron in estuarine and coastal waters using flow injection with chemiluminescence detection. *Analyst*, **125**(1): 51-57.

Carey E., and Taillefert M., **2005**. The role of soluble Fe(III) in the cycling of iron and sulfur in coastal marine sediments. *Limnology and Oceanography*, **50**(4): 1129-1141.

Chang C.A., and Patterson H.H., **1980**. Halide ion enhancement of chromium(III), iron(II), and cobalt(II) catalysis of luminol chemiluminescence. *Analytical Chemistry*, **52**: 653-656.

Chase Z., Johnson K.S., Elrod V.A., Plant J.N., Fitzwater S.E., Pickell L., and Sakamoto C.M., **2005**. Manganese and iron distributions off central California influenced by upwelling and shelf width. *Marine Chemistry*, **95**: 235-254.

Chen M., Dei R.C.H., Wang W.-X., and Guo L., **2003**. Marine diatom uptake of iron bound with natural colloids of different origins. *Marine Chemistry*, **81**(3-4): 177-189.

Chester R., **1990**. Marine Geochemistry. London, Chapman & Hall, 698pp.

Chisholm S.W., Falkowski P.G., and Cullen J.J., **2001**. Dis-crediting ocean fertilization. *Science*, **294**: 309-310.

Coale K.H., Fitzwater S.E., Gordon R.M., Johnson K.S., and Barber R.T., **1996a**. Control of community growth and export production by upwelled iron in the equatorial Pacific Ocean. *Nature*, **379**: 621-624.

Coale K.H., Johnson K.S., Fitzwater S.E., Gordon R.M., Tanner S.J., Chavez F.P., Ferioli L., Sakamoto C., Rogers P., Millero F.J., Steinberg P., Nightingale P., Cooper D., Cochlan W.P., Landry M.R., Constantinou J., Rollwagen G., Trasvina A., and Kudela R.M., **1996b**. A massive phytoplankton bloom induced by an ecosystem-scale iron fertilization experiment in the equatorial Pacific Ocean. *Nature*, **383**: 495-501.

Coale K.H., Johnson K.S., Chavez F.P., Buesseler K.O., Barber R.T., Brzezinski M.A., Cochlan W.P., Millero F.J., Falkowski P.G., Bauer J.E., Wanninkhof R.H., Kudela R.M., Altabet M.A., Hales B.E., Takahashi T., Landry M.R., Bidigare R.R., Wang X., Chase Z., Strutton P.G., Friederich G.E., Gorbunov M.Y., Lance V.P., Hilting A.K., Hiscock M.R., Demarest M., Hiscock W.T., Sullivan K.F., Tanner S.J., Gordon R.M., Hunter C.N., Elrod V.A., Fitzwater S.E., Jones J.L., Tozzi S., Koblizek M., Roberts A.E., Hemdon J., Brewster J., Ladizinsky N.,

Smith G.J., Cooper D., Timothy D., Brown S.L., Selph K.E., Sheridan C.C., Twining B.S., and Johnson Z.I., **2004**. Southern Ocean iron enrichment experiment: Carbon cycling in high- and low-Si waters. *Science*, **304**: 408-414.

Cotté-Krief M.-H., Thomas A.J., and Martin J.-M., **2002**. Trace metal (Cd, Cu, Ni and Pb) cycling in the upper water column near the shelf edge of the European continental margin (Celtic Sea). *Marine Chemistry*, **79**: 1-26.

Croot P.L., and Hunter K.A., **1998**. Trace metal distributions across the continental shelf near Otago Peninsula, New Zealand. *Marine Chemistry*, **62**: 185-201.

Croot P.L., and Johansson M., **2000**. Determination of iron speciation by cathodic stripping voltammetry in seawater using the competing ligand 2-(2-thiazolylazo)-p-cresol (TAC). *Electroanalysis*, **12**(8): 565-576.

Croot P.L., and Laan P., **2002**. Continuous shipboard determination of Fe(II) in polar waters using flow injection analysis with chemiluminescence detection. *Analytica Chimica Acta*, **466**: 261-273.

Croot P.L., Andersson K., Öztürk M., and Turner D.R., **2004a**. The distribution and speciation of iron along 6°E in the Southern Ocean. *Deep-Sea Research II*, **51**: 2857-2879.

Croot P.L., Streu P., and Baker A.R., **2004b**. Short residence time for iron in surface seawater impacted by atmospheric dry deposition from Saharan dust events. *Geophysical Research Letters*, **31**: L23S08.

Dalton R., **2002**. Ocean tests raise doubts over use of algae as carbon sink. *Nature*, **420**: 722.

de Baar H.J.W., de Jong J.T.M., Nolting R.F., Timmermans K.R., van Leeuwen M.A., Bathmann U., van der Loeff M.R., and Sildam J., **1999**. Low dissolved Fe and the absence of diatom blooms in remote Pacific waters of the Southern Ocean. *Marine Chemistry*, **66**(1-2): 1-34.

de Baar H.J.W., and de Jong J.T.M., **2001**. Distributions, sources and sinks of iron in seawater. In: *The Biogeochemistry of Iron in Seawater*. Turner D.R., and Hunter K.A., Chichester, John Wiley & Sons, **IUPAC 7:** 123-253.

de Jong J.T.M., den Das J., Bathmann U., Stoll M.H.C., Kattner G., Nolting R.F., and de Baar H.J.W., **1998**. Dissolved iron at subnanomolar levels in the Southern Ocean as determined by ship-board analysis. *Analytica Chimica Acta*, **377**(2-3): 113-124.

Dehairs F., Baeyens W., and van Gansbeke D., **1989**. Tight coupling between enrichment of iron and manganese in North Sea suspended matter and sedimentary redox processes: evidence for seasonal variability. *Estuarine, Coastal and Shelf Science*, **29**: 457-471.

Dickson R.R., and Gurbutt P.A., **1980**. Satellite evidence of enhanced upwelling along the European continental slope. *Journal of Physical Oceanography*, **10**: 813-819.

Dickson R.R., and McCave I.N., **1986**. Nepheloid layers on the continental slope west of Porcupine Bank. *Deep-Sea Research I*, **33**(6): 791-818.

Dierssen H., Balzer W., and Landing W.M., **2001**. Simplified synthesis of an 8-hydroxyquinoline chelating resin and a study of trace metal profiles from Jellyfish Lake, Palau. *Marine Chemistry*, **73**(3-4): 173-192.

Duce R.A., Liss P.S., Merrill J.T., Atlas E.L., Buat-Menard P., Hicks B.B., Miller J.M., Prospero J.M., Arimoto R., Church T.M., Ellis W., Galloway J.N., Hansen L., Jickells T.D., Knap A.H., Reinhardt K.H., Schneider B., Soudine A., Tokos J.J., Tsunogai S., Wollast R., and Zhou M., **1991**. The atmospheric input of trace species to the world ocean. *Global Biogeochemical Cycles*, **5**: 193-259.

Duce R.A., and Tindale N.W., **1991**. Atmospheric transport of iron and its deposition in the ocean. *Limnology and Oceanography*, **36**(8): 1715-1726.

Elderfield H., **1981**. Metal-organic associations in interstitial waters for Narragansett Bay sediments. *American Journal of Science*, **281**: 1184-1196.

Elrod V.A., Berelson W.M., Coale K.H., and Johnson K.S., **2004**. The flux of iron from continental shelf sediments: A missing source for global budgets. *Geophysical Research Letters*, **31**(L12307): 1-4.

Field M.P., and Sherrell R.M., **2000**. Dissolved and particulate Fe in a hydrothermal plume at $9^{o}45'$N, East Pacific Rise: Slow Fe(II) oxidation kinetics in Pacific plumes. *Geochimica et Cosmochimica Acta*, **64**(4): 619-628.

Firme G.F., Rue E.L., Weeks D.A., Bruland K.W., and Hutchins D.A., **2003**. Spatial and temporal variability in phytoplankton iron limitation along the California coast and consequences for Si, N, and C biogeochemistry. *Global Biogeochemical Cycles*, **17**(1): 1016.

Fitzwater S.E., Johnson K.S., Elrod V.A., Ryan J.P., Coletti L.J., Tanner S.J., Gordon R.M., and Chavez F.P., **2003**. Iron, nutrient and phytoplankton biomass relationships in upwelled waters of the California coastal system. *Continental Shelf Research*, **23**: 1523-1544.

Fouquet Y., Charlou J.L., Costa I., Donval J.P., Radford-Knoery J., Pellé H., Ondréas H., Lourenço N., Ségonzac M., and Tivey M.K., **1994**. A detailed study of the Lucky Strike hydrothermal site and discoveryof a new hydrothermal site : Menez Gwen. Preliminary results of the DIVA-1 cruise. *InterRidge News*, **3**(2): 14-17.

Geider R.J., **1999**. Complex lessons of iron uptake. *Nature*, **400**(6747): 815-816.

German C.R., Campbell A.C., and Edmond J.M., **1991**. Hydrothermal scavenging at the Mid-Atlantic Ridge: Modification of trace element dissolved fluxes. *Earth and Planetary Science Letters*, **107**: 101-114.

Gervais F., Rievesell U., and Gorbunov M.Y., **2002**. Changes in primary productivity and chlorophyll *a* in response to iron fertilization in the Southern Polar Frontal Zone. *Limnology and Oceanography*, **47**(5): 1324-1335.

Gledhill M., and van den Berg C.M.G., **1995**. Measurement of the redox speciation of iron in seawater by catalytic cathodic stripping voltammetry. *Marine Chemistry*, **50**(1-4): 51-61.

Gordon R.M., Coale K.H., and Johnson K.S., **1997**. Iron distributions in the equatorial Pacific: Implications for new production. *Limnology and Oceanography*, **42**(3): 419-431.

Gran H.H., **1931**. On the conditions for the production of plankton in the sea. *Rapp. Proc. Verb. Reun. Conn. Int. Expl. Mer*, **75**: 37-46.

Granger J., and Price N.M., **1999**. The importance of siderophores in iron nutrition of heterotrophic marine bacteria. *Limnology and Oceanography*, **44**(3): 541-555.

Grotti M., Soggia F., Abelmoschi M.L., Rivaro P., Magi E., and Frache R., **2001**. Temporal distribution of trace metals in Antarctic coastal waters. *Marine Chemistry*, **76**(3): 189-209.

Guéguen C., Belin C., Thomas B.A., Monna F., Favarger P.-Y., and Dominik J., **1999**. The effect of freshwater UV-irradiation prior to resin preconcentration of trace metals. *Analytica Chimica Acta*, **386**: 155-159.

Guieu C., Bozec Y., Blain S., Ridame C., Sarthou G., and Leblond N., **2002**. Impact of high Saharan dust inputs on dissolved iron concentrations in the Mediterranean Sea. *Geophysical Research Letters*, **29**(19): 1911.

Heathershaw A.D., New A.L., and Edwards P.D., **1987**. Internal tides and sediment transport at the shelf break in the Celtic Sea. *Continental Shelf Research*, **7**(5): 485-517.

Helmers E., and Schrems O., **1995**. Wet deposition of metals to the tropical North and the South Atlantic Ocean. *Atmospheric Environment*, **29**(18): 2475-2484.

Ho T.-Y., Quigg A., Finkel Z.V., Milligan A.J., Falkowski P.G., and Morel F.M.M., **2003**. The elemental composition of some marine phytoplankton. *Journal of Phycology*, **39**: 1145-1159.

Holeton C.L., Nédélec F., Sanders R., Brown L., Moore M.C., Stevens D.P., Heywood K.J., Statham P.J., and Lucas C., **2005**. Physiological state of phytoplankton communities from the Southwest Atlantic sector of the Southern Ocean, as measured by fast repetition rate fluorometry. *Polar Biology*, **29**: 44-52.

Hong H., and Kester D.R., **1986**. Redox state of iron in the offshore waters of Peru. *Limnology and Oceanography*, **31**(3): 512-524.

Hudson R.J.M., and Morel F.M.M., **1990**. Iron transport in marine phytoplankton: Kinetics of cellular and medium coordination reactions. *Limnology and Oceanography*, **35**(5): 1002-1020.

Hutchins D.A., DiTullio G.R., and Bruland K.W., **1993**. Iron and regenerated production : Evidence for biological iron recycling in two marine environments. *Limnology and Oceanography*, **38**(6): 1242-1255.

Hutchins D.A., and Bruland K.W., **1994**. Grazer-mediated regeneration and assimilation of Fe, Zn and Mn from planktonic prey. *Marine Ecology-Progress Series*, **110**(2-3): 259-269.

Hutchins D.A., and Bruland K.W., **1998**. Iron-limited diatom growth and Si:N uptake ratios in a coastal upwelling regime. *Nature*, **393**: 561-564.

Hutchins D.A., DiTullio G.R., Zhang Y., and Bruland K.W., **1998**. An iron limitation mosaic in the California upwelling regime. *Limnology and Oceanography*, **43**(6): 1037-1057.

Hutchins D.A., Witter A.E., Butler A., and Luther III G.W., **1999**. Competition among marine phytoplankton for different chelated iron species. *Nature*, **400**: 858-861.

Hutchins D.A., Hare C.E., Weaver R.S., Zhang Y., Firme G.F., DiTullio G.R., Alm M.B., Riseman S.F., Maucher J.M., Geesey M.E., Trick C.G., Smith G.J., Rue E.L., Conn J., and Bruland K.W., **2002**. Phytoplankton iron limitation in the Humboldt Current and Peru Upwelling. *Limnology and Oceanography*, **47**(4): 997-1011.

Huthnance J.M., Coelho H., Griffiths C.R., Knight P.J., Rees A.P., Sinha B., Vangriesheim A., White M., and Chatwin P.G., **2001**. Physical structures, advection and mixing in the region of Goban spur. *Deep-Sea Research II*, **48**: 2979-3021.

Huthnance J.M., Humphery J.D., Knight P.J., Chatwin P.G., Thomsen L., and White M., **2002**. Near-bed turbulence measurements, stress estimates and sediment mobility at the continental shelf edge. *Progress in Oceanography*, **52**: 171-194.

Hydes D.J., Le Gall A.C., Miller A.E.J., Brockmann U., Raabe T., Holley S.E., Alvarez-Salgado X., Antia A.N., Balzer W., Chou L., Elskens M., Helder W., Joint I., and Orren M., **2001**. Supply and demand of nutrients and dissolved organic matter at and across the NW European shelf break in relation to hydrography and biogeochemical activity. *Deep-Sea Research II*, **48**: 3023-3047.

Jago C.F., Jones S.E., Latter R.J., McCandliss R.R., Hearn M.R., and Howarth M.J., **2002**. Resuspension of benthic fluff by tidal currents in deep stratified waters, northern North Sea. *Journal of Sea Research*, **48**: 259-269.

Jahnke R.A., Reimers C.E., and Craven D.B., **1990**. Intensification of recycling of organic matter at the sea floor near ocean margins. *Nature*, **348**: 50-54.

Jickells T.D., and Spokes L.J., **2001**. Atmospheric iron inputs to the oceans. In: *The Biogeochemistry of Iron in Seawater*. Turner D.R., and Hunter K.A., Chichester, John Wiley & Sons, **IUPAC 7:** 85-121.

Johnson K.S., Gordon R.M., and Coale K.H., **1997**. What controls dissolved iron concentrations in the world ocean ? *Marine Chemistry*, **57**(3-4): 137-161.

Johnson K.S., Chavez F.P., and Friederich G.E., **1999**. Continental-shelf sediment as a primary source of iron for coastal phytoplankton. *Nature*, **398**: 697-700.

Johnson K.S., and Karl D.M., **2002**. Is ocean fertilization credible and creditable. *Science*, **296**: 467-468.

Johnson K.S., Elrod V.A., Fitzwater S.E., Plant J.N., Chavez F.P., Tanner S.J., Gordon R.M., Westphal D.L., Perry K.D., Wu J., and Karl D.M., **2003**. Surface ocean-

lower atmosphere interactions in the Northeast Pacific Ocean Gyre: Aerosols, iron, and the ecosystem response. *Global Biogeochemical Cycles*, **17**(2): 32.

Johnson W.K., Miller L.A., Sutherland N.E., and Wong C.S., **2005**. Iron transport by mesoscale Haida eddies in the Gulf of Alaska. *Deep-Sea Research II*, **52**: 933-953.

Joint I., Wollast R., Chou L., Batten S., Elskens M., Edwards E., Hirst A., Burkill P., Groom S., Gibb S., Miller A., Hydes D., Dehairs F., Antia A., Barlow R., Rees A., Pomroy A., Brockmann U., Cummings D., Lampitt R., Loijens M., Mantoura F., Miller P., Raabe T., Alvarez-Salgado X., Stelfox C., and Woolfenden J., **2001**. Pelagic production at the Celtic Sea shelf break. *Deep-Sea Research II*, **48**: 3049-3081.

Kieber R.J., Williams K., Willey J.D., Skrabal S., and Avery Jr. G.B., **2001**. Iron speciation in coastal rainwater: concentration and deposition to seawater. *Marine Chemistry*, **73**(2): 83-95.

Kieber R.J., Hardison D.R., Whitehead R.F., and Willey J.D., **2003**. Photochemical production of Fe(II) in rainwater. *Environmental Science and Technology*, **37**: 4610-4616.

Kim Y.-N., **In preparation**. Effect of changes in different hydrographic environments on photosynthetic performance, as measured by FRRF, of different size fractions of marine phytoplankton. School of Ocean and Earth Sciences. Southampton, University of Southampton.

King D.W., Lin J., and Kester D.R., **1991**. Spectrophotometric determination of iron(II) in seawater at nanomolar concentrations. *Analytica Chimica Acta*, **247**(1): 125-132.

King D.W., Aldrich R.A., and Charnecki S.E., **1993**. Photochemical redox cycling of iron in NaCl solutions. *Marine Chemistry*, **44**(2-4): 105-120.

King D.W., Lounsbury H.A., and Millero F.J., **1995**. Rates and mechanism of Fe(II) oxidation at nanomolar total iron concentrations. *Environmental Science and Technology*, **29**(3): 818-824.

Klopf L.L., and Nieman T.A., **1983**. Effect of iron(II), cobalt(II), copper(II) and manganese(II) on the chemiluminescence of luminol in the absence of hydrogen peroxide. *Analytical Chemistry*, **55**(7): 1080-1083.

Korb R.E., and Whitehouse M.J., **2004**. Contrasting primary production regimes around South Georgia, Southern Ocean: large blooms versus high nutrient, low chlorophyll waters. *Deep-Sea Research I*, **51**: 721-738.

Korb R.E., Whitehouse M.J., and Ward P., **2004**. SeaWiFS in the southern ocean: spatial and temporal variability in phytoplankton biomass around South Georgia. *Deep-Sea Research II*, **51**: 99-116.

Kremling K., **1983**. Trace metal fronts in European shelf waters. *Nature*, **303**: 225-227.

Kuma K., Nakabayashi S., Suzuki Y., and Matsunaga K., **1992**. Dissolution rate and solubility of colloidal hydrous ferric oxide in seawater. *Marine Chemistry*, **38**: 133-143.

Kuma K., Katsumoto A., Nishioka J., and Matsunaga K., **1998**. Size-fractionated iron concentrations and Fe(III) hydroxide solubilities in various coastal waters. *Estuarine, Coastal and Shelf Science*, **47**(3): 275-283.

Laes A., Blain S., Laan P., Achterberg E.P., Sarthou G., and de Baar H.J.W., **2003**. Deep dissolved iron profiles in the eastern North Atlantic in relation to water masses. *Geophysical Research Letters*, **30**(17): 1902.

Lan Z.H., and Mottola H.A., **1996**. Carbon dioxide-enhanced luminol chemiluminescence in the absence of added oxidant. *Analyst*, **121**: 211-218.

Landing W.M., Haraldsson C., and Paxeus N., **1986**. Vinyl polymer agglomerate based transition metal cation chelating ion-exchange resin containing the 8-hydroxyquinoline functional group. *Analytical Chemistry*, **58**(14): 3031-3035.

Landing W.M., and Bruland K.W., **1987**. The contrasting biogeochemistry of iron and manganese in the Pacific Ocean. *Geochimica et Cosmochimica Acta*, **51**(1): 29-43.

Le Gall A.C., Statham P.J., Morley N.H., Hydes D.J., and Hunt C.H., **1999**. Processes influencing distributions and concentrations of Cd, Cu, Mn and Ni at the North West European shelf break. *Marine Chemistry*, **68**: 97-115.

Lind J., Merenyi G., and Eriksen T.E., **1983**. Chemiluminescence mechanism of cyclic hydrazides such as luminol in aqueous solutions. *Journal of American Chemical Society*, **105**: 7655-7661.

Liu X., and Millero F.J., **2002**. The solubility of iron in seawater. *Marine Chemistry*, **77**(1): 43-54.

Lohan M.C., Aguilar-Islas A.M., Franks R.P., and Bruland K.W., **2005**. Determination of iron and copper in seawater at pH 1.7 with a new commercially available chelating resin, NTA Superflow. *Analytica Chimica Acta*, **530**: 121-129.

Lohse L., Helder W., Epping E.H.G., and Balzer W., **1998**. Recycling of organic matter along a shelf-slope transect across the N.W. European Continental Margin (Goban Spur). *Progress in Oceanography*, **42**: 77-110.

Loscher B.M., de Baar H.J.W., de Jong J.T.M., Veth C., and Dehairs F., **1997**. The distribution of Fe in the Antarctic Circumpolar Current. *Deep-Sea Research II*, **44**(1-2): 143-188.

Mackey D.J., O'Sullivan J.E., and Watson R.J., **2002**. Iron in the western Pacific: a riverine or hydrothermal source for iron in the Equatorial Undercurrent ? *Deep-Sea Research I*, **49**(5): 877-893.

Mackie D.S., Boyd P.W., Hunter K.A., and McTainsh G.H., **2005**. Simulating the cloud processing of iron in Australian dust: pH and dust concentration. *Geophysical Research Letters*, **32**: L06809.

Macrellis H.M., Trick C.G., Rue E.L., Smith G.J., and Bruland K.W., **2001**. Collection and detection of natural iron-binding ligands from seawater. *Marine Chemistry*, **76**(3): 175-187.

Maldonado M.T., and Price N.M., **2000**. Nitrate regulation of Fe reduction and transport by Fe-limited *Thalassiosira oceanica*. *Limnology and Oceanography*, **45**(4): 814-826.

Martin J.H., and Gordon R.M., **1988**. Northeast Pacific iron distributions in relation to phytoplankton productivity. *Deep-Sea Research I*, **35**(2): 177-196.

Martin J.H., **1990**. Glacial-interglacial CO_2 change : The iron hypothesis. *Paleoceanography*, **5**: 1-13.

Martin J.H., Gordon R.M., and Fitzwater S.E., **1990**. Iron in Antarctic waters. *Nature*, **345**: 156-158.

Martin J.H., Fitzwater S.E., Gordon R.M., Hunter C.N., and Tanner S.J., **1993**. Iron, primary production and carbon-nitrogen flux studies during the JGOFS North Atlantic Bloom Experiment. *Deep-Sea Research II*, **40**(1-2): 115-134.

Martin J.H., Coale K.H., Johnson K.S., Fitzwater S.E., Gordon R.M., Tanner S.J., Hunter C.N., Elrod V.A., Nowicki J.L., Coley T.L., Barber R.T., Lindley S., Watson A.J., van Scoy K., Law C.S., Liddicoat M.I., Ling R., Stanton T.P., Stockel J., Collins C., Anderson A., Bidigare R.R., Ondrusek M., Latasa M., Millero F.J., Lee K., Yao W., Zhang J.Z., Friederich G.E., Sakamoto C., Chavez F.P., Buck K., Kolber Z., Greene R.M., Falkowski P.G., Chisholm S.W., Hoge F., Swift R., Yungel J., Turner S., Nightingale P., Hatton A., Liss P.S., and Tindale N.W., **1994**. Testing the iron hypothesis in ecosystems of the equatorial Pacific Ocean. *Nature*, **371**: 123-129.

McCave I.N., Hall I.R., Antia A.N., Chou L., Dehairs F., Lampitt R.S., Thomsen L., van Weering T.C.E., and Wollast R., **2001**. Distribution, composition and flux of particulate material over the European margin at 47^o - 50^oN. *Deep-Sea Research II*, **48**(14-15): 3107-3139.

Measures C.I., Yuan J., and Resing J.A., **1995**. Determination of iron in seawater by flow injection analysis using in-line preconcentration and spectrophotometric detection. *Marine Chemistry*, **50**(1-4): 3-12.

Measures C.I., **1999**. The role of entrained sediments in sea ice in the distribution of aluminium and iron in the surface waters of the Arctic Ocean. *Marine Chemistry*, **68**: 59-70.

Millero F.J., **1989**. Effect of Ionic Interactions on the Oxidation of Fe(II) and Cu(I) in Natural Waters. *Marine Chemistry*, **28**: 1-18.

Millero F.J., González-Dávila M., and Santana-Casiano J.M., **1995a**. Reduction of Fe(III) with sulfite in natural waters. *Journal of Geophysical Research*, **100**(D4): 7235-7244.

Millero F.J., Yao W., and Aicher J., **1995b**. The speciation of Fe(II) and Fe(III) in natural waters. *Marine Chemistry*, **50**(1-4): 21-39.

Mills M.M., Ridame C., Davey M., La Roche J., and Geider R.J., **2004**. Iron and phosphorus co-limit nitrogen fixation in the eastern tropical North Atlantic. *Nature*, **429**: 292-294.

Millward G.E., Morris A.W., and Tappin A.D., **1998**. Trace metals at two sites in the southern North Sea: Results from a sediment resuspension study. *Continental Shelf Research*, **18**: 1381-1400.

Moffett J.W., **2001**. Transformations among different forms of iron in the ocean. In: *The Biogeochemistry of Iron in Seawater*. Turner D.R., and Hunter K.A., Chichester, John Wiley & Sons, **IUPAC 7:** 343-372.

Moody J.R., and Lindstrom R.M., **1977**. Selection and cleaning of plastic containers for storage of trace element samples. *Analytical Chemistry*, **49**(14): 2264-2267.

Moody J.R., **1982**. The sampling, handling and storage of materials for trace analysis. *Philosophical Transactions of the Royal Society of London. Series A, Mathematical and Physical Sciences*, **305**(1491): 669-680.

Moran S.B., Yeats P.A., and Balls P.W., **1996**. On the role of colloids in trace metal solid-solution partitioning in continental shelf waters: a comparison of model results and field data. *Continental Shelf Research*, **16**(3): 397-408.

Muller F.L.L., Tappin A.D., Statham P.J., Burton J.D., and Hydes D.J., **1994**. Trace metal fronts in waters of the Celtic Sea. *Oceanologica Acta*, **17**(4): 383-396.

Ndung'u K., Francks R.P., Bruland K.W., and Flegal A.R., **2003**. Organic complexation and total dissolved trace metal analysis in estuarine waters: comparison of solvent-extraction graphite furnace atomic absorption spectrometric and chelating resin flow injection inductively coupled plasma-mass spectrometric analysis. *Analytica Chimica Acta*, **481**: 127-138.

Nishioka J., Takeda S., Wong C.S., and Johnson W.K., **2001**. Size-fractionated iron concentrations in the northeast Pacific Ocean: distribution of soluble and small colloidal iron. *Marine Chemistry*, **74**(2-3): 157-179.

Nodwell L.M., and Price N.M., **2001**. Direct use of inorganic colloidal iron by marine mixotrophic phytoplankton. *Limnology and Oceanography*, **46**(4): 765-777.

Obata H., Karatani H., and Nakayama E., **1993**. Automated determination of iron in seawater by chelating resin concentration and chemiluminescence detection. *Analytical Chemistry*, **65**: 1524-1528.

Obata H., Karatani H., Matsui M., and Nakayama E., **1997**. Fundamental studies for chemical speciation of iron in seawater with an improved analytical method. *Marine Chemistry*, **56**(1-2): 97-106.

Obata H., and van den Berg C.M.G., **2001**. Determination of picomolar levels of iron in seawater using catalytic cathodic stripping voltammetry. *Analytical Chemistry*, **73**: 2522-2528.

O'Sullivan D.W., Hanson Jr. A.K., Miller W.L., and Kester D.R., **1991**. Measurement of Fe(II) in surface water of the Equatorial Pacific. *Limnology and Oceanography*, **36**(8): 1727-1741.

O'Sullivan D.W., Hanson Jr. A.K., and Kester D.R., **1995**. Stopped flow luminol chemiluminescence determination of Fe(II) and reducible iron in seawater at subnanomolar levels. *Marine Chemistry*, **49**(1): 65-77.

Otto S., and Balzer W., **1998**. Release of dissolved organic carbon (DOC) from sediments of the N.W. European Continental Margin (Goban Spur) and its significance for benthic carbon cycling. *Progress in Oceanography*, **42**: 127-144.

Paillet J., Arhan M., and McCartney M.S., **1998**. Spreading of Labrador Sea Water in the eastern North Atlantic. *Journal of Geophysical Research*, **103**(C5): 10,223-10,239.

Parekh P., Follows M.J., and Boyle E.A., **2004**. Modeling the global ocean iron cycle. *Global Biogeochemical Cycles*, **18**: 1002.

Perez F.F., Mourino C., Fraga F., and Rios A.F., **1993**. Displacement of water masses and remineralization rates off the Iberian Peninsula by nutrient anomalies. *Journal of Marine Research*, **51**: 869-892.

Pingree R.D., Mardell G.T., and New A.L., **1986**. Propagation of internal tides from the upper slopes of the Bay of Biscay. *Nature*, **321**: 154-158.

Pingree R.D., and Le Cann B., **1989**. Celtic and Armorican slope and shelf residual currents. *Progress in Oceanography*, **23**: 303-338.

Pingree R.D., Sinha B., and Griffiths C.R., **1999**. Seasonality of the European slope current (Goban Spur) and ocean margin exchange. *Continental Shelf Research*, **19**: 929-975.

Pollard R.T., Griffiths M.J., Cunningham S.A., Read J.F., Perez F.F., and Rios A.F., **1996**. Vivaldi 1991 - A study of the formation, circulation and ventilation of Eastern North Atlantic Central Water. *Progress in Oceanography*, **37**: 167-192.

Pollard R.T., **2004**. Iron rations. *Planet Earth*, **Spring 2004**: 19.

Powell R.T., King D.W., and Landing W.M., **1995**. Iron distributions in surface waters of the south Atlantic. *Marine Chemistry*, **50**(1-4): 13-20.

Powell R.T., and Donat J.R., **2001**. Organic complexation and speciation of iron in the South and Equatorial Atlantic. *Deep-Sea Research II*, **48**(13): 2877-2893.

Price N.B., **2005**. The elemental stoichiometry and composition of an iron-limited diatom. *Limnology and Oceanography*, **50**(4): 1159-1171.

Price N.M., Andersen L.F., and Morel F.M.M., **1991**. Iron and nitrogen nutrition of equatorial Pacific plankton. *Deep-Sea Research I*, **38**(11): 1361-1378.

Prospero J.M., and Lamb P.J., **2003**. African droughts and dust transport to the caribbean: Climate change implications. *Science*, **302**: 1024-1027.

Read J.F., Lucas M.I., Holley S.E., and Pollard R.T., **2000**. Phytoplankton, nutrients and hydrography in the frontal zone between the Southwest Indian Subtropical gyre and the Southern Ocean. *Deep-Sea Research I,* **47**(12): 2341-2368.

Redfield A.C., Ketchum B.H., and Richards F.A., **1963**. The influence of organisms on the compositions of sea-water. New York, John Wiley & Sons, 554pp.

Rich H.W., and Morel F.M.M., **1990**. Availability of well-defined iron colloids to the marine diatom *Thalassiosira weissflogii*. *Limnology and Oceanography,* **35**(3): 652-662.

Rose A.L., and Waite T.D., **2001**. Chemiluminescence of luminol in the presence of iron(II) and oxygen: Oxidation mechanism and implications for its analytical use. *Analytical Chemistry,* **73**: 5909-5920.

Rose A.L., and Waite D.T., **2002**. Kinetic model for Fe(II) oxidation in seawater in the absence and presence of natural organic matter. *Environmental Science and Technology*, **36**: 433-444.

Rose A.L., and Waite T.D., **2003a**. Kinetics of hydrolysis and precipitation of ferric iron in seawater. *Environmental Science and Technology*, **37**: 3897-3903.

Rose A.L., and Waite T.D., **2003b**. Kinetics of iron complexation by dissolved natural organic matter in coastal waters. *Marine Chemistry*, **84**: 85-103.

Rue E.L., and Bruland K.W., **1995**. Complexation of iron(III) by natural organic ligands in the Central North Pacific as determined by a new competitive ligand equilibration/adsorptive cathodic stripping voltammetric method. *Marine Chemistry*, **50**(1-4): 117-138.

Rue E.L., and Bruland K.W., **1997**. The role of organic complexation on ambient iron chemistry in the equatorial Pacific Ocean and the response of a mesoscale iron addition experiment. *Limnology and Oceanography*, **42**(5): 901-910.

Rue E.L., and Bruland K.W., **2001**. Domoic acid binds iron and copper: a possible role for the toxin produced by the marine diatom *Pseudo-nitzschia*. *Marine Chemistry*, **76**(1-2): 127-134.

Santschi P.H., Höhener P., Gaboury B., and Buchholtz-ten Brink M., **1990**. Chemical processes at the sediment-water interface. *Marine Chemistry*, **30**: 269-315.

Sarthou G., and Jeandel C., **2001**. Seasonal variations of iron concentrations in the Ligurian Sea and iron budget in the Western Mediterranean Sea. *Marine Chemistry*, **74**: 115-129.

Sarthou G., Baker A.R., Blain S., Achterberg E.P., Boye M., Bowie A.R., Croot P.L., Laan P., de Baar H.J.W., Jickells T.D., and Worsfold P.J., **2003**. Atmospheric iron deposition and sea-surface dissolved iron concentrations in the eastern Atlantic Ocean. *Deep-Sea Research I,* **50**: 1339-1352.

Schiermeier Q., **2003**. The oresmen. *Nature*, **421**: 109-110.

Schlitzer R., **2002**. http://www.awi-bremerhaven.de/GEO/ODV.

Schueller G., **1999**. Testing the waters. *New Scientist*: 34-37.

Sedlak D.L., and Hoigne J., **1994**. Oxidation of S(IV) in atmospheric water by photooxidants and iron in the presence of copper. *Environmental Science and Technology*, **28**(11): 1898-1906.

Sedwick P.N., and DiTullio G.R., **1997**. Regulation of algal blooms in Antarctic shelf waters by the release of iron from melting sea ice. *Geophysical Research Letters*, **24**(20): 2515-2518.

Sedwick P.N., DiTullio G.R., and Mackey D.J., **2000**. Iron and manganese in the Ross Sea, Antarctica: Seasonal iron limitation in Antarctic shelf waters. *Journal of Geophysical Research*, **105**(C5): 11,321-11,336.

Seitz W.R., and Hercules D.M., **1972**. Determination of trace amounts of iron(II) using chemiluminescence analysis. *Analytical Chemistry*, **44**(13): 2143-2149.

Sharples J., Moore M.C., Rippeth T.P., Holligan P.M., Hydes D.J., Fisher N.R., and Simpson J.H., **2001**. Phytoplankton distribution and survival in the thermocline. *Limnology and Oceanography*, **46**(3): 486-496.

Sherrell R.M., and Boyle E.A., **1988**. Zinc, chromium, vanadium and iron in the Mediterranean Sea. *Deep-Sea Research*, **35**: 1319-1334.

Sholkovitz E.R., **1978**. The flocculation of dissolved Fe, Mn, Al, Cu, Ni, Co and Cd during estuarine mixing. *Earth and Planetary Science Letters*, **41**(1): 77-86.

Sholkovitz E.R., Boyle E.A., and Price N.B., **1978**. The removal of dissolved humic acids and iron during estuarine mixing. *Earth and Planetary Science Letters*, **40**: 130-136.

Skrabal S.A., Donat J.R., and Burdige D.J., **2000**. Pore water distributions of dissolved copper and copper-complexing ligands in estuarine and coastal marine sediments. *Geochimica et Cosmochimica Acta*, **64**(11): 1843-1857.

Sohrin Y., Iwamoto S.-i., Akiyama S., Fujita T., Kugii T., Obata H., Nakayama E., Goda S., Fujishima Y., Hasegawa H., Ueda K., and Matsui M., **1998**. Determination of trace elements in seawater by fluorinated metal alkoxide glass-immobilized 8-hydroxyquinoline concentration and high-resolution inductively coupled plasma mass spectrometry detection. *Analytica Chimica Acta*, **363**: 11-19.

Sokolowski A., Wolowicz M., and Hummel H., **2001**. Distribution of dissolved and labile particulate trace metals in the overlying bottom water in the Vistula River plume (Southern Baltic Sea). *Marine Pollution Bulletin*, **42**(10): 967-980.

Souza A.J., Simpson J.H., Harikrishnan M., and Malarkey J., **2001**. Flow structure and seasonality in the Hebridean slope current. *Oceanologica Acta*, **24**(S63-S76).

Statham P.J., German C.R., and Connelly D.P., **2005**. Iron(II) distribution and oxidation kinetics in hydrothermal plumes at the Kairei and Edmond vent sites, Indian Ocean. *Earth and Planetary Science Letters*, **236**: 588-596.

Statham P.J., and Hart V., **2005**. Dissolved iron in the Cretan Sea (eastern Mediterranean). *Limnology and Oceanography*, **50**(4): 1142-1148.

Sturgeon R.E., Berman S.S., Willie S.N., and Desaulniers A.H., **1981**. Preconcentration of trace elements from seawater with silica-immobilized 8-hydroxyquinoline. *Analytical Chemistry*, **53**(14): 2337-2340.

Sulzberger B., and Laubscher H., **1995**. Reactivity of various types of iron(III) (hydr)oxides towards light-induced dissolution. *Marine Chemistry*, **50**: 103-115.

Sunda W.G., and Huntsman S.A., **1995**. Iron uptake and growth limitation in oceanic and coastal phytoplankton. *Marine Chemistry*, **50**(1-4): 189-206.

Sunda W.G., and Huntsman S.A., **1997**. Interrelated influence of iron, light and cell size on marine phytoplankton growth. *Nature*, **390**: 389-392.

Sunda W.G., **2001**. Bioavailability and bioaccumulation of iron in the sea. In: *The Biogeochemistry of Iron in Seawater*. Turner D.R., and Hunter K.A., Chichester, John Wiley & Sons, **IUPAC 7:** 41-84.

Swap R., Ulanski S., Cobbett M., and Garstand M., **1996**. Temporal and spatial characteristics of Saharan dust outbreaks. *Journal of Geophysical Research*, **101**(D2): 4205-4220.

Takeda S., and Tsuda A., **2005**. An in situ iron-enrichment experiment in the western subarctic Pacific (SEEDS): Introduction and summary. *Progress in Oceanography*, **64**: 95-109.

Talley L.D., and McCartney M.S., **1982**. Distribution and Circulation of Labrador Sea Water. *Journal of Physical Oceanography*, **12**: 1189-1205.

Thomsen L., and van Weering T.C.E., **1998**. Spatial and temporal variability of particulate matter in the benthic boundary layer at the N.W. European Continental Margin (Goban Spur). *Progress in Oceanography*, **42**: 61-76.

Thorpe S.A., and White M., **1988**. A deep intermediate nepheloid layer. *Deep-Sea Research I*, **35**(9): 1665-1671.

Tsuchiya M., Talley L.D., and McCartney M.S., **1992**. An eastern Atlantic section from Iceland southward across the equator. *Deep-Sea Research*, **39**(11-12): 1885-1917.

Turner A., and Millward G.E., **2000**. Particle dynamics and trace metal reactivity in estuarine plumes. *Estuarine, Coastal and Shelf Science*, **50**: 761-774.

Ussher S.J., Achterberg E.P., and Worsfold P.J., **2004**. Marine biogeochemistry of iron. *Environmental Chemistry*, **1**: 67-80.

Ussher S.J., Yaqoob M., Achterberg E.P., Nabi A., and Worsfold P.J., **2005**. Effect of model ligands on iron redox speciation in natural waters using flow injection with luminol chemiluminescence detection. *Analytical Chemistry*, **77**: 1971-1978.

van Aken H.M., **2000**. The hydrography of the mid-latitude Northeast Atlantic Ocean II : The intermediate water masses. *Deep-Sea Research I*, **47**: 789-824.

van den Berg C.M.G., **1995**. Evidence for organic complexation of iron in seawater. *Marine Chemistry*, **50**(1-4): 139-157.

van Weering T.C.E., Hall I.R., de Stigter H.C., McCave I.N., and Thomsen L., **1998**. Recent sediments, sediment accumulation and carbon burial at Goban Spur, N.W. European Continental Margin (47-50^{o}N). *Progress in Oceanography*, **42**: 5-35.

van Weering T.C.E., de Stigter H.C., Balzer W., Epping E.H.G., Graf G., Hall I.R., Helder W., Khripounoff A., Lohse L., McCave I.N., Thomsen L., and Vangriesheim A., **2001**. Benthic dynamics and carbon fluxes on the NW European continental margin. *Deep-Sea Research II*, **48**: 3191-3221.

Vink S., Boyle E.A., Measures C.I., and Yuan J., **2000**. Automated high resolution determination of the trace elements iron and aluminium in the surface ocean using a towed Fish coupled to flow injection analysis. *Deep-Sea Research I*, **47**(6): 1141-1156.

Vink S., and Measures C.I., **2001**. The role of dust deposition in determining surface water distributions of Al and Fe in the South West Atlantic. *Deep-Sea Research II*, **48**: 2787-2809.

Voelker B.M., and Sedlak D.L., **1995**. Iron reduction by photoproduced superoxide in seawater. *Marine Chemistry*, **50**(1-4): 93-102.

Waite D.T., **2001**. Thermodynamics of the iron system in seawater. In: *The Biogeochemistry of Iron in Seawater*. Turner D.R., and Hunter K.A., Chichester, John Wiley & Sons, **IUPAC 7:** 291-342.

Wang J.H., **1955**. On the detailed mechanism of a new type of catalase-like action. *Journal of American Chemical Society*: 4715-4719.

Wang W.-X., and Dei R.C.H., **2001**. Biological uptake and assimilation of iron by marine plankton: influences of macronutrients. *Marine Chemistry*, **74**(2-3): 213-226.

Watson A.J., **2001**. Iron Limitation in the Oceans. In: *The biogeochemistry of iron in seawater*. Turner D.R., and Hunter K.A., Chichester, John Wiley & Sons, **IUPAC 7:** 9-39.

Weeks D.A., and Bruland K.W., **2002**. Improved method for shipboard determination of iron in seawater by flow injection analysis. *Analytica Chimica Acta*, **453**: 21-32.

Weinstein S.E., and Moran S.B., **2004**. Distribution of size-fractionated particulate trace metals collected by bottles and in-situ pumps in the Gulf of Maine-Scotian shelf and Labrador Sea. *Marine Chemistry*, **87**: 121-135.

Wells M.L., and Goldberg E.D., **1991**. Occurence of small colloids in sea water. *Nature*, **353**: 342-344.

Wells M.L., and Goldberg E.D., **1993**. Colloid aggregation in seawater. *Marine Chemistry*, **41**: 353-358.

Wells M.L., and Goldberg E.D., **1994**. The distribution of colloids in the North Atlantic and Southern Oceans. *Limnology and Oceanography*, **39**(2): 286-302.

Whitfield M., **2001**. Interactions between phytoplankton and trace metals in the ocean. *Advances in Marine Biology*, **41**: 1-128.

Wollast R., and Chou L., **2001**. The carbon cycle at the ocean margin in the northern Gulf of Biscay. *Deep-Sea Research II*, **48**: 3265-3293.

Wright, and Jeffrey S.W., **1987**. Fucoxanthin pigment markers of marine phytoplankton analysed by HPLC and HPTLC. *Marine Ecology Progress Series*, **38**: 259-266.

Wright S.W., Jeffrey S.W., Mantoura R.F.C., Llewellyn C.A., Bjornland T., Repeta D., and Welschmeyer N.A., **1991**. Improved HPLC method for the analysis of chlorophylls and carotenoids from marine phytoplankton. *Marine Ecology Progress Series*, **77**: 183-196.

Wu J., and Luther III G.W., **1995**. Complexation of Fe(III) by natural organic ligands in the Northwest Atlantic Ocean by a competitive ligand equilibration method and a kinetic approach. *Marine Chemistry*, **50**(1-4): 159-177.

Wu J., and Luther III G.W., **1996**. Spatial and temporal distribution of iron in the surface water of the northwestern Atlantic Ocean. *Geochimica et Cosmochimica Acta*, **60**(15): 2729-2741.

Wu J., and Boyle E.A., **1998**. Determination of iron in seawater by high-resolution isotope dilution inductively coupled plasma mass spectrometry after $Mg(OH)_2$ coprecipitation. *Analytica Chimica Acta*, **367**: 183-191.

Wu J., Boyle E.A., Sunda W.G., and Wen L.-S., **2001**. Soluble and colloidal iron in the oligotrophic North Atlantic and North Pacific. *Science*, **293**(5531): 847-849.

Xiao C., King D.W., Palmer D.A., and Wesolowski D.J., **2000**. Study of enhancement effetcs in the chemiluminescence method for Cr(III) in the $ng.l^{-1}$ range. *Analytica Chimica Acta*, **415**: 209-219.

Xiao C., Palmer D.A., Wesolowski D.J., Lovitz S.B., and King D.W., **2002**. Carbon dioxide effects on luminol and 1,10-phenanthroline chemiluminescence. *Analytical Chemistry*, **74**(9): 2210-2216.

Zeebe R.E., and Archer D., **2005**. Feasibility of ocean fertilization and its impact on future atmospheric CO_2 levels. *Geophysical Research Letters*, **32**: L09703.

Zhu X., Prospero J.M., Savoie D.L., Millero F.J., Zika R.G., and Saltzman E.S., **1993**. Photoreduction of iron(III) in marine mineral aerosol solutions. *Journal of Geophysical Research*, **98**(D5): 9,039-9,046.

Zhuang G., Duce R.A., and Kester D.R., **1990**. The dissolution of atmospheric iron in surface seawater of the open ocean. *Journal of Geophysical Research*, **95**(C9): 16,207-16,2016.

Zhuang G., Yi Z., Duce R.A., and Brown P.R., **1992**. Link between iron and sulphur cycles suggested by detection of Fe(II) in remote marine aerosols. *Nature*, **355**: 537-539.